NGU Report 2011.004

Resistivity measurements and structural geology along the railroad tunnel transect Oslo - Ski.

Geological Survey of Norway
NO-7441 Trondheim, Norway
Tel.: 47 73 90 40 00
Telefax 47 73 92 16 20

REPORT

Report no.: 2011.004 | ISSN 0800-3416 | Grading: Open

Title:
Resistivity measurements and structural geology along the railroad tunnel transect Oslo - Ski.

Authors:
Aline Saintot, Einar Dalsegg & Jan S. Rønning

Client:
Jernbaneverket Utbygningsdivisjonen -NGU

County:
Oslo & Akershus

Commune:
Oslo, Oppegård & Ski

Map-sheet name (M=1:250.000)
Oslo

Map-sheet no. and -name (M=1:50.000)
1914 III Ski, 1914 IV Oslo

Deposit name and grid-reference:

Number of pages: 143 Price (NOK): 950,-
Map enclosures:

Fieldwork carried out:	Date of report:	Project no.:	Person responsible:
July & October 2010	20.12.2010	336000	Guri V. Ganerød

Summary:

In connection with the detailed planning of new double track railway tunnel approx. 23.5 km long from Oslo to Ski, the Geological Survey of Norway (NGU) on request from the Norwegian Rail Road Authority (Jernbaneverket Utbyggingsdivisjonen) conducted an upgrade of the geological and geophysical background material at a regional scale and delivered it in a digital form in 2007 (Lutro et al. 2007). This work contributed to provide the best possible basis and assessment to the engineering geological and hydrogeological conditions for further planning of the tunnels. In the following years, the same authorities deviated the trends of the planned tunnel traces and requested to NGU for additional geophysical and geological data.

All together, 19 resistivity profiles were measured using the Lund system mainly with electrode separation 5 meters, giving a maximum penetration of 60 meters. Three profiles were measured using 10 meters electrode separation were maximum penetration depth is 120 meters. In this study, both soil cover and fracture zones in bedrock were of interest. Due to this, the data were processed focusing both on horizontal and vertical structures (vertical/horizontal filter equal 0,5 and 2). To get control of technical installations and possible sulphides in bedrock, induced polarization (IP) were measured. All measured data are presented in colour sections with interpretation of soil cover and fracture zones. In addition, fracture zones are listed in a table with classification of fracture zone thickness, depth extent and dip. All together, 52 fracture zones are indicated. Unfortunately, the measurements in the northern part of the area seem to be influenced by technical installations giving disturbances in the resistivity level. Due to this, some of the indicated fracture zones are uncertain.

Structural observations were made at 21 locations. Strike and dip of different structures are presented in stereo nets (Smith's projection) and as rose diagrams with dip indicators. In addition, rock quality is documented in pictures. All types of structures are included in the analysis. They comprise (1) the metamorphic foliation and the ductile folding deformation, (2) the brittle deformation classified as joints, joint sets, mineralized fractures, striated fault surfaces, faults with crushed zones or fault rocks (breccias, gouge, etc) as well as dykes linked to the magmatic activity of the Oslo rift development.

Keywords:	Geophysics	Structural geology
	Tunnels	Resistivity
		Scientific report

CONTENTS

FIGURES

1. INTRODUCTION

In connection with the detailed planning of the new double track railway tunnel approx. 23.5 km long from Oslo to Ski, the Geological Survey of Norway (NGU) on request from the Norwegian Rail Road Authority (Jernbaneverket Utbygging) conducted an upgrade of the geological and geophysical background material at a regional scale and delivered it in a digital form in 2007 (Lutro et al. 2007). This work contributed to provide the best possible basis and assessment to the engineering geological and hydrogeological conditions for further planning of the tunnels. In the following years, the same authorities deviated the trends of the planned tunnel traces and requested to NGU for additional geophysical and geological data.

Within the project ""Miljø- og Samfunnstjenlige tunneler (Tunnels for the citizen)", which was conducted in the period 2001 to 2003, 2D resistivity method was introduced as an interesting technique of studies for tunnel planning (Rønning, 2003). The electric resistivity measurements along the planned Lunner tunnel trace allowed to propose a model for the characterization of weakness zones (Rønning et al., 2003). With the prevailing geological conditions of the Oslo region, the intact intrusives and sediments (syenites and sandstones) indicated resistivity values higher than about 3000 Ωm while major water leakages were characterized by zones of resistivity in the range of 500 to 3000 Ωm and zones where resistivity was lower than 500 Ωm was considered to correspond to unstable bedrock. Afterwards NGU performed simulations to show that resistivity methods also provide a geometric characterization of weakness zones (Reiser et al., 2009) by indicating not only depth and width of weakness zones but also their dip angles. The conclusion was that resistivity method has the potential to localize the weak zones, to give their geometry and the mineralogical characterization of the zones. Electronic leading minerals like sulphides, metallic oxides and graphite may increase the electrical conductivity (or reduce the resistivity), and thereby give anomalies of the same type as the water-filled weakness zones with or without clay. However, the method is limited in some known cases: contrast of resistivity between intact (not fractured) intrinsically less resistive bedrock and weakness zones can be too low to be detected; a thick conductive cover (as made of clays) may prevent the current to penetrate the bedrock at depth. Both these effects reduce the potentiality for mapping zones of weakness. In addition, the modelling showed that there may be artificial effects in the inversion of the measured data. The characterization of weakness zones using resistivity data is a new technology, and the projects that NGU works on in cooperation with the Norwegian Road and Rail Road authorities may be part of efforts to build up expertise in the interpretation of such data (see for example, in Dalsegg et al. 2010).

Based on these experiences to provide reliable information for tunneling with the 2D electric resistivity method, NGU carried out measurement profiles at places specifically assigned by the Norwegian Rail Road Authorities to be critical for the stability of the Oslo-Ski planned tunnels. A total of 11.4 km, divided in 18 profiles of 400 to 1400 m length, was acquired in summer 2010. In addition to these resistivity measurements with the purpose of detecting and characterizing weakness zones, the areas close to the profiles were geologically investigated to gain a better understanding of the structures as fracture zones and faults that can cause both leakage and stability problems in the tunnels. All types of structures are included in the analysis. They comprise (1) the metamorphic foliation and the ductile folding deformation (2) the brittle deformation classified as joints, joint sets, mineralized fractures, striated fault surfaces, faults with crushed zones or fault rocks (breccias, gouge, etc) as well as dykes linked to the magmatic activity of the Oslo rift development. The resistivity data are processed and interpreted with, for the latter, the integration of existing and newly acquired geological data. The structures observed at the scale of the outcrops are also interpreted in a wider context in terms of extent and regional significance. Such analysis allows for an estimate of the importance of the different structures and the completion of the interpretation of the 2D resistivity data.

2. PREVIOUS NGU WORK ON THE PLANNED OSLO-SKI DOUBLE TRACK RAILWAY TUNNEL

The background data of the current report and specifically of the maps in figures are from Lutro et al. (2007).

They issued from:

- Publications, maps and datasets (geological, geophysical and remote sensing) of the NGU archives
- Topographic data from the Norwegian Mapping Authority (Statens Kartverk)
- Reports of previous investigations on geology and engineering geology of the Oslo-Ski tunnel (provided by the Norwegian Rail Road Authority).

Based on this material and other available data sets, the NGU produced and delivered in Lutro et al. (2007):

- a new bedrock geological map (at scale 1:5000) and a geological profile along the Oslo-Ski planned tunnel trace with bedrock limits, dykes, regional faults and fractures zones (maps 2007.048-1 to -5 in Lutro et al. 2007)
- a Digital Elevation Model and its derived map of lineaments, both included in the bedrock geological map at scale 1:5000 (the Digital Elevation Model as shaded relief) (maps 2007.048-6 to -10 in Lutro et al. 2007)
- information on subsidence based on NGU inSAR-data (satellite radardata) (maps 2007.048-11 to -15 in Lutro et al. 2007)
- a map of zones possibly affected by deep-weathering, issued from magnetic data and displayed on the shaded relief Digital Elevation Model at scale 1:20000 (map 2007.048-16 in Lutro et al. 2007)
- a quaternary map at scale 1:5000 (maps 2007.048-17 to -21 in Lutro et al. 2007)
- a map combining the shaded relief Digital Elevation Model, the quaternary map and the inSAR-data to localise the zones of subsidence (maps 2007.048-22 to -26 in Lutro et al. 2007).

3. OVERVIEW OF THE GEOLOGY ALONG THE OSLO-SKI PLANNED RAILROAD TUNNELS

The bedrock map is displayed on Figure 1 together with the trace of planned rail road tunnels, the important faults or/and lineaments, some foliation values, the field localities for the structural analysis and the 2D resistivity profiles.

The bedrock belongs to the Precambrian basement of southeastern Norway. They have an age of ca. 1500-1600 million years, and underwent deformation and metamorphism about 1000 million years ago (Sveconorwegian Orogeny). At this time a penetrative foliation which is generally oriented NNW-SSE to N-S developed in the rocks. Folds are observed at many places. The most common folds are tight with steep axial planes and axes that plunge towards the NNW.

The Precambrian rocks displayed at the scale of Figure 1 consists of three main types: (1) a tonalitic to granitic, middle to coarse grained, grey gneiss, (2) a biotite-rich augen gneiss (granitic to granodioritic gneiss, migmatitic and biotite-rich with 1-2 cm large eye-shaped K-feldspars in Graversen et al. 2009) and (3) a quartz-feldspathic gneiss (supracrustal) (garnet-

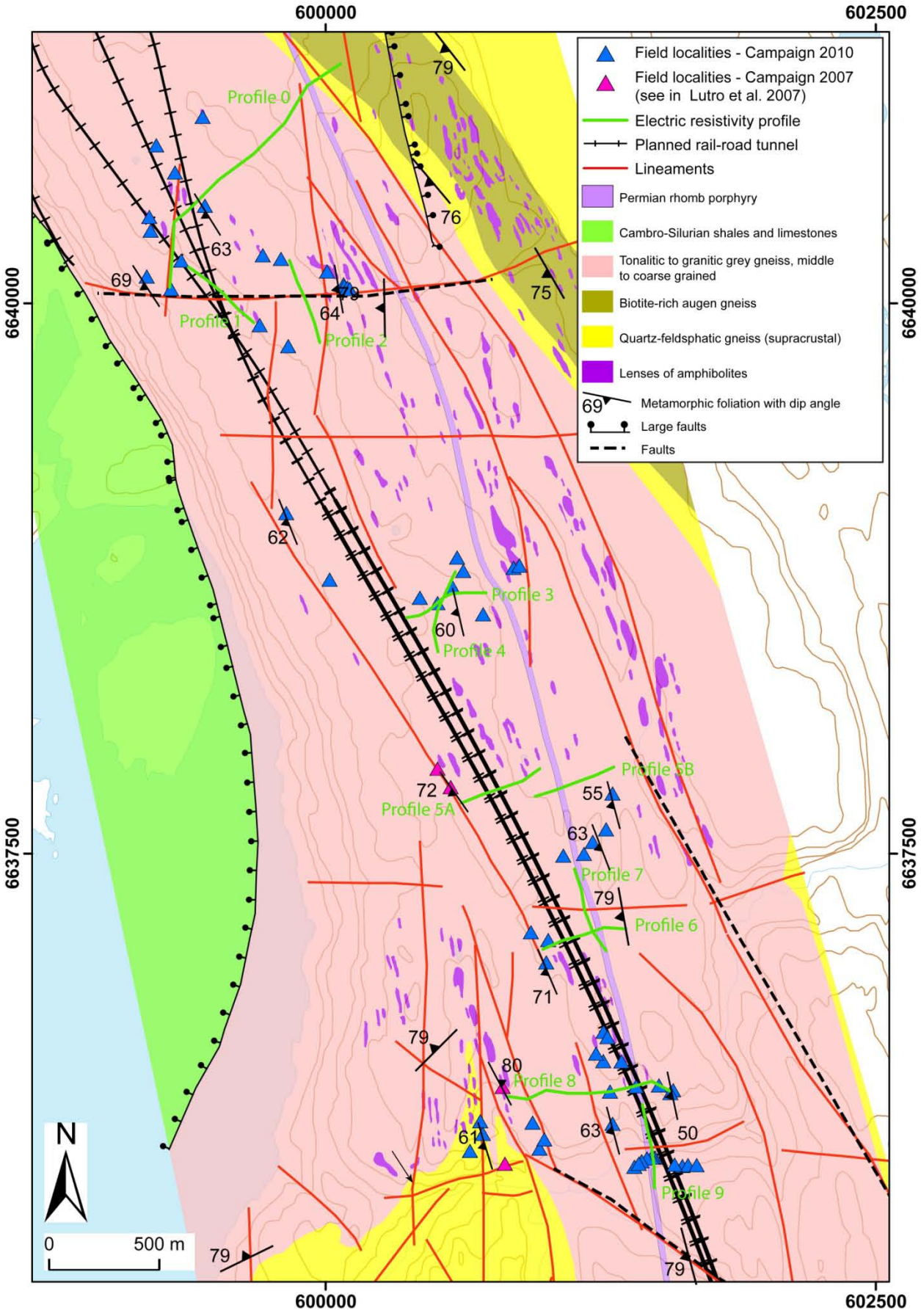

Figure 1. Geological map around the Oslo-Ski planned rail road tunnels with the important faults or/and lineaments, some foliation values, the field localities for the structural analysis and the 2D resistivity profiles presented in this report.

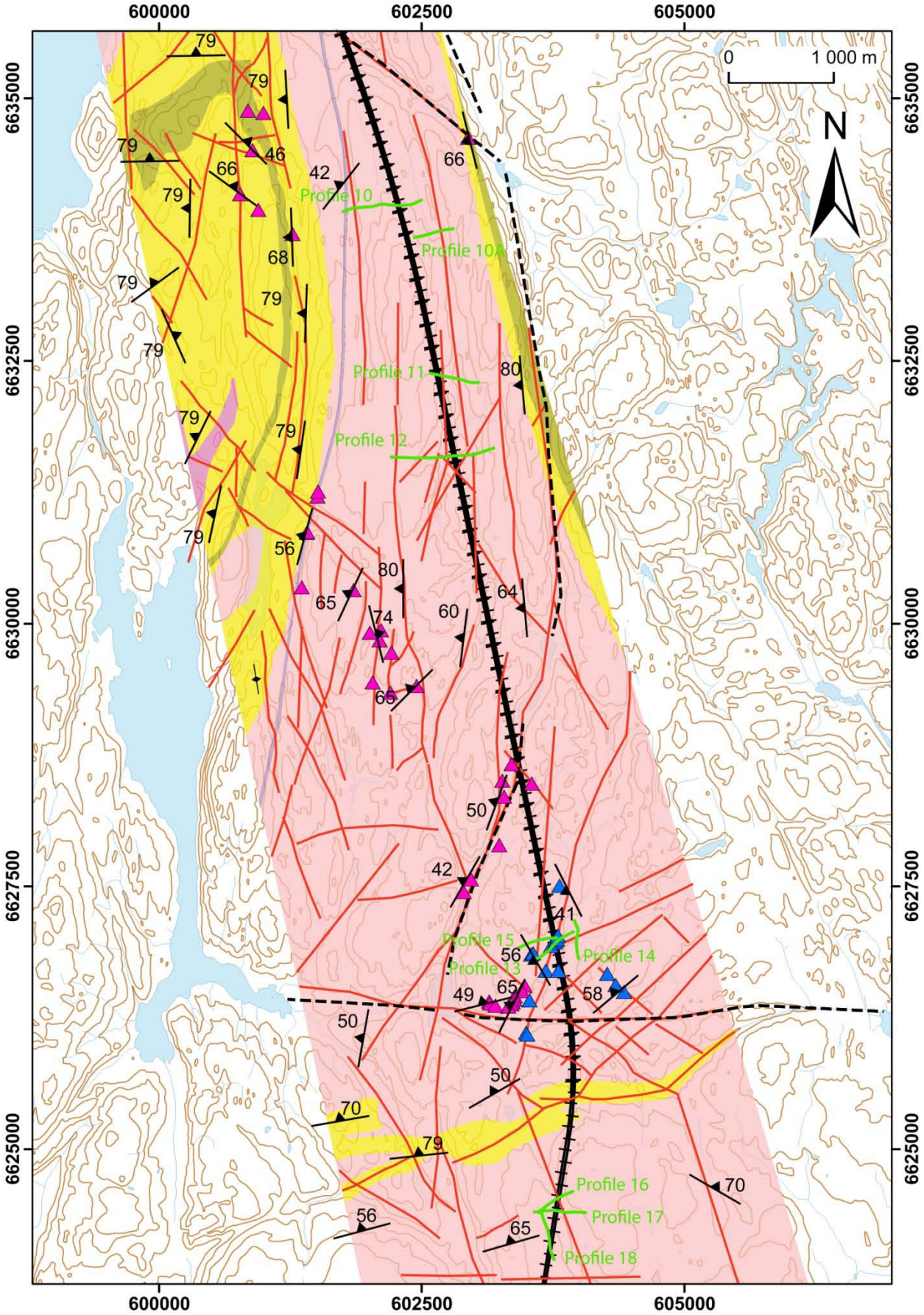

Figure 1 continued.

biotite gneiss, biotite-muscovite gneiss, locally with amphibolite and lenses of calc-silicate rocks – Stora Le-Marstrand Formation- in Graversen et al. 2009); (more information on the three units is in Lutro et al. 2007 and a detailed petrographic description, in Graversen, 1984). Whereas the planned tunnels in 2007 were expected to cross these three units, the new tunnel traces are deviated to the east and should only be across the first unit (Figure 1). Many bodies of various types of amphibolites are reported in the unit (Graversen, 1984). Their shapes are generally lenticular and of some meter extent but 20-30 m large bodies are also reported (see in Lutro et al. 2007). Amphibolite lenses mapped by Gudmund Grammeltvedt (document by courtesy of the Norwegian Rail Road Authority) in the northern part of the studied area are added to the updated map produced by Lutro et al. (2007) (Figure 1). However, the accuracy in the position of these amphibolitic lenses is very low and may severely be deviated of the reality.

The formation of the Permian Oslo Rift has also affected these Precambrian rocks with the development of fractures and faults. The latter correspond to more or less pronounced lineaments as elongated topographic depressions. The planned tunnels is also expected to cross many Permian dykes intruded in the Precambrian bedrocks along major fractures and / or foliation. The dykes are commonly not wider than half a meter and orientated NW-SE to N-S to NE-SW. Among them, a N-S trending, 10 to 20 m wide, rhomb porphyry dyke is remarkable (Brøgger 1933; Figure 1).

4. GEOPHYSICS – 2D RESISTIVITY AND INDUCED POLARIZATION (IP)

4.1 Method: Resistivity

2D resistivity and induced polarization (IP) was measured in this geophysical survey. IP and resistivity are measured simultaneously which extended the measuring time slightly. Indeed, the combination of the two kinds of data significantly reduced the risk of misinterpretation. For example the conductive minerals (sulphides, graphite, metallic oxides) which can be misinterpreted as a water filled damage zone of the bedrock with only resistivity data have in turn a clear signature as minerals in the IP data. In this survey, the IP data can also be an indicator of technical installations in the neighbourhood of the profiles. The method is shortly described herein but a detailed description is available in http://www.ngu.no/no/hm/Norges-geologi/Geofysikk/Bakkegeofysikk/Elektriske-metoder/ (in Norwegian).

4.1.1 Acquisition

Data are collected using a cable system developed by the Institute of Technology of Lund University, called the LUND-system (Dahlin 1993). The system consists of a relay box (Electrode Selector ES10-64) and of two or four multi-electrode cables. The ABEM Terrameter SAS 4000 (ABEM 1999) resistivity and IP instrument contains an integrated PC for full control of data acquisition process and storage of data. In this survey, four cables were used with a GRADIENT electrode configuration and 5m to 10 m electrode spacing. A maximum depth range of about 120 meters may be reach with the latter configuration, while with 5 m electrode spacing the penetrating depth is ca. 60 m The resolution decreases with depth and resistivity data deeper than ca. 80 and 30 meters, respectively of the two configurations, are by experience of low reliability. The entire system can be rolled along the profile so that the extent of a profile is unlimited.

The profiles 0, 10 and 12 were acquired using a 10 m electrode interval, while a 5 m electrode interval was used on the remaining profiles. Crossing profiles are acquired since this increases the reliability of the interpretation of the weakness zones.

4.1.2 Electric currents and data quality

The electric currents varied quite a lot during the Oslo-Ski measurements. In the heavily populated areas to the north, the ground consists of dry sand and gravel, and here the maximum currents were from 10 to 50 mA. Further to the south, where the profiles were in open areas with natural soil, the current strength was from 100 to 200 mA.

Low current strength and technical installations (metallic fences a.o.) in the northern part, resulted in a low data quality. Obvious noisy data points were removed from the data before inversion. However, the technical installations gave reduced resistivity level due to channeling of the currents in the ground, which resulted in less reliable interpretations. In the southern part of the area, from profile no. 9 and upwards, the data quality was good, giving reliable interpretation. Increased IP values in the north is an indication of metallic conductors such as fences, reinforced concrete and metallic pipes in the ground.

4.1.3 Inversion

All resistivity measurements give an apparent resistivity value. This latter represents a weighted average resistivity which resulted from resistivity of each heterogeneous volume in the surrounding of the measurement points (note: heterogeneous volume in terms of resistivity and size for the purpose of the study). To find the specific resistivity of each part of the heterogeneous investigated volume, the data are inverted. This is made by dividing the profile into blocks each characterized by specific resistivity values. The resistivity values of the blocks are adjusted following an iterative procedure until the theoretical model fits the measured data.

Resistivity measurements were inverted using the computer program RES2DINV (Loke, 2007). Different methods of inversion are applied (”Least Square” and ”Robust”) with variation in the inversion parameters, attenuation factors and filters. This did not result in fundamental changes in the main features of the inverted profiles, but only in minor variations. However, the use of the vertical / horizontal filter 2 highlights the vertical structures (Reiser et al., 2009) while vertical/horizontal filter 0.5 highlights horizontal layering. In this survey, both subvertical structures such as fracture zones in bedrock, and subhorizontal soil layers at the surface were of interest. Due to this, the inversion results are presented with both filters (V/H = 2 and 0.5) in addition to IP values, with H/V-filter equal 2. The zones becoming wider at depth are an artefact of the inversion procedure, and not the real geometric attitudes of the zones. Actually, it is more likely that the zones are narrower at depth due to the increase of pressure with depth.

4.1.4 Interpretation

To provide an interpretation directly applicable for engineering geologists, we propose a classification of the zone according to their depth, width and resistivity value. Classes are from 1 to 4, where 1 corresponds to a good rock mass while 4 suggests a problematic rock mass (Table 1). Increased zone width is assumed to cause more problems, and low resistivity values could indicate presence of clay minerals in fractures and thus unstable conditions (Rønning el al., 2009). Such a characterization is given for each resistivity profile. Zones that are interpreted to be fracture zones or faults are added to the profiles. A +/- 5 m accuracy locations of the zones are also given in a table with both coordinates along the profile and UTM coordinates. The deduced strike and dip angle of each zone are also available. The dip angles of zones obtained by a 2D resistivity method cannot be accurately determined so they are classified according to their general attitude as "steep, moderate and gentle" (Table 2).

The purpose of providing both the coordinates at the surface and the dip angle of the zones is to allow their projection to the tunnel level. The profiles are displayed with horizontal and vertical scale ratio 1:1 to allow a straightforward projection of the zones to the planned tunnel trace following their dip angle. However, due to the uncertainty on the value of the dip angles of the zones, the exact locations at depth of the zone and tunnel intersections are not predictable.

A- depth of zone	B- Width of zone	C- Resistivity of zone	Class
0-20 m	0-10 m	>3000 Ωm	1
20-40 m	10-20 m	3000-1000 Ωm	2
40-60 m	20-40 m	1000-500 Ωm	3
>60 m	>40 m	<500 Ωm	4

Table 1. Classification of fracture and/or fault zones. Zones that are observed with 2D resistivity methods are in four classes according to their depth (A), width (B) and resistivity value (C).

Class	**Dip angle**
Steep	80-90°
Moderate	45-80°
Gentle	<45°

Table 2. Classification of dip angles.

In addition, we indicate the possibility for the presence of electronic conducting minerals (sulphides, oxides or graphite) or responses from technical installations in case of low resistivity values. In some of the measured profiles, the resistivity level is influenced by technical installations. Consequently, it is not possible to interpret whether or not there is clay within the fracture zones (see Introduction).

In the presentation of the resistivity/IP data, an interpretation of soil thickness is indicated on the V/H-filter equal 0.5 inverted data, while fracture zones in bedrock are drawn on the V/H equal 2 inversion.

4.2 2D resistivity profiles along the Oslo-Ski planned railroad tunnels

The locations of the resistivity profiles are displayed on the 1/10 000 topographic maps in Appendix 1. In section 5, the resistivity profiles 0–9 and 13–15 also appear on very detailed topographic maps together with the field localities, structural measurements and geological units. In the following, a short description of each profile is given. A summary of all profiles are presented in Table 3 after the profile description.

4.2.1 2D resistivity profiles 0, 1 and 2

2D resistivity profile 0

Along profile 0 presented in Figure 2, no obvious soil cover is interpreted. This may relay on lack of resistivity contrast in case of sand/gravel above bedrock. Altogether 8 possible fracture zones are interpreted (for details see Table 3). High IP values may indicate that general low resistivity can be caused by technical installations. However, shallow relative variations along the profile may indicate real fracture zones.

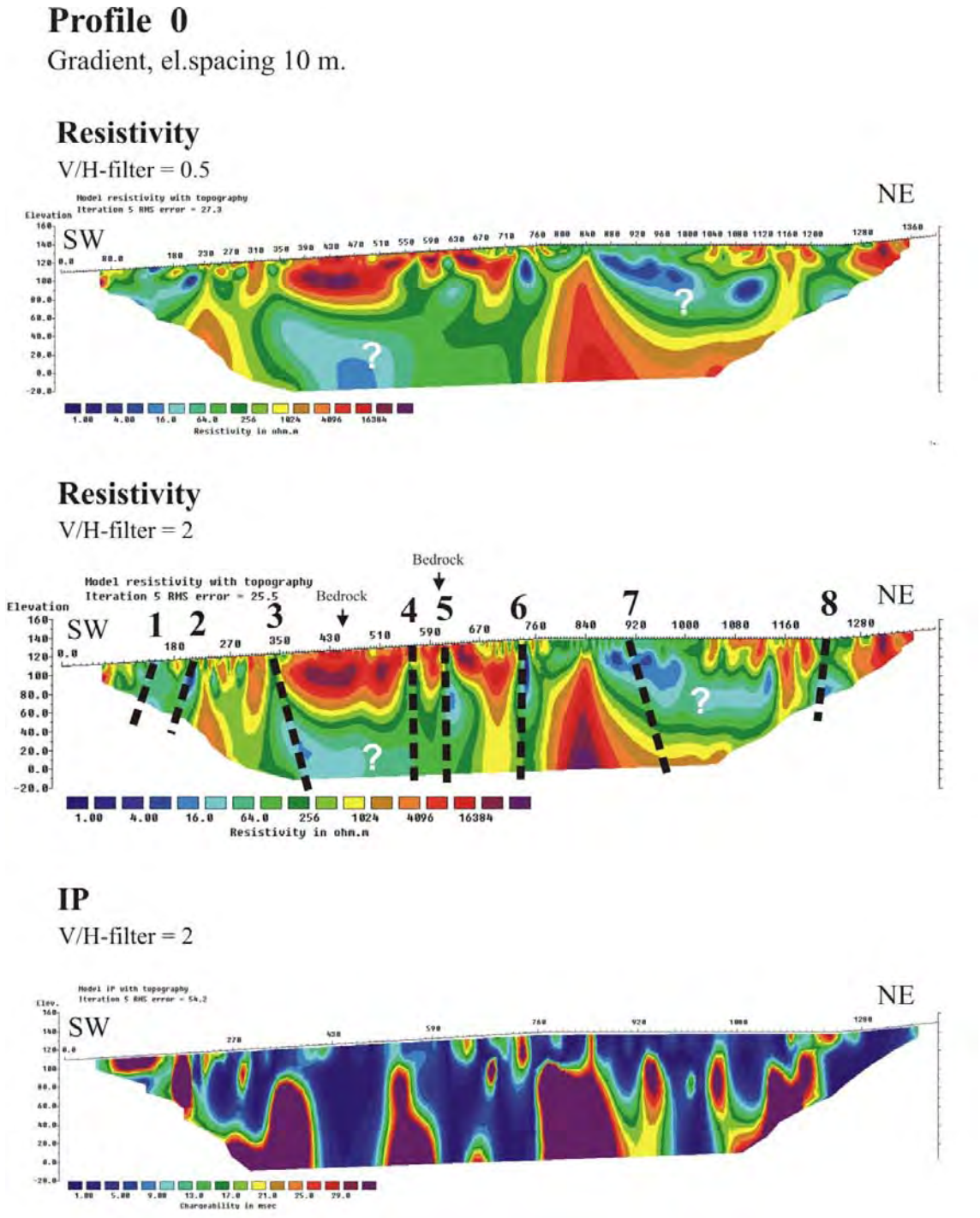

Figure 2. Profile 0, resistivity and IP with interpreted zones (fracture zones as thick dashed lines).

2D resistivity profile 1

Along profile 1 presented in Figure 3, a soil cover is interpreted between coordinates 130 and 240, with a maximum depth of ca. 15 m. Altogether 2 possible fracture zones are interpreted (for details see Table 3). High IP values towards SE may indicate that general low resistivity in this area can be caused by technical installations. However, shallow relative variations along the profile may indicate real fracture zones.

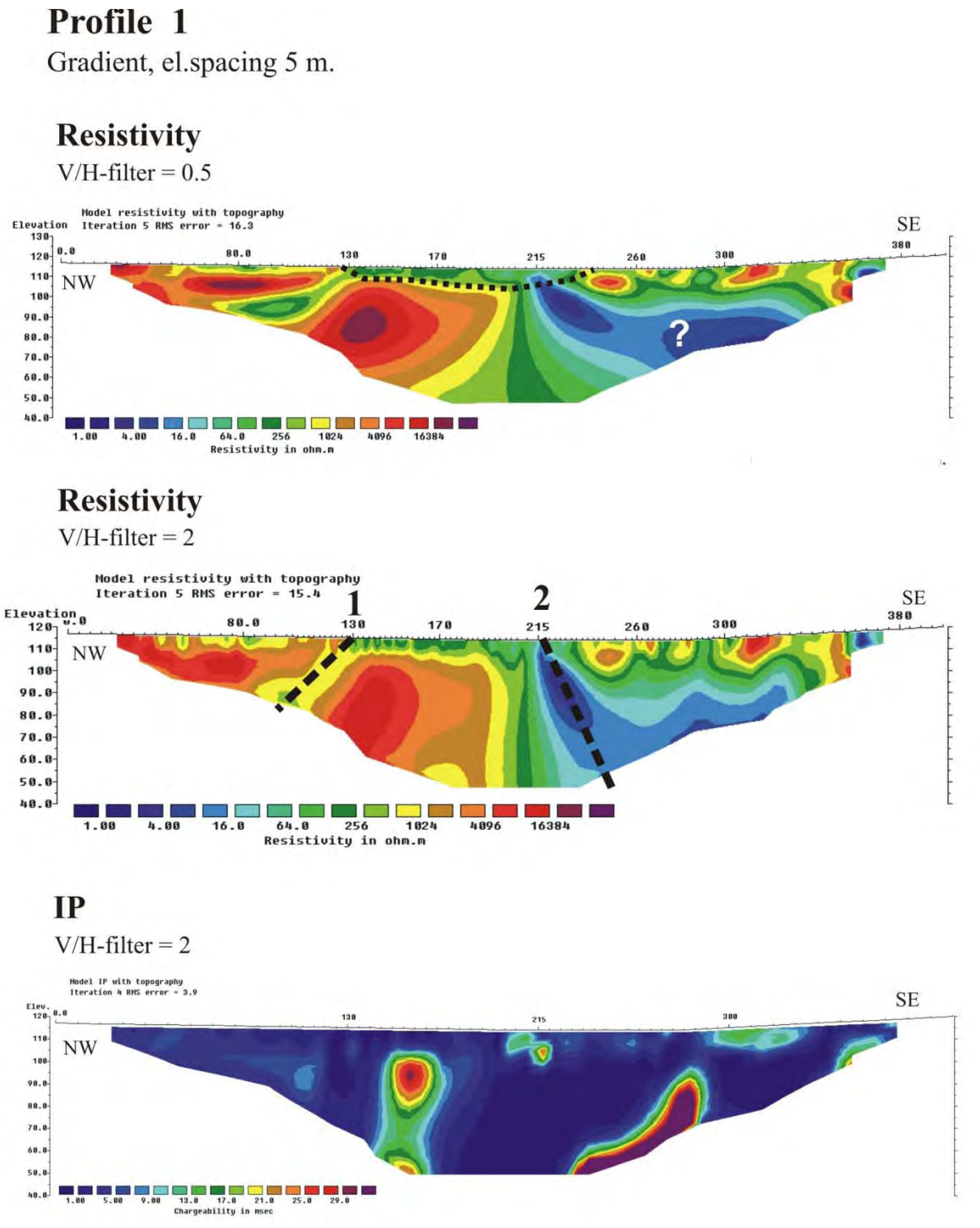

Figure 3. Profile 1, resistivity and IP with interpreted zones (fracture zones as thick dashed lines; soil cover limited at depth by a thin dashed line).

2D resistivity profile 2

Along profile 2 presented in Figure 4, no obvious soil cover is interpreted. This may relay on lack of resistivity contrast in case of sand/gravel above bedrock. One possible fracture zones is interpreted (for details see Table 3). High IP values may indicate that general low resistivity can be caused by technical installations. However, the indicated fracture zone seems to be real.

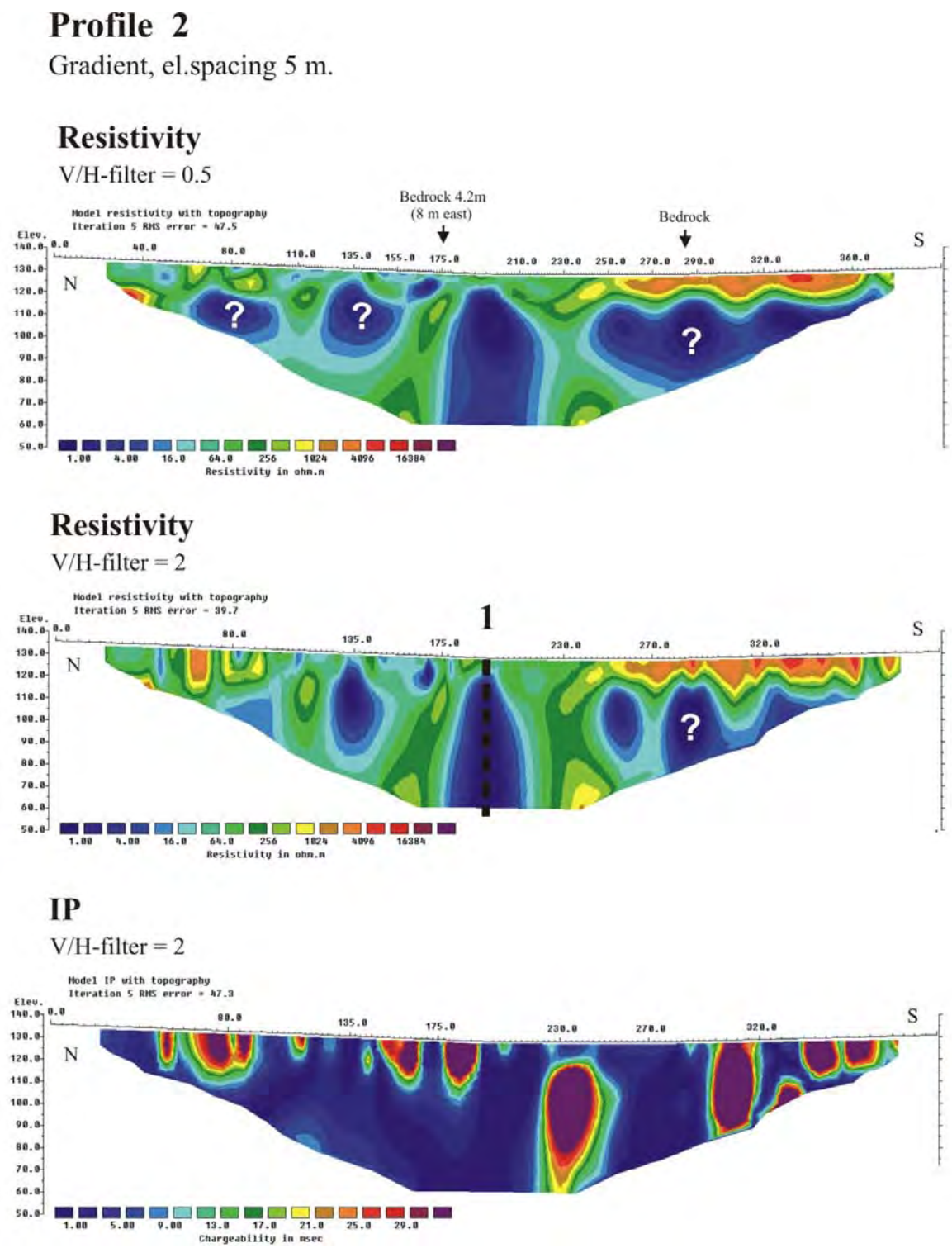

Figure 4. Profile 2, resistivity and IP with interpreted zones (fracture zone as a thick dashed line).

Map of resistivity anomalies along profiles 0, 1 and 2

Figure 5 presents on the geological map the resistivity anomalies along profiles 0, 1 and 2 which may be related to fracture zones. It includes the uncertainty of the anomaly interpretation and the dip angle of the anomaly.

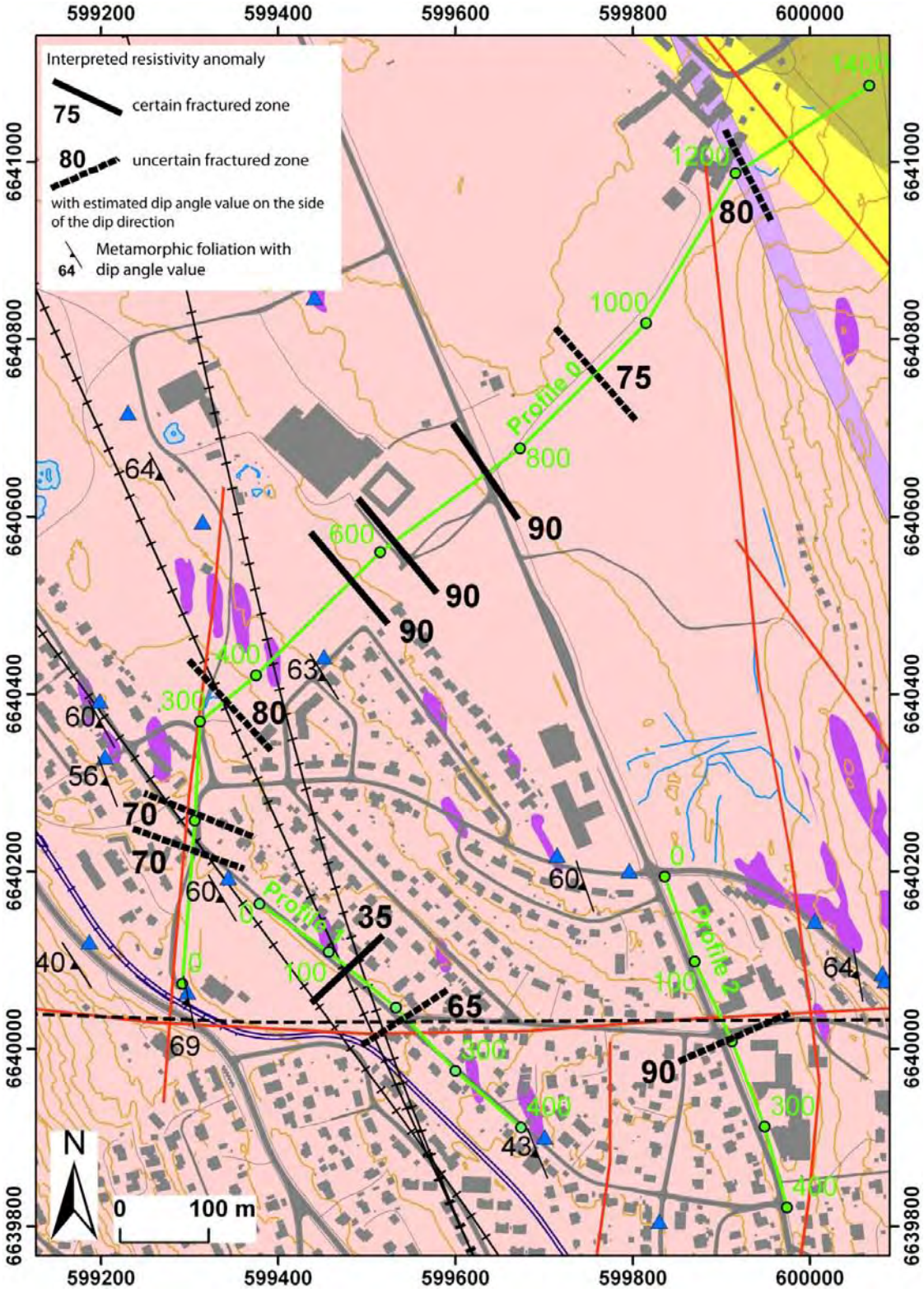

Figure 5. Map of resistivity anomalies along profiles 0, 1 and 2 (background as for Figure 1). (Approximate dip direction of the zone mapped by 2D resistivity method is indicated by which side of the line the angle of dip is written.)

4.2.2 2D resistivity profiles 3 and 4

2D resistivity profile 3

Along profile 3 presented in Figure 6, a soil cover is interpreted in the west end of the profile, where the soil cover becomes thicker westward, approximately of 10-15 m. Altogether 3 possible fracture zones are interpreted (for details see Table 3). High IP values may indicate that the general low resistivity can be caused by technical installations in the western part of the profile. However, the three interpreted fracture zones seem to be real, but the resistivity level is influenced by technical installations.

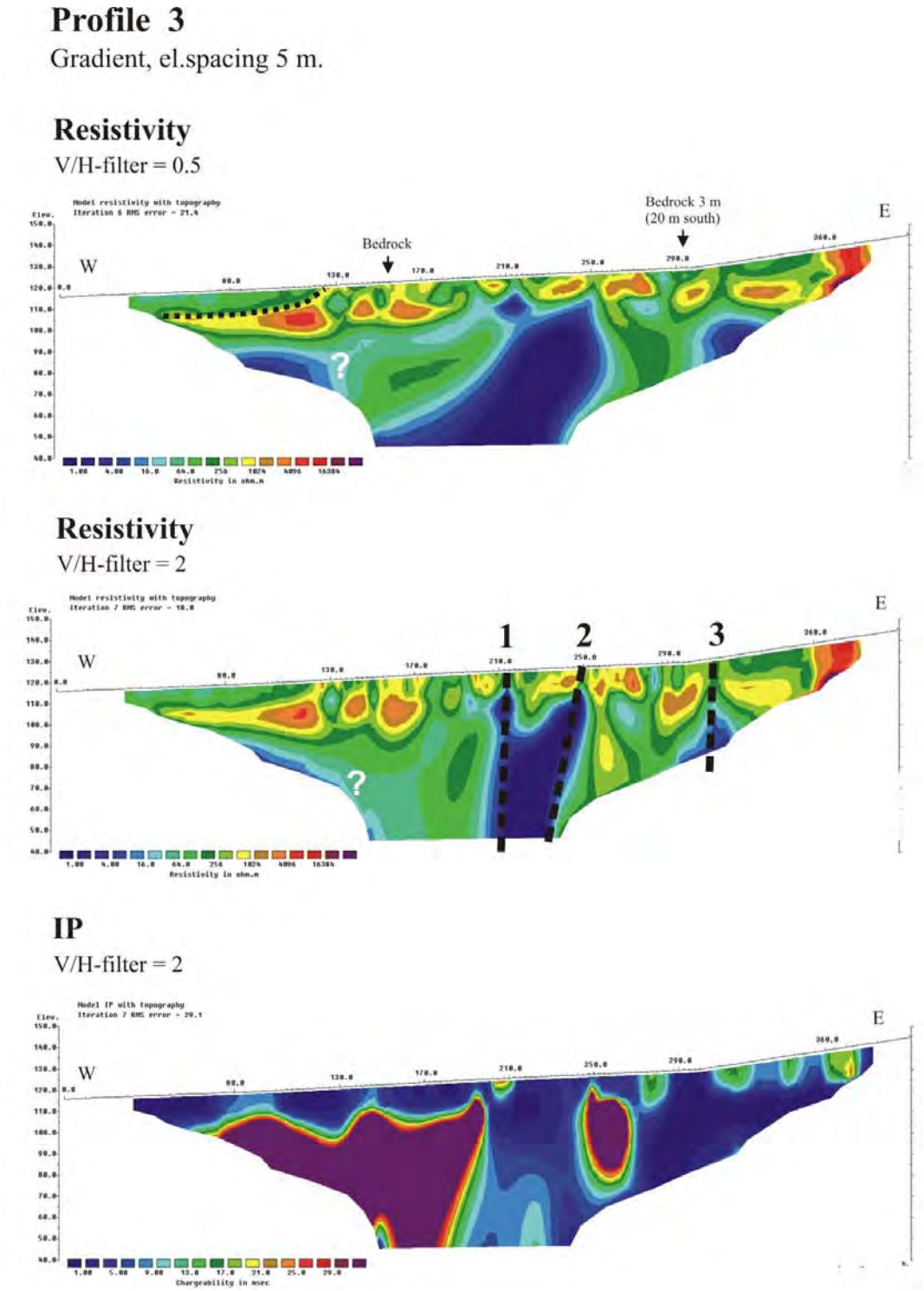

Figure 6. Profile 3, resistivity and IP with interpreted zones (fracture zones as thick dashed lines; soil cover limited at depth by a thin dashed line).

2D resistivity profile 4

Along profile 4, a soil cover is interpreted between coordinate 20 and coordinate 180, with a maximum depth of ca. 15 m (Figure 7). Two possible fracture zones are interpreted (for details see Table 3). High IP values may indicate that general low resistivity in the central part of the profile can be caused by technical installations or electronic conducing minerals. However, shallow relative variations along the profile may indicate the fracture zones to be real.

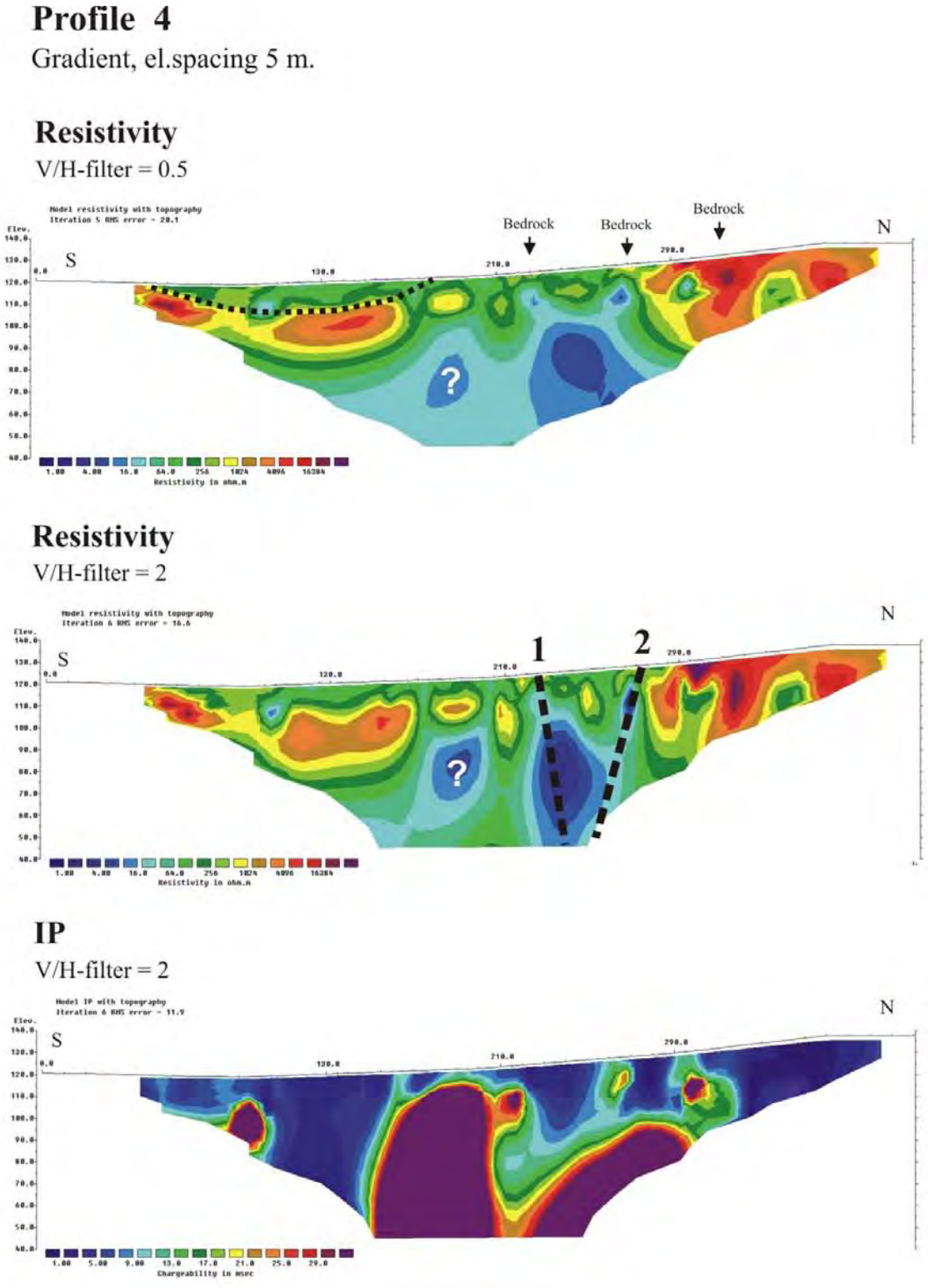

Figure 7. Profile 4, resistivity and IP with interpreted zones (fracture zones as thick dashed lines; soil cover limited at depth by a thin dashed line).

Map of resistivity anomalies along profiles 3 and 4

Figure 8 presents on the geological map the resistivity anomalies along profiles 3 and 4 which may be related to fracture zones. It includes the uncertainty of the anomaly interpretation and the dip angle of the anomaly.

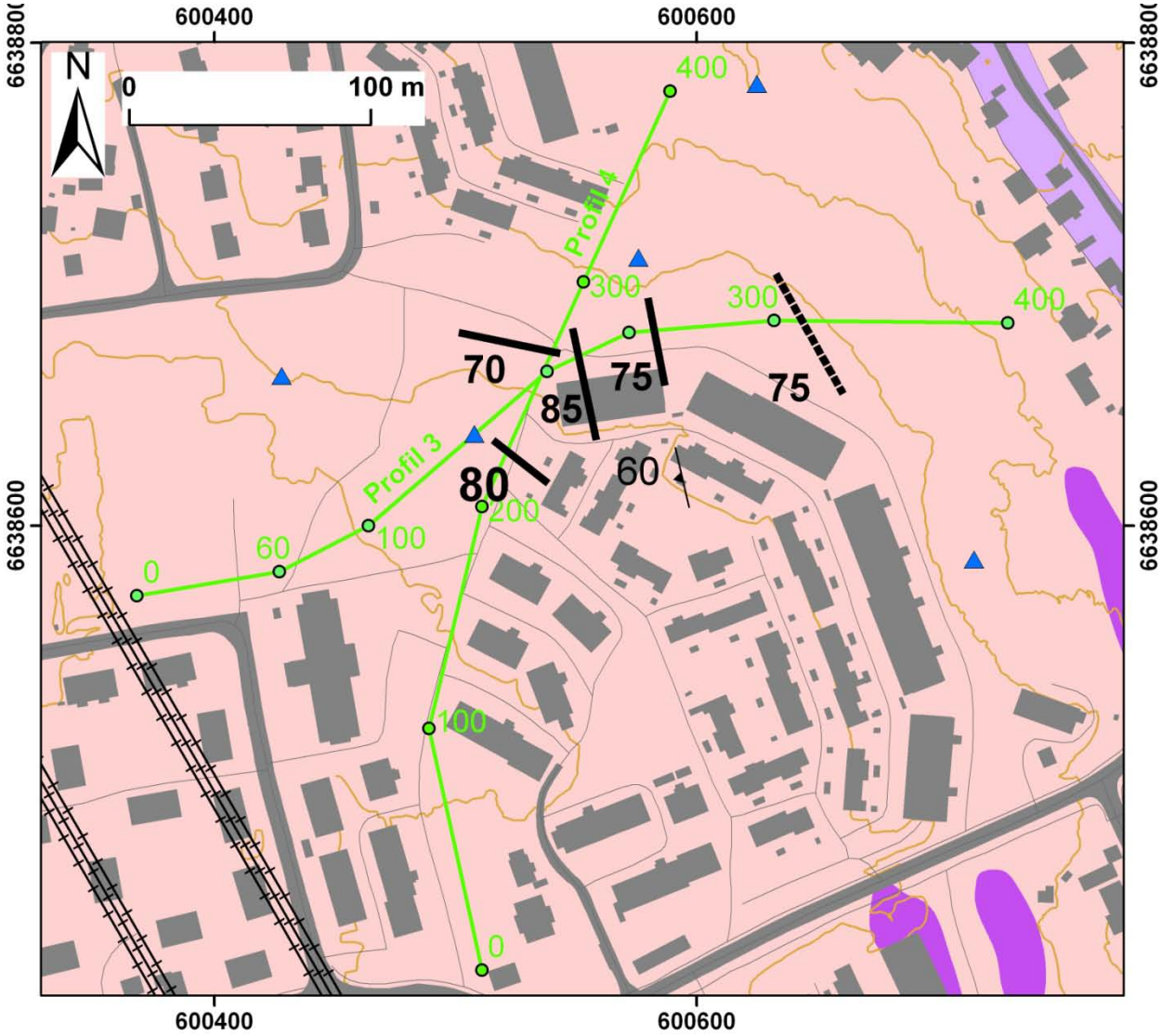

Figure 8. Map of resistivity anomalies along profiles 3 and 4 (legend as for Figure 5 and background as for Figure 1). (Approximate dip direction of the zone mapped by 2D resistivity method is indicated by which side of the line the angle of dip is written.)

4.2.3 2D resistivity profiles 5A and 5B

2D resistivity profiles 5A

Along profile 5A presented in Figure 9, no obvious soil cover is interpreted. This may relay on lack of resistivity contrast in case of sand/gravel above bedrock. One possible fracture zones is interpreted (for details see Table 3). High IP values may indicate that general low resistivity can be caused by technical installations or electronic conduction minerals. However, the indicated fracture zone may be real unless there is a good mineralisation.

Profile 5A

Gradient, el.spacing 5 m.

Resistivity

V/H-filter = 0.5

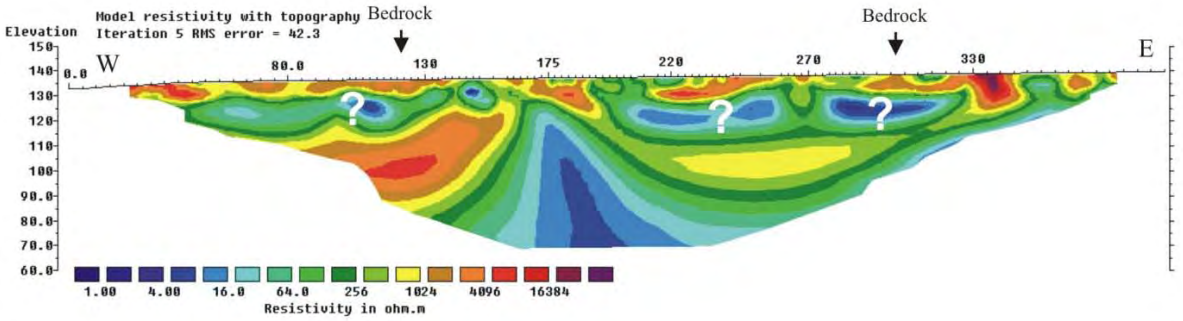

Resistivity

V/H-filter = 2

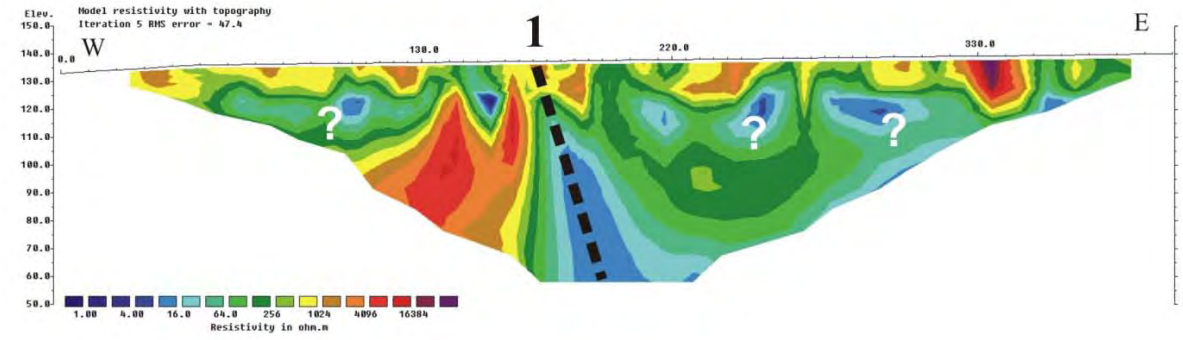

IP

V/H-filter = 2

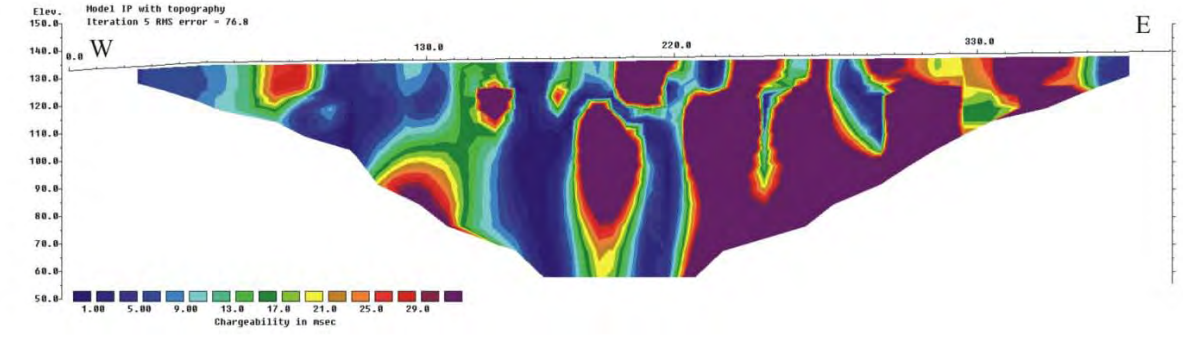

Figure 9. Profile 5A, resistivity and IP with interpreted zones (fracture zone as a thick dashed line).

2D resistivity profile 5B

Along profile 5B presented in Figure 10, no obvious soil cover is interpreted. This may relay on lack of resistivity contrast in case of sand/gravel above bedrock since a cover was drilled toward the eastern tip of the profile. Altogether 3 possible fracture zones are interpreted (for details see Table 3). High IP values may indicate that general low resistivity can be caused by technical installations. At this profile, the fracture zone interpretation is uncertain.

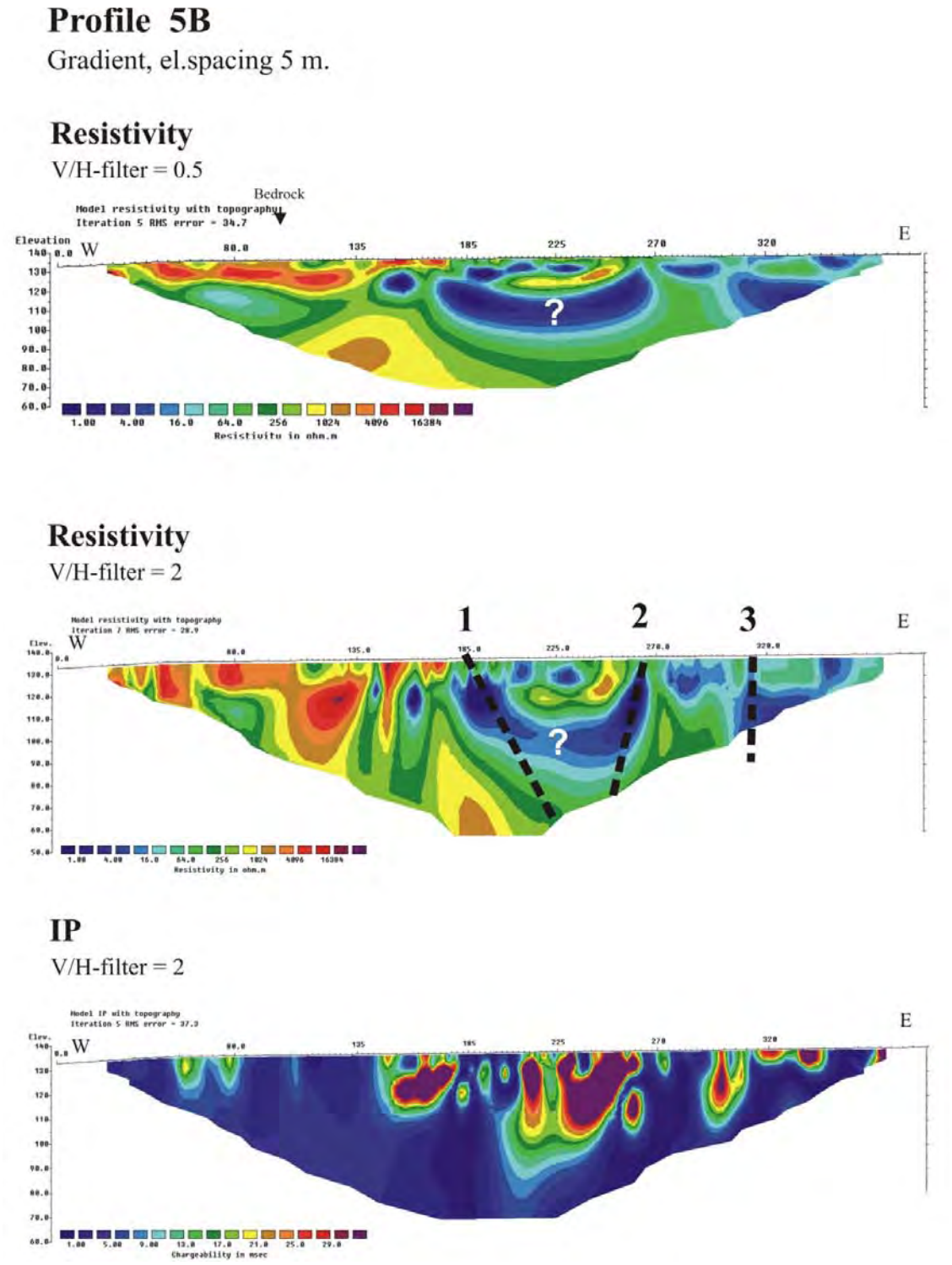

Figure 10. Profile 5B, resistivity and IP with interpreted zones (fracture zones as thick dashed lines).

Map of resistivity anomalies along profiles 5A and 5B

Figure 11 presents on the geological map the resistivity anomalies along profiles 5A and 5B which may be related to fracture zones. It includes the uncertainty of the anomaly interpretation and the dip angle of the anomaly.

Figure 11. Map of resistivity anomalies along profiles 5A and 5B (legend as for Figure 5 and background as for Figure 1). (Approximate dip direction of the zone mapped by 2D resistivity method is indicated by which side of the line the angle of dip is written.)

4.2.4 2D resistivity profiles 6 and 7

2D resistivity profile 6

Along profile 6 presented in Figure 12, a soil cover is interpreted between coordinate 40 and 130, with a maximum depth of ca. 10 m. This may continue for the entire profile, but there is no resistivity contrast to bedrock. Two possible fracture zones are interpreted (for details see Table 3). High IP values may indicate that general low resistivity can be caused by technical installations or electronic conducting minerals. At this profile, the fracture zone interpretation is uncertain, especially the dip interpretation.

2D resistivity profile 7

Along profile 7 presented in Figure 13, a soil cover is interpreted between coordinate 20 and 200, with a maximum depth of 10-15 m at coordinate 170. This may continue for the entire profile, but there is no resistivity contrast to bedrock. Two possible fracture zones are interpreted (for details see Table 3). High IP values may indicate that general low resistivity can be caused by technical installations or electronic conducting minerals. At this profile, the fracture zone interpretation is uncertain, especially the dip interpretation.

Profile 6

Gradient, el.spacing 5 m.

Resistivity

V/H-filter = 0.5

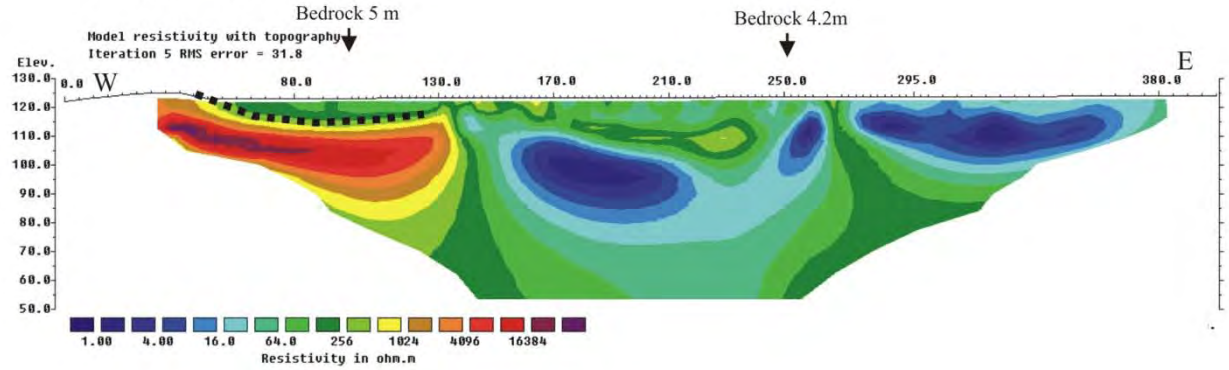

Resistivity

V/H-filter = 2

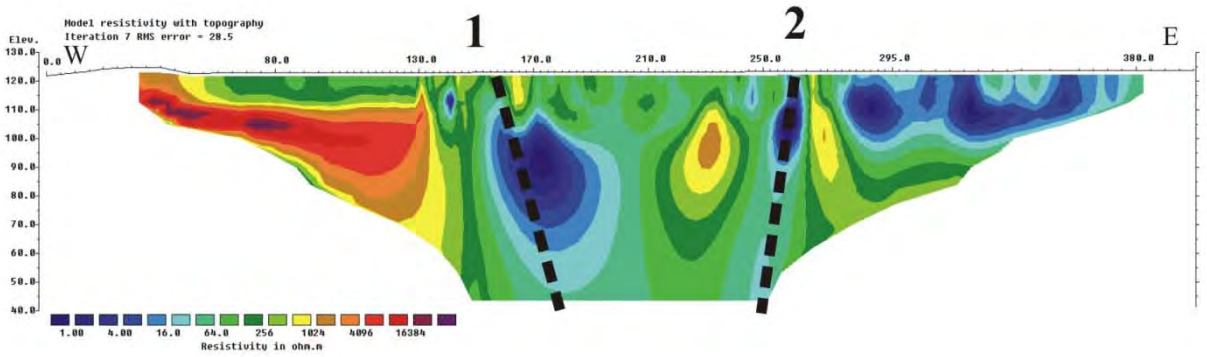

IP

V/H-filter = 2

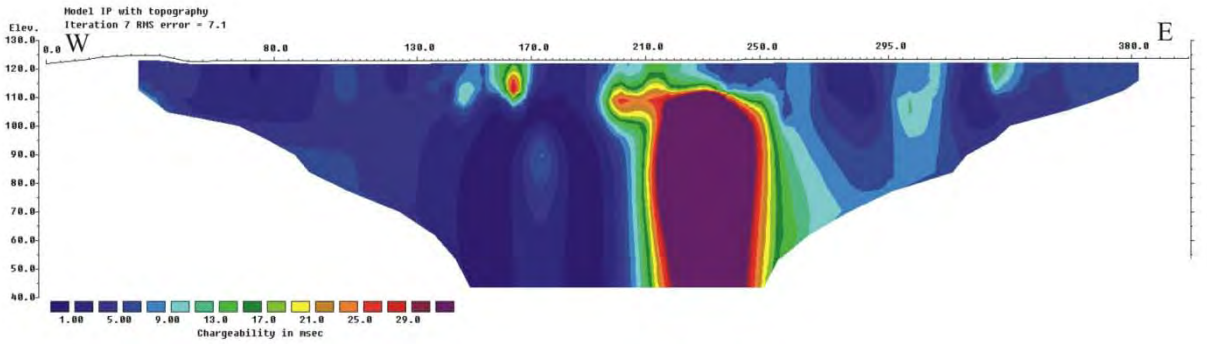

Figure 12. Profile 6, resistivity and IP with interpreted zones (fracture zones as thick dashed lines; soil cover limited at depth by a thin dashed line).

Profile 7

Gradient, el.spacing 5 m.

Resistivity

V/H-filter = 0.5

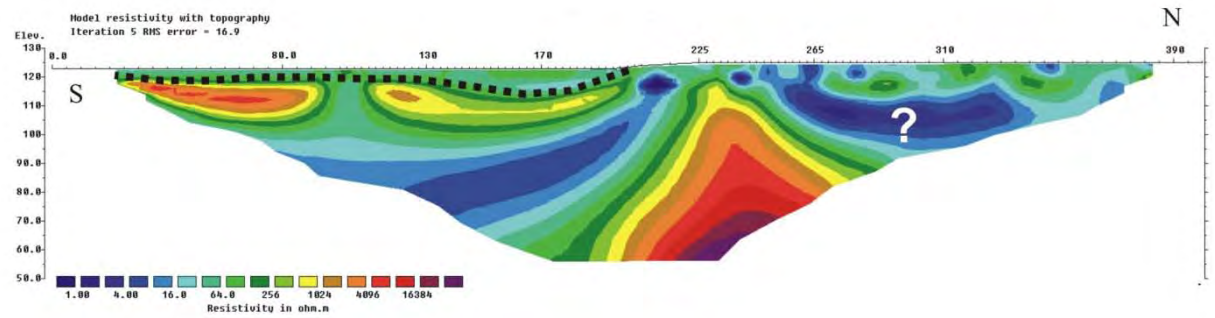

Resistivity

V/H-filter = 2

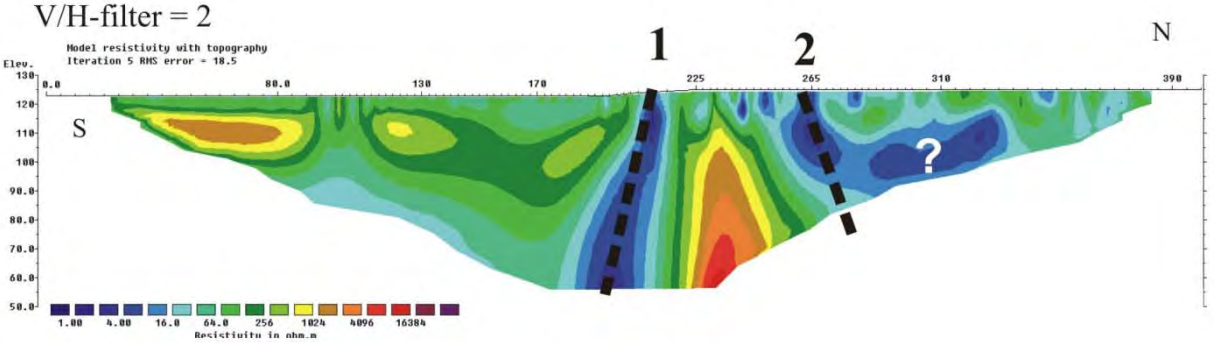

IP

V/H-filter = 2

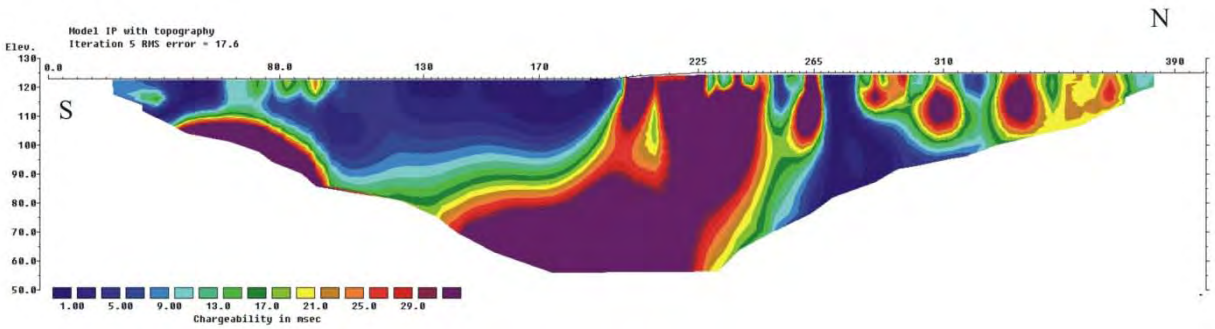

Figure 13. Profile 7, resistivity and IP with interpreted zones (fracture zones as thick dashed lines; soil cover limited at depth by a thin dashed line).

Map of resistivity anomalies along profiles 6 and 7

Figure 14 presents on the geological map the resistivity anomalies along profiles 6 and 7 which may be related to fracture zones. It includes the uncertainty of the anomaly interpretation and the dip angle of the anomaly.

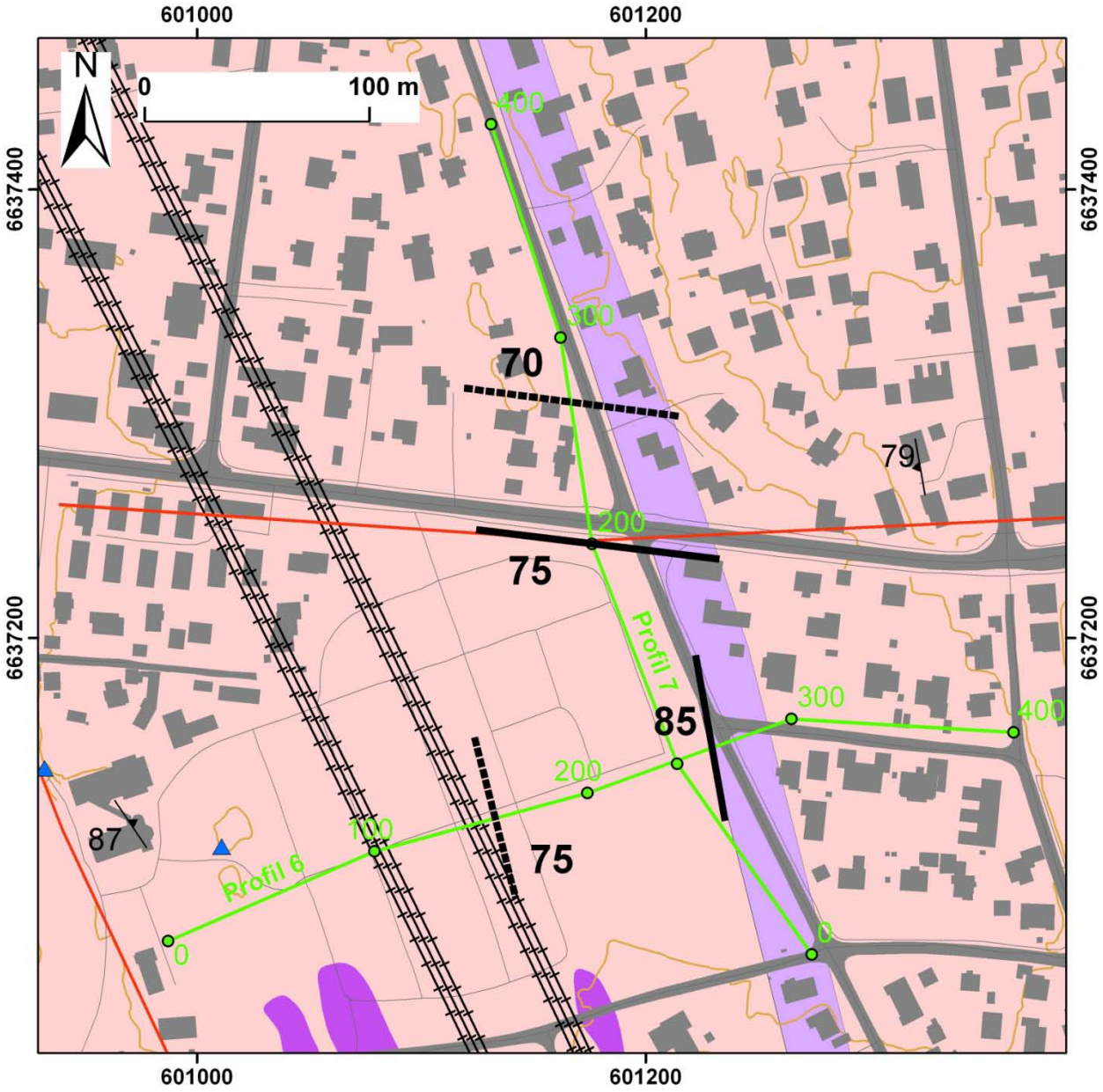

Figure 14. Map of resistivity anomalies along profiles 6 and 7 (legend as for Figure 5 and background as for Figure 1). (Approximate dip direction of the zone mapped by 2D resistivity method is indicated by which side of the line the angle of dip is written.)

4.2.5 2D resistivity profiles 8 and 9

2D resistivity profile 8

Along profile 8 presented in Figure 15, no soil cover is interpreted. Exposed bedrock is registered along almost the entire profile, despite of low resistivity in the shallow part of the profile. High IP values may indicate that general low resistivity can be caused by technical installations or electronic conducting minerals. Altogether 7 possible fracture zones are interpreted (for details see Table 3Table 3). However, these interpretations are uncertain.

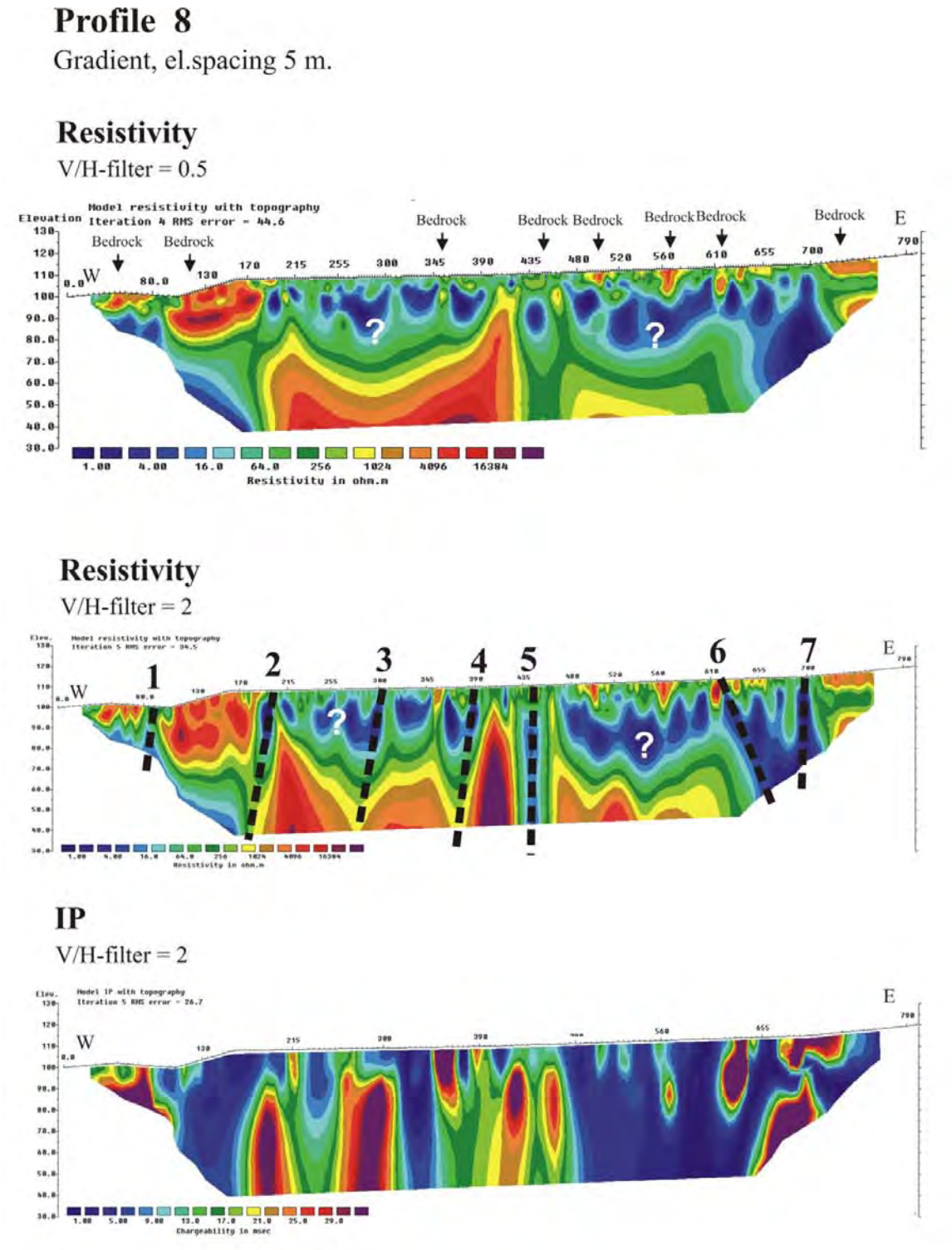

Figure 15. Profile 8, resistivity and IP with interpreted zones (fracture zones as thick dashed lines).

2D resistivity profile 9

The general resistivity along profile 9, presented in Figure 16, is higher than 4000 Ωm, which is expected in this geological environment. No IP effect indicates clean conditions saying that no artificial resistivity anomalies are present. No soil cover is indicated but this may relay on lack of resistivity contrast between possible dry sand above bedrock. Two fracture zones are indicated (for details see Table 3).

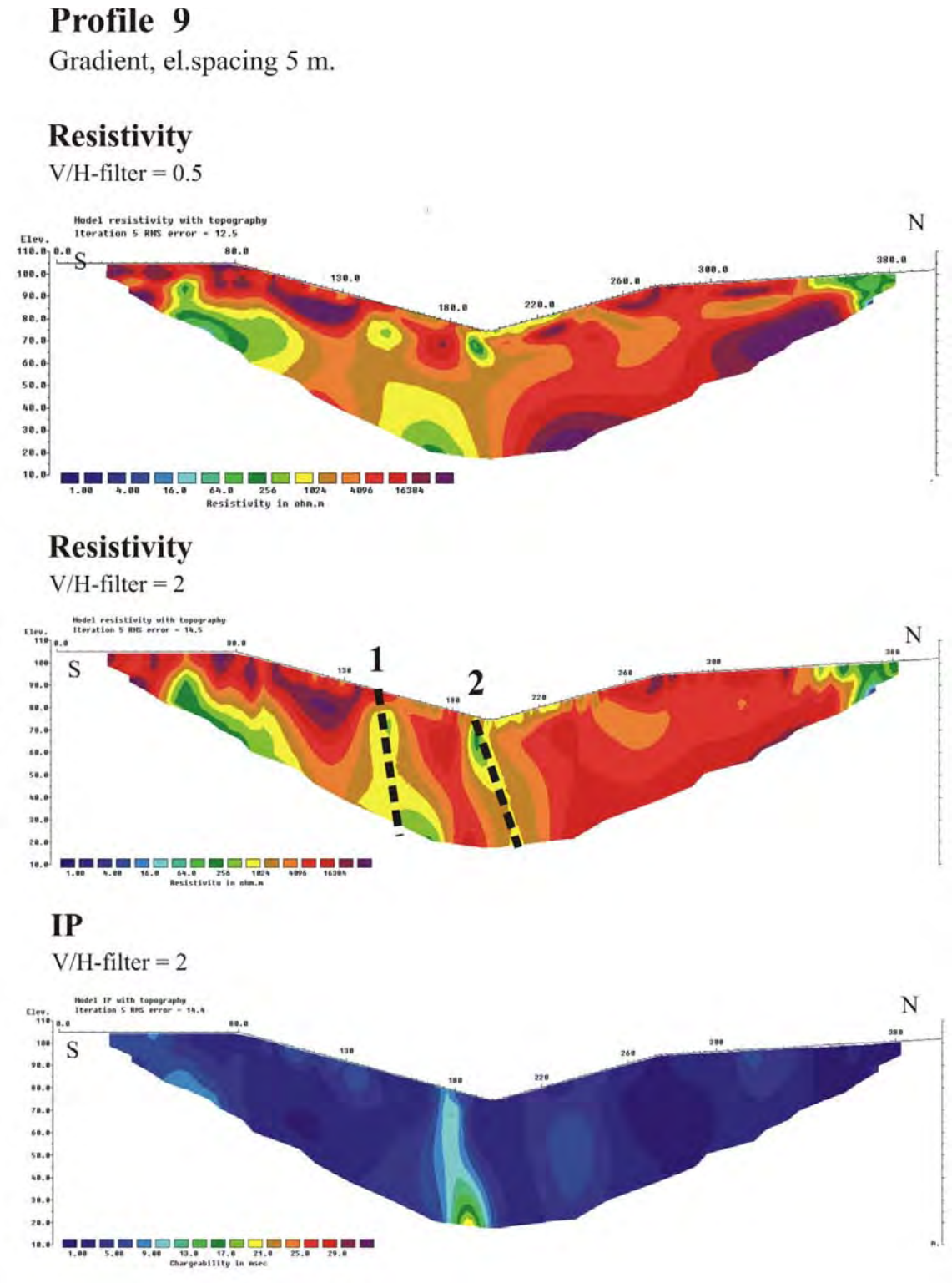

Figure 16. Profile 9, resistivity and IP with interpreted zones (fracture zones as thick dashed lines).

Map of resistivity anomalies along profiles 8 and 9

Figure 17 presents on the geological map the resistivity anomalies along profiles 8 and 9 which may be related to fracture zones. It includes the uncertainty of the anomaly interpretation and the dip angle of the anomaly.

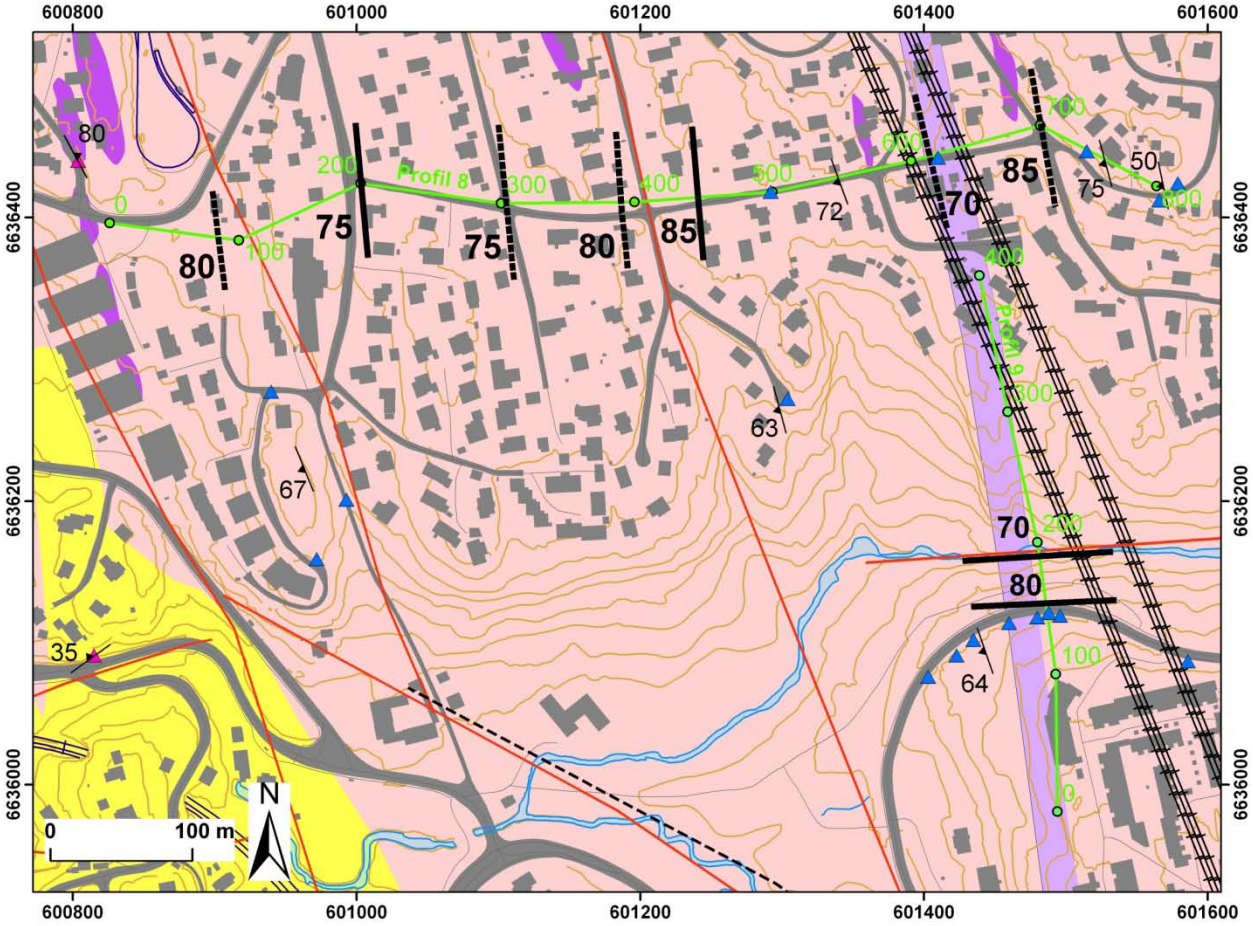

Figure 17. Map of resistivity anomalies along profiles 8 and 9 (legend as for Figure 5 and background as for Figure 1). (Approximate dip direction of the zone mapped by 2D resistivity method is indicated by which side of the line the angle of dip is written.)

4.2.6 2D resistivity profiles 10 and 10A

2D resistivity profile 10

The general resistivity along profile 10, presented in Figure 18, is higher than 4000 Ωm, which is expected in this geological environment. No IP effect indicates clean conditions saying that no artificial resistivity anomalies are present. Two small pockets of soil cover are indicated, with depths up to ca. 25 m. One weak fracture zone is indicated (for details, see Table 3).

Profile 10

Gradient, el.spacing 10 m.

Resistivity

V/H-filter = 0.5

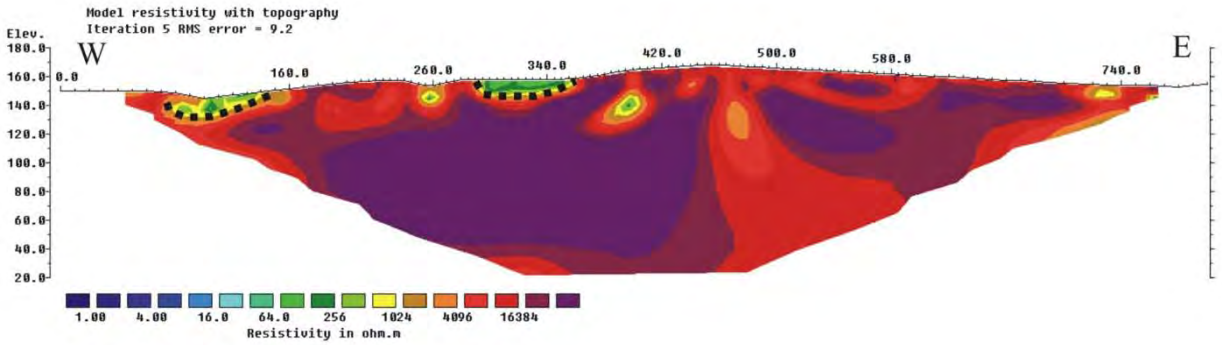

Resistivity

V/H-filter = 2

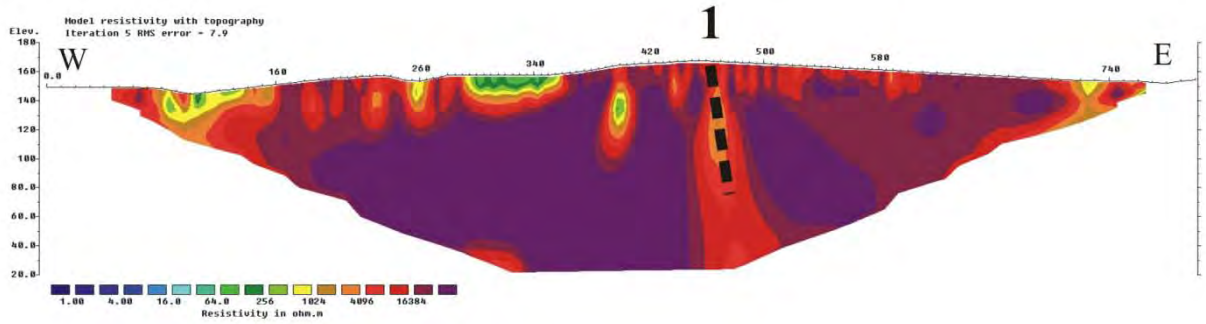

IP

V/H-filter = 2

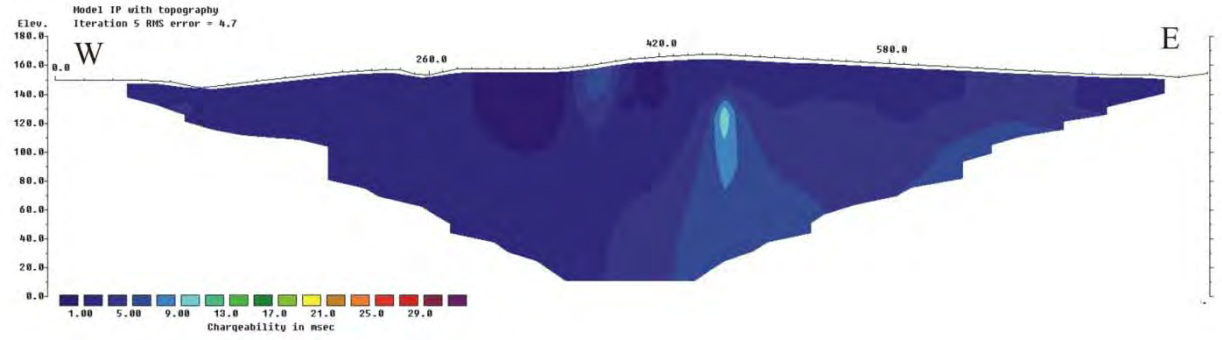

Figure 18. Profile 10, resistivity and IP with interpreted zones (fracture zone as a thick dashed line; soil cover limited at depth by a thin dashed line).

2D resistivity profile 10A

The general resistivity along profile 10A, presented in Figure 19, is higher than 4000 Ωm, which is expected in this geological environment. Low shallow resistivity in the central part of the profile indicates a soil cover, with depth up to ca. 15 m. Three fracture zones are indicated (for details see Table 3). High IP effect in the deeper part of zone 1 may indicate electronic conducting minerals or technical installations.

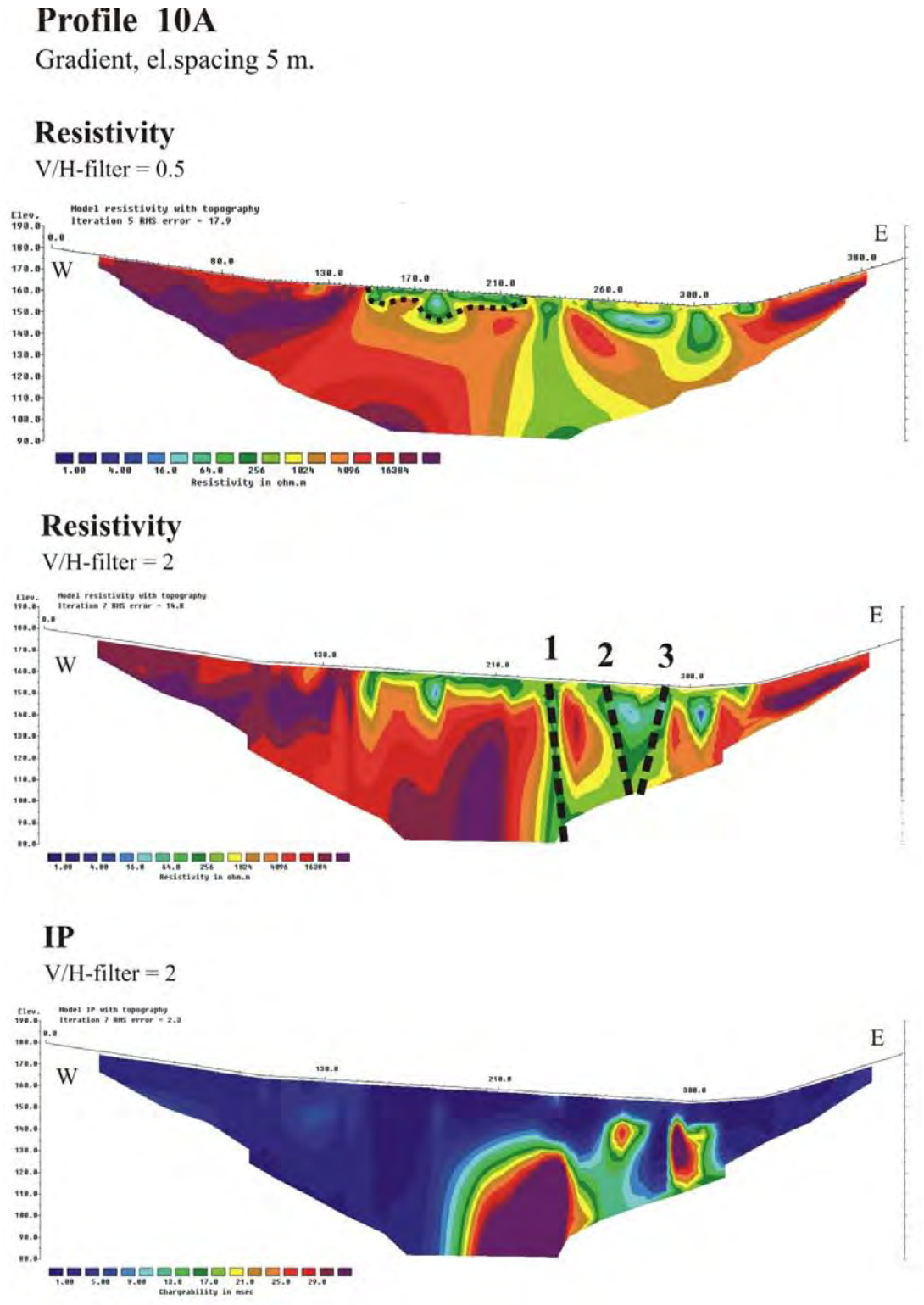

Figure 19. Profile 10A, resistivity and IP with interpreted zones (fracture zones as thick dashed lines; soil cover limited at depth by a thin dashed line).

Map of resistivity anomalies along profiles 10 and 10A

Figure 20 presents on the geological map the resistivity anomalies along profiles 10 and 10A which may be related to fracture zones. It includes the uncertainty of the anomaly interpretation and the dip angle of the anomaly.

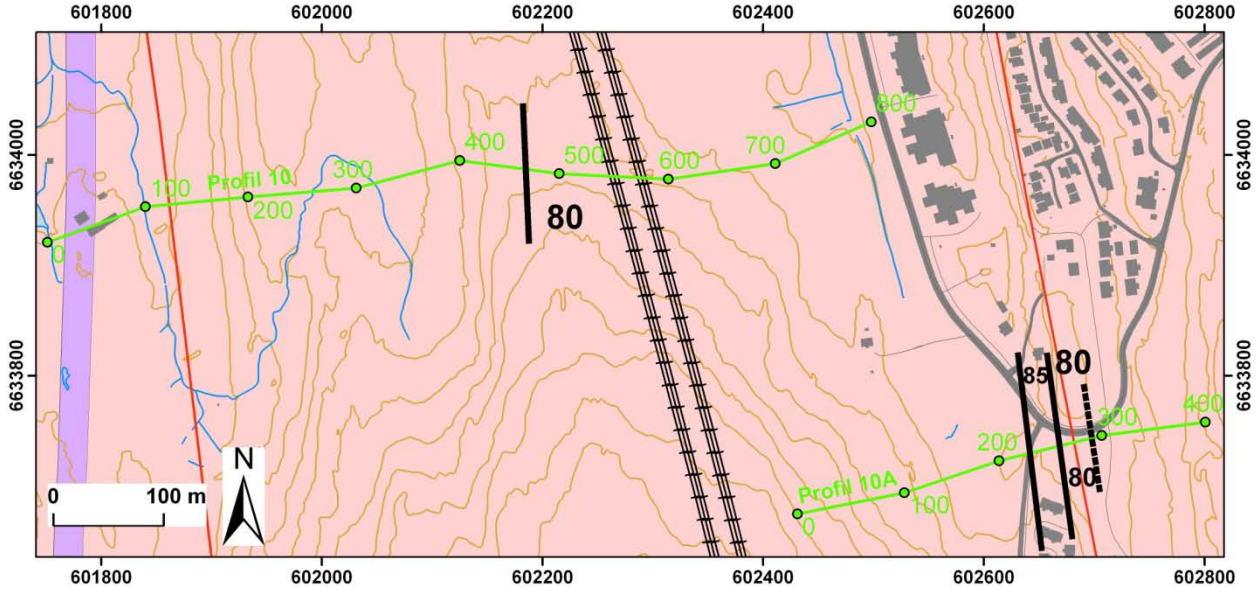

Figure 20. Map of resistivity anomalies along profiles 10 and 10A (legend as for Figure 5 and background as for Figure 1). (Approximate dip direction of the zone mapped by 2D resistivity method is indicated by which side of the line the angle of dip is written.)

4.2.7 2D resistivity profiles 11 and 12

2D resistivity profile 11

The general resistivity along profile 11, presented in Figure 21, is higher than 4000 Ωm, which is expected in this geological environment. No IP effect indicates clean conditions saying that no artificial resistivity anomalies are present. A soil cover is indicated between coordinates 210 and 360, with a maximum depth of ca. 15 m. Two fracture zones are indicated (for details see Table 3).

2D resistivity profile 12

The general resistivity along profile 12 presented in Figure 22 is higher than 4000 Ωm, which is expected in this geological environment. No IP effect in critical positions indicates clean conditions saying that no artificial resistivity anomalies are present. A soil cover is indicated in three pockets along the profile, with a maximum depth of ca. 20m. Two shallow fracture zones are indicated (for details see Table 3).

Profile 11

Gradient, el.spacing 5 m.

Resistivity

V/H-filter = 0.5

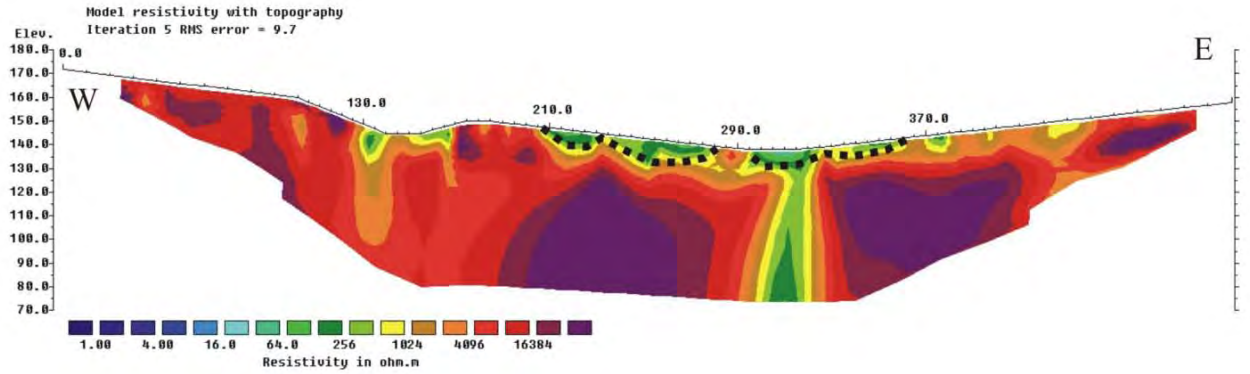

Resistivity

V/H-filter = 2

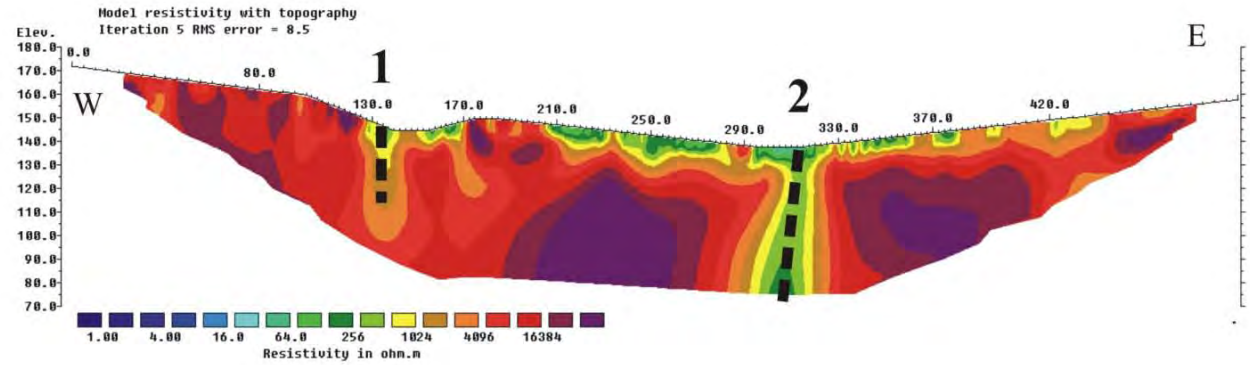

IP

V/H-filter = 2

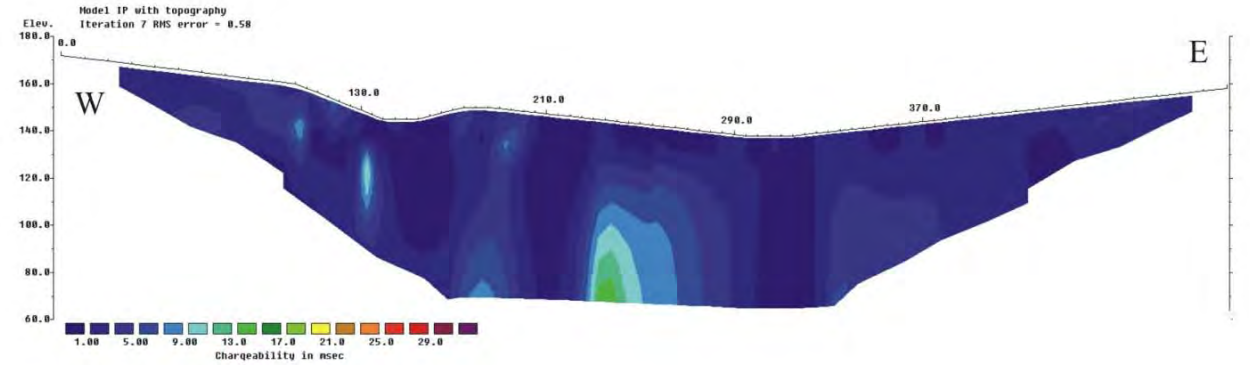

Figure 21. Profile 11, resistivity and IP with interpreted zones (fracture zones as thick dashed lines; soil cover limited at depth by a thin dashed line).

Profile 12

Gradient, el.spacing 10 m.

Resistivity

V/H-filter = 0.5

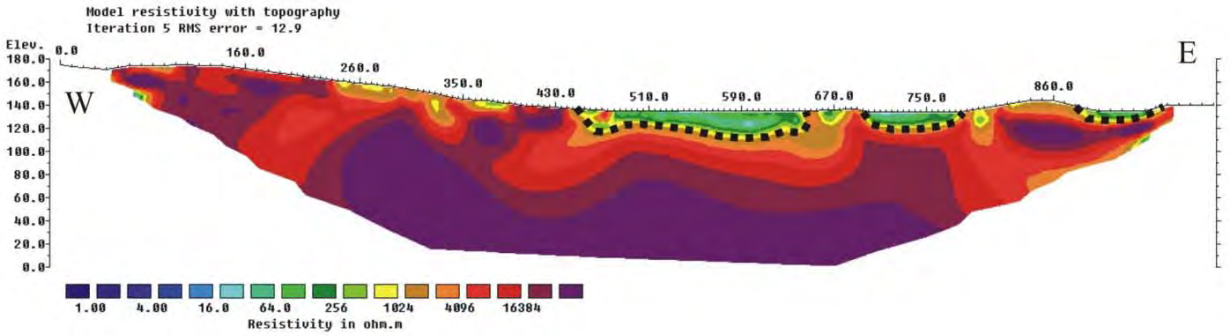

Resistivity

V/H-filter = 2

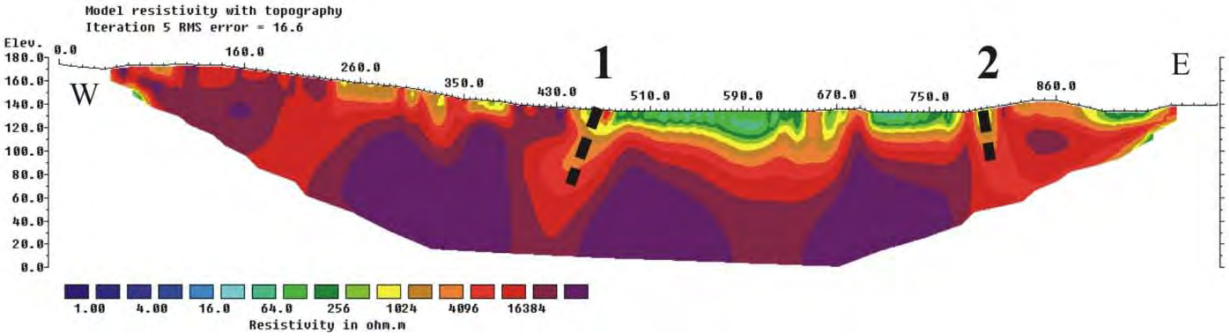

IP

V/H-filter = 2

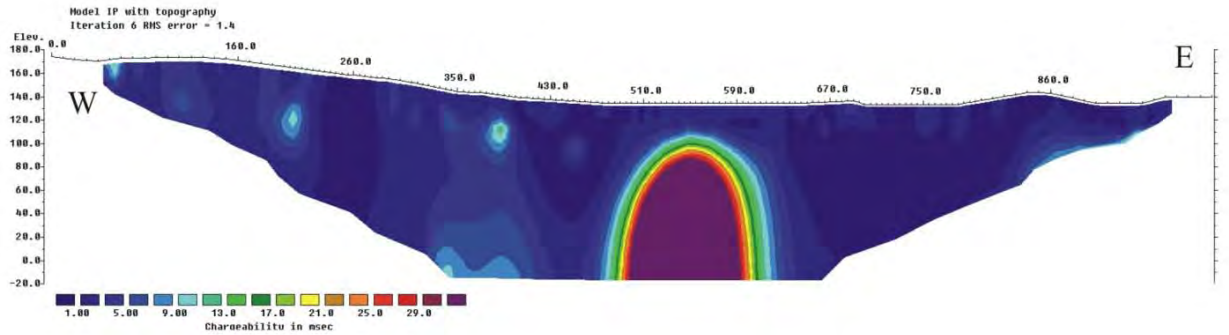

Figure 22. Profile 12, resistivity and IP with interpreted zones (fracture zones as thick dashed lines; soil cover limited at depth by a thin dashed line).

Map of resistivity anomalies along profiles 11 and 12

Figure 23 presents on the geological map the resistivity anomalies along profiles 11 and 12 which may be related to fracture zones. It includes the uncertainty of the anomaly interpretation and the dip angle of the anomaly.

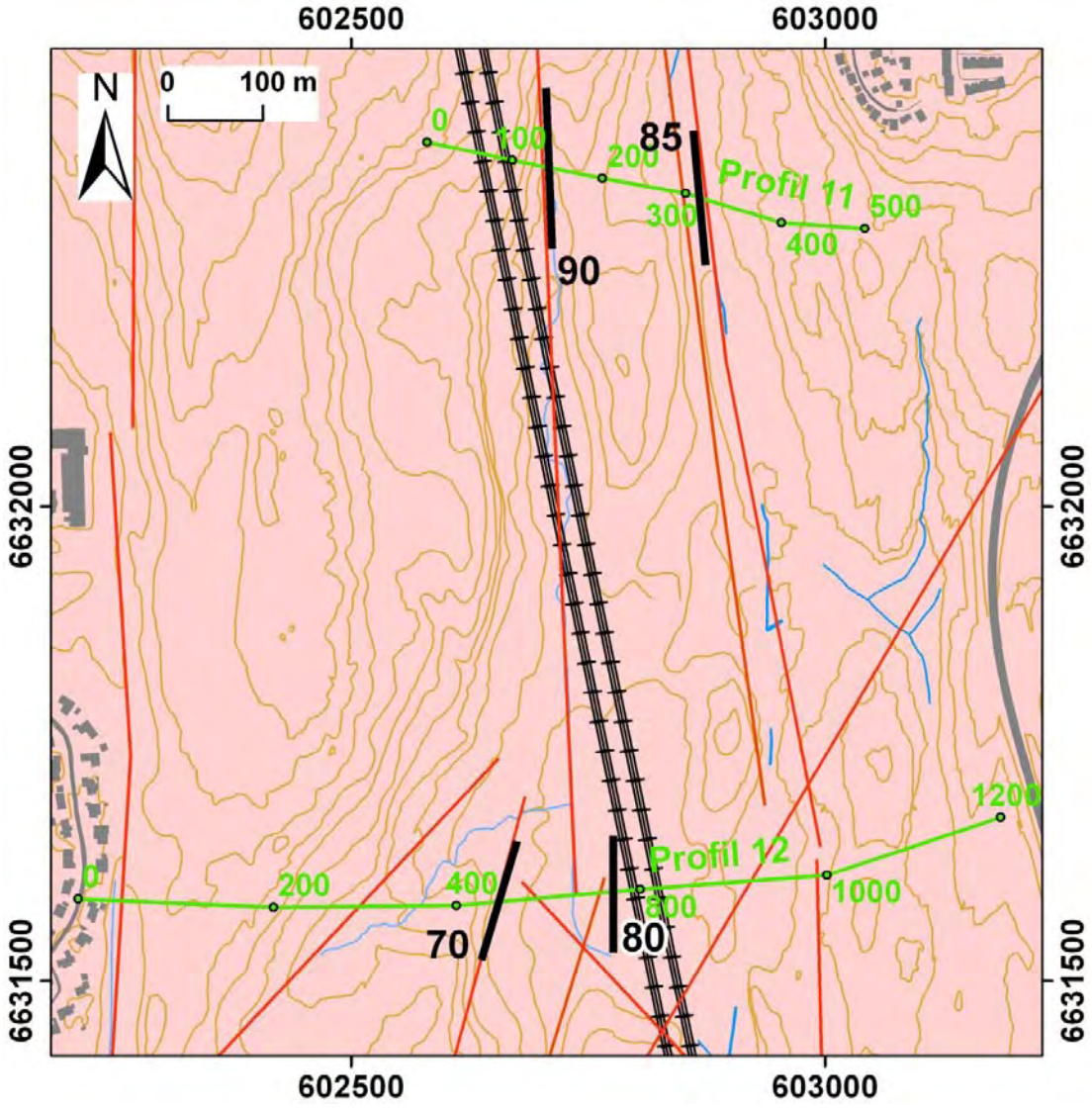

Figure 23. Map of resistivity anomalies along profiles 11 and 12 (legend as for Figure 5 and background as for Figure 1). (Approximate dip direction of the zone mapped by 2D resistivity method is indicated by which side of the line the angle of dip is written.)

4.2.8 2D resistivity profiles 13, 14 and 15

2D resistivity profile 13

The resistivity along profile 13, presented in Figure 24, is general higher than 4000 Ωm, which is expected in this geological environment. A reduced level in the central part of the profile may be caused by deep weathering. Two fracture zones are indicated (for details see Table 3). There is an IP effect in the deeper part of fracture № 2 which may indicate electronic conducting minerals or metallic water pipeline which is located here. A lack of resistivity contrast between possible dry sand above bedrock makes difficult to identify the soil cover. However, we interpret 3 zones with low resistivity at the sub-surface to correspond to a discontinuous soil cover, with depths up to ca. 25 m.

Profile 13

Gradient, el.spacing 5 m.

Resistivity

V/H-filter = 0.5

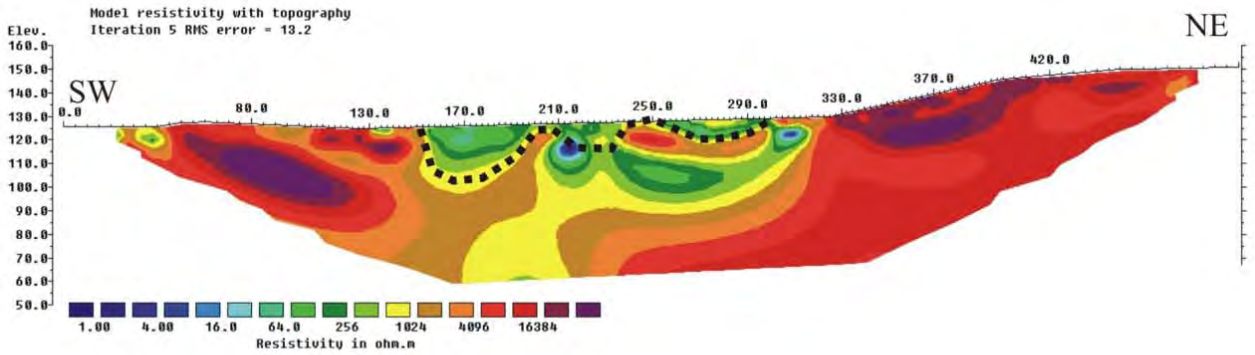

Resistivity

V/H-filter = 2

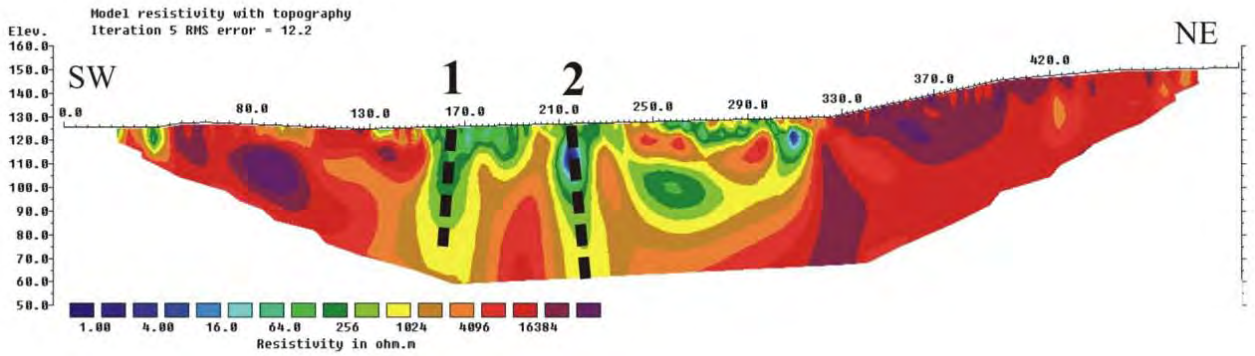

IP

V/H-filter = 2

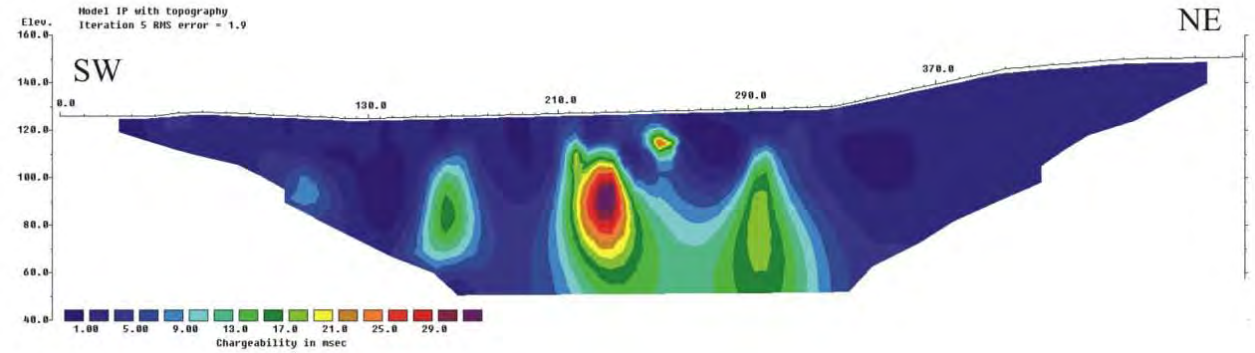

Figure 24. Profile 13, resistivity and IP with interpreted zones (fracture zones as thick dashed lines; soil cover limited at depth by a thin dashed line).

2D resistivity profile 14

The general resistivity along profile 14 presented in Figure 25 is higher than 4000 Ωm, which is expected in this geological environment. Special high resistivity values north of coordinate 230 may indicate another bedrock type. No IP effect indicates clean conditions saying that no artificial resistivity anomalies are present. A thin soil cover, less than 10 meters thick, is indicated between coordinates 80 and 350. One weak fracture zone is indicated (for details see Table 3).

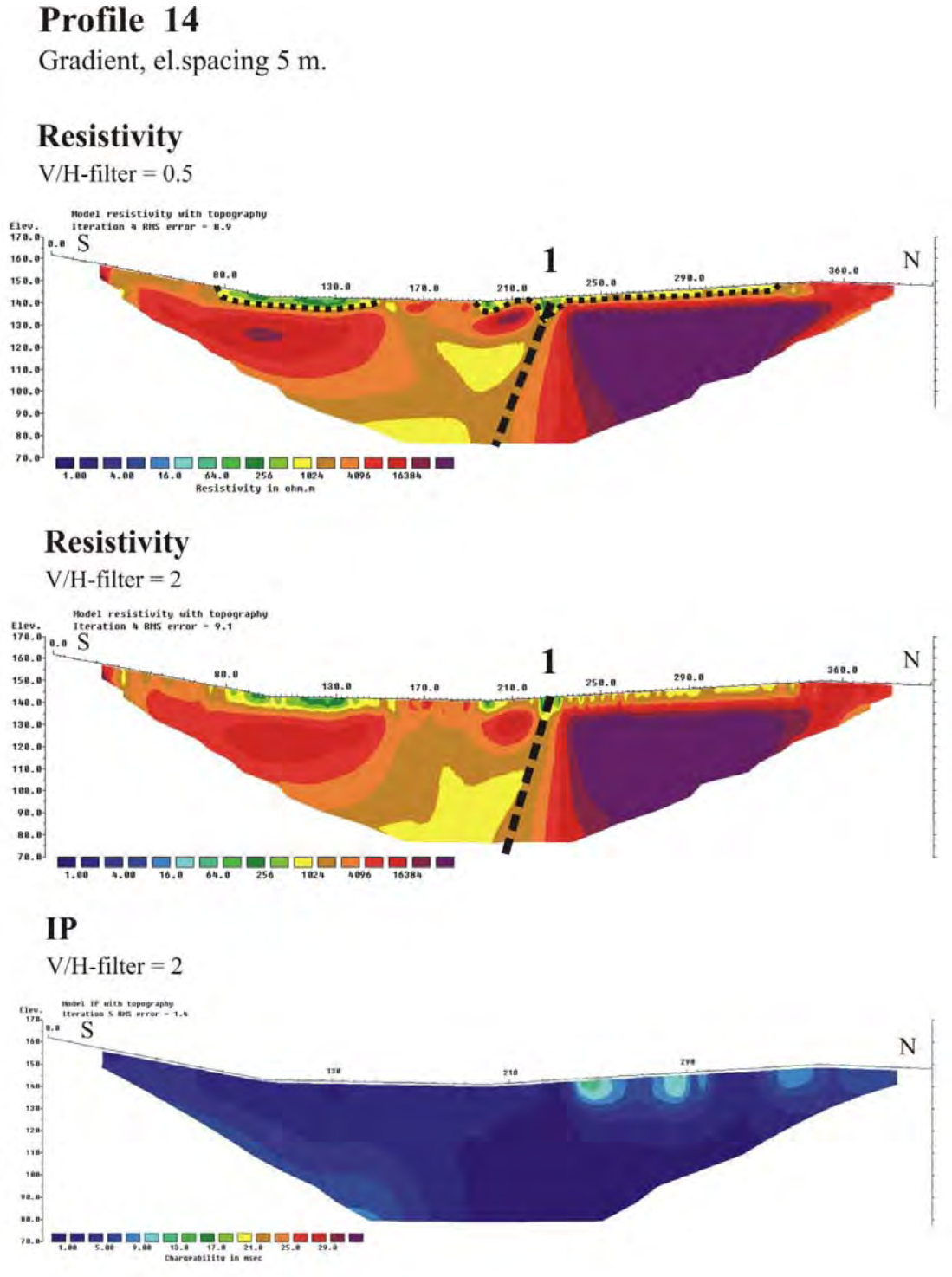

Figure 25. Profile 14, resistivity and IP with interpreted zones (fracture zone as a thick dashed line; soil cover limited at depth by a thin dashed line).

2D resistivity profile 15

The general resistivity along profile 15, presented in Figure 26, is higher than 4000 Ωm, which is expected in this geological environment. No soil cover is indicated but this may relay on lack of resistivity contrast between possible dry sand above bedrock. Two fracture zones are indicated (for details see Table 3). The low resistivity value between these zones at depth is an artefact. High IP values at depth may indicate electronic conducting minerals of technical installations. However, these do not seem to influence the resistivity level.

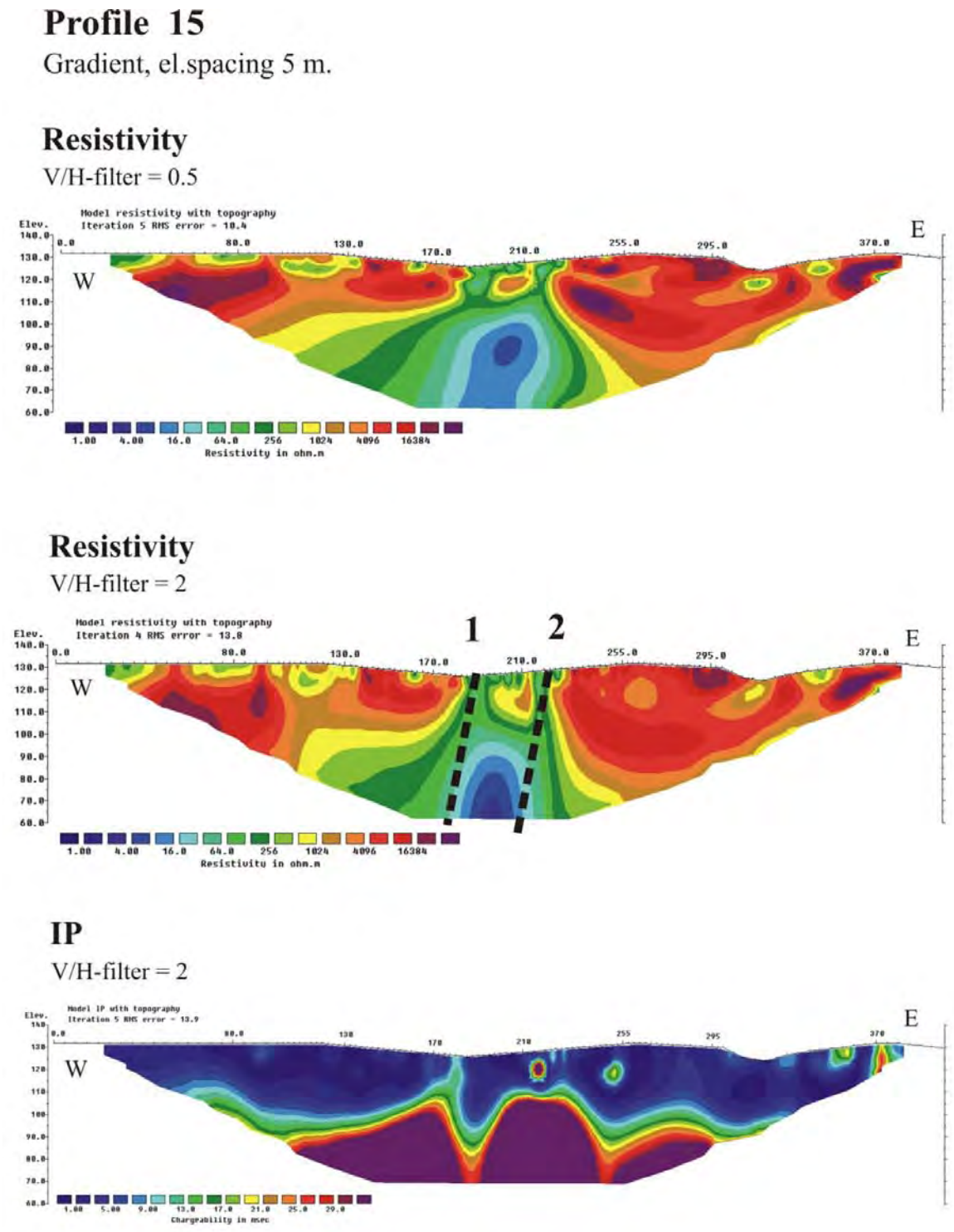

Figure 26. Profile 15, resistivity and IP with interpreted zones (fracture zones as thick dashed lines).

Map of resistivity anomalies along profiles 13, 14 and 15

Figure 27 presents on the geological map the resistivity anomalies along profiles 13, 14 and 15 which may be related to fracture zones. It includes the uncertainty of the anomaly interpretation and the dip angle of the anomaly.

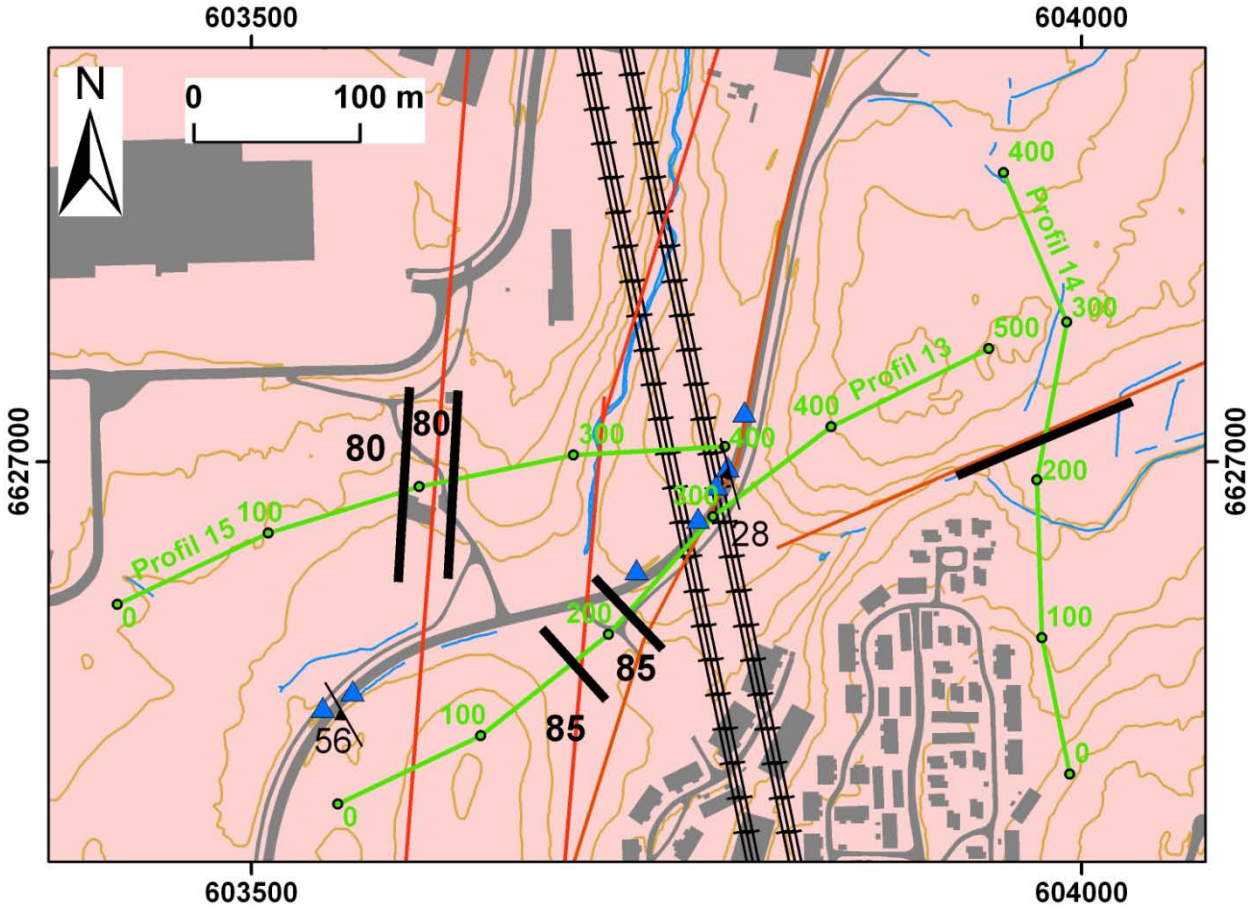

Figure 27. Map of resistivity anomalies along profiles 13, 14 and 15 (legend as for Figure 5 and background as for Figure 1). (Approximate dip direction of the zone mapped by 2D resistivity method is indicated by which side of the line the angle of dip is written.)

4.2.9 2D resistivity profiles 16, 17 and 18

2D resistivity profile 16

The general resistivity along profile 16, presented in Figure 28, is higher than 4000 Ωm, which is expected in this geological environment. In the central part of the profile, general low resistivity values may indicate deep weathering. There are registered high IP values in the same area. However, the patchy pattern cannot explain the low resistivity. Three fracture zones are indicated (for details, see Table 3). A soil cover is indicated in the central part of the profile, with a maximum depth of ca. 15 m.

Profile 16

Gradient, el.spacing 5 m.

Resistivity

V/H-filter = 0.5

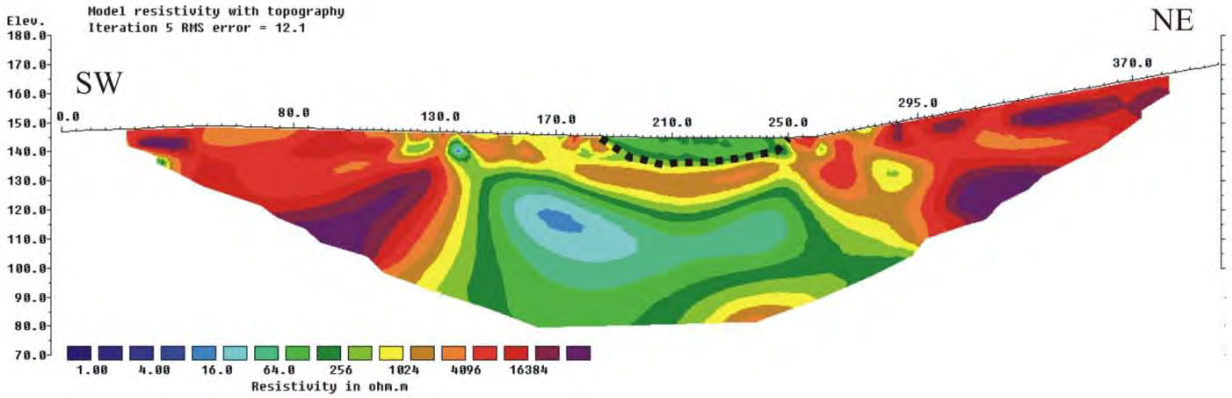

Resistivity

V/H-filter = 2

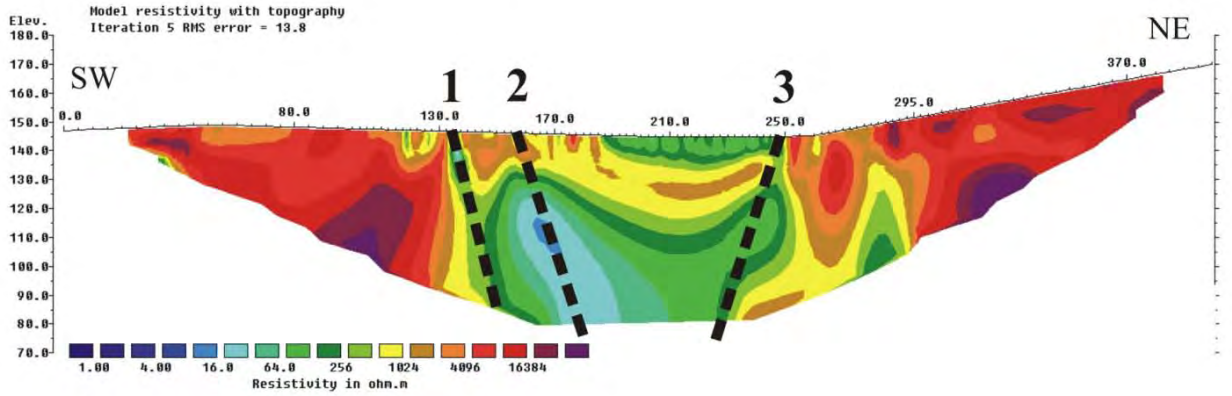

IP

V/H-filter = 2

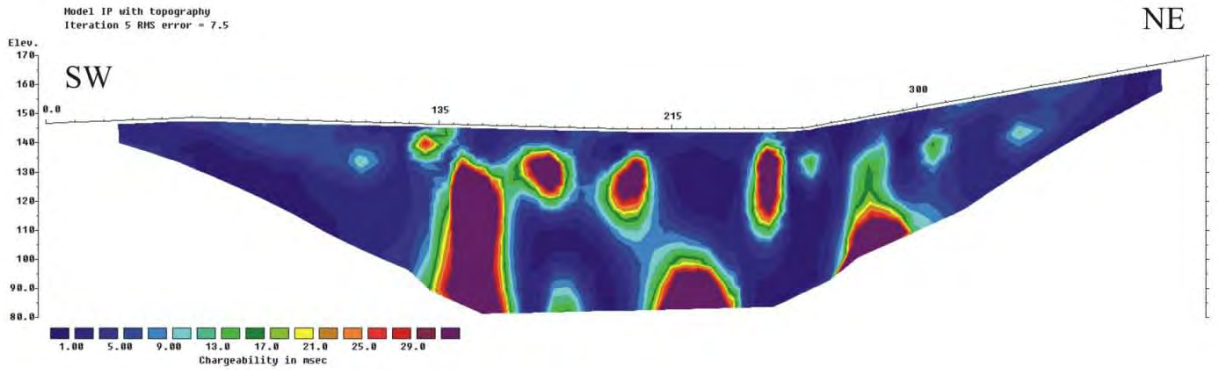

Figure 28. Profile 16, resistivity and IP with interpreted zones (fracture zones as thick dashed lines; soil cover limited at depth by a thin dashed line).

2D resistivity profile 17

The general resistivity along profile 17, presented in Figure 29, is higher than 4000 Ωm, which is expected in this geological environment. A soil cover is indicated from point 190 and eastwards, with a maximum depth of ca. 20 m. Soil thickness is interpreted partly based on observations from drilling (Gammelsæter, personal communication). Two weak fracture zones are indicated (for details see Table 3). High IP values at depth may indicate electronic conducting minerals of technical installations

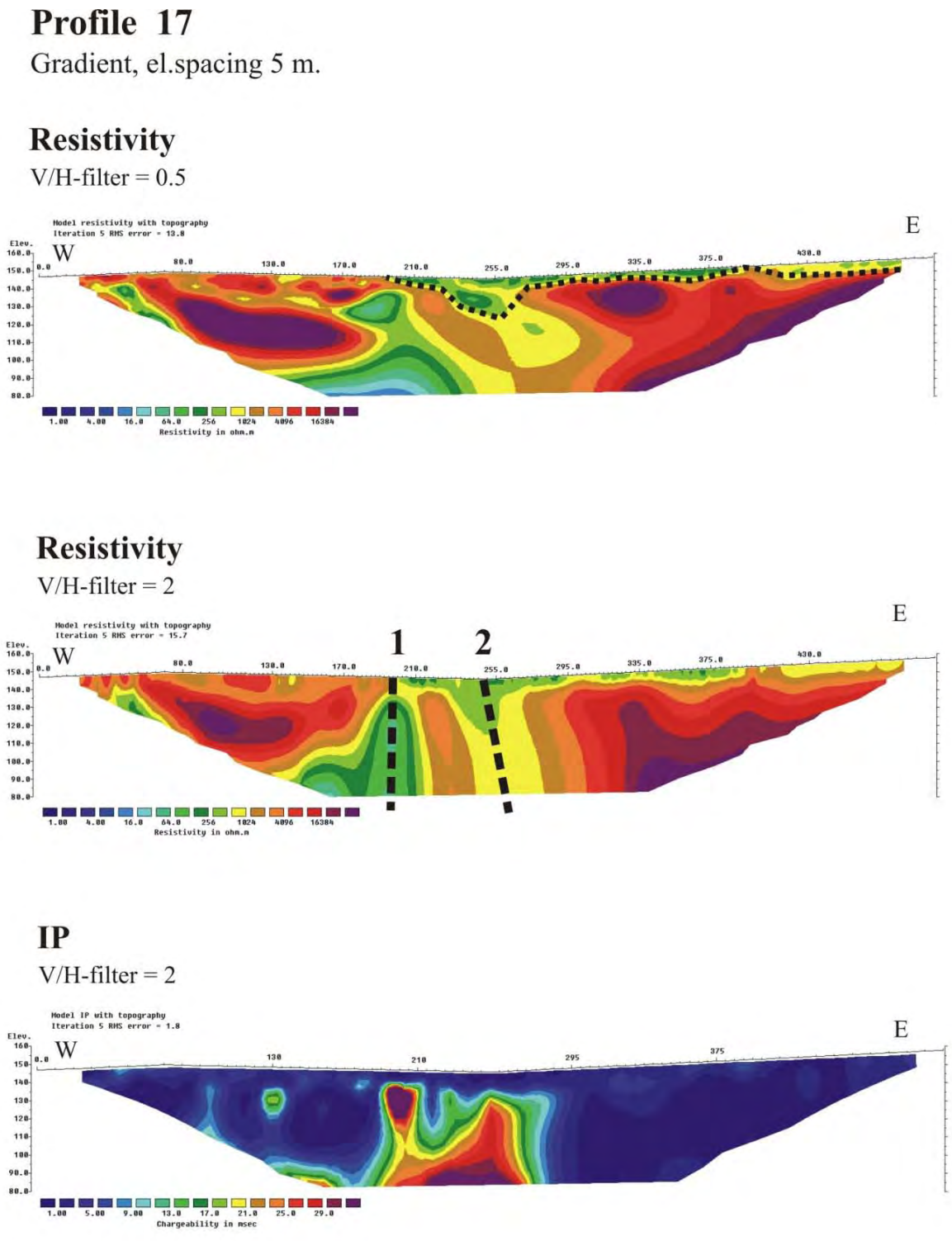

Figure 29. Profile 17, resistivity and IP with interpreted zones (fracture zones as thick dashed lines; soil cover limited at depth by a thin dashed line).

2D resistivity profile 18

The general resistivity along profile 18, presented in Figure 30, is higher than 4000 Ωm, which is expected in this geological environment. Two pockets of soil cover are indicated, with depths of ca. 15 m and the depth of the southern soil cover increases southward. One clear fracture zone is indicated (for details see Table 3). High IP values at depth do not influence on the fracture zone resistivity.

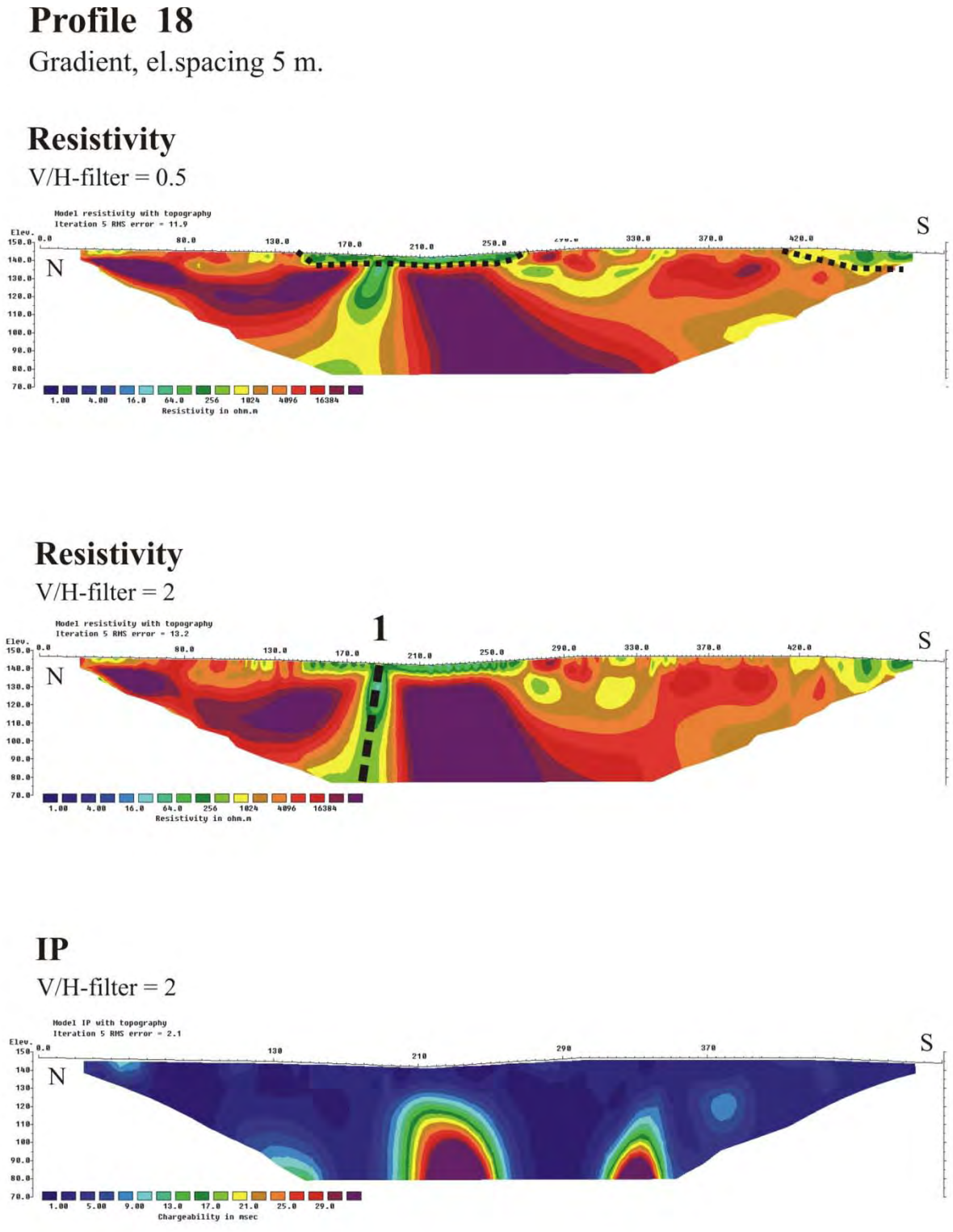

Figure 30. Profile 18, resistivity and IP with interpreted zones (fracture zone as a thick dashed line; soil cover limited at depth by a thin dashed line).

Map of resistivity anomalies along profiles 16, 17 and 18

Figure 31 presents on the geological map the resistivity anomalies along profiles 16, 17 and 18 which may be related to fracture zones. It includes the uncertainty of the anomaly interpretation and the dip angle of the anomaly.

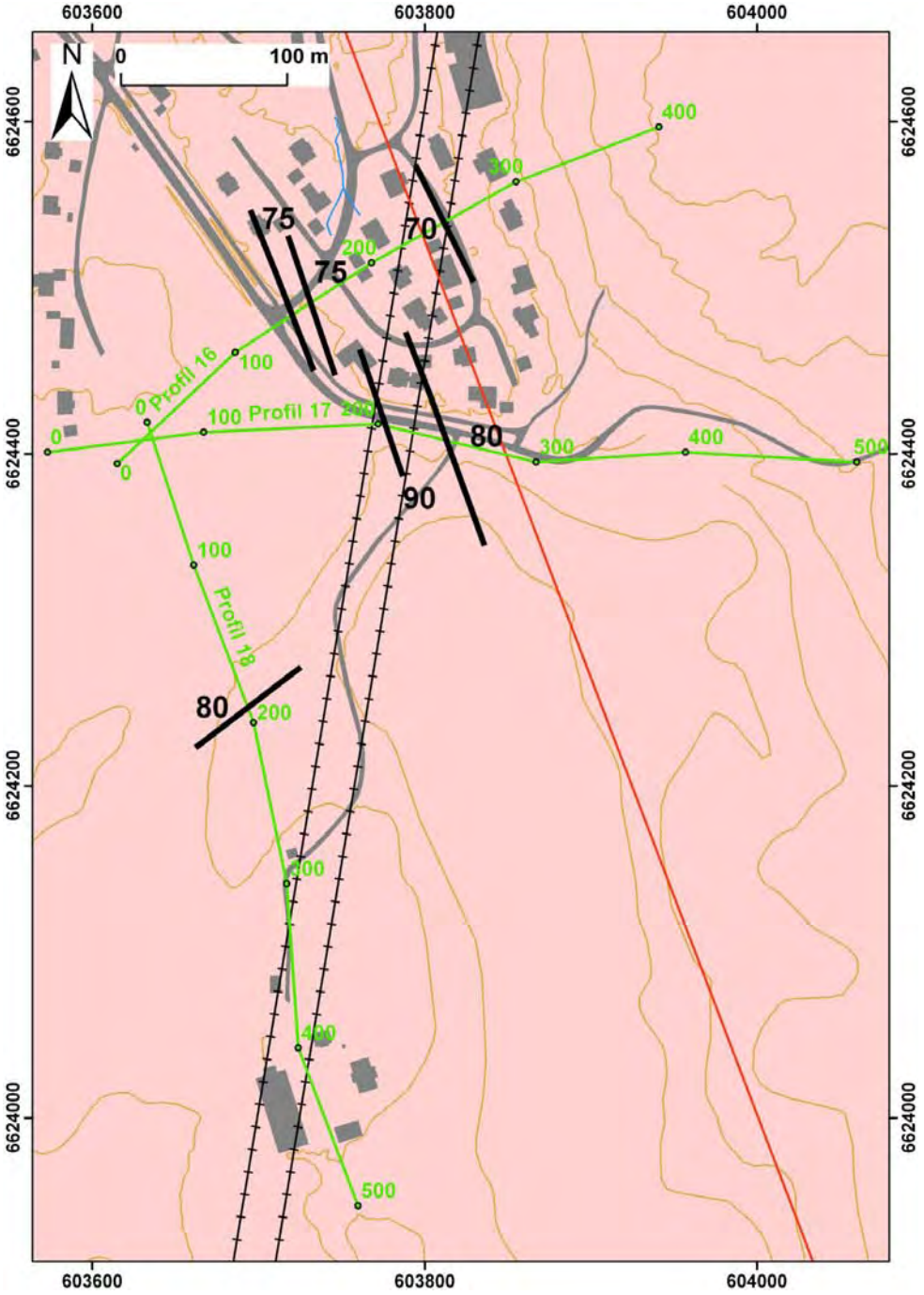

Figure 31. Map of resistivity anomalies along profiles 16, 17 and 18 (legend as for Figure 5 and background as for Figure 1). (Approximate dip direction of the zone mapped by 2D resistivity method is indicated by which side of the line the angle of dip is written.)

4.2.10 Summary of the anomalies detected along the 2D resistivity profiles in the Oslo-Ski planned railroad tunnel area.

Table 3 summarizes the main characteristics of the anomalies detected along the 2D resistivity profiles in the Oslo-Ski rail road planned tunnel area.

Coordinates along the profile	**Zone №**	**X** WGS 84, UTM 32	**Y** WGS 84, UTM 32	**Dip direction**	**Dip angle (c.^{o})**	**Depth extend of zone**	**Width of zone**	**Class of resistivity**	**Comments**
P 0 - 150	1	599303	6640223	SW	70	2	?		Uncertain interpretation due to noise both for the resistivity and IP measurements
P 0 - 205	2	599306	6640263	SW	70	2	?		Uncertain interpretation due to noise both for the resistivity and IP measurements
P 0 - 335	3	599338	6640391	NE	80	4	1		Uncertain interpretation due to noise both for the resistivity and IP measurements
P 0 - 550	4	599481	6640527		90	4	1	*3*	Due to noise in the profile the resistivity class is an uncertain interpretation.
P 0 - 620	5	599530	6640571		90	4	1	*3*	Due to noise in the profile the resistivity class is an uncertain interpretation.
P 0 - 750	6	599634	6640648		90	4	1	*3*	Due to noise in the profile the resistivity class is an uncertain interpretation.
P 0 - 920	7	599757	6640761	NE	75	4	?		Uncertain interpretation due to noise both for the resistivity and IP measurements
P 0 - 1210	8	599925	6640992	SW	80	2	2		Uncertain interpretation due to noise both for the resistivity and IP measurements
P 1 - 130	1	599479	6640090	NW	35	3	2	*2*	Due to noise in the profile the resistivity class is an uncertain interpretation.
P 1 - 215	2	599543	6640035	SE	65	4	2		Uncertain interpretation due to noise both for the resistivity and IP measurements
P 2 - 195	1	599910	6640011		90	4	?		Uncertain interpretation due to noise both for the resistivity and IP measurements
P 3 - 215	1	600551	6638670	W	85	4	1	*4*	Due to noise in the profile the resistivity class is an uncertain interpretation.
P 3 - 250	2	600582	6638680	W	75	4	1	*4*	Due to noise in the profile the resistivity class is an uncertain interpretation.
P 3 - 310	3	600643	6638684	W	80	4	1		Uncertain interpretation due to noise both for the resistivity and IP measurements

P 4 - 225	1	600521	6638630	N	80	4	2	*4*	Due to noise in the profile the resistivity class is an uncertain interpretation.
P 4 - 270	2	600539	6638671	S	70	4	1	*4*	Due to noise in the profile the resistivity class is an uncertain interpretation.
P 5A - 170	1	600775	6637789	E	70	4	1	*4*	Due to noise in the profile the resistivity class is an uncertain interpretation.
P 5B - 185	1	601119	6637816	E	60	4	?		Uncertain interpretation due to noise both for the resistivity and IP measurements
P 5B - 260	2	601191	6637842	W	70	3	?		Uncertain interpretation due to noise both for the resistivity and IP measurements
P 5B - 315	3	601241	6637862	W	75	3	1		Uncertain interpretation due to noise both for the resistivity and IP measurements
P 6 - 155	1	601131	6637119	E	75	4	?		Uncertain interpretation due to noise both for the resistivity and IP measurements
P 6 - 260	2	601230	6637151	W	85	4	1	*4*	Due to noise in the profile the resistivity class is an uncertain interpretation.
P 7 - 200	1	601175	6637242	S	75	4	1	*4*	Due to noise in the profile the resistivity class is an uncertain interpretation.
P 7 - 265	2	601166	6637305	N	70	3	?		Uncertain interpretation due to noise both for the resistivity and IP measurements
P 8 - 85	1	600902	6636385	W	80	2	1		Uncertain interpretation due to noise both for the resistivity and IP measurements
P 8 - 200	2	601002	6636424	W	75	4	1	*3*	Due to noise in the profile the resistivity class is an uncertain interpretation.
P 8 - 305	3	601106	6636410	W	75	3	?		Uncertain interpretation due to noise both for the resistivity and IP measurements
P 8 - 390	4	601185	6636410	W	80	4	1		Uncertain interpretation due to noise both for the resistivity and IP measurements
P 8 - 445	5	601240	6636414	W	85	4	2	*4*	Due to noise in the profile the resistivity class is an uncertain interpretation.
P 8 - 615	6	601404	6636443	E	70	4	1		Uncertain interpretation due to noise both for the resistivity and IP

									measurements
P 8 - 700	7	601482	6636465	W	85	4	1		Uncertain interpretation due to noise both for the resistivity and IP measurements
P 9 - 150	1	601486	6636128	N	80	4	1	2	
P 9 - 190	2	601481	6636161	N	70	4	1	2	
P 10 - 460	1	602184	6633987	E	80	2	1	0	
P 10A - 230	1	602642	6633729	E	85	4	1	3	
P 10A - 260	2	602668	6633736	E	80	3	?	3	
P 10A - 290	3	602697	6633743	W	80	3	?	3	Uncertain interpretation of zone
P 11 - 140	1	602708	6632357		90	2	1	1	
P 11 - 315	2	602867	6632325	W	85	4	1	2	
P 12 - 445	1	602655	6631582	W	70	2	2	0	
P 12 - 770	2	602775	6631593	E	80	2	2	0	
P 13 - 165	1	603688	6626875	SW	85	3	2	3	
P 13 - 215	2	603724	6626907	NE	85	4	1	3	
P 14 - 225	1	603975	6627014	S	75	4	2	1	
P 15 - 190	1	603591	6626982	W	80	4	2	3	
P 15 - 220	2	603620	6626989	W	80	4	2	3	
P 16 - 135	1	603714	6624480	NE	75	4	1	3	
P 16 - 150	2	603727	6624488	NE	75	4	3	3	
P 16 - 250	3	603811	6624539	SW	70	4	?	3	
P 17 - 205	1	603776	6624417		90	4	3	3	
P 17 - 245	2	603815	6624407	E	80	4	3	1	
P 18 - 190	1	603693	6624247	N	80	4	2	3	

Table 3. Classification of zones along the profiles. Classes for depth extent, width and resistivity are described in **Table 1**.

5. STRUCTURAL GEOLOGY

Localities for fieldwork were selected as close as possible to the 2D resistivity profiles, with the aim to characterize the nature of the resistivity anomalies encountered along the profiles. The profiles selected for detailed structural mapping on the surface was made according to the degree of geological knowledge of the area surrounding the profiles, i.e. to the degree of difficulty to interpret the resistivity anomalies. The task of the fieldwork was therefore to get an overview of the main structural grain of the various selected areas. The analyzed structures consist of faults, joints, dykes and metamorphic foliation. The data and results are presented by areas surrounding a group of profiles or a single profile. The structural data are displayed on stereonets and rose diagrams.

5.1 Keys to read stereonet

In following sub-sections, detailed analyses of fractures are given with representation of planes on stereonets (southern hemisphere, Schmidt's projection) with the convention below (Figure 32 and Figure 33).

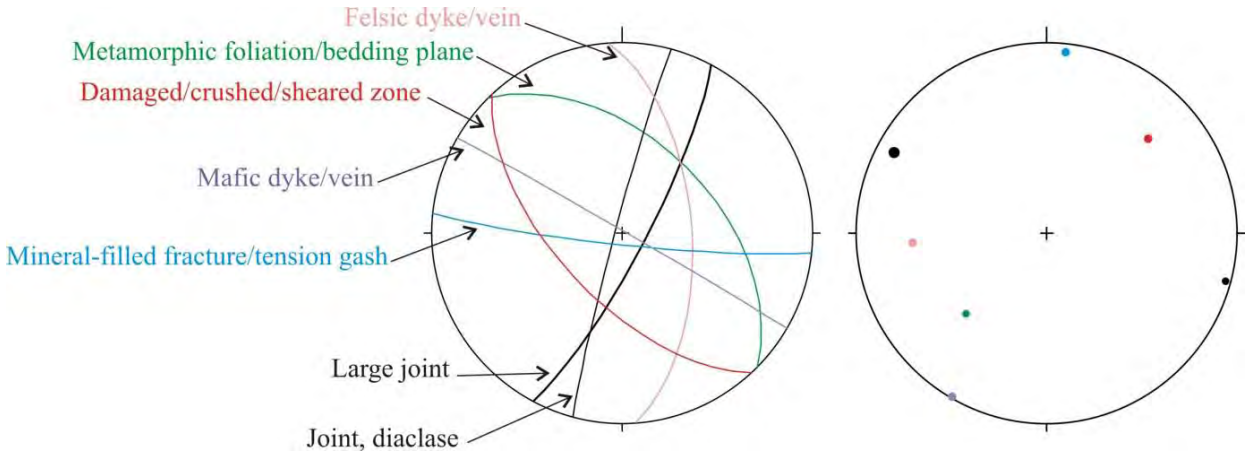

Figure 32. Example of stereonet for planar structures, Schmidt's projection, lower hemisphere (left, stereonet of planes; right, stereonet of poles of planes).

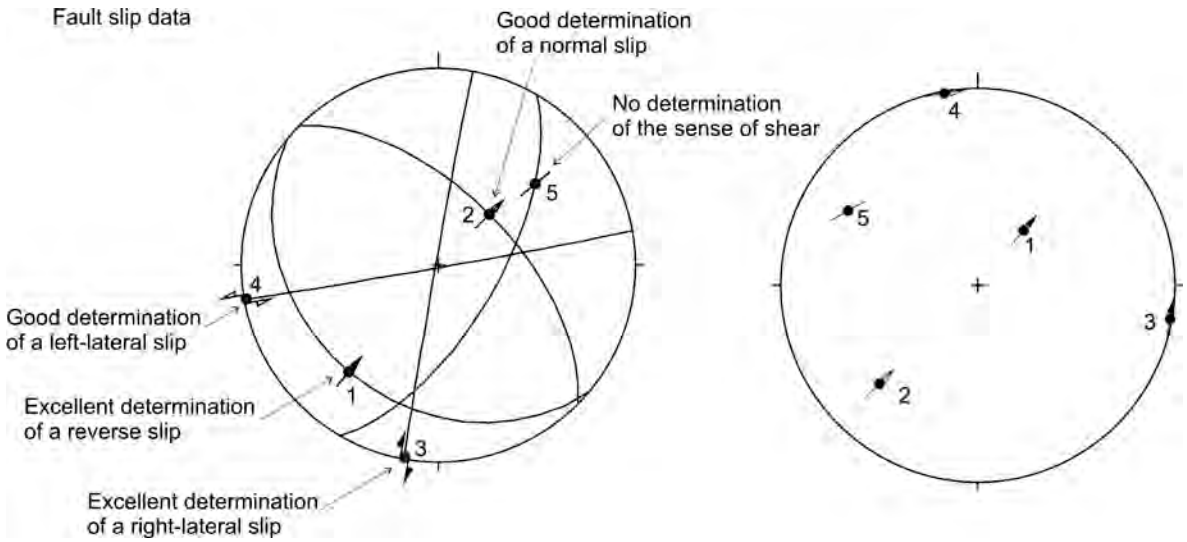

Figure 33. Example of stereonets for fault slip data, Schmidt's projection, lower hemisphere (left, stereonet of fault planes; right, stereonet of poles of fault planes). Keys for striae: An arrow indicates the sense of movement of the hanging wall block; inward directed arrow: reverse stria (number 1 on stereonet); outward directed arrow: normal stria (number 2); couple of arrows: strike-slip stria (numbers 3 and 4); full black arrow: excellent constrains on the sense of shear (numbers 1 and 3); empty arrow: good constrains on the sense of shear (numbers 2 and 4); thin line: no determination of the sense of shear (number 5).

5.2 Structural analysis around resistivity profiles 0-2

Twelve field localities with outcrops of variable size were visited in order to carry on the structural analysis needed in the vicinity of the 2D resistivity profiles 0, 1 and 2 (Figure 34). All measurements and field observations are listed in Appendix 2.

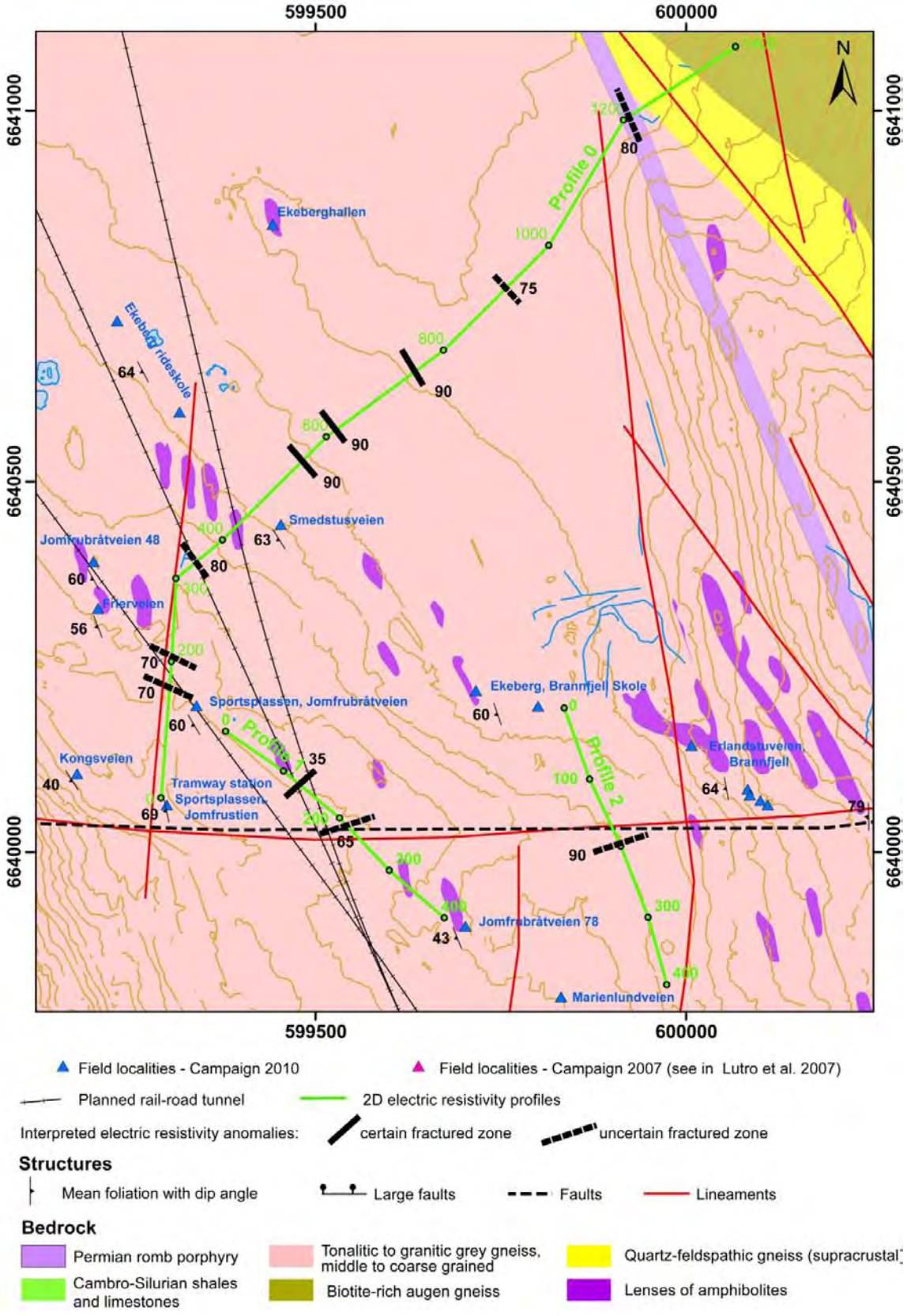

Figure 34. Field localities for structural analysis in the surrounding area of resistivity profiles 0, 1 and 2.

5.2.1 Field localities ”Ekeberghallen”, ”Ekeberg Rideskole” and ”Smedstusveien”

Three field localities are described in detail in this section to attempt to determine the causes of 2 of the resistivity anomalies observed along the profile 0 (Figure 35).

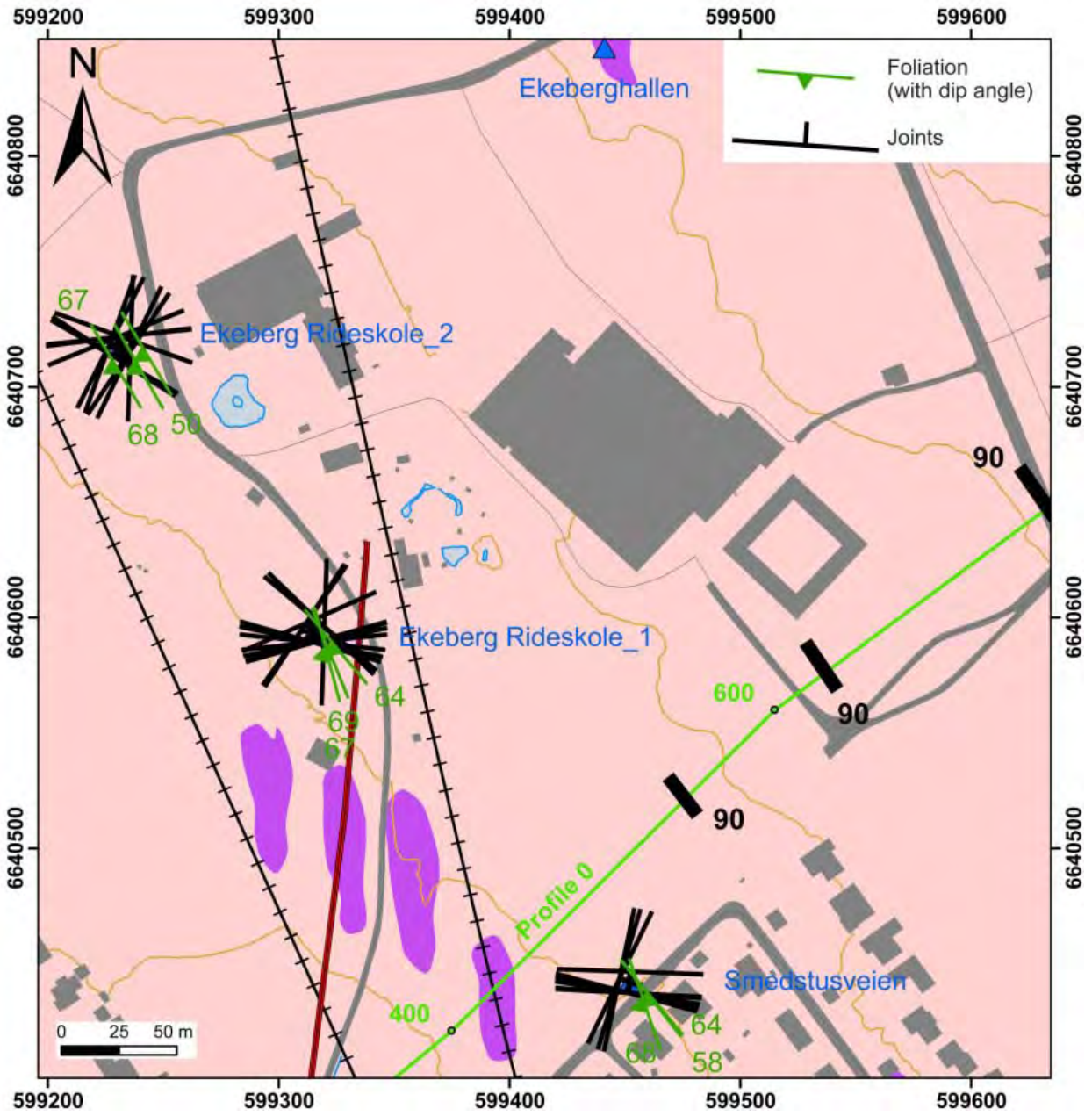

Figure 35. Structural field measurements at localities close to resistivity profile 0 (caption of background map as Figure 34 and of interpreted resistivity anomalies as Figure 5).

Field locality “Ekeberghallen”

The field locality “Ekeberghallen” is nearly in line with anomalies displayed by 2D resistivity profile 0 (Figure 35). However, the outcrop is a flat smoothed rock surface, also very limited in size, and structural measurements were not possible to handle. The only observation is the presence of WSW-ENE 40 cm wide and E-W 10 cm wide pegmatite veins in the host amphibolitic rocks.

Field locality "Ekeberg Rideskole"

At the field locality "Ekeberg Rideskole" the outcrops are widespread flat surfaces on the ground. This locality is close to resistivity profile 0 (Figure 35). A high dispersion of joints is observed. However, the two main trends commonly displayed at the regional scale are present and correspond to the steep WSW-ENE and WNW-ESE orientated sets (Figure 35 and Figure 36). The metamorphic foliation has an average value of 70° dipping to the WSW. At field point "Ekeberg Rideskole_2" (located on Figure 35) the rocks are amphibolitic lenses and large pegmatitic bodies.

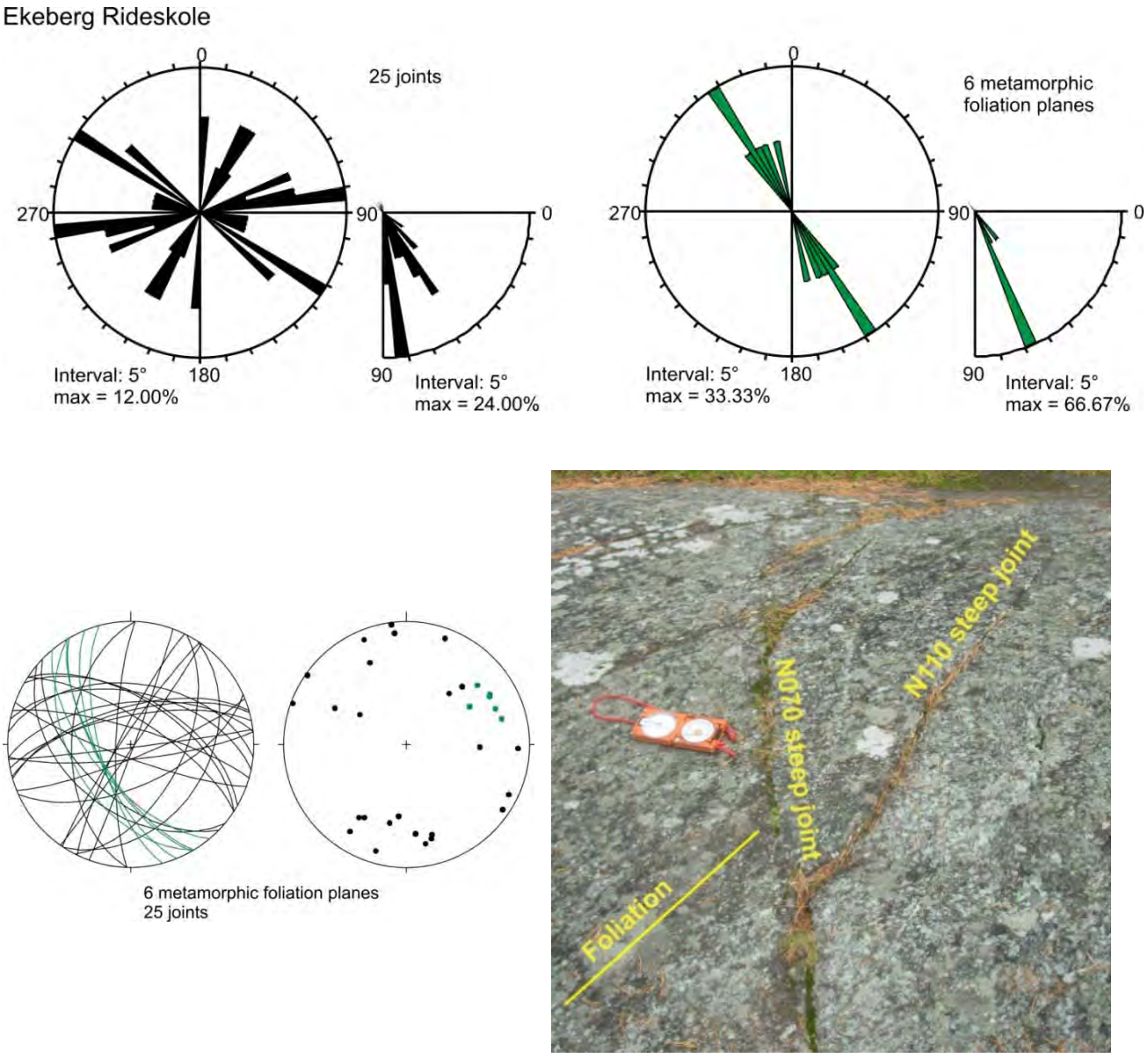

Figure 36. Structural field measurements displayed by rose diagrams and on stereonets at locality "Ekeberg Rideskole" close to resistivity profile 0 (keys to stereonets on Figure 32) and photograph of two fractures which belong to the two main sets of joints commonly found at the regional scale, which are the steep WSW-ENE and WNW-ESE orientated sets.

Field locality "Smedstusveien"

The field locality "Smedstusveien" close to resistivity profile 0 (Figure 35) is tens of meters long and 1 m high outcrop of gneiss. The metamorphic foliation dips from 65° to 80° toward the SW and WSW reflecting well its regional attitude (Figure 35 and Figure 37). The two sets of joints correspond to nearly vertical NE-SW/NNE-SSW fractures and to shallow to steep N-dipping E-W trending fractures (Figure 35 and Figure 37).

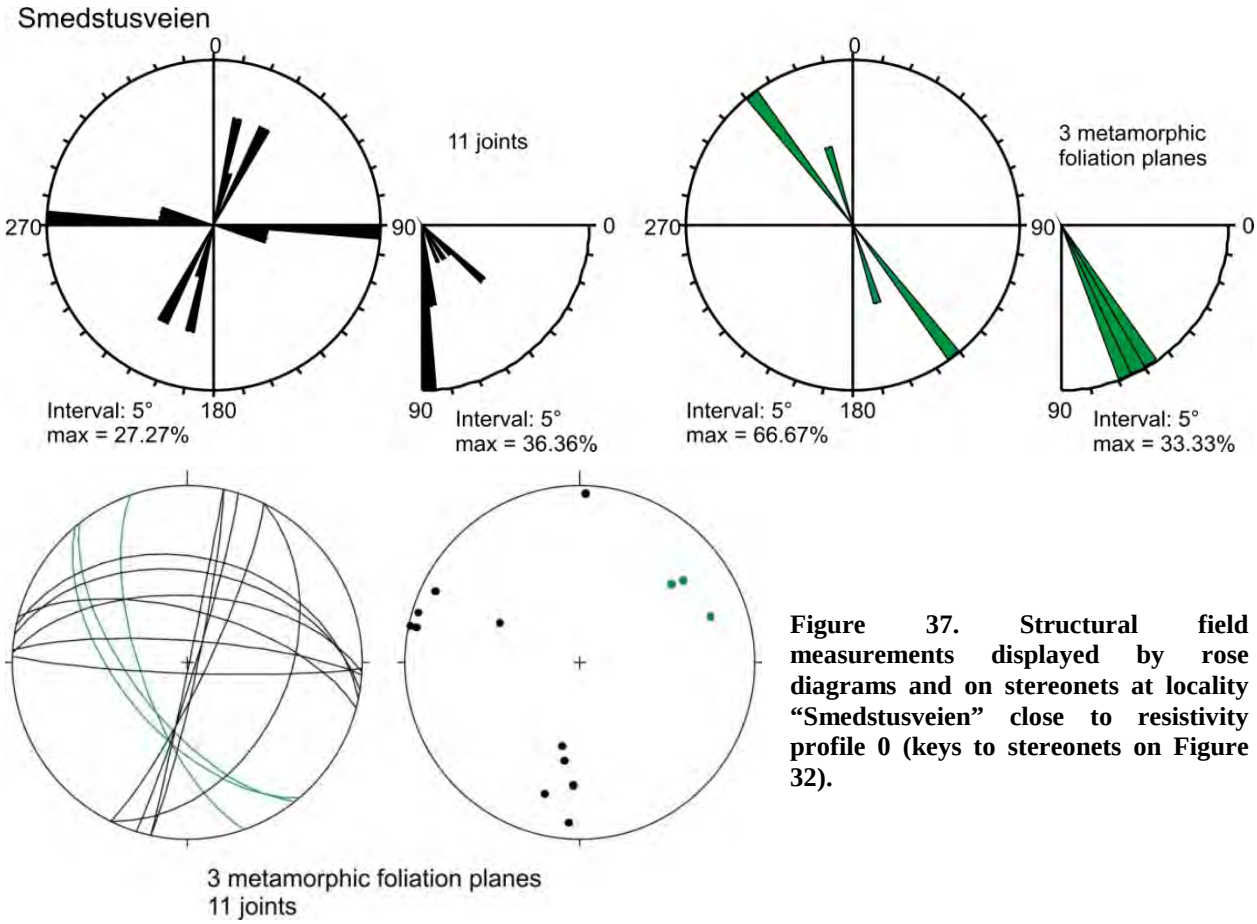

Figure 37. Structural field measurements displayed by rose diagrams and on stereonets at locality "Smedstusveien" close to resistivity profile 0 (keys to stereonets on Figure 32).

5.2.2 Field localities "Jomfrubråtveien, 48", "Frierveien", "Sportsplassen, Jomfrubråtveien", "Kongsveien" and "Tramway station Sportsplassen, Jomfrustien"

Five field localities are described in detail and in term of structural geology in this section to better constrain what can be the nature of the 5 anomalies along the resistivity profiles 0 and 1 (Figure 38).

Field locality "Jomfrubråtveien, 48"

The field locality "Jomfrubråtveien, 48" is a small outcrop close to resistivity profile 0 (Figure 38). Of interest was the presence of 30 cm wide, nearly vertical basaltic dyke trending approximately E-W (Figure 38 and Figure 39). It trends parallel to a set of joints (Figure 38 and Figure 39). The other structures correspond to (1) a steep ENE-WSW fracture set with one fracture displaying an important chlorite-coating and to (2) the foliation dipping moderately to steeply toward the SW and WSW (Figure 38 and Figure 39).

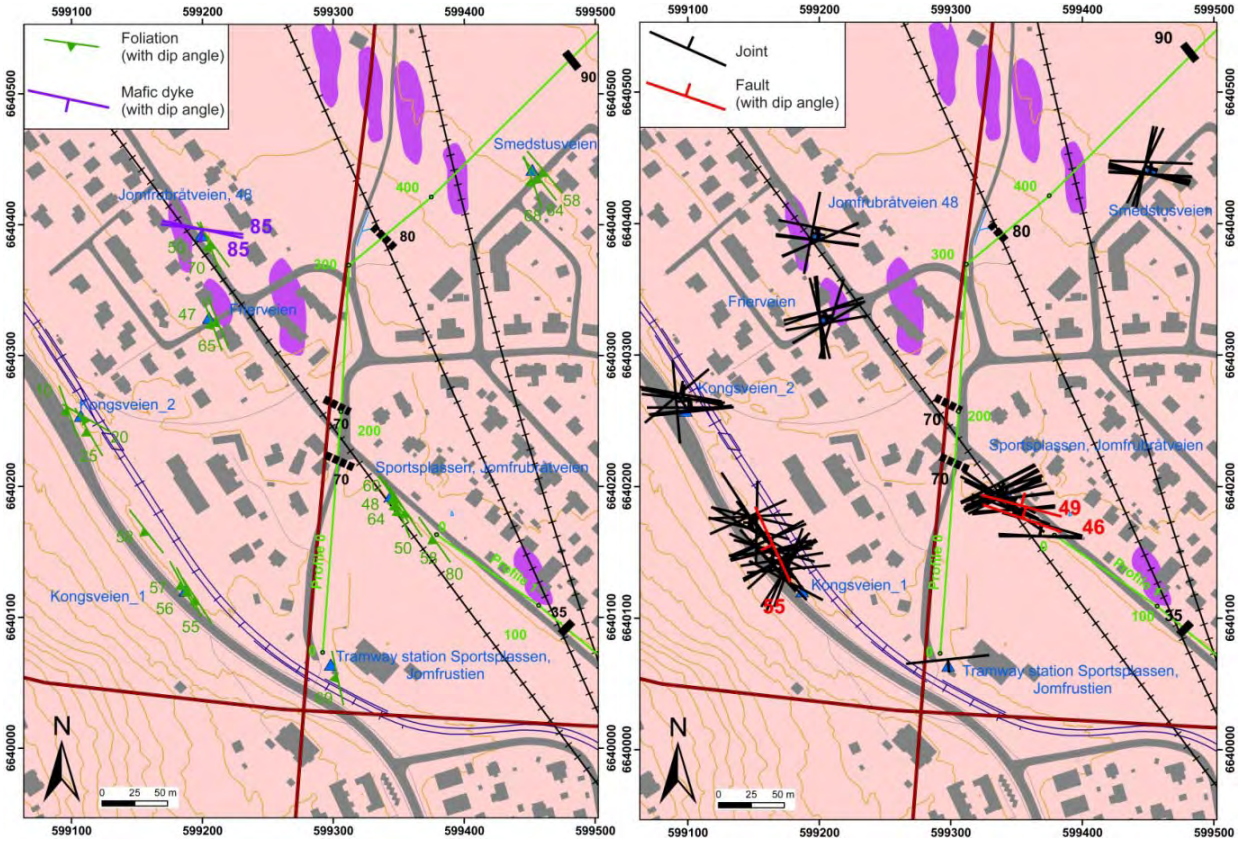

Figure 38. Structural field measurements at localities close to resistivity profiles 0 and 1 (caption of background map as Figure 34 and of interpreted resistivity anomalies as Figure 5).

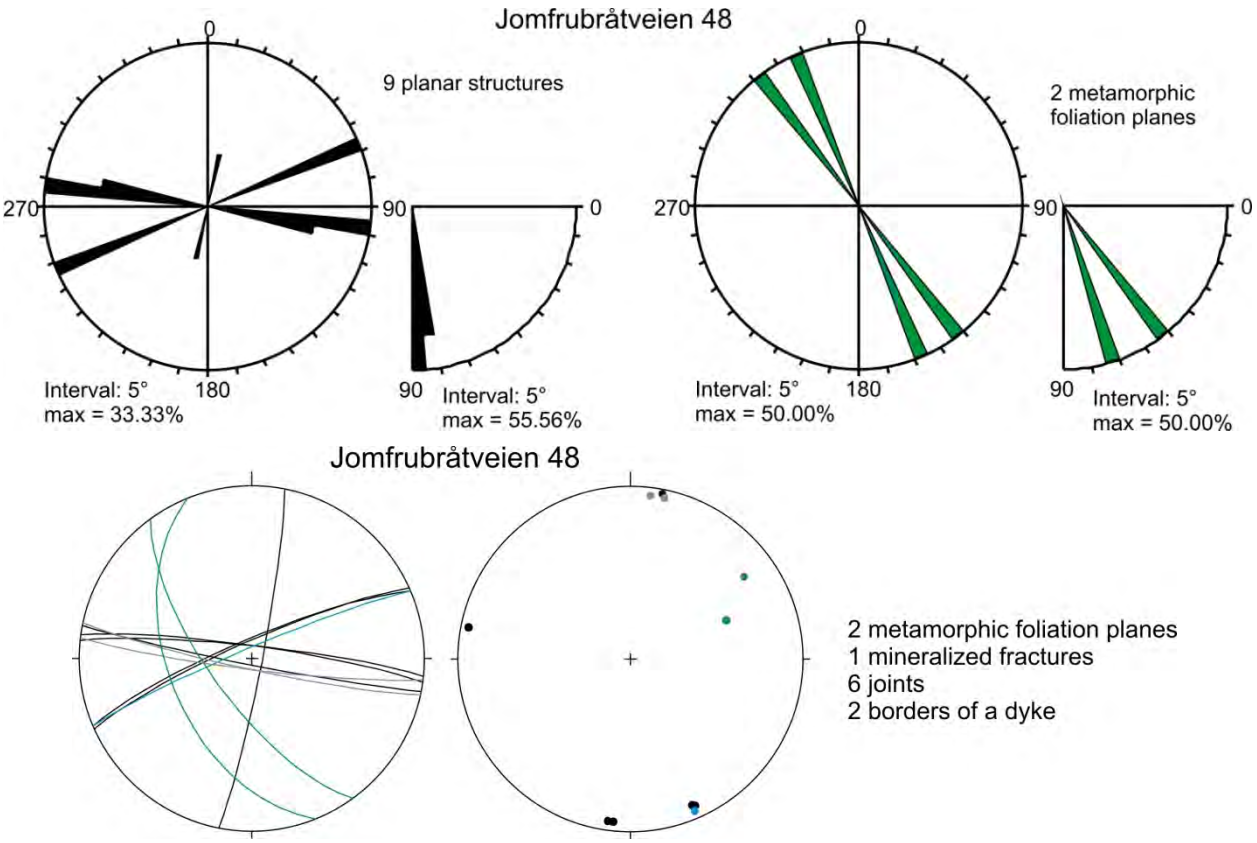

Figure 39. Structural field measurements displayed by rose diagrams and on stereonets at locality "Jomfrubråtveien, 48" close to resistivity profile 0 (keys to stereonets on Figure 32).

Field locality "Frierveien"

The field locality "Frierveien" is like the previous one, a small outcrop close to resistivity profile 0 (Figure 38). Besides the common trends of the metamorphic foliation and of the main set of joints, that are moderately to steeply WSW-dipping and vertically ENE-WSW striking, respectively, we can observe a singular set of steeply ENE-dipping joints (Figure 38 and Figure 40).

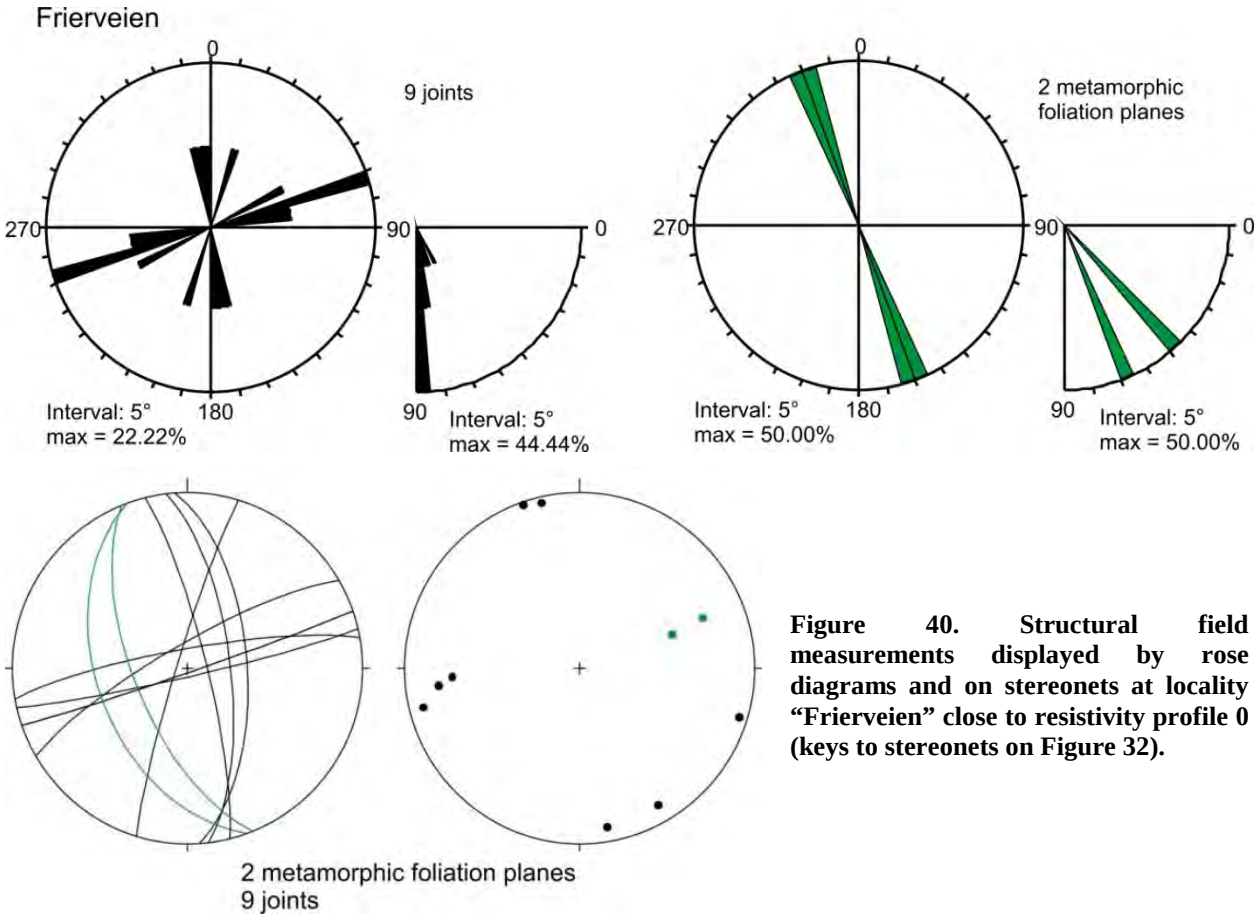

Figure 40. Structural field measurements displayed by rose diagrams and on stereonets at locality "Frierveien" close to resistivity profile 0 (keys to stereonets on Figure 32).

Field locality "Sportsplassen, Jomfrubråtveien"

The field locality "Sportsplassen, Jomfrubråtveien" is located between resistivity profiles 0 and 1 and aligned with one of the anomalies found along profile 0 (Figure 38). The outcrop is some tens of meters long and about 2 m high. The metamorphic foliation is steeply to moderately dipping to the WSW (Figure 38 and Figure 41). Two joint sets are well defined: one set dipping c. 60° to the NNE and another one, vertical and striking ENE-WSW (Figure 41). Mineralized fractures form a third set of roughly E-W directed structures steeply N- or S-dipping (Figure 41). Two of these measurements are along a striated fault surface, which extends several meters and approximately follow the steeply dipping E-W trend (Figure 38, Figure 41 and Figure 42). This large fault is aligned with the anomaly observed along resistivity profile 0 (Figure 38) and therefore we suggest that this anomaly may correspond to a large N-dipping E-W trending fault zone.

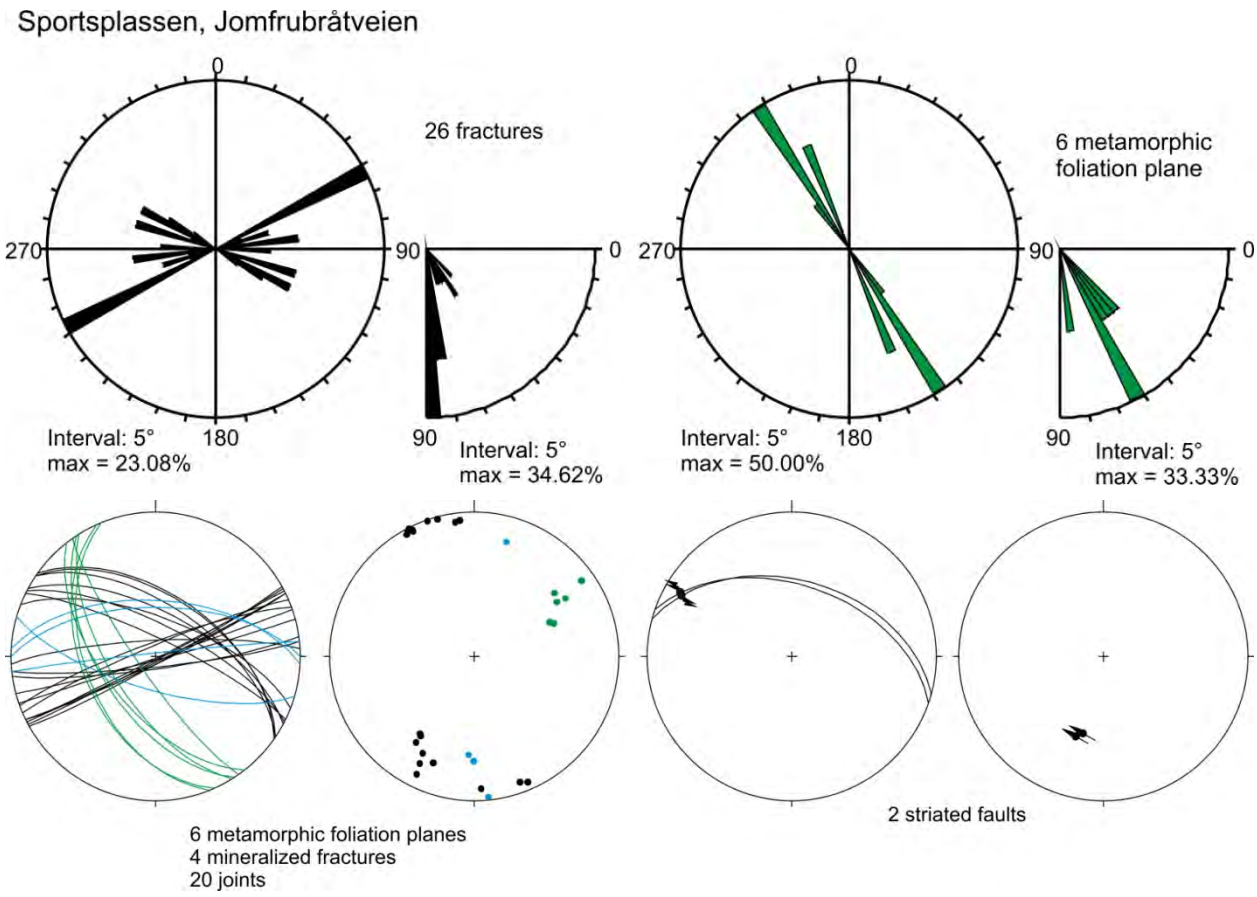

Figure 41. Structural field measurements displayed by rose diagrams and on stereonets at locality "Sportsplassen, Jomfrubråtveien" close to resistivity profiles 0 and 1 (keys to stereonets on Figure 32 and Figure 33).

Figure 42. Illustration of the striated surface of a sinistral fault (strike/dip 285/46; pitch: 20W) which extends several meters at locality "Sportsplassen, Jomfrubråtveien".

Field locality "Kongsveien"

The field locality "Kongsveien" is west of resistivity profile 0 and the field point "Kongsveien_2" is aligned with one of the anomalies along the profile (Figure 38). The outcrop is discontinuous from field point "Kongsveien_1" to field point "Kongsveien_2" but each of them has large extent. The metamorphic foliation is moderately dipping toward the WSW at field point "Kongsveien_1" and severely flattens toward the field point "Kongsveien_2" (Figure 38 and Figure 43). The metamorphic foliation planes at field point "Kongsveien_1" displayed weathered features and a dip-slip faulting occurred along one of these surfaces (Figure 38, Figure 43 and Figure 44). The joints are quite dispersed both in terms of orientation and dip angle with, however, a preferential steep WSW-ENE trend. This trend corresponds to a regional geometry, which is perpendicular to the regional metamorphic foliation (Figure 38 and Figure 43). Chlorite- or quartz-coated fractures developed along the metamorphic foliation surface as well as along the main set of steep WSW-ENE joints (Figure 43 and Figure 44).

Field locality "Tramway station Sportsplassen, Jomfrustien"

The field locality "Tramway station Sportsplassen, Jomfrustien" is a poor outcrop visited because of its close vicinity to resistivity profile 0 (Figure 38). The observation allows confirming the regional trends of the steeply WSW-dipping metamorphic foliation and of the main set of vertical ENE-WSW orientated joints (Figure 38 and Figure 45).

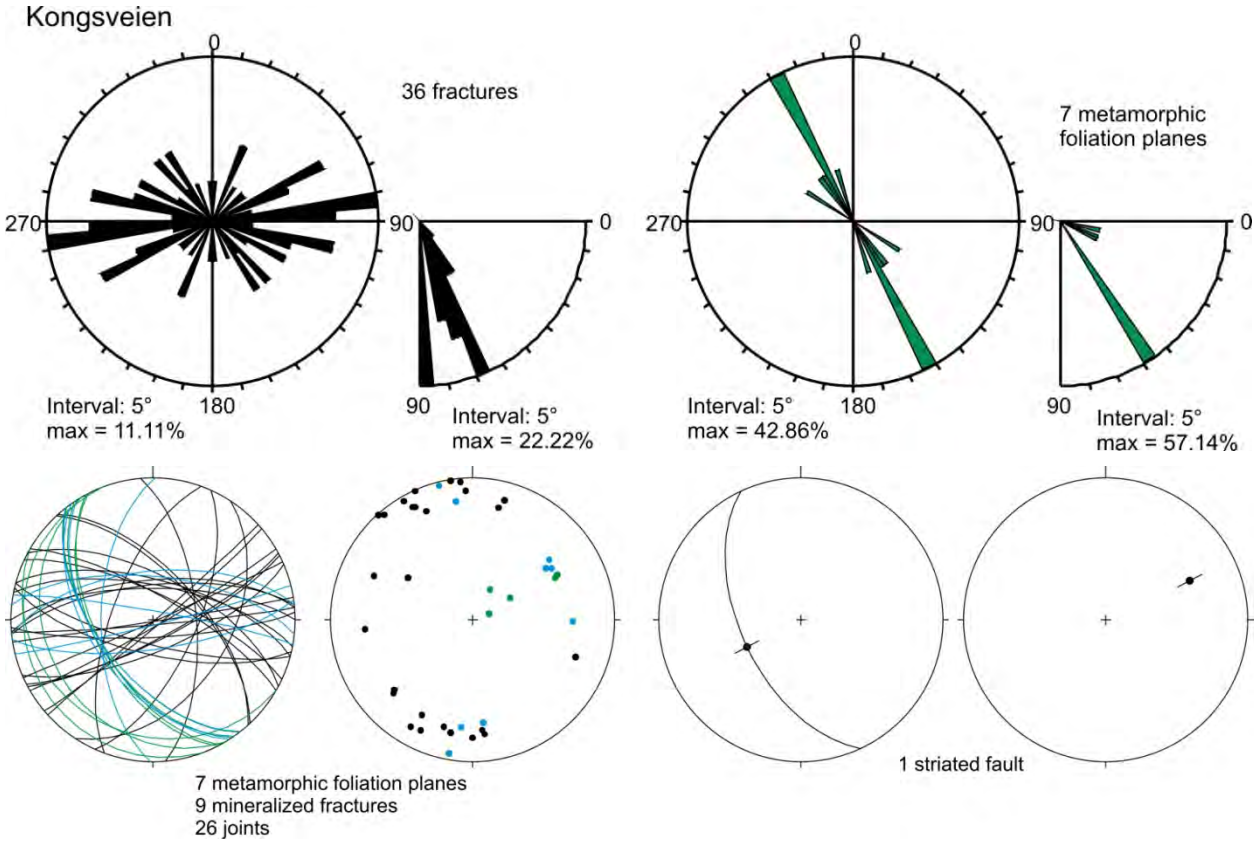

Figure 43. Structural field measurements displayed by rose diagrams and on stereonets at locality "Kongsveien" close to resistivity profile 0 (keys to stereonets on Figure 32 and Figure 33).

Figure 44. Left: weathered surface along a 55º WSW-dipping foliation plane observed at field point "Kongsveien_1"; right: steep north-dipping quartz-coated fracture at field point "Kongsveien_2"; (location of field points on Figure 38).

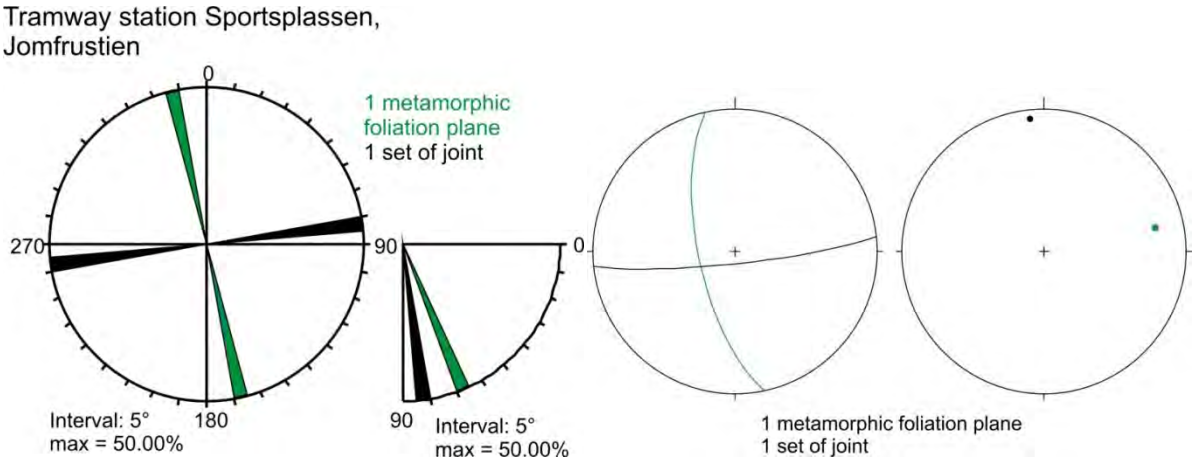

Figure 45. Structural field measurements displayed by rose diagrams and on stereonets at locality "Tramway station Sportsplassen, Jomfrustien" close to resistivity profile 0 (keys to stereonets on Figure 32).

5.2.3 Field localities "Ekeberg Brannfjell Skole", "Jomfrubråtveien, 78" and "Marienlundveien"

Three field localities are analysed in this section to get the structural grain surrounding the anomalies found along resistivity profile 1 (Figure 46).

Field locality "Ekeberg Brannfjell Skole"

The field locality "Ekeberg Brannfjell Skole" is close to resistivity profiles 1 and 2, with the first showing an anomaly to identify. The outcrop is some tens of meters long but only 1 m high. However, structures of interest are observed. The foliation attitude corresponds to the regional NNW-SSE trend with a steep dip angle to the WSW (Figure 46 and Figure 47). Fractures are steep and two orientations predominate: WNW-ESE and WSW-ENE (Figure 46 and Figure 47). One in each of these fracture sets is a striated fault plane, and these two faults (Figure 48) are also parallel to chlorite- and calcite-coated fractures (Figure 46 and Figure 47).

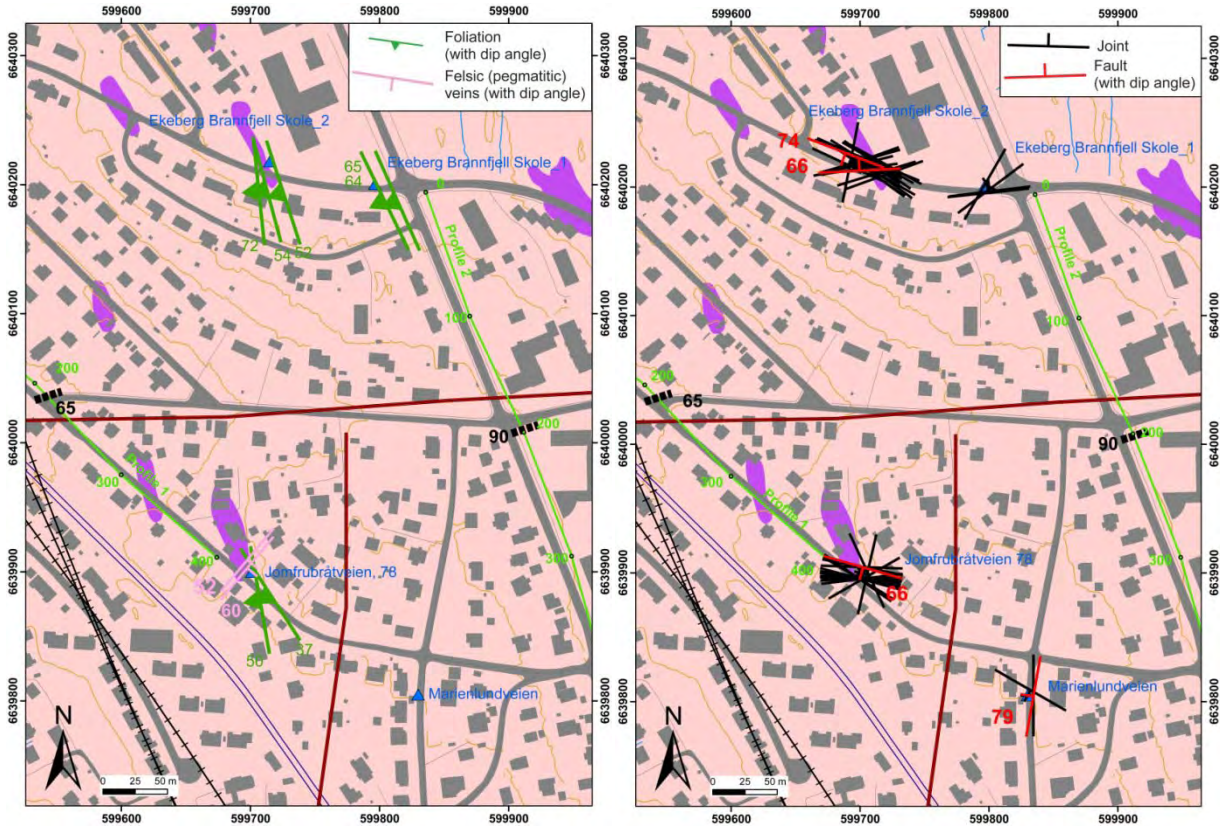

Figure 46. Structural field measurements at localities close to resistivity profiles 1 and 2 (caption of background map as Figure 34 and of interpreted resistivity anomalies as Figure 5).

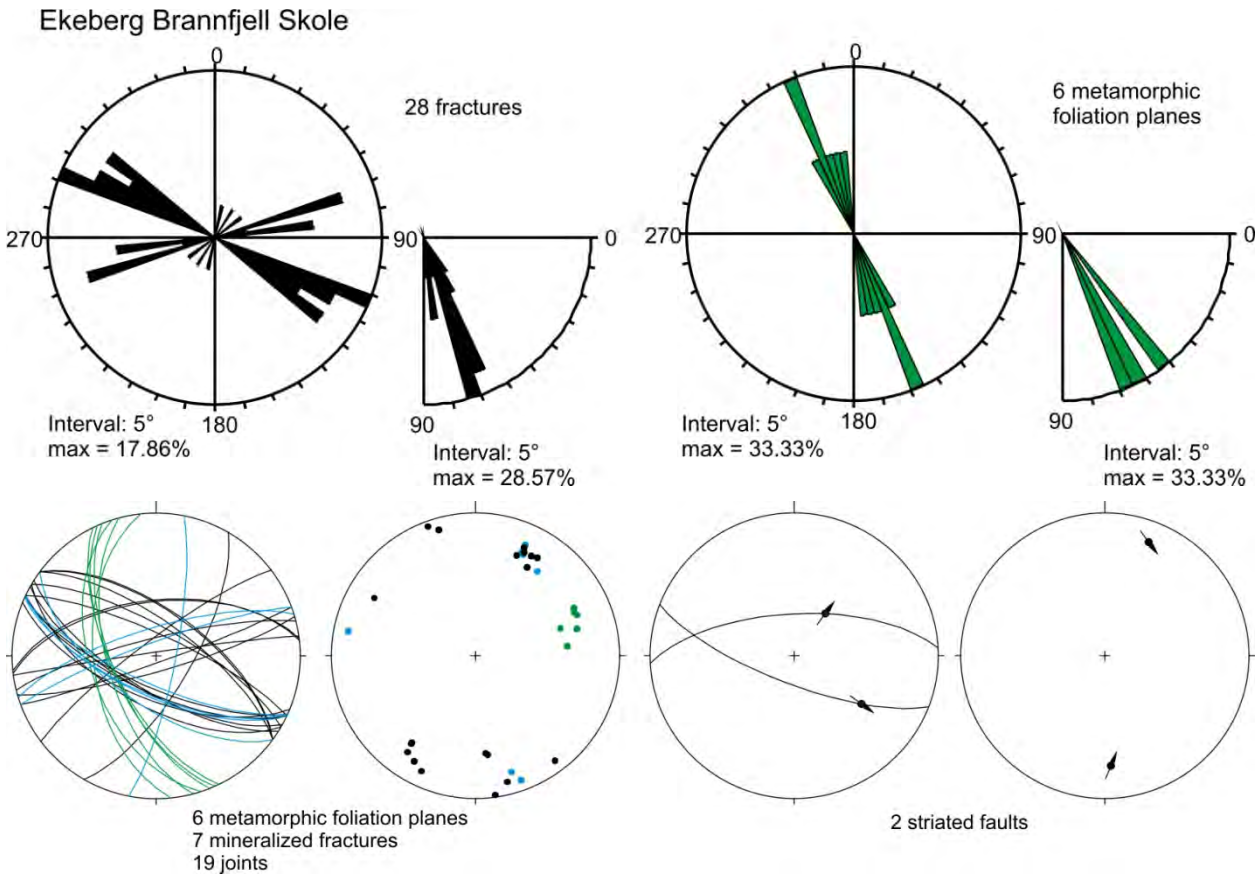

Figure 47. Structural field measurements displayed by rose diagrams and on stereonets at locality "Ekeberg Brannfjell Skole" close to resistivity profile 2 (keys to stereonets on Figure 32 and Figure 33).

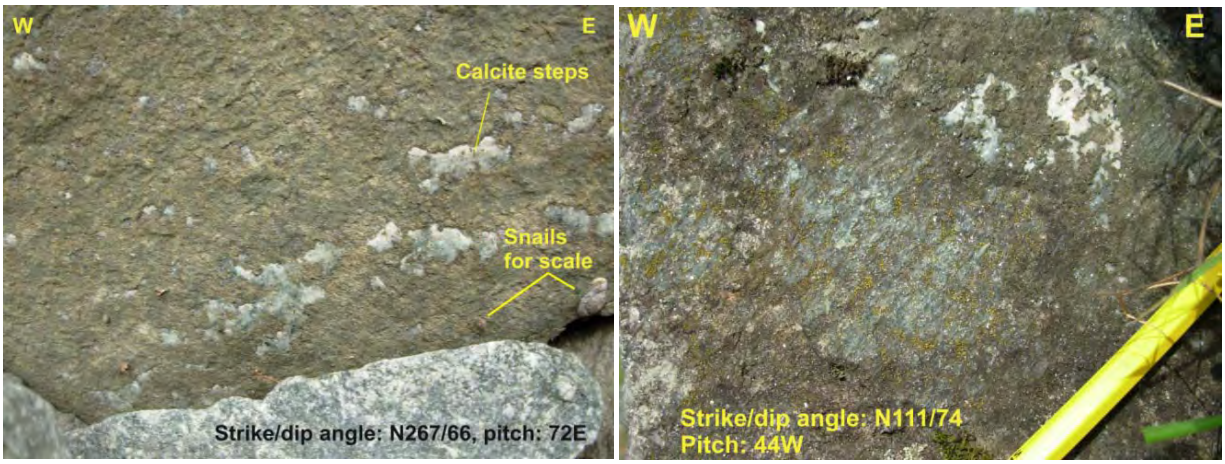

Figure 48. Photographs of striated normal faults observed at field locality "Ekeberg Brannfjell Skole"

Field locality "Jomfrubråtveien, 78"

The field locality "Jomfrubråtveien, 78" is located at the southeastern end of the resistivity profile 1 (Figure 46). The metamorphic foliation is shallow dipping to the WSW and SW (Figure 46 and Figure 49). The main set of joint dips towards the north and NNE with a quite important dispersion in the angle from vertical to shallow values (Figure 46 and Figure 49). Two distinct trends correspond to two mineralised fractures (Figure 49) which exhibits chlorite- calcite and quartz-calcite respectively. One is exactly parallel to the unique striated fault (Figure 46 and Figure 49) measured at the field locality. Two pegmatitic veins of 4 and 20 cm wide, cut the gneiss rocks in a NE-SW direction with a dip of c. 52° and 60° (Figure 46 and Figure 49).

Field locality "Marienlundveien"

The field locality "Marienlundveien" (Figure 46) was visited because of the observation of a hematite-striated fault. The fault strike steeply N-S (Figure 50) which corresponds to a lineament mapped some 50 m toward the west (Figure 46). The two other measurements fit with this fault and with the regional WNW-ESE steep trend of fractures (Figure 46 and Figure 50).

5.2.4 Field locality "Erlandstuveien"

The field locality "Erlandstuveien" is not particularly close to any of the resistivity profiles (Figure 51) but is a very large outcrop that may allow a good identification of regional structural features which by correlation may be helpful to determine the nature of the resistivity anomalies elsewhere.

The metamorphic foliation is slightly disturbed and from the regional steeply WSW-dipping trend, it is deviated toward a vertical NNE-SSW trend (Figure 52). The presence of large amphibolitic bodies along the outcrop and in the area in general (Figure 51) may explain the disturbance. In addition to the amphibolitic lenses, several NE-SW trending basaltic dykes (Figure 52) crop out, and they are more fractured than the gneissic host rock (Figure 53). The fractures within the dykes form a main set of steep brittle structures (Figure 52), while the other main set of fractures is moderately to steeply N-dipping and includes a striated fault (Figure 52 and Figure 53). This latter trend is parallel to the trend of a mapped lineament south of this field locality (Figure 51).

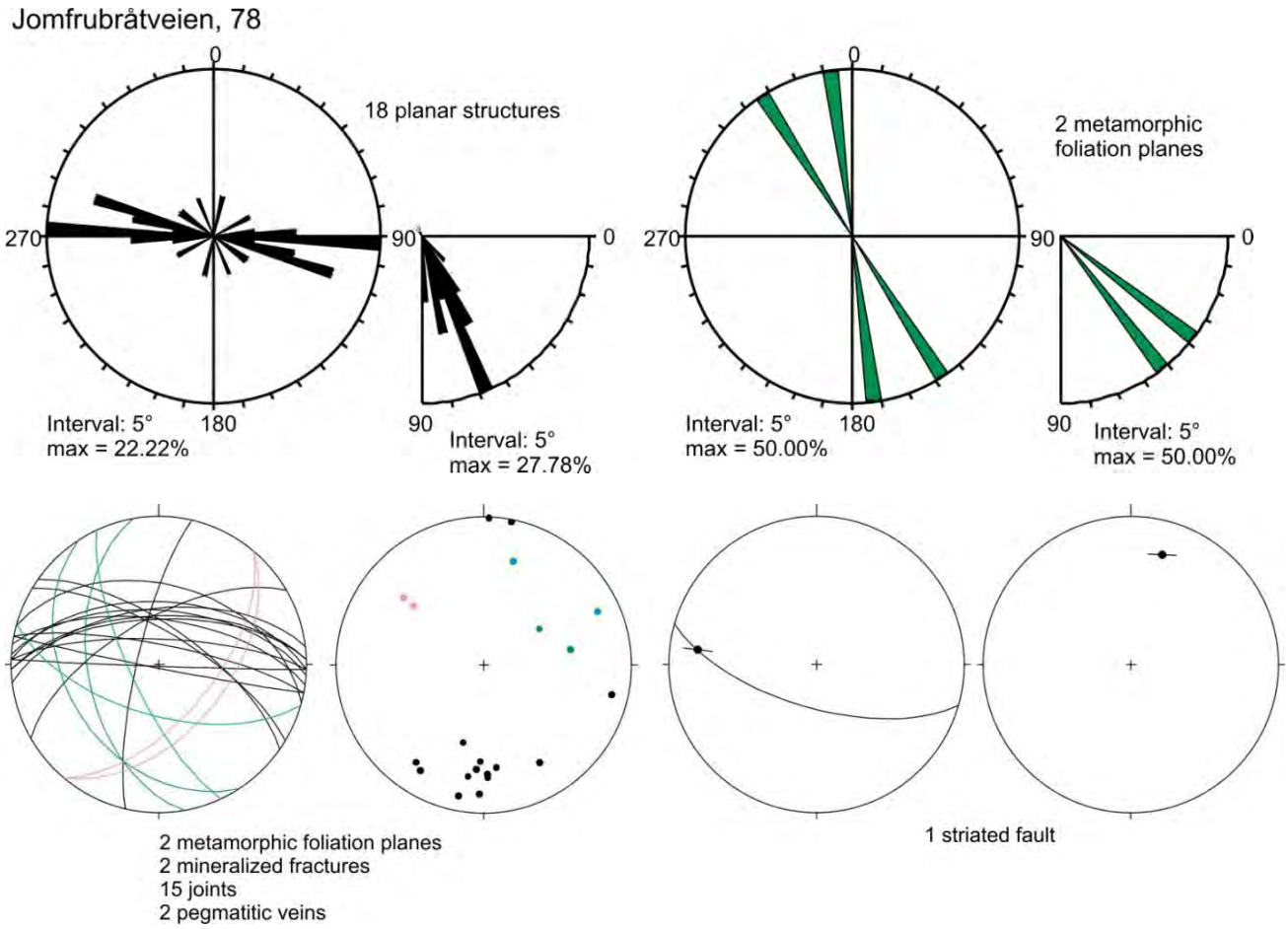

Figure 49. Structural field measurements displayed by rose diagrams and on stereonets at locality "Jomfrubråtveien, 78" close to resistivity profile 1 (keys to stereonets on Figure 32 and Figure 33).

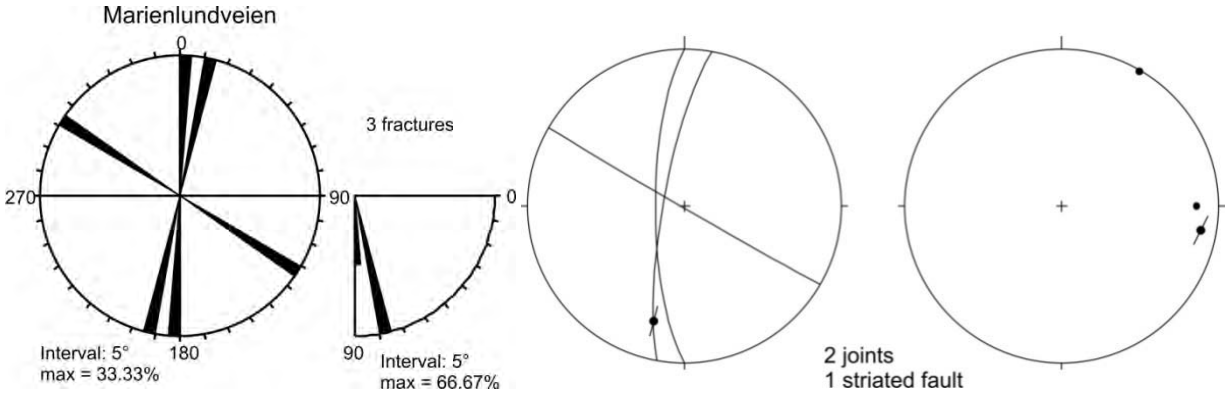

Figure 50. Structural field measurements displayed by rose diagrams and on stereonets at locality "Marienlundveien" close to resistivity profiles 0 and 1 (keys to stereonets on Figure 32 and Figure 33).

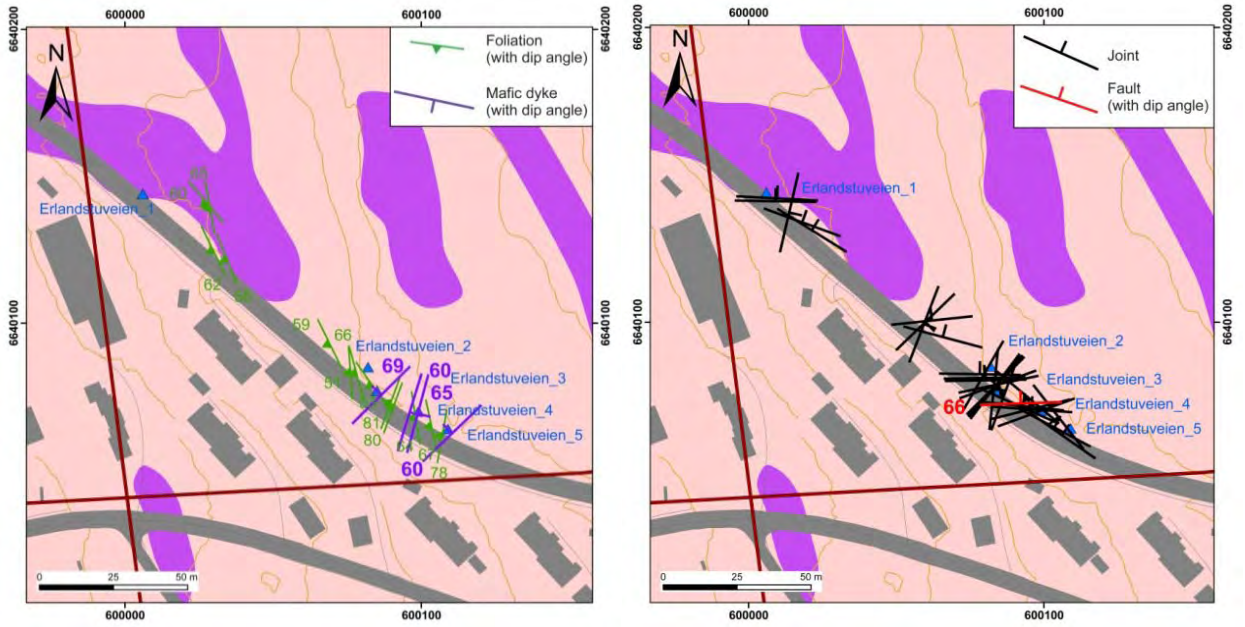

Figure 51. Structural field measurements at locality "Erlandstuveien" in the vicinity of resistivity profile 2 (caption of background map as Figure 34).

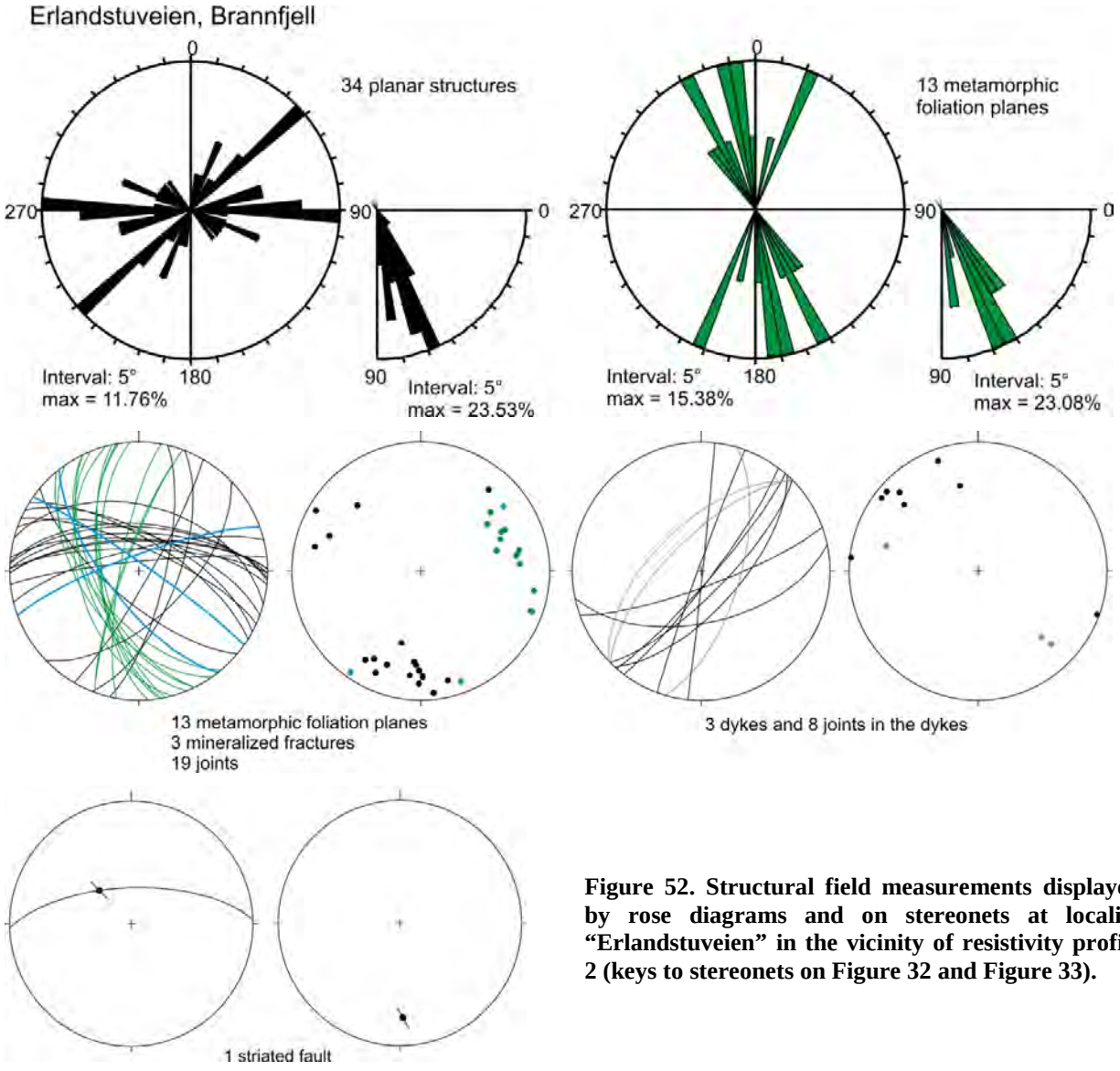

Figure 52. Structural field measurements displayed by rose diagrams and on stereonets at locality "Erlandstuveien" in the vicinity of resistivity profile 2 (keys to stereonets on Figure 32 and Figure 33).

Figure 53. Left: western border of 5 m wide, steep NE-SW basaltic dyke at field point "Erlandstuveien_3"; note the high frequency of vertical NE-SW joints within the dyke; right: the north-dipping striated fault observed at field point "Erlandstuveien_4"; (field points are located on Figure 51).

5.2.5 Structural analysis around resistivity profiles 0-2: summary

There is one large fault at field locality "Sportsplassen, Jomfrubråtveien" that may fit with one of the anomalies detected along resistivity profile 0 (Figure 38). Where the resistivity profile 0 trends NE-SW in its northwestern part the anomalies may reflect a heterogeneous lithology in the bedrocks like amphibolitic bodies trending parallel to the foliation (Figure 34). One of the anomalies detected at the north-eastern tip of profile 0 obviously corresponds to the regional rhomb porphyry dyke (Figure 34).

One of the anomalies along resistivity profile 1 may correspond to a lineament already mapped as a fault (Figure 34). Parallel trend of striated faults is observed at several field localities in the area ("Ekeberg Brannfjell Skole" and "Jomfrubråtveien, 78", Figure 46 and "Erlandstuveien", Figure 51) and emphasizes that the cause of the anomaly may correspond to an E-W striking steep fault.

5.3 Structural analysis around resistivity profiles 3-4

Four field localities with outcrops of variable size were visited in order to carry on the structural analysis needed for the interpretation of the 2D resistivity profiles 3 and 4 (Figure 54). All measurements and field observations are listed in Appendix 2.

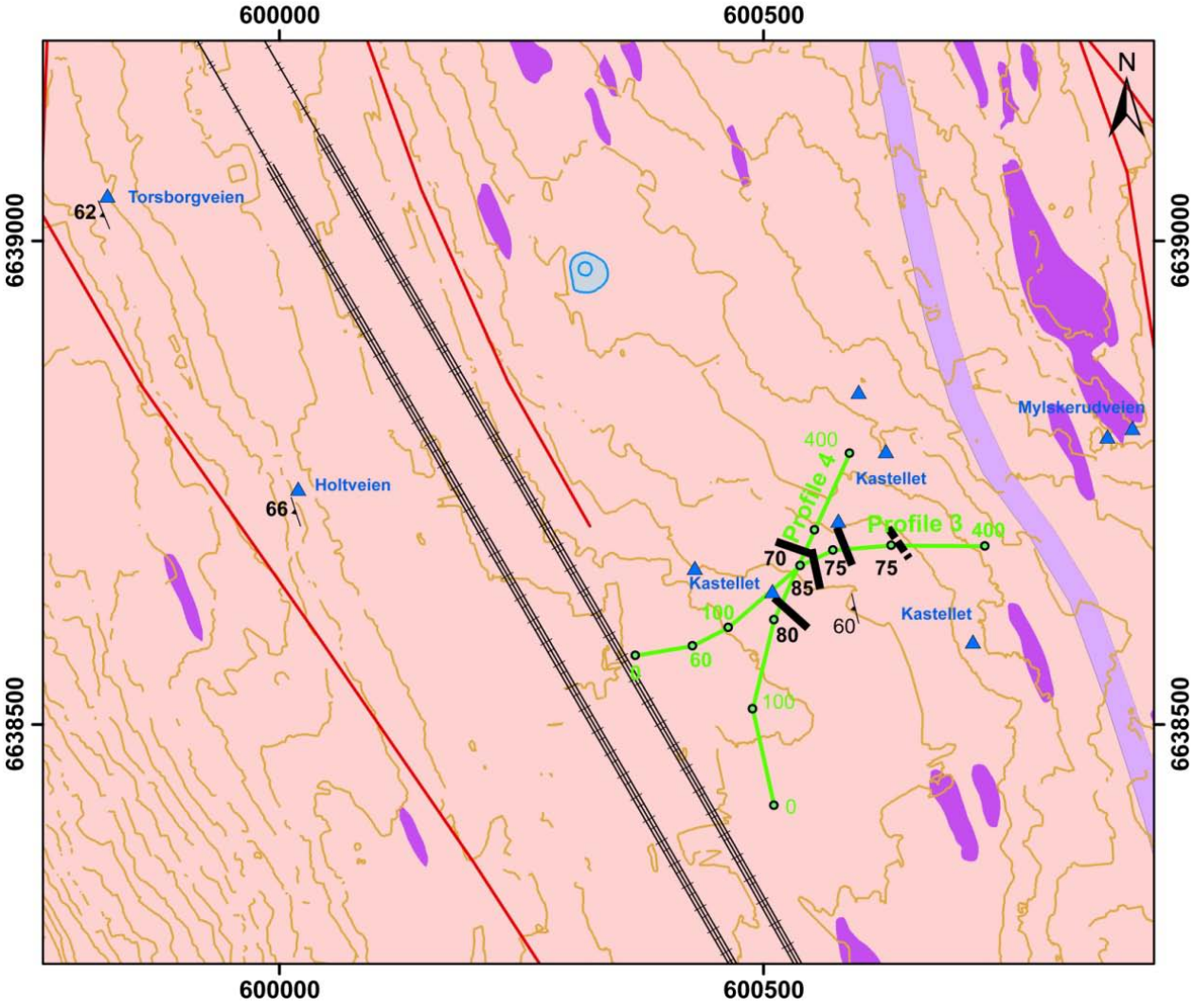

Figure 54. Field localities for structural analysis in the surrounding area of resistivity profiles 3 and 4 (caption as for Figure 34).

5.3.1 Field localities "Kastellet" and "Mylskerudveien"

The field localities "Kastellet" and "Mylskerudveien" are located close to resistivity profiles 3 and 4 that revealed five anomalies (Figure 55).

Field locality "Kastellet"

"Kastellet" field locality is a group of 6 field points (called "Kastellet_1" to "Kastellet_6") in the close vicinity of the resistivity profiles 3 and 4 (Figure 55). The metamorphic foliation is steeply dipping to the WSW in agreement with its regional attitude (Figure 55 and Figure 56). Two sets of joints are observed: one is steep to vertical and trending from E-W to NW-SE and the other one is about 60° dipping to the SE (Figure 55 and Figure 56).

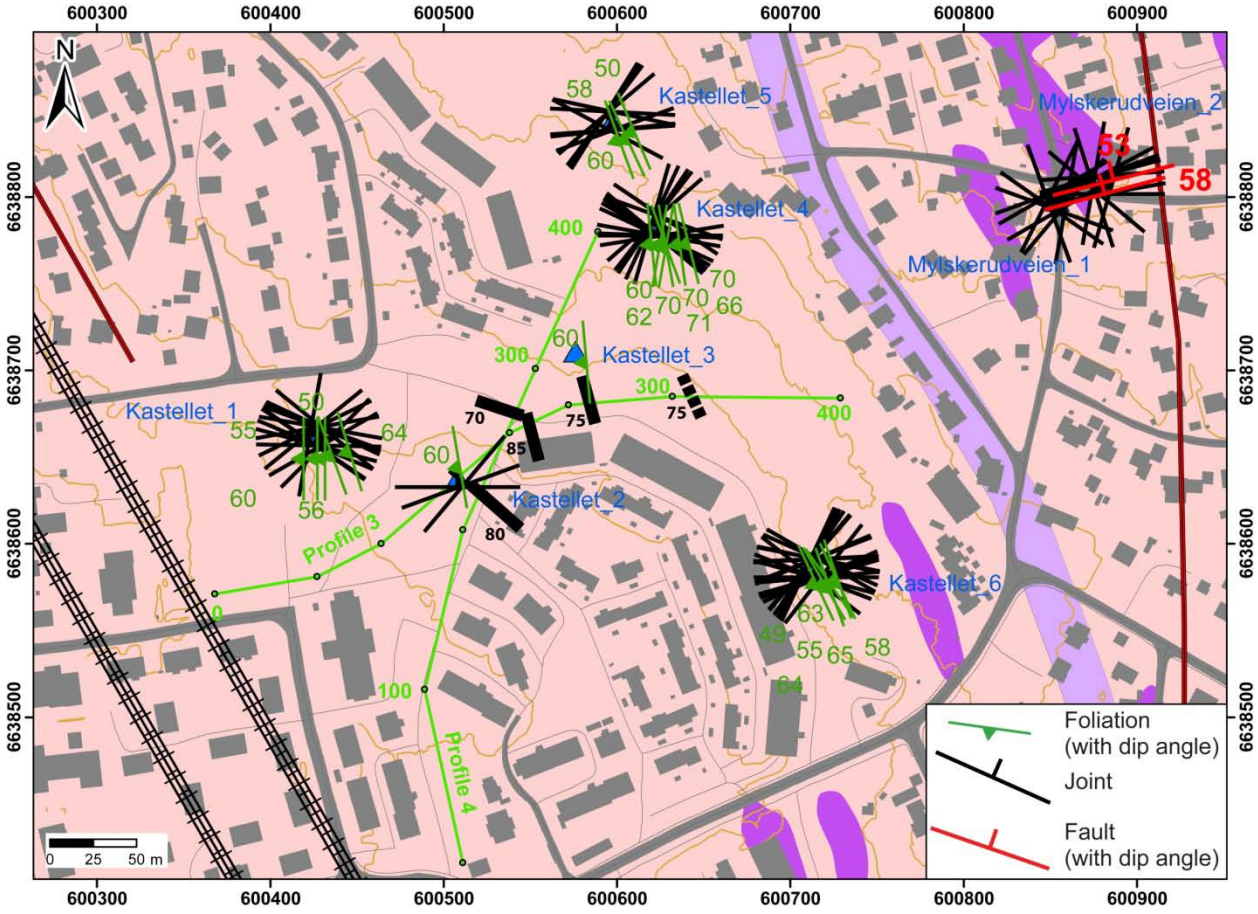

Figure 55. Structural field measurements at localities close to resistivity profiles 3 and 4 (caption of background map as Figure 34 and of interpreted resistivity anomalies as Figure 5).

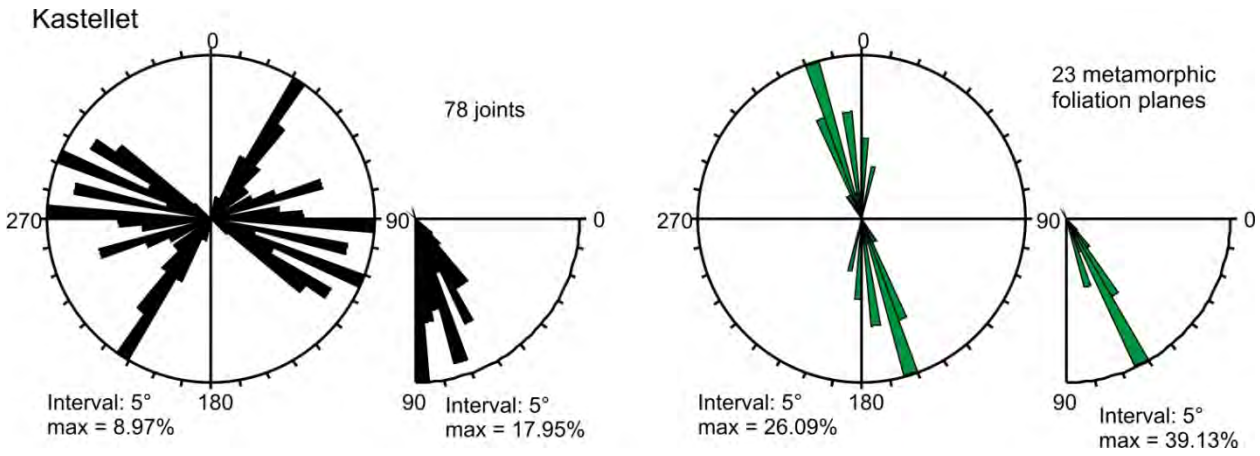

Figure 56 to be continued

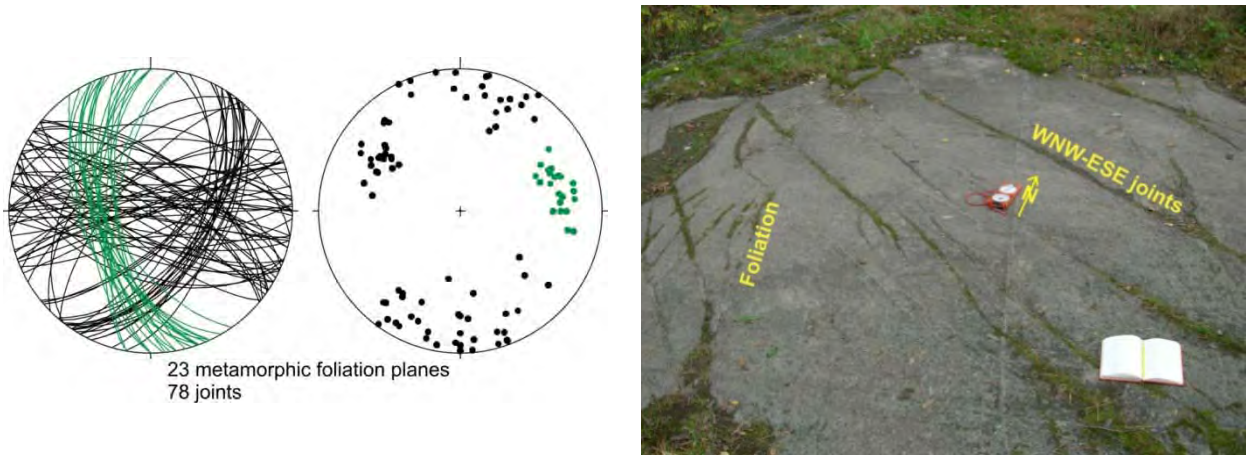

Figure 56. Structural field measurements displayed by rose diagrams and on stereonets at locality "Kastellet" close to resistivity profiles 3 and 4 (keys to stereonets on Figure 32) and photograph of the outcrop at field point "Kastellet_4" (located on Figure 55) displaying the foliation and a main set of WNW-ESE joints.

Field locality "Mylskerudveien"

"Mylskerudveien" field locality is an outcrop of amphibolites that is located just west of a N-S trending lineament (Figure 55). A set of WSW-ENE steep joints predominates while the rocks show a very scarce fracturation (Figure 57). Two striated faults are moderately dipping towards the WNW. The nature of the N-S trending lineament is difficult to define according to these observations.

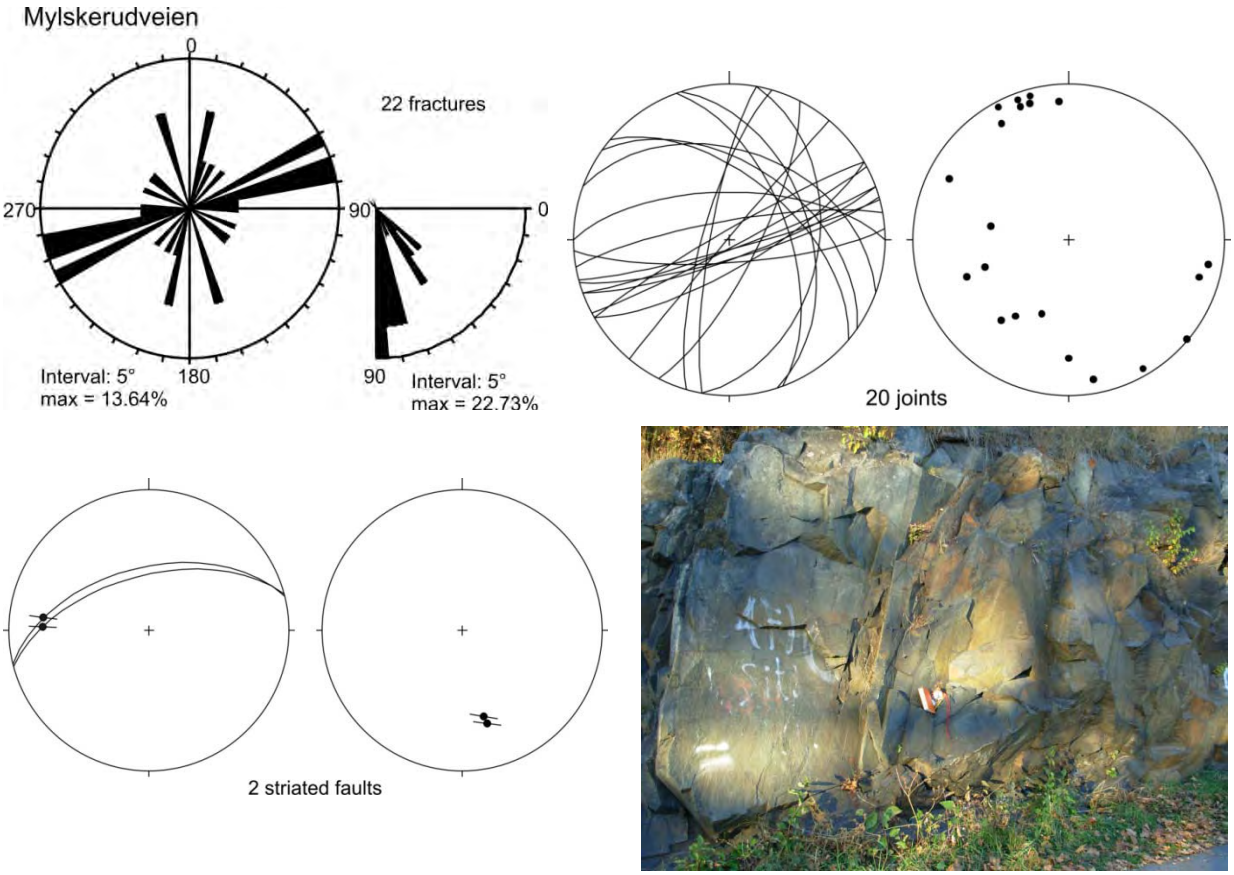

Figure 57. Structural field measurements displayed by rose diagrams and on stereonets at locality "Mylskerudveien" close to resistivity profiles 3 and 4 (keys to stereonets on Figure 32 and Figure 33) and photograph showing the scarcity of fractures in the massive amphibolites.

5.3.2 Field localities “Holtveien” and “Torsborgveien”

The two field localities “Holtveien” and “Torsborgveien” are far from any of the 2D resistivity profiles but will be analysed in the aim to correlate structures at the regional scale (Figure 58).

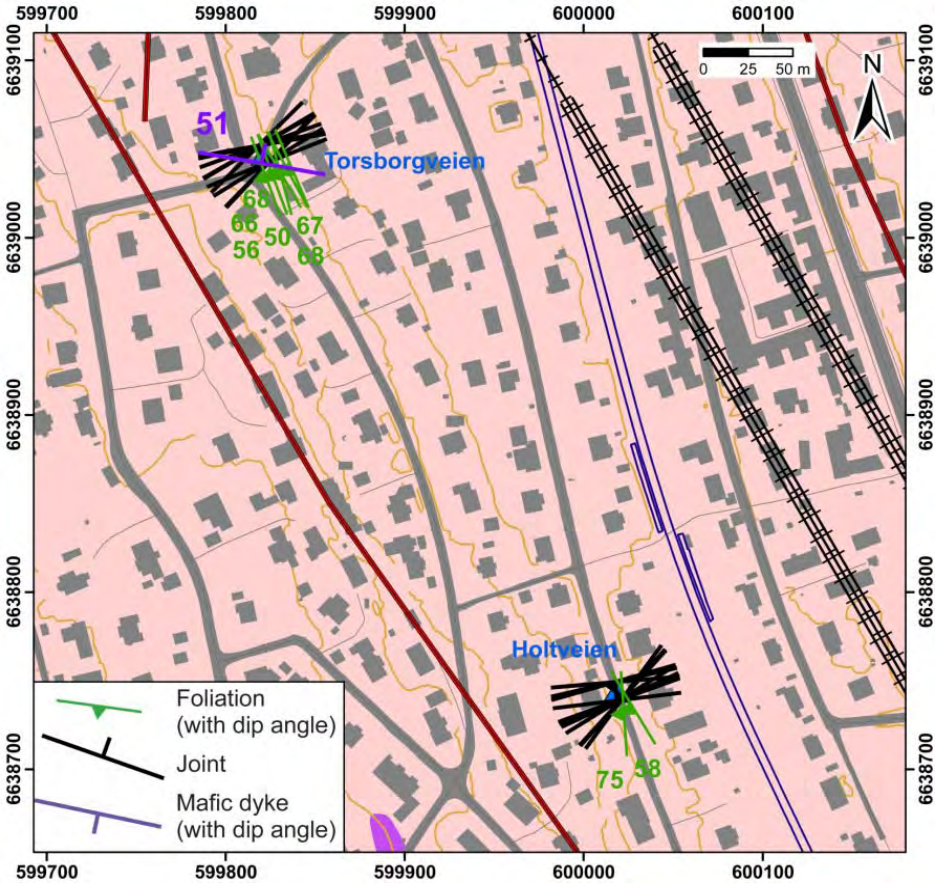

Figure 58. Structural field measurements at localities “Holtveien” and “Torsborgveien”, west of profiles 3 and 4 (caption of background map as Figure 34).

Field locality “Holtveien”

The Field locality “Holtveien” (Figure 58) gives a particular good view of the structural pattern of the region. The two regional structures are solely represented, which are the steep foliation dipping to the WSW and W, and the perpendicular set of nearly vertical ENE-WSW joints (Figure 58 and Figure 59). The frequency of this unique joint set is of about 2/m.

Field locality “Torsborgveien”

At the field locality “Torsborgveien” (Figure 58) the structural pattern is similar to that of field locality “Holtveien” with the exception of a north shallow dipping, 3 cm thick basaltic dyke observed along the few meters large outcrop (Figure 58 and Figure 60).

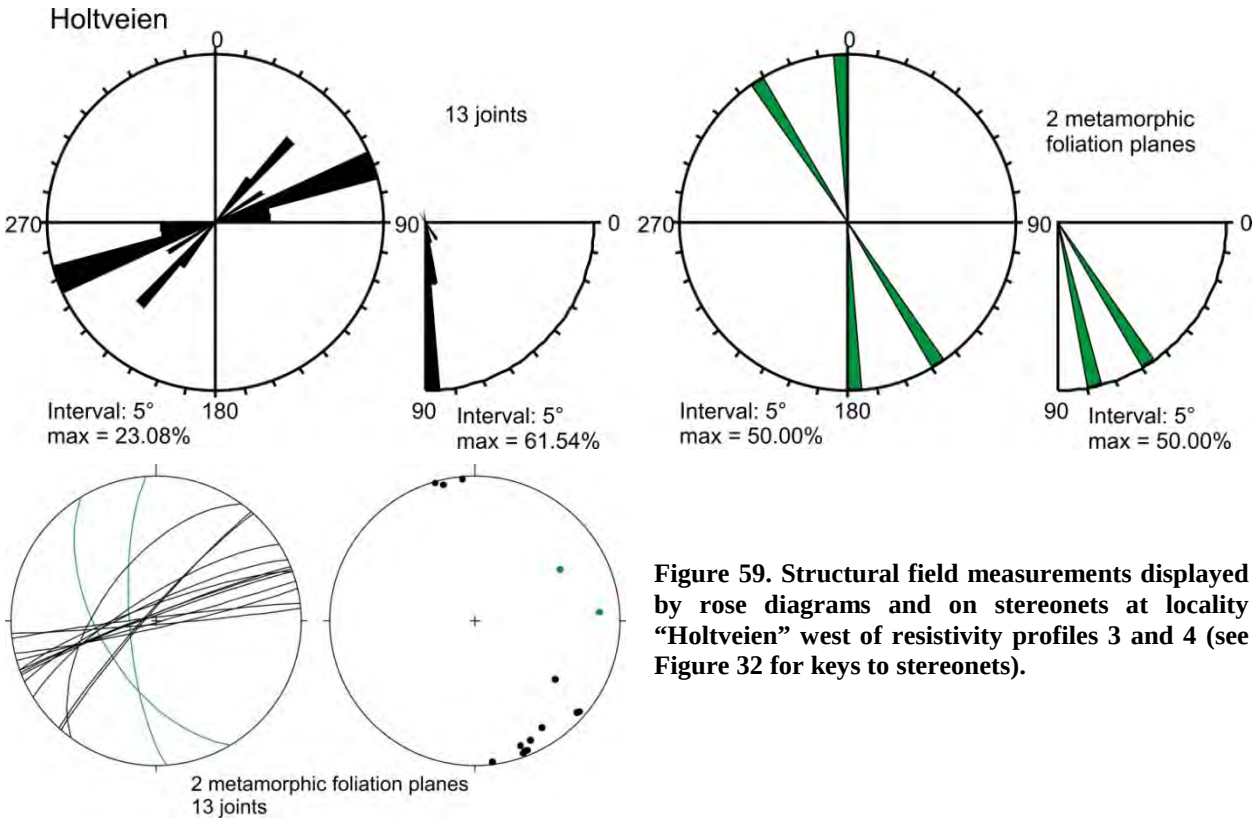

Figure 59. Structural field measurements displayed by rose diagrams and on stereonets at locality "Holtveien" west of resistivity profiles 3 and 4 (see Figure 32 for keys to stereonets).

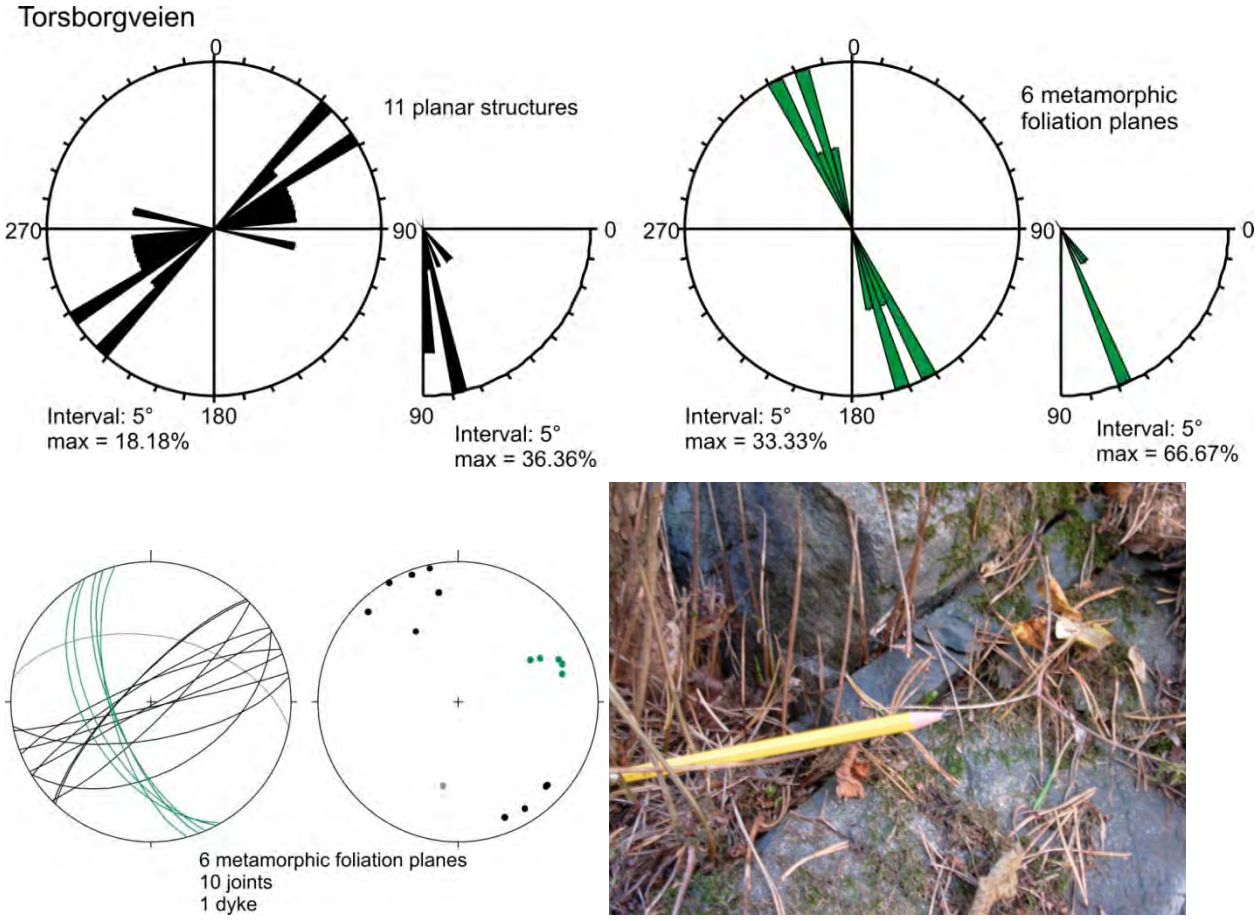

Figure 60. Structural field measurements displayed by rose diagrams and on stereonets at locality "Torsborgveien" northwest of resistivity profiles 3 and 4 (keys to stereonets on Figure 32) and photograph of a north shallow dipping 3 cm thick basaltic dyke.

5.3.3 Structural analysis around resistivity profiles 3-4: summary

The observations made at the two field localities "Kastellet" and "Mylskerudveien" in the vicinity of the resistivity profiles 3 and 4 (Figure 55) do not allow to accurately identifying the cause of the resistivity anomalies. No brittle structures that may indicate the presence of a large fault zone are observed. The only structures that would trend parallel to the anomalies are the persistent set of E-W to NW-SE trending steep joints.
The structural data at field localities "Torsborgveien" and "Holtveien" do not unravel the presence of regional structure in the area.

5.4 Structural analysis around resistivity profiles 5-7

Four field localities with outcrops of variable size were visited in order to carry on the structural analysis needed to interpret the 2D resistivity profiles 5A, 5B, 6 and 7 (Figure 61). All measurements and field observations are listed in Appendix 2.
During the field campaign 2007, examination of a nearly 100 m long outcrop close to profile 5A (site 35 on Figure 61) allowed to propose that the NW-SE striking lineament corresponds indeed to the foliation and that the brittle structures as faults, joints and mineral-filled fractures are roughly E-W and characterized by three crushed zones (one being 20 cm wide) and a zone of high joint frequency (up to 8 joints per dm; Lutro et al. 2007).

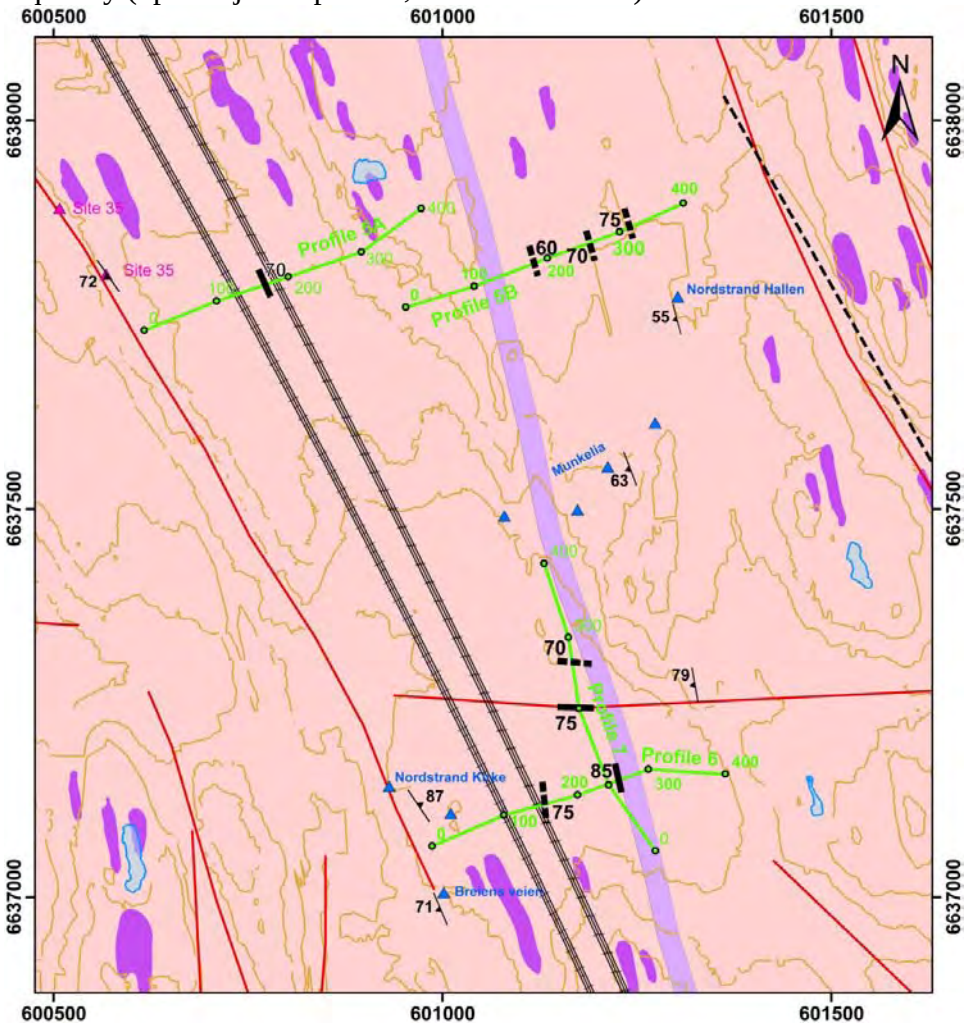

Figure 61. Field localities for structural analysis in the surrounding area of resistivity profiles 5A, 5B, 6 and 7 (caption as for Figure 34).

5.4.1 Field localities “Nordstrand Hallen” and “Munkelia”

The two field localities “Nordstrand Hallen” and “Munkelia” were studied in order to better assign the origin of the four resistivity anomalies recorded along the profiles 5A and 5B (Figure 62).

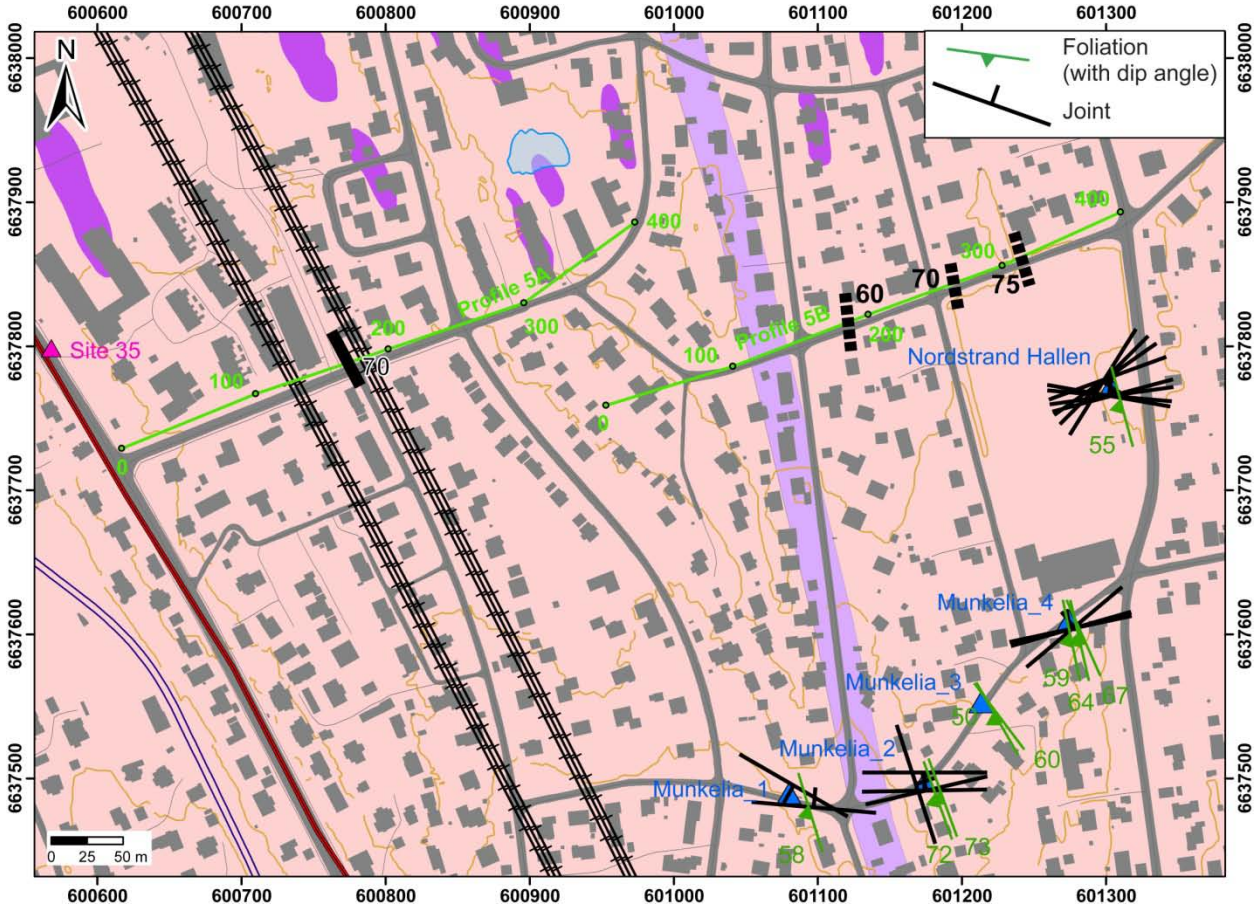

Figure 62. Structural field measurements at localities close to resistivity profiles 5A and 5B (caption of background map as Figure 34 and of interpreted resistivity anomalies as Figure 5).

Field locality “Nordstrand Hallen”

The field locality “Nordstrand Hallen” (Figure 62) is a very limited outcrop corresponding to a polished glaciated surface. However it is the closest field locality surrounding the resistivity profiles 5A and 5B. The metamorphic foliation is, like its regional trend, 55° to the WSW (Figure 62 and Figure 63). Joints dip from 60° to vertical and strike from NE–SW to ESE–WNW.

Field locality “Munkelia”

The field locality “Munkelia” is a discontinuous outcrop parallel to the resistivity profile 5B along which 3 anomalies are detected (Figure 62). The metamorphic foliation trends NNW-SSE and steeply dips to the WSW. The main set of fractures is a regional steep set trending perpendicular to the foliation (Figure 62 and Figure 64). A single joint dips 54° to the ENE (Figure 64). Two WNW-ESE, north and south 70° dipping calcite-coated fractures (Figure 64) are the only remarkable structures observed at field point “Munkelia_1” (located on Figure 62).

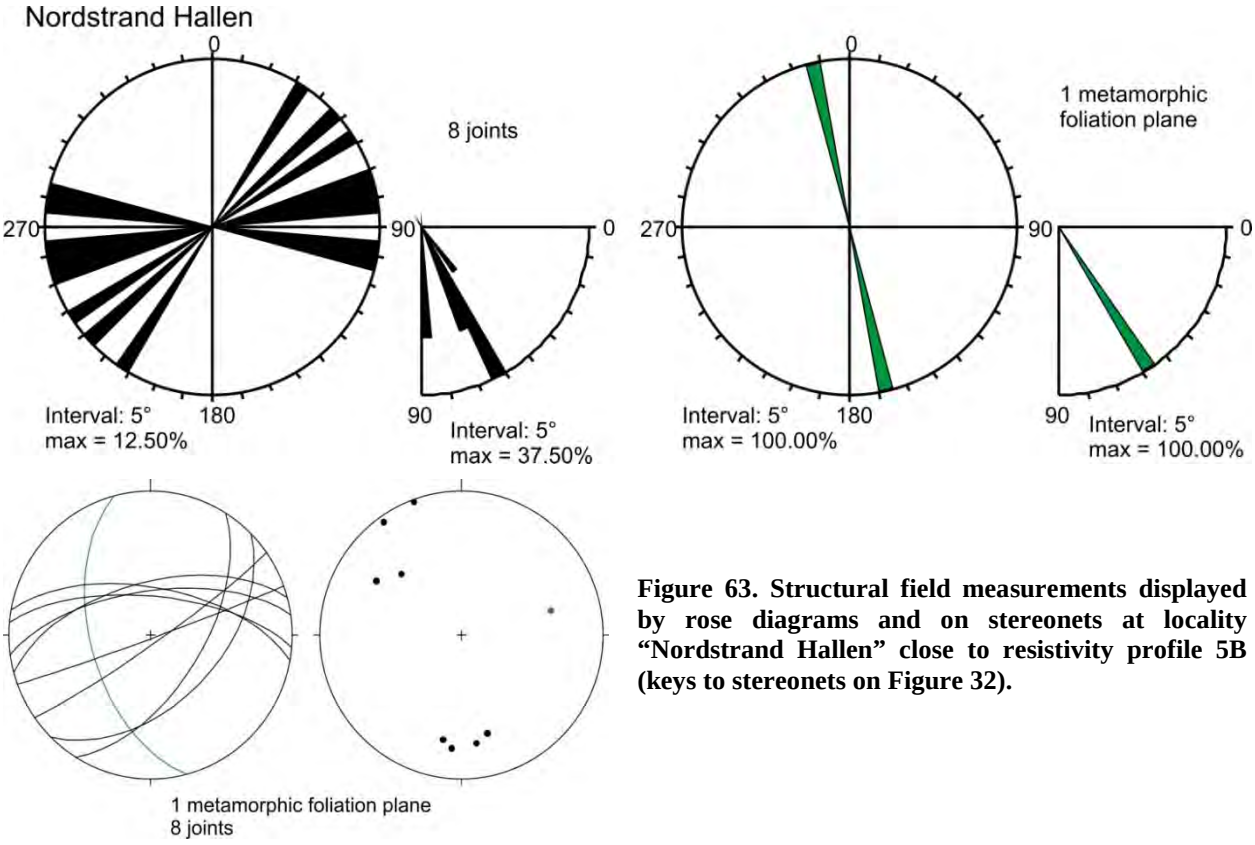

Figure 63. Structural field measurements displayed by rose diagrams and on stereonets at locality "Nordstrand Hallen" close to resistivity profile 5B (keys to stereonets on Figure 32).

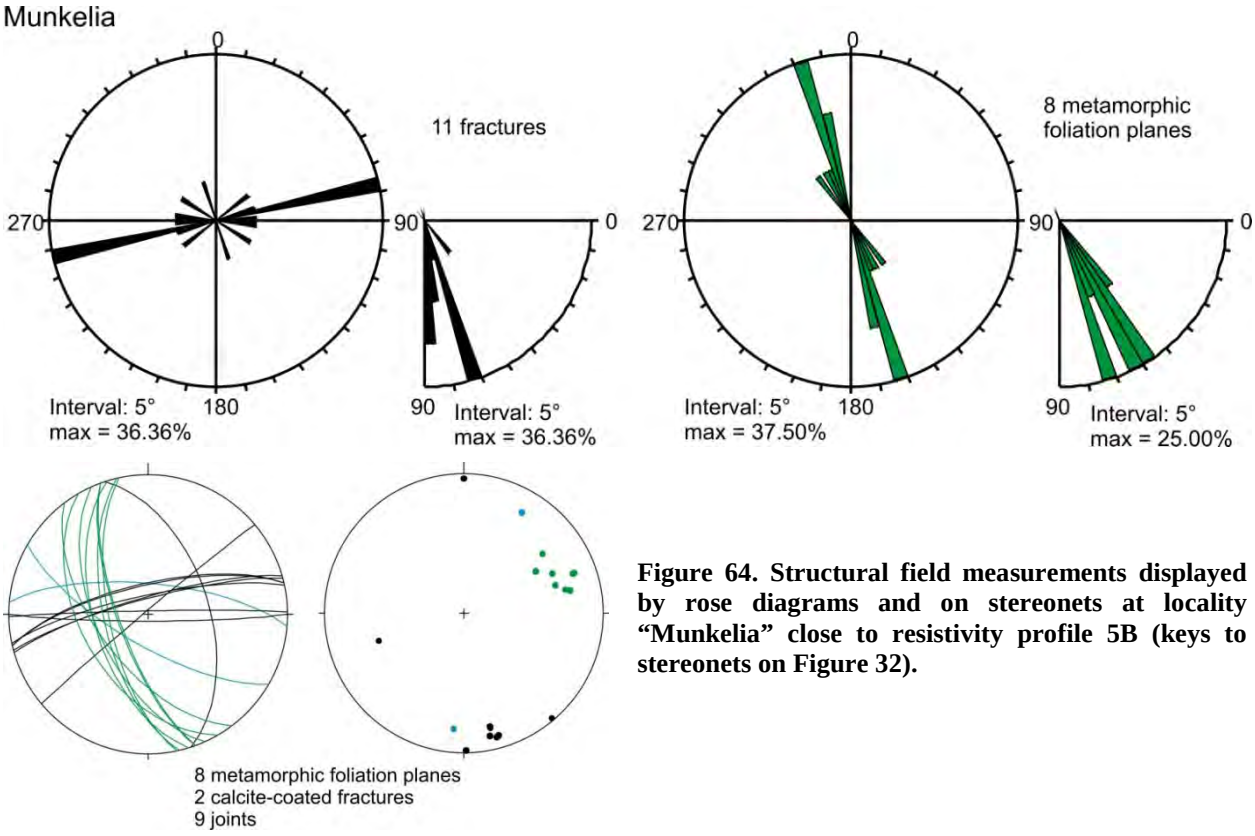

Figure 64. Structural field measurements displayed by rose diagrams and on stereonets at locality "Munkelia" close to resistivity profile 5B (keys to stereonets on Figure 32).

5.4.2 Field localities ”Nordstrand Kirke” and ”Breiens veien”

The structural field analysis carried out at the two field localities ”Nordstrand Kirke” and ”Breiens veien” are expected to provide information in order to determine the nature of the resistivity anomalies of profiles 6 and 7 (Figure 65).

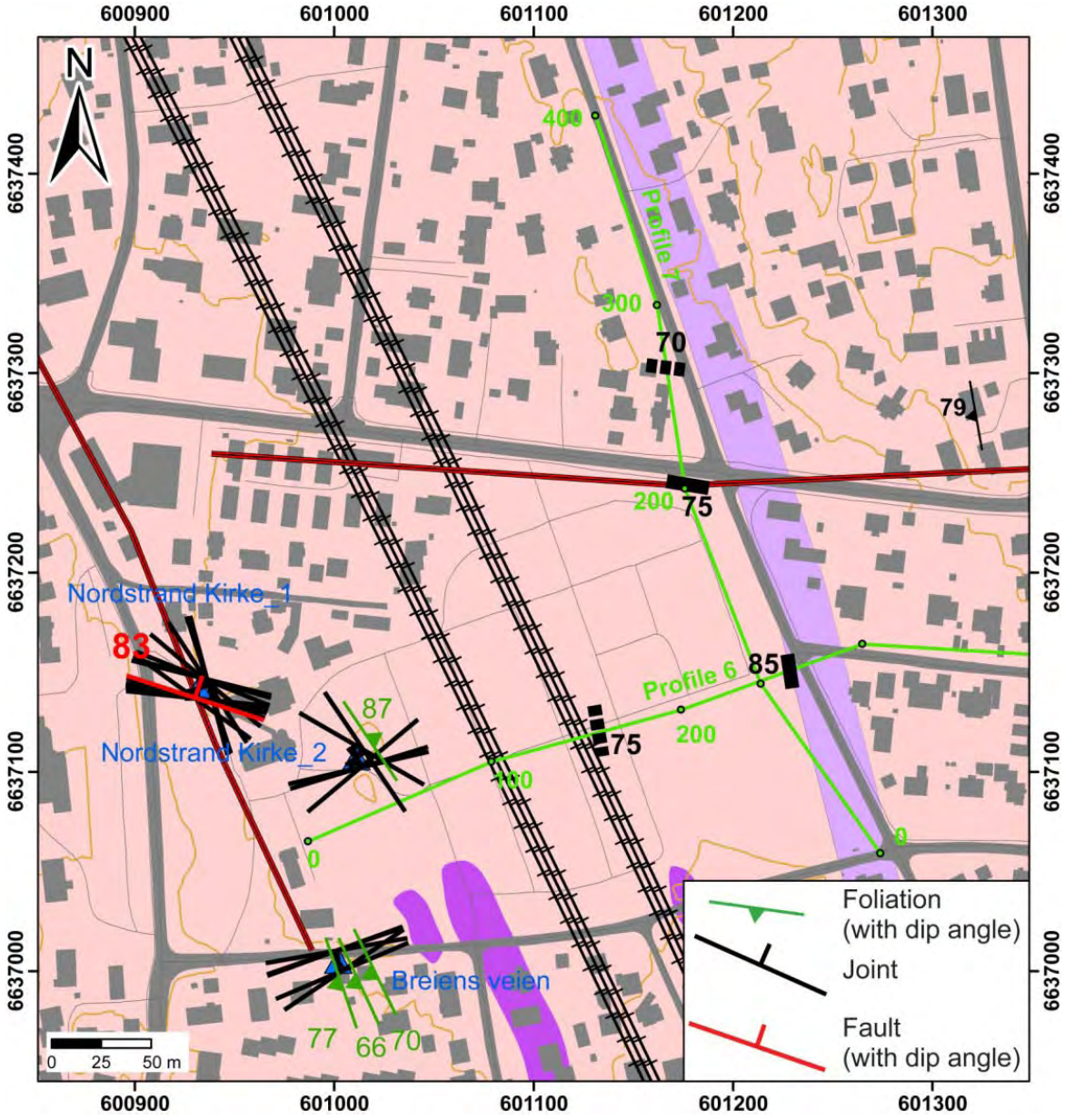

Figure 65. Structural field measurements at localities close to resistivity profiles 6 and 7 (caption of background map as Figure 34 and of interpreted resistivity anomalies as Figure 5).

Field locality “Nordstrand Kirke”

The field locality “Nordstrand Kirke” in the vicinity of resistivity profile 6 (Figure 65) consists of small outcrops of amphibolites. The metamorphic foliation is nearly vertical and strikes WNW-ESE (Figure 66). The joints have moderate to steep dip angles and dispersed around a WNW-ESE orientation (Figure 65 and Figure 66). A striated fault at field point “Nordstrand Kirke_2” trends parallel to the mean value of the joint set (Figure 65 and Figure 66). Whereas the field point “Nordstrand Kirke_2” is on a NNW-SSE lineament, the striated fault reminds of the WNW-ESE lineament located c. 100 m northward (Figure 65). However, at the same field point “Nordstrand Kirke_2”, some joints are well deviated from the WNW-ESE mean value

toward a NNW-SSE orientation which actually trends parallel to the NNW-SSE lineament and may represent the damage fractured zone of a large-scale fault.

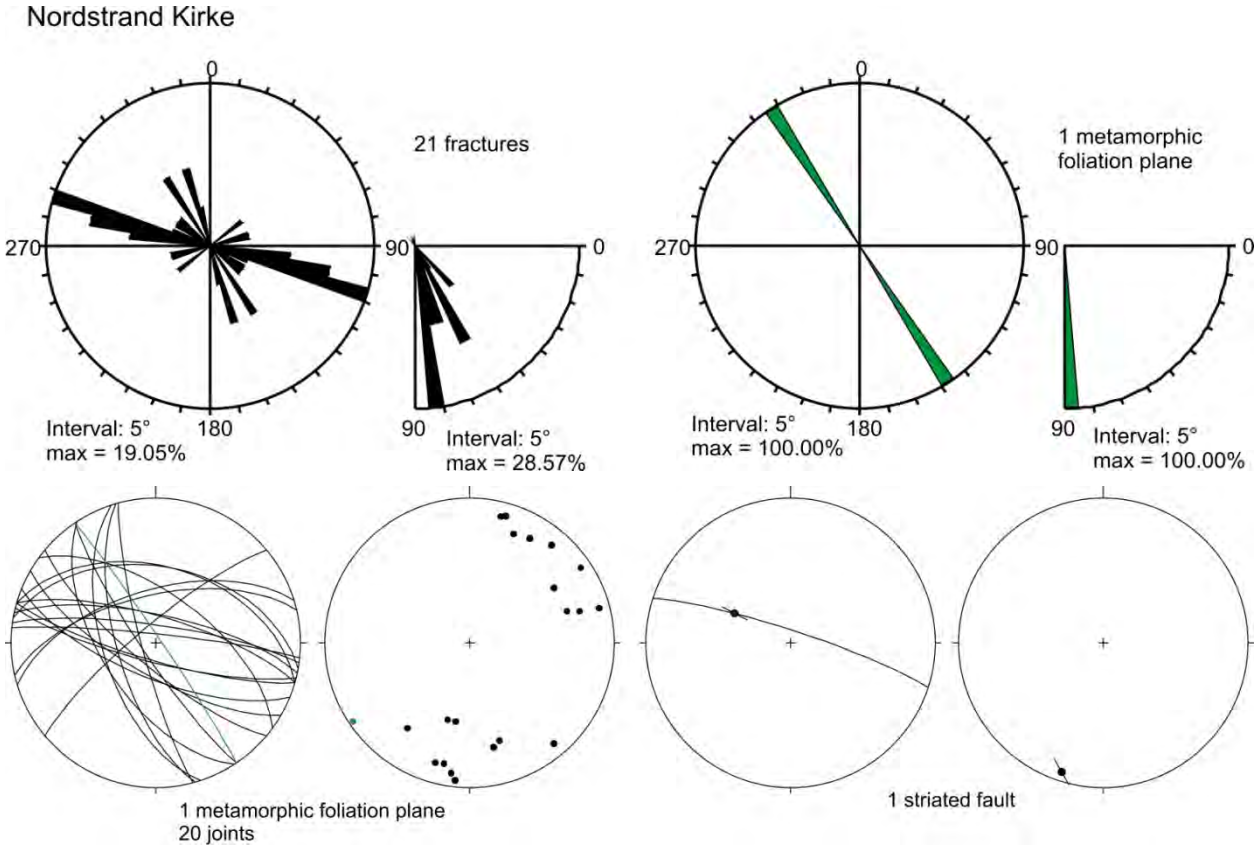

Figure 66. Structural field measurements displayed by rose diagrams and on stereonets at locality "Nordstrand Kirke" close to resistivity profile 6 (keys to stereonets on Figure 32 and Figure 33).

Field locality "Breiens veien"

The field locality "Breiens veien" is close to the resistivity profile 6 (Figure 65) displays a small some meters wide outcrop of strongly foliated gneiss and amphibolites (Figure 67). The metamorphic foliation is typical of the region with a steep dip toward the WSW (Figure 65 and Figure 67) as well as the only set of joints found is nearly vertical and WSW-ENE trending, therefore, perpendicular to the foliation (Figure 65 and Figure 67).

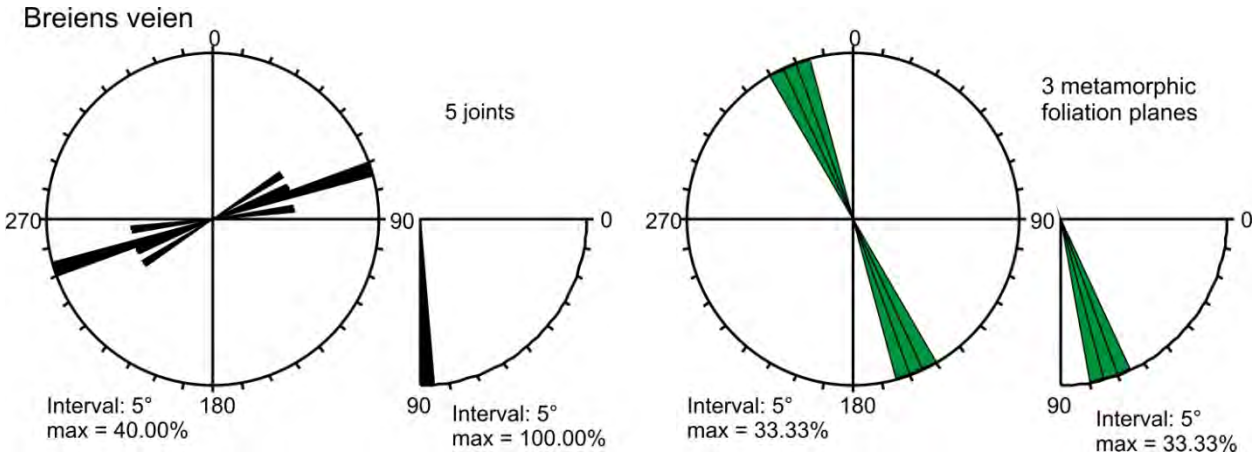

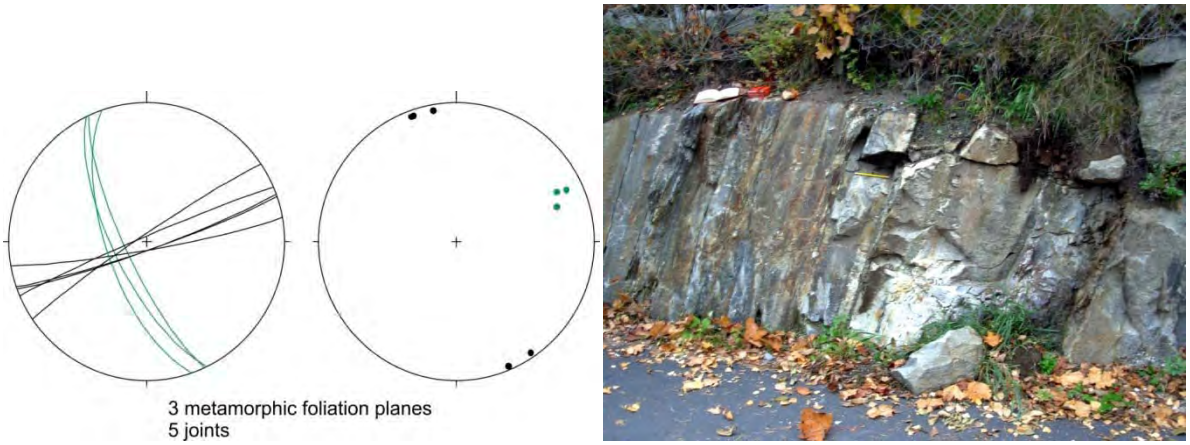

Figure 67. Structural field measurements displayed by rose diagrams and on stereonets at locality "Breiens veien" close to resistivity profile 6 (keys to stereonets on Figure 32) and photograph showing the strongly foliated gneiss and amphibolite at the outcrop.

5.4.3 Structural analysis around resistivity profiles 5-7: summary

None of the brittle structures observed at the field localities surrounding resistivity profiles 5A and 5B may explain the anomalies. It cannot be ruled out that the anomalies along both profiles 5A and 5B are due to the presence of amphibolitic lenses, which are mapped just north of the profiles (Figure 62).

One of the anomalies along resistivity profile 7 lays along a WNW-ESE lineament and one anomaly is parallel to a minor fault, observed at field locality "Nordstrand Kirke", as well as a large population of WNW-ESE brittle structures. It cannot be rules out that the WNW-ESE lineament may correspond to a fault zone detected along the resistivity profile 7 (Figure 65).

Whereas no brittle structures parallel to the NW-SE lineaments are observed at site 35 (Lutro et al. 2007), a set of NW-SE fractures are found at field locality "Nordstrand Kirke". Therefore it may be difficult to conclude that the NW-SE lineament corresponds to the metamorphic foliation and not to a large brittle structure. The anomalies along resistivity profile 7 may reflect similar NW-SE trending features and the presence of NW-SE elongated amphibolitic bodies in the vicinity may be the cause of the anomalies (Figure 61).

5.5 Structural analysis around resistivity profiles 8-9

Eight field localities with outcrops of variable size were studied in order to carry on the structural analysis needed to interpret the 2D resistivity profiles 8 and 9 (Figure 68). All measurements and field observations are listed in Appendix 2.

During the field campaign 2007, two field localities were visited in the vicinity of resistivity profile 8 (Figure 68). At site 34, a population of minor striated faults reflects the NNW-SSE trend of the lineaments of the area (Figure 68; Lutro et al. 2007). At site 32, steep minor faults trends strictly parallel to the lineament passing by the site (Figure 68; Lutro et al. 2007).

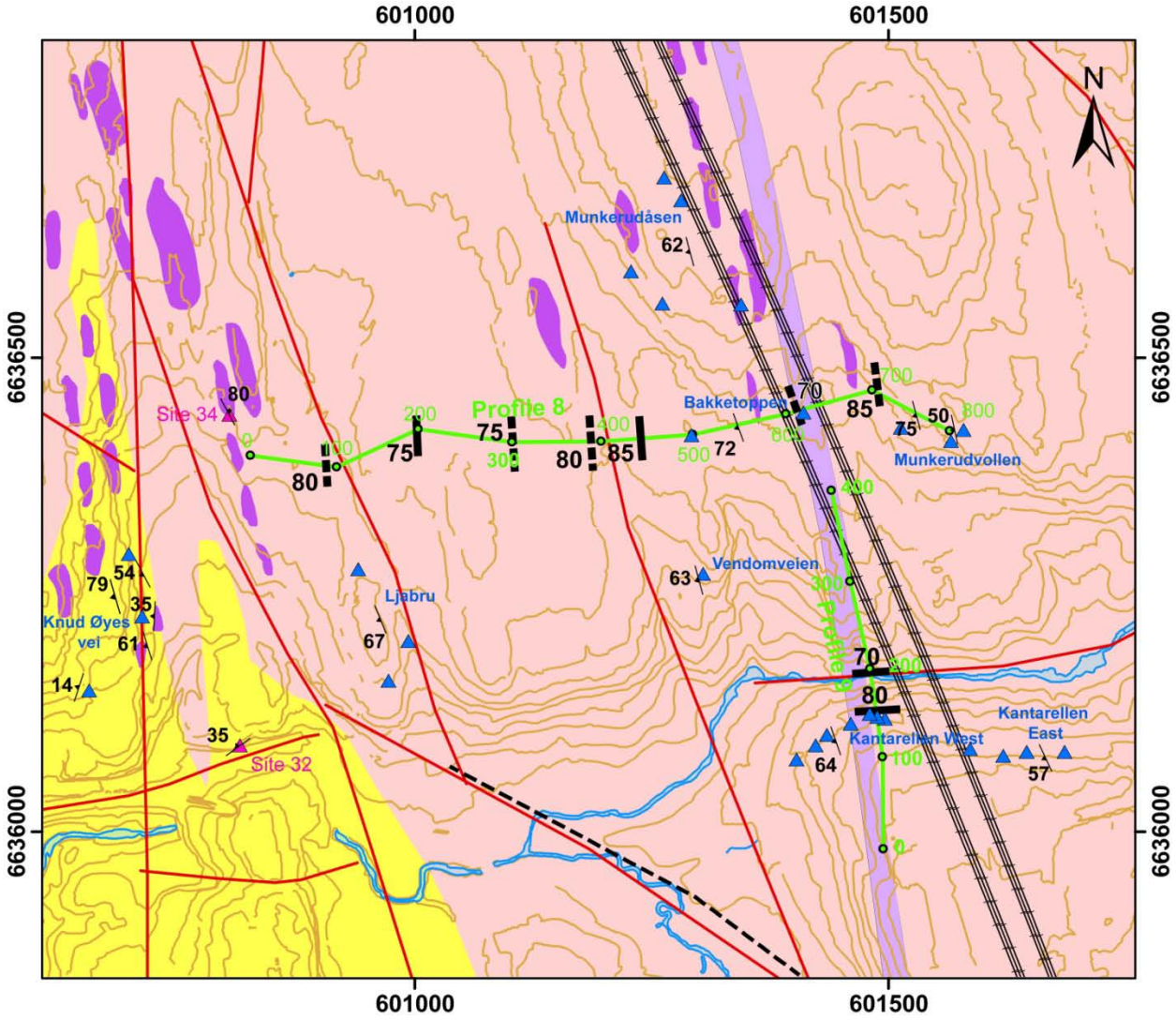

Figure 68. Field localities for structural analysis in the surrounding area of resistivity profiles 8 and 9 (caption as for Figure 34).

5.5.1 Field localities ”Munkerudåsen”, ”Bakketoppen” and ”Vendomveien”

The structural field study at the three localities ”Munkerudåsen”, ”Bakketoppen” and ”Vendomveien” may allow to better determine the cause of the anomalies detected along the resistivity profile 8 (Figure 69).

Field locality “Munkerudåsen”

The field locality “Munkerudåsen” is a 700 m long discontinuous outcrop divided in 5 points of observations (from “Munkerudåsen_1” to “Munkerudåsen_5”; Figure 69).

The metamorphic foliation follows the regional trend that is about 60° dipping to the WSW (Figure 69 and Figure 70). Other structures are also rather steep and roughly E-W trending including two large pegmatitic veins of 60 cm and 2 m wide, at field points “Munkerudåsen_2” and “Munkerudåsen_5” respectively (Figure 69 and Figure 70). Two striated faults dipping steeply to the north are observed and they are underlined by a set of mineralized fractures (Figure 69, Figure 70 and Figure 71).

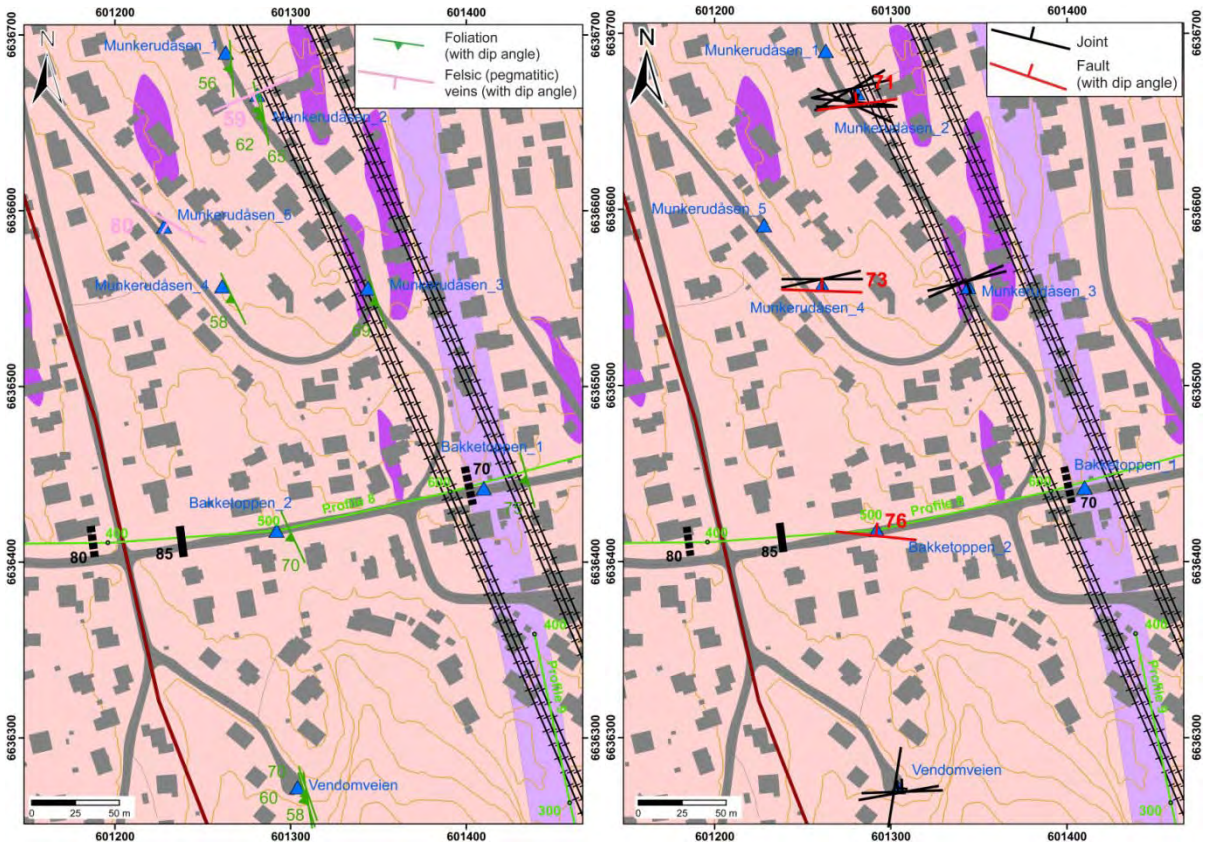

Figure 69. Structural field measurements at localities ”Munkerudåsen”, ”Bakketoppen” and ”Vendomveien” close to resistivity profiles 8 and 9 (caption of background map as Figure 34 and of interpreted resistivity anomalies as Figure 5).

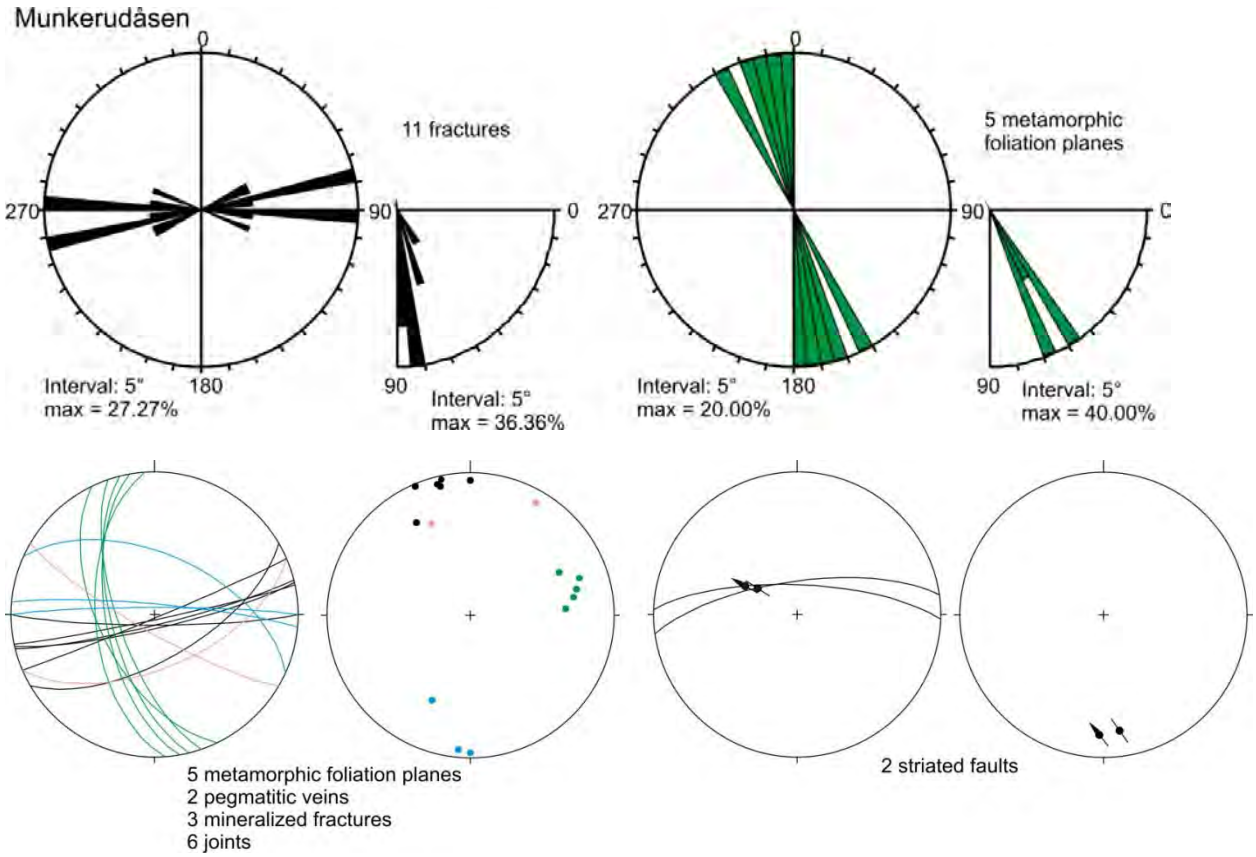

Figure 70. Structural field measurements displayed by rose diagrams and on stereonets at locality “Munkerudåsen” close to resistivity profile 8 (keys to stereonets on Figure 32 and Figure 33).

Figure 71. Photograph of a calcite- and chlorite-coated striated normal fault observed at field point "Munkerudåsen_4" (see location on Figure 69)

Field locality "Bakketoppen"

The field locality "Bakketoppen" is a discontinuous 100 m long outcrop along the resistivity profile 8 (Figure 69). One of the anomalies along the profile 8 obviously corresponds to the regional 20m wide rhomb porphyry dyke (Figure 69). The metamorphic foliation steeply dips to the WSW and one steep north-dipping striated fault is observed (Figure 72) that mirrors the faults found at the field locality "Munkerudåsen" close by (see preceding section and Figure 70).

Field locality "Vendomveien"

The field locality "Vendomveien" was investigated because it is located just south of a resistivity anomaly detected along profile 8 (Figure 69). However, the size of the outcrop is rather limited and only few measurements display the structure at this site. The metamorphic foliation resembles the one at the regional scale (Figure 69 and Figure 73). Besides the regionally well-represented E-W steep joint set a singular N-S shallow east-dipping large joint is also observed (Figure 69 and Figure 73).

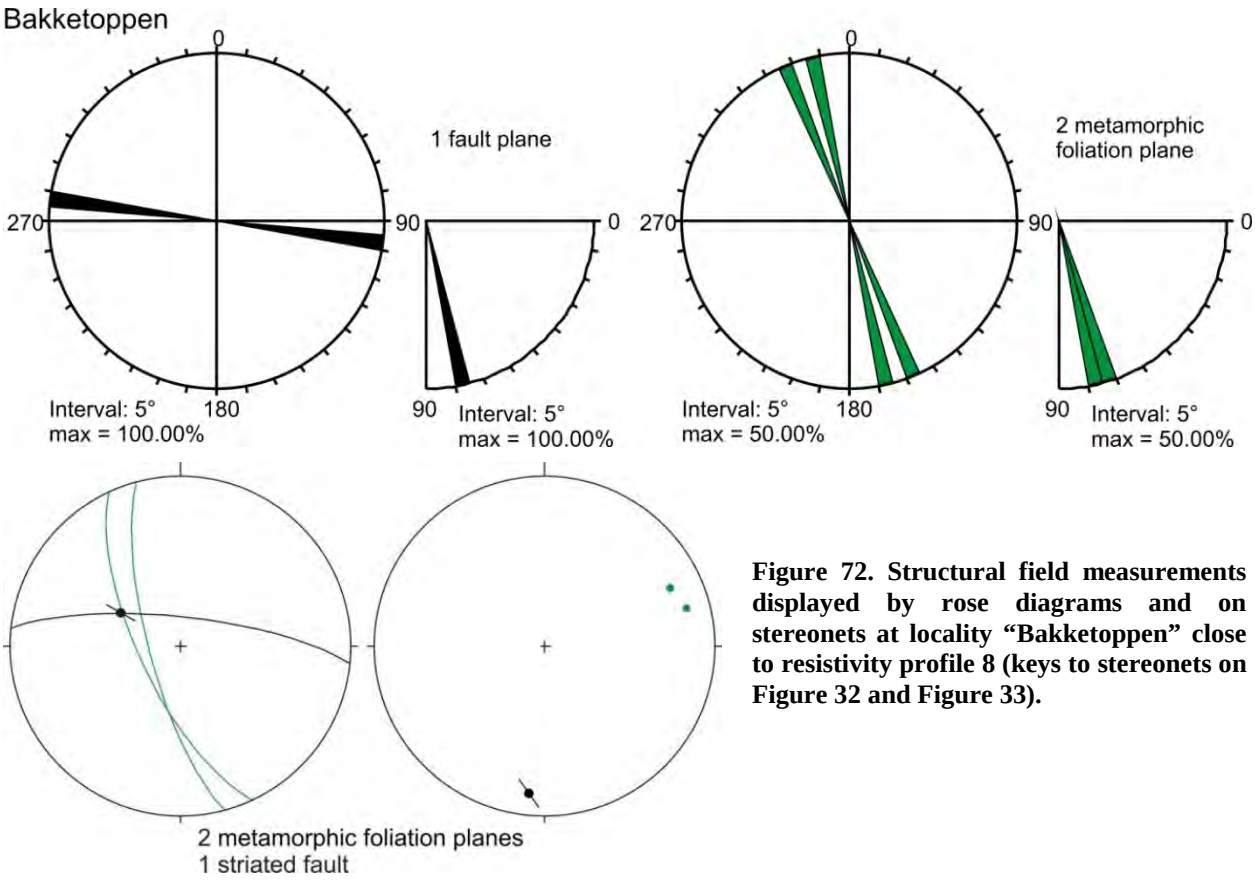

Figure 72. Structural field measurements displayed by rose diagrams and on stereonets at locality "Bakketoppen" close to resistivity profile 8 (keys to stereonets on Figure 32 and Figure 33).

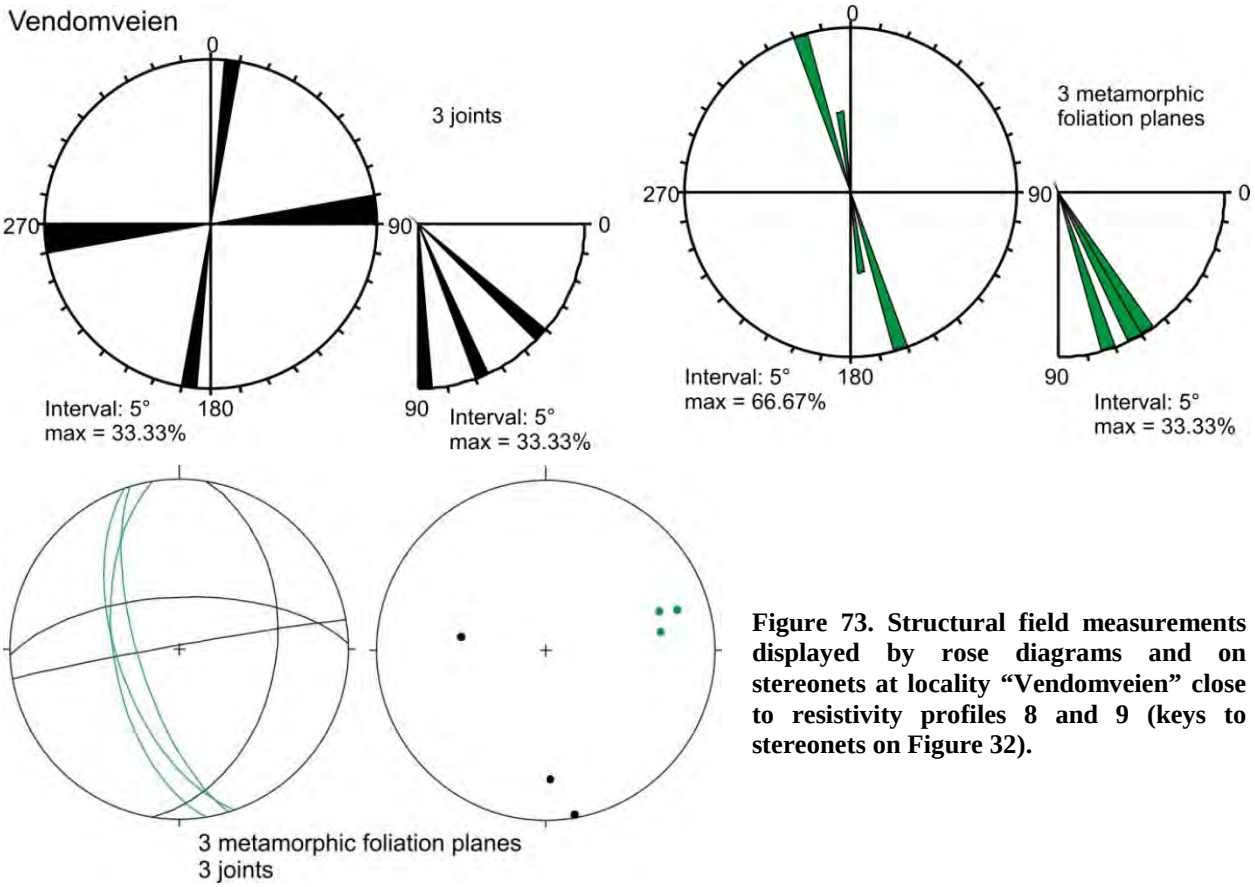

Figure 73. Structural field measurements displayed by rose diagrams and on stereonets at locality "Vendomveien" close to resistivity profiles 8 and 9 (keys to stereonets on Figure 32).

5.5.2 Field locality “Munkerudvollen”

The field locality “Munkerudvollen” is a road cut along the resistivity profile 8 where an anomaly is indicated west of point “Munkerudvollen_3” (Figure 74).

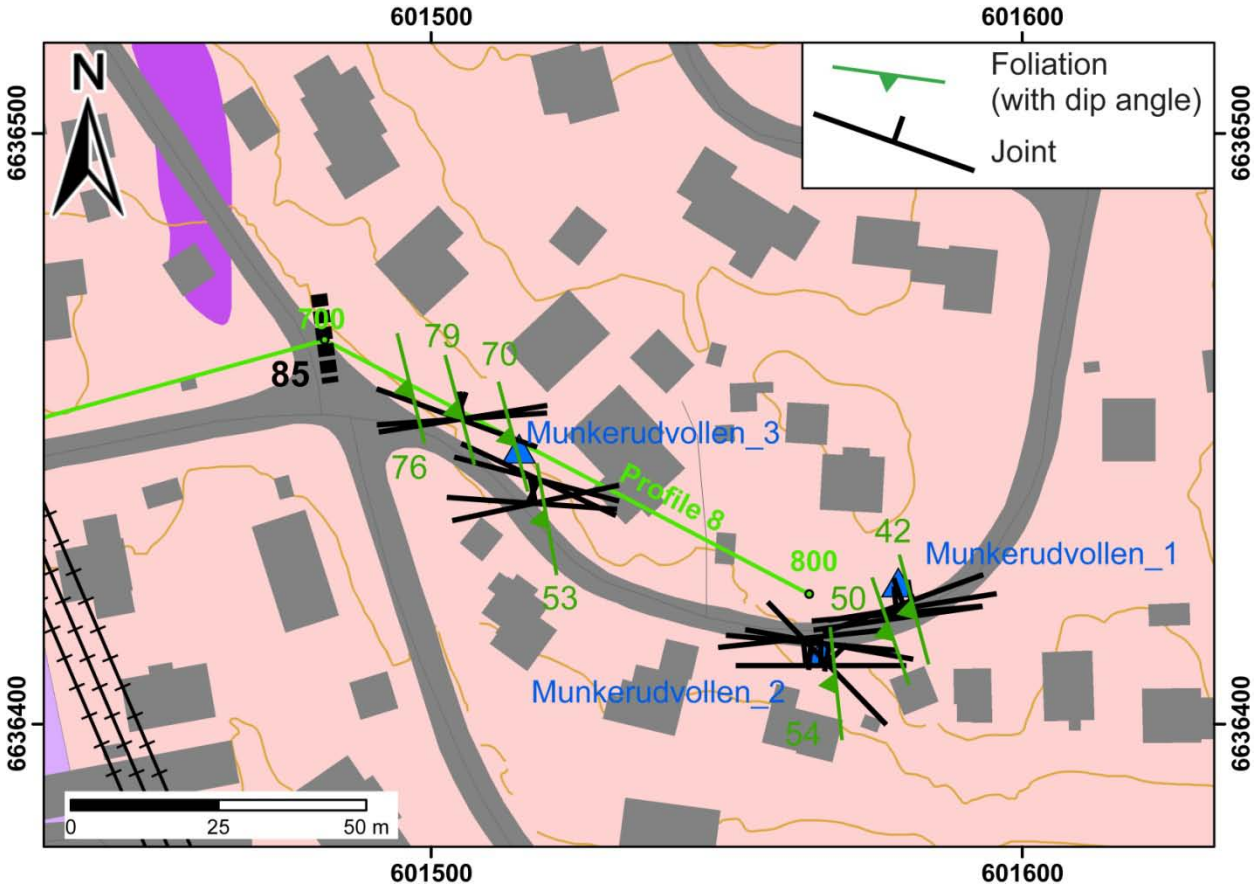

Figure 74. Structural field measurements at locality “Munkerudvollen” close to resistivity profile 8 (caption of background map as Figure 34 and of interpreted resistivity anomalies as Figure 5).

The foliation strikes NNW-SSE and steepens from east to west along the outcrop with dip angles from c. 50° to above 75° (Figure 74 and Figure 75). The joints strike perpendicular to the foliation and are steep. Mineral-, mostly quartz-coating is frequent along the fractures (Figure 74 and Figure 75).

There is no brittle structure that strikes parallel to the resistivity anomaly. However, a lens of amphibolites is mapped close to the anomaly and because its location is uncertain on the map, it may be what the anomaly reflects.

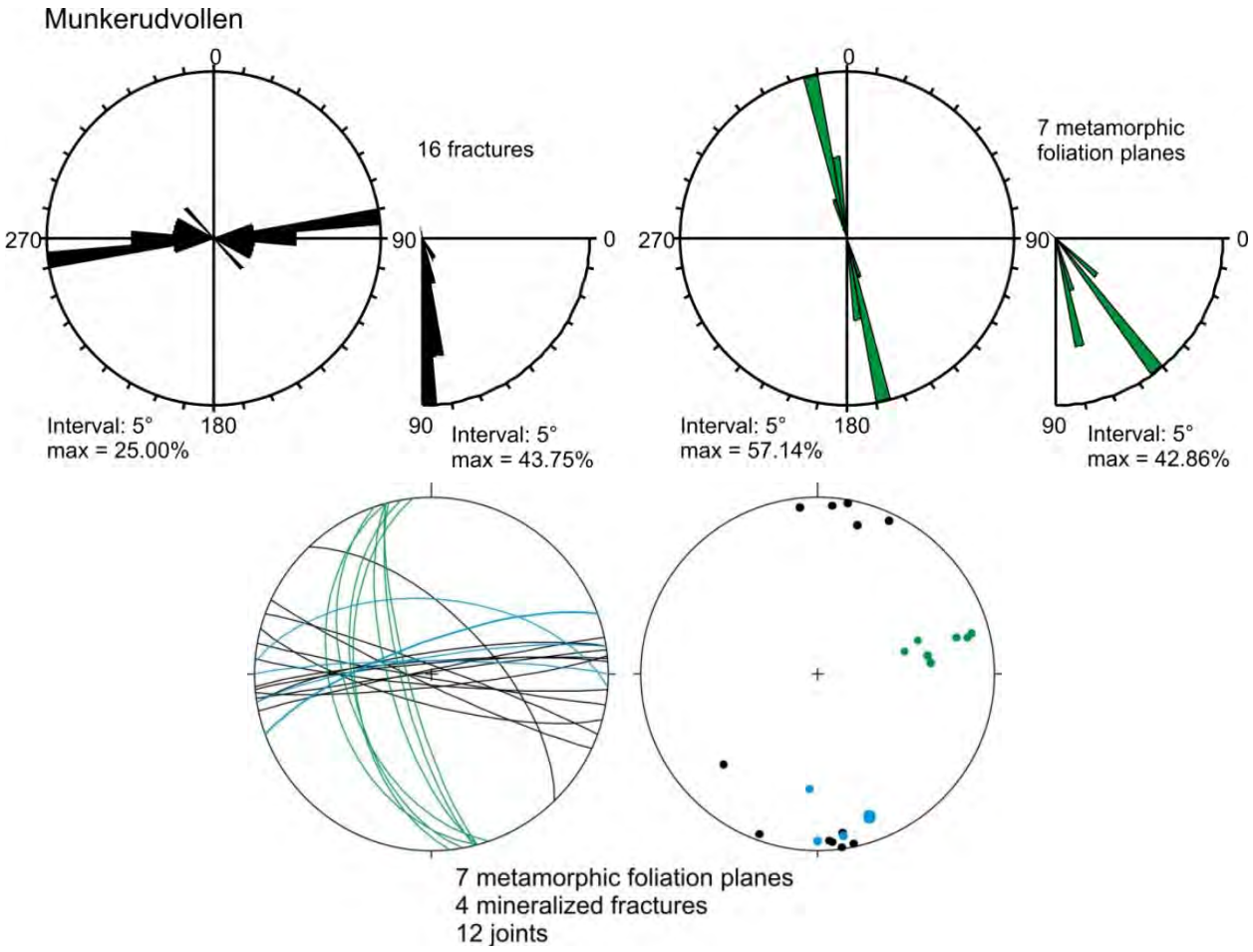

Figure 75. Structural field measurements displayed by rose diagrams and on stereonets at locality "Munkerudvollen" close to resistivity profile 8 (keys to stereonets on Figure 32).

5.5.3 Field localities "Ljabru" and "Knud Øyes vei"

The two field localities "Ljabru" and "Knud Øyes vei" are in the vicinity of the eastern tip of resistivity profile 8 (Figure 76).

Field locality "Ljabru"

The field locality "Ljabru" is just south of a resistivity anomaly detected along profile 8, which is also in line with a NNW-SSE lineament (Figure 76). From field point "Ljabru_1" to field point "Ljabru_2" a continuous, several meters high outcrop of garnet-rich gneiss is exposed. The metamorphic foliation is steeply dipping to the WSW in agreement with its regional attitude (Figure 76 and Figure 77). Steep to vertical WNW-ESE trending fractures form the main set of joints, which also corresponds to oblique – and strike-slip faults (Figure 77 and Figure 78). They are located on field point "Ljabru_1" and reflect the trend of the lineament mapped some 50 m farther south (Figure 76).Two other sets of joints are well defined: one dips about 60° to the north and the other one is vertical and striking ENE-ESE. The most remarkable structures along the outcrop are two large normal faults that developed along the foliation with, on one of the plane, the observation of a proto-breccia (Figure 77 and Figure 79).

The field point "Ljabru_3" is a very small outcrop which, however, displays one vertical fault plane trending parallel to the close NNW-SSE lineament (Figure 76).

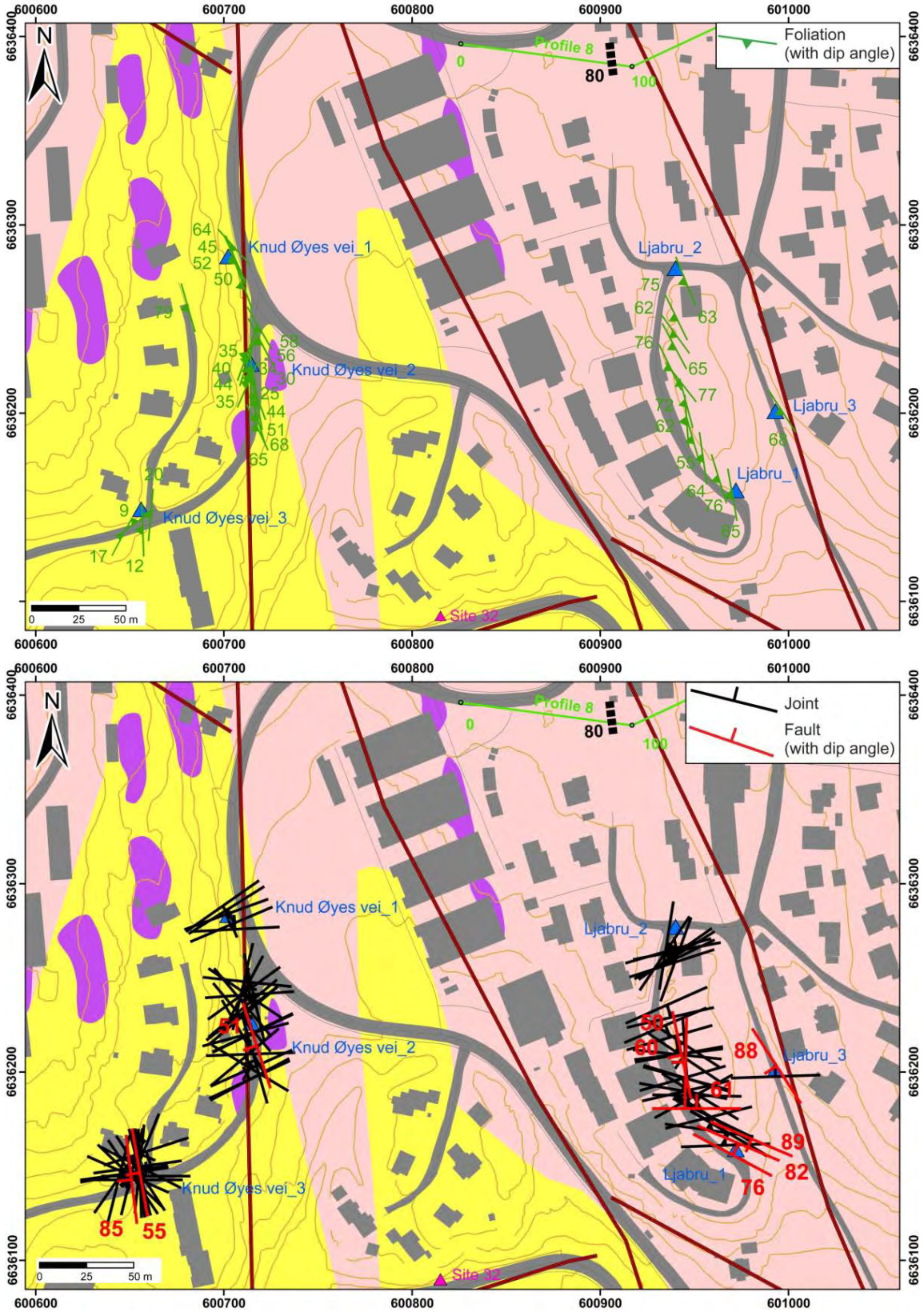

Figure 76. Structural field measurements at localities close to resistivity profile 8 (caption of background map as Figure 34 and of interpreted resistivity anomalies as Figure 5).

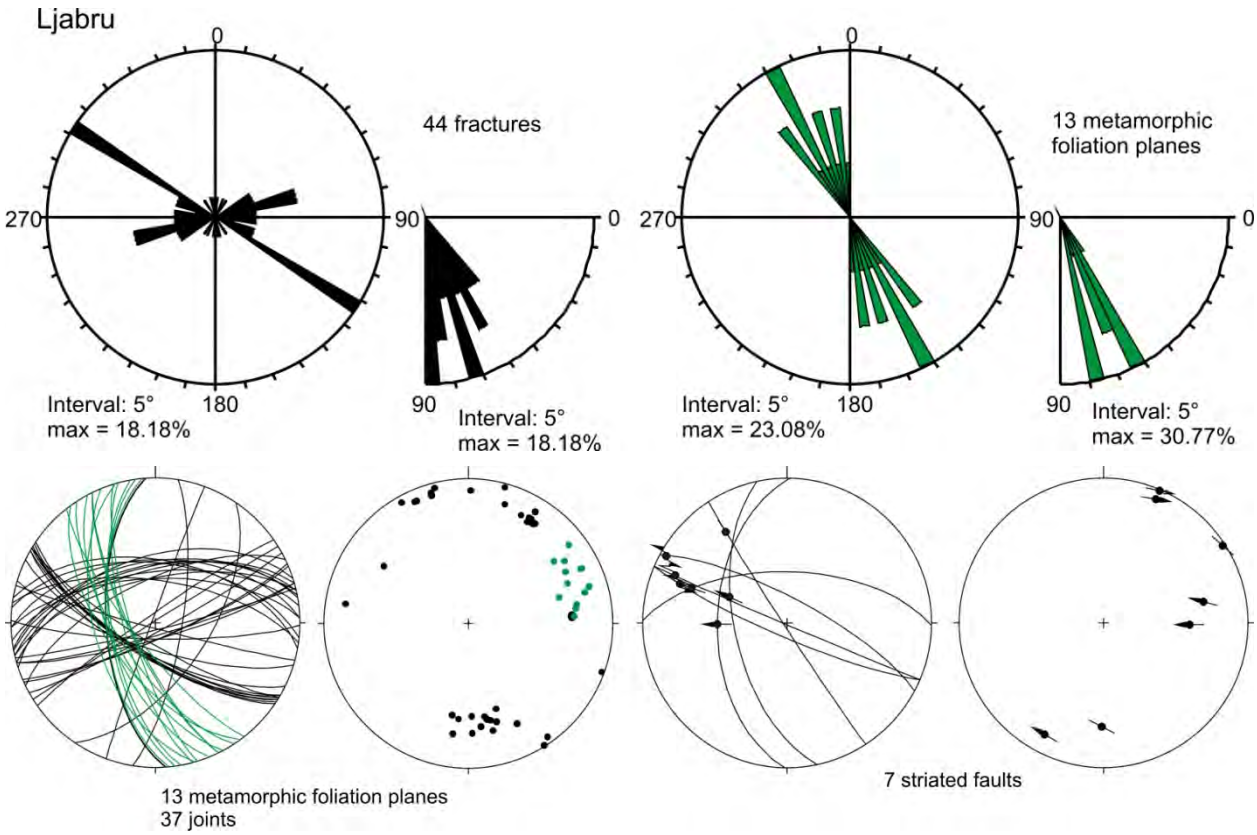

Figure 77. Structural field measurements displayed by rose diagrams and on stereonets at locality "Ljabru" close to resistivity profile 8 (keys to stereonets on Figure 32 and Figure 33).

Figure 78. Photograph of a sinistral WNW-ESE steep fault at field point "Ljabru_1" (located on Figure 76).

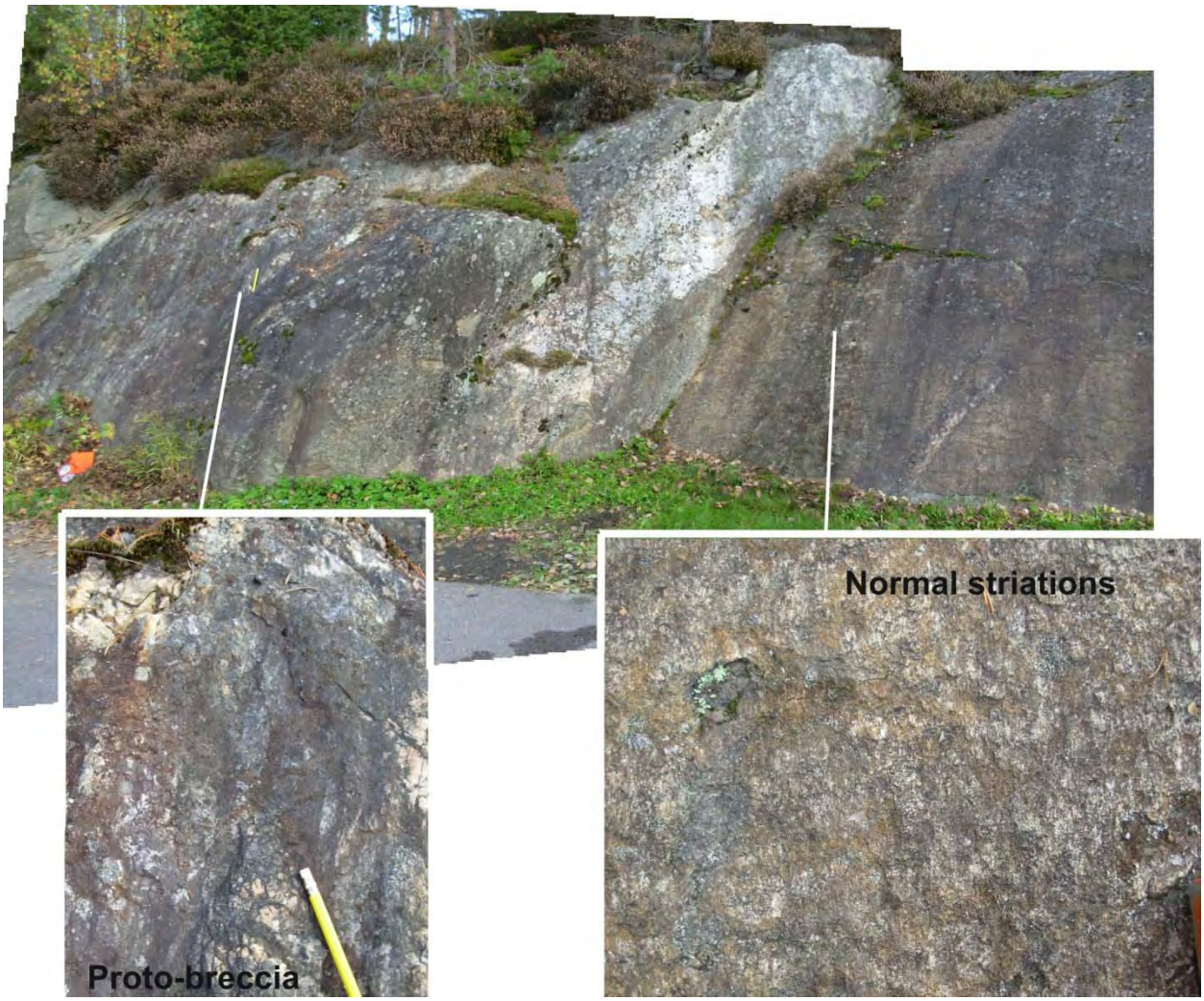

Figure 79. Photographs of normal faults which developed along the metamorphic foliation between field points ”Ljabru_1” and ”Ljabru_2” (located on Figure 76).

Field locality “Knud Øyes vei”

The field locality “Knud Øyes vei” is some hundred meters SW of resistivity profile 8 (Figure 76). The outcrop is discontinuous from field point “Knud Øyes vei_1” to field point “Knud Øyes vei_3” and display mafic units as biotite-rich gneiss and amphibolites but also felsic units as large ductilly deformed pegmatites (Figure 80). The metamorphic foliation is NNW-SSE trending with moderate to shallow dip angles, which flattens towards the west with dip angles below 20° at field point “Knud Øyes vei_3” (Figure 76, Figure 80 and Figure 81). There is dispersion in the fracturation of the rocks. However, a main set corresponds to steep joints trending SW-NE to WSW-ENE (Figure 76 and Figure 81). A set of large vertical chlorite-coated fractures forms a predominant structural grain, specifically at field point “Knud Øyes vei_3” (Figure 80 and Figure 81). Of interest is the presence of fractures including striated faults (Figure 76, Figure 81 and Figure 82) trending nearly parallel to a mapped N-S lineament passing by the two field points “Knud Øyes vei_1” and “Knud Øyes vei_2” (Figure 76). This lineament may correspond to a regional west-dipping fault.

Figure 80. Photographs of the outcrops at field point "Knud Øyes vei_1" displaying a large pegmatitic body juxtaposed to the shallow-dipping biotite-rich gneiss (left) and at field point "Knud Øyes vei_3" (view to W) where the foliation is close to horizontal (right), note the presence of large E-W trending and vertical joints; (field points located on Figure 76).

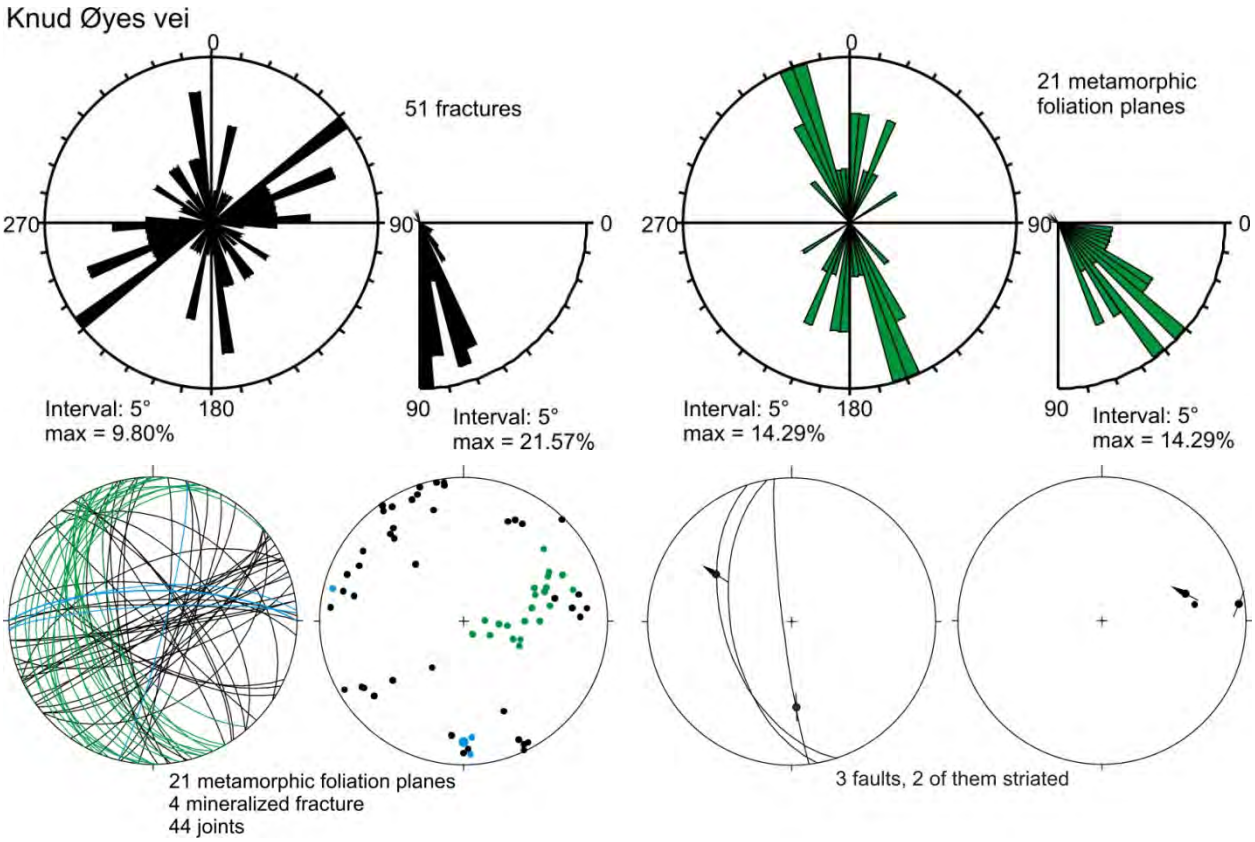

Figure 81. Structural field measurements displayed by rose diagrams and on stereonets at locality "Knud Øyes vei" close to resistivity profile 8 (keys to stereonets on Figure 32 and Figure 33).

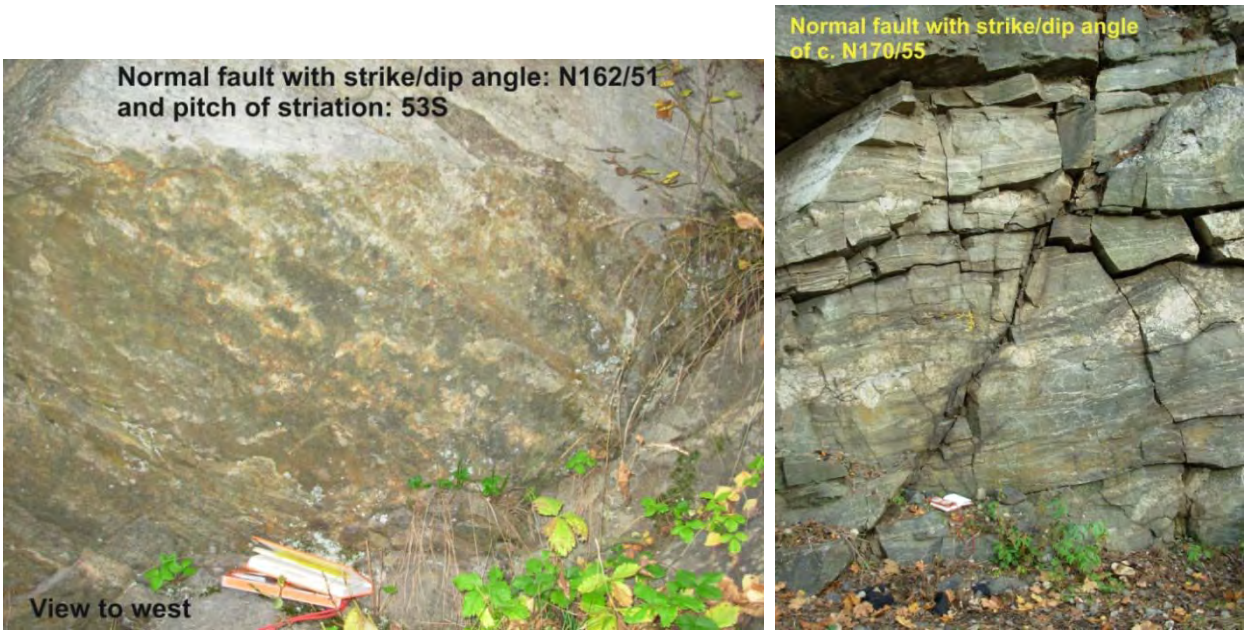

Figure 82. Photographs of normal faults at field point "Knud Øyes vei_2" displaying intense striations (left) and at field point "Knud Øyes vei_3" with an intense vertical fracturation in the vicinity of the main fault plane (right); (field points located on Figure 76).

5.5.4 Field localities "East Kantarellen" and "West Kantarellen"

The two field localities called "East Kantarellen" and "West Kantarellen" are close to resistivity profile 9 and to two resistivity anomalies approximately striking E-W; one of the anomalies superimposed on a E-W lineament (Figure 83).

Field locality "East Kantarellen"

The c. 50 m long outcrop at field locality "East Kantarellen" displays pegmatitic gneiss. The metamorphic foliation dips in average 60° to the WSW (Figure 83 and Figure 84). The main set of joints is E-W striking and steeply dipping to the north (Figure 83 and Figure 84). Between the field points "East Kantarellen_2" and "East Kantarellen_3" (Figure 83) the spacing of these joints is about 30-50 cm. At point "East Kantarellen_1" a meter thick pegmatitic vein is observed; it trends N080 and dips steeply to the NNW (Figure 83 and Figure 84). At point "East Kantarellen_2" a 1,5 m wide basaltic dyke is observed with a N016 strike and asub-vertical dip (Figure 83 and Figure 84).

Field locality "West Kantarellen"

The field locality "West Kantarellen" is a c. 150 m long outcrop. The metamorphic foliation is steeper than eastward along the "East Kantarellen" outcrop but keeps the same strike (Figure 83 and Figure 85). The same E-W trending and steep joint set is observed (Figure 83 and Figure 85). At point "West Kantarellen_4" a 10 cm basaltic dyke has developed parallel to foliation (Figure 83 and Figure 85). Between points "West Kantarellen_7" and "West Kantarellen_8" the regional 20 m wide rhomb porphyry dyke crops out (see on Figure 1); its eastern border strike strictly N-S (Figure 83 and Figure 85).
The most important observation along the outcrop is the set of 8 steep E-W to WNW-ESE trending faults, seven of them dipping toward the south (Figure 83, Figure 85 and Figure 86).

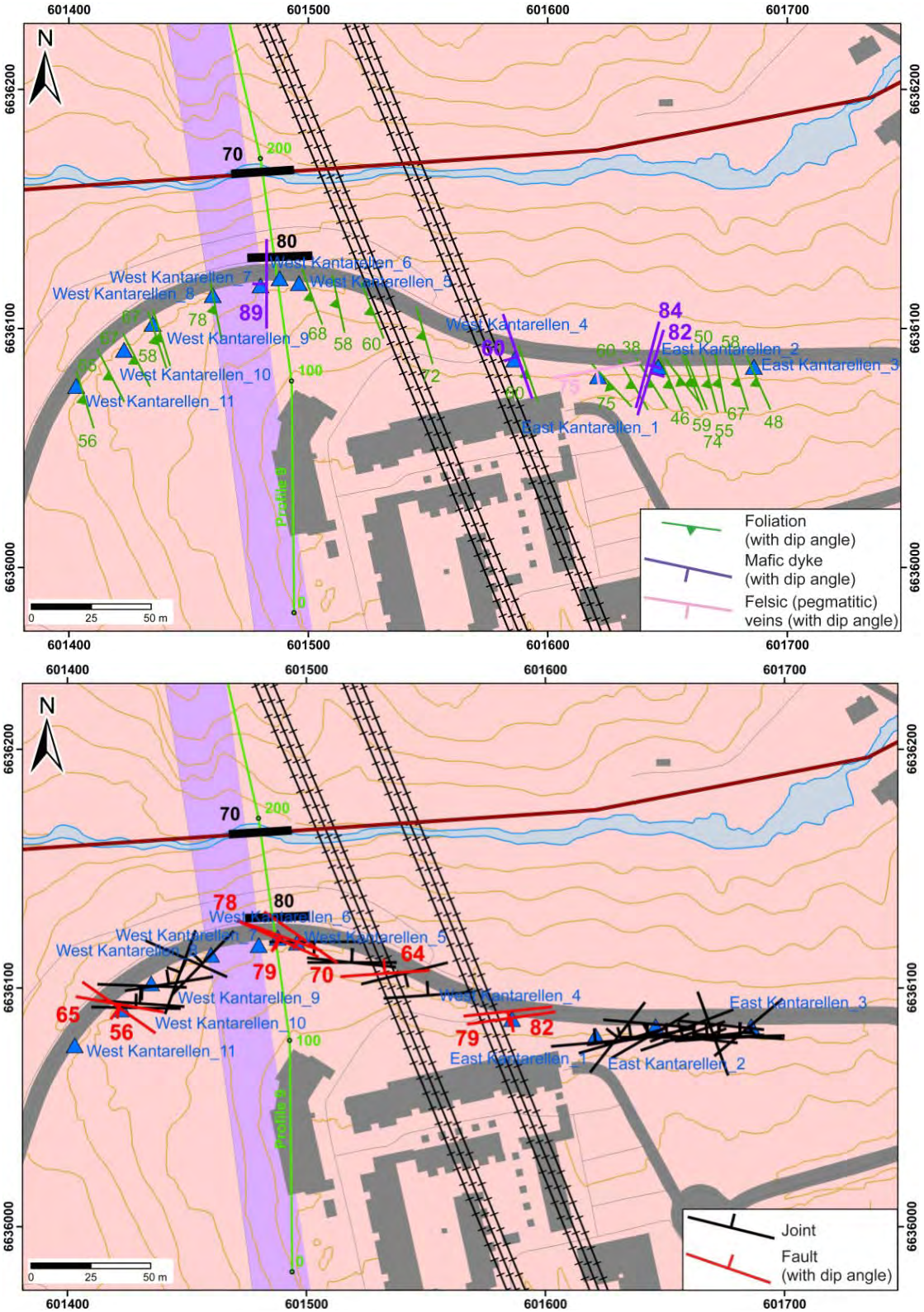

Figure 83. Structural field measurements at localities "East Kantarellen" and "West Kantarellen" close to resistivity profile 9 (caption of background map as Figure 34 and of interpreted resistivity anomalies as Figure 5).

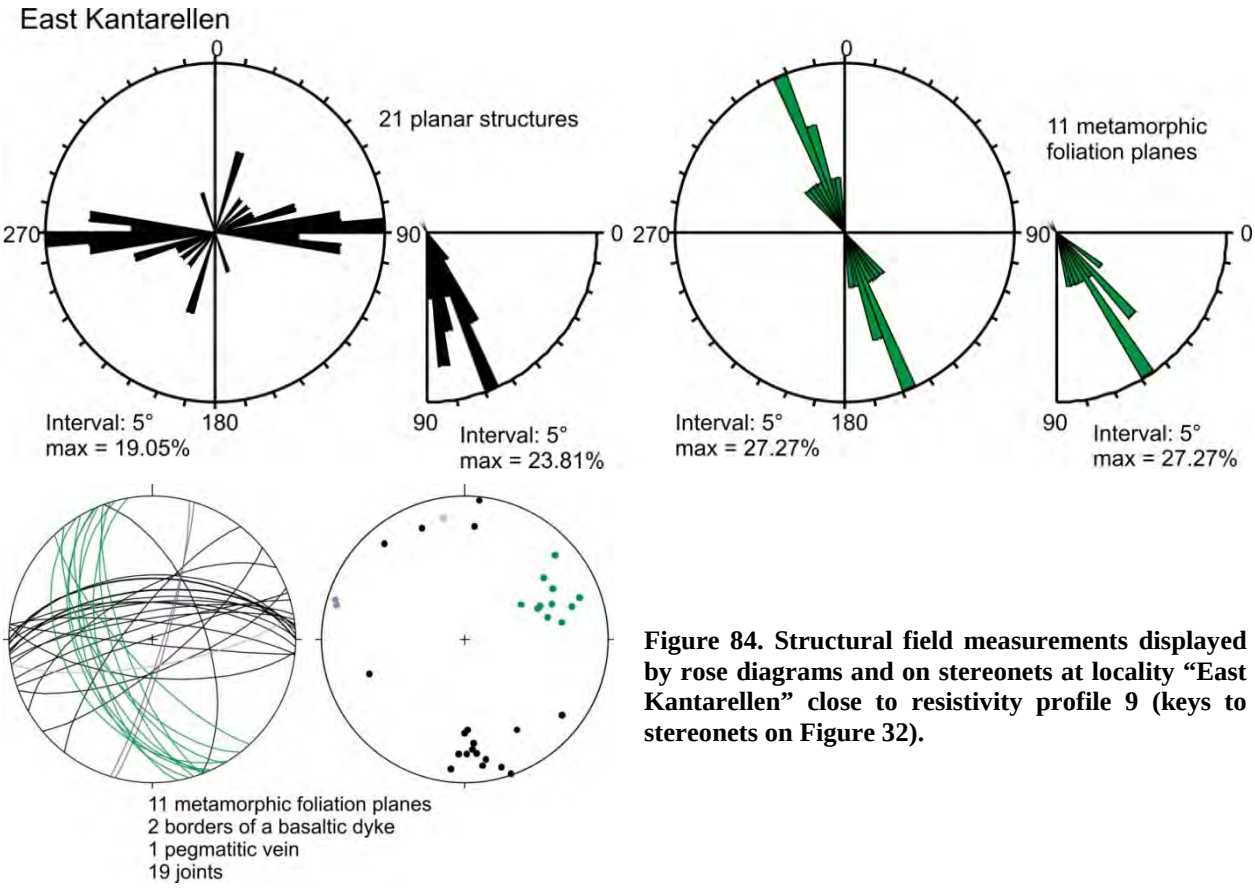

Figure 84. Structural field measurements displayed by rose diagrams and on stereonets at locality "East Kantarellen" close to resistivity profile 9 (keys to stereonets on Figure 32).

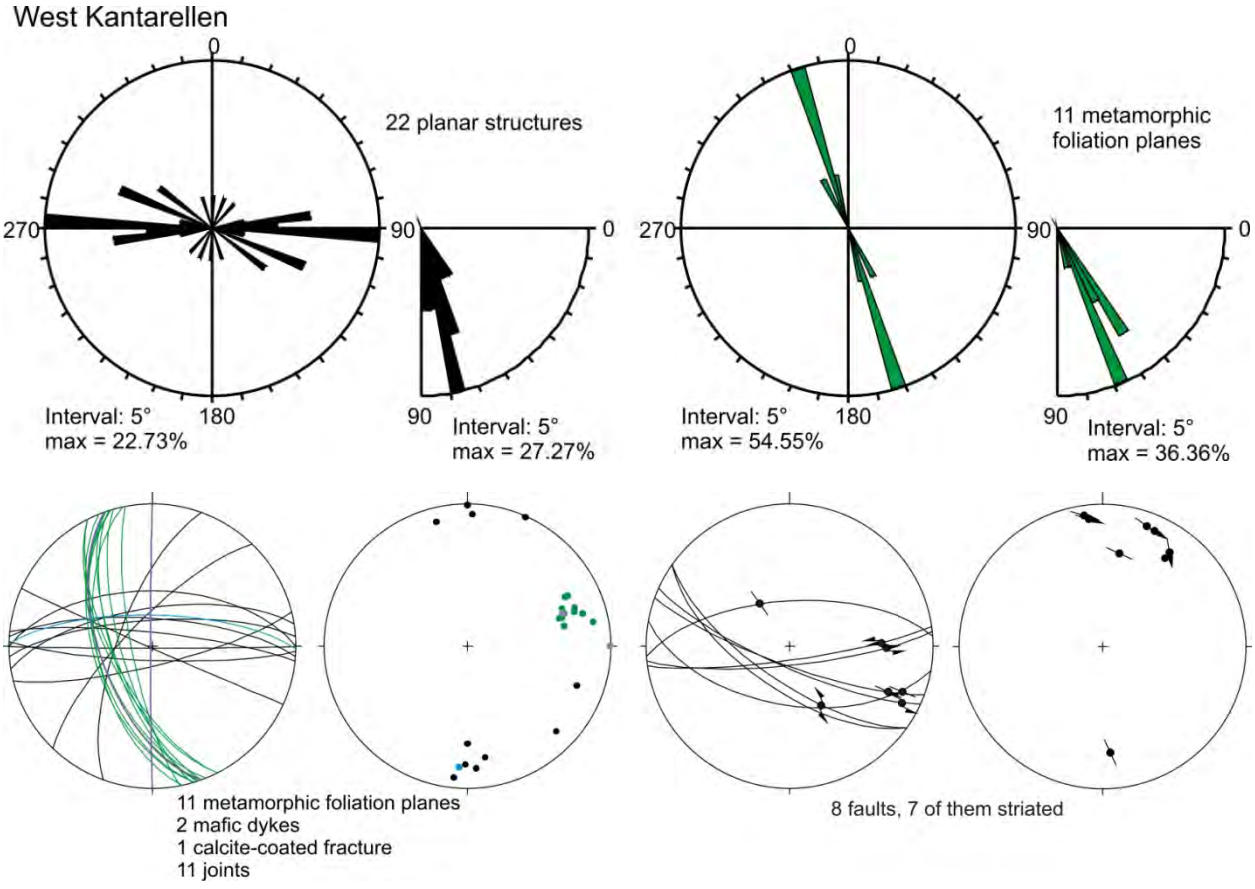

Figure 85. Structural field measurements displayed by rose diagrams and on stereonets at locality "West Kantarellen" close to resistivity profile 9 (keys to stereonets on Figure 32 and Figure 33).

Figure 86. Photographs of striated fault surfaces along the outcrop of field locality "West Kantarellen".

5.5.5 Structural analysis around resistivity profiles 8-9: summary

One of the anomalies along resistivity profile 8 obviously corresponds to the regional rhomb porphyry dyke as seen on Figure 68.

The other anomalies along the same profile 8 may correspond to foliation and amphibolitic lenses parallel to the foliation (Figure 68), but also to faults if we consider the large amount of striated faults trending roughly N-S collected at field localities "Ljabru", "Knud Øyes vei" and "Site 34". However, these faults might be restricted to the western part of the studied area (Figure 76) since the study of the field localities of the eastern part of the area ("Munkerudåsen", "Bakketoppen", "Vendomveien" and "Munkerudvollen") does not appear to unravel such brittle structures (see on Figure 69 and Figure 74).

Because of the predominant number of E-W brittle structures and specifically of striated faults along the outcrops of "East Kantarellen" and "West Kantarellen" field localities, we may assume that the E-W lineament located c. 50 m farther north (see on Figure 83) would be a steep regional fault zone that would be revealed by the resistivity anomalies along profile 9. Such a trend of faults is also commonly observed north at the field localities "Munkerudåsen" and "Bakketoppen" (Figure 69).

5.6 Structural analysis around resistivity profiles 13-15

Nine field localities with outcrops of variable size were mapped in order to carry on the structural analysis needed to interpret the anomalies of the 2D resistivity profiles 13, 14 and 15 (Figure 87). All measurements and field observations are listed in Appendix 2. One can note the change of the attitude of the metamorphic foliation from a NW-SE/NNW-SSE regional direction to a NE-SW direction, respectively from the northern to the southern parts of the area, and as displayed on the map on Figure 87.

During the field campaign 2007, field study was carried out at several sites in the area (Figure 87). Data from this previous study also shows that the foliation changes in attitude in the southern studied region and becomes NW-dipping (while it is WSW-dipping in the northern region; Figure 87). A large population of striated faults were observed at these sites and strikes from NW-SE to NE-SW (Lutro et al. 2007). An E-W set of faults underlines an already mapped fault (Figure 87).

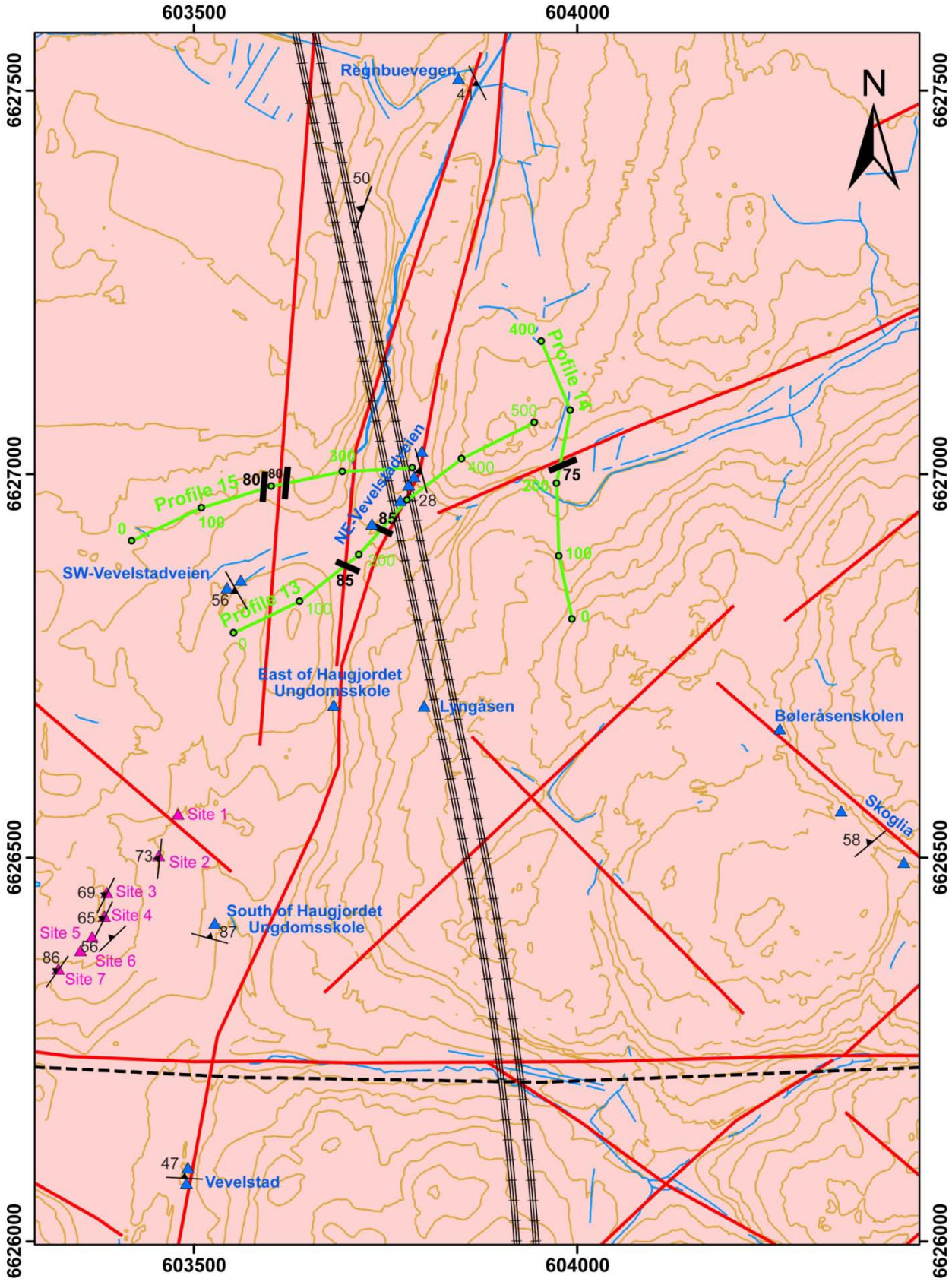

Figure 87. Field localities for structural analysis in the surrounding area of resistivity profiles 13, 14 and 15 (caption as for Figure 34); note the change in the attitude of foliation from a NW-SE/NNW-SSE direction to a NE-SW direction, from the northern to the southern parts of the area, respectively.

5.6.1 Field locality “Regnbuevegen”

Although the field locality “Regnbuevegen” is somehow far from the resistivity profiles 13, 14 and 15, which are investigated in this section, it is close to two of the N-S trending lineaments commonly observed in the region (Figure 87). The purpose of the study at this site was mainly to better characterise the nature of this lineament set.

The 100 m large outcrop at the field locality “Regnbuevegen” consists of amphibolites and patches of felsic gneiss units in its eastern part and of coarse massive gneissic rocks in its western part. The metamorphic foliation along the outcrop is NW-SE to NNW-SSE orientated and variably dips from about 30º to 60º toward the WSW and SW (Figure 88 and Figure 89).

The 34 fractures measured at this field locality display a rather significant geometrical dispersion (Figure 89). However, a set trending N-S with steep dip, parallel to the mapped lineaments in the area, predominates (Figure 88 and Figure 89). Nearly vertical WNW-ESE fractures and c. 50º north-dipping fractures are also two important sets (Figure 88 and Figure 89). Coating by quartz, hematite, orange zeolite or chlorite, is observed on all trends of fractures (Figure 89).

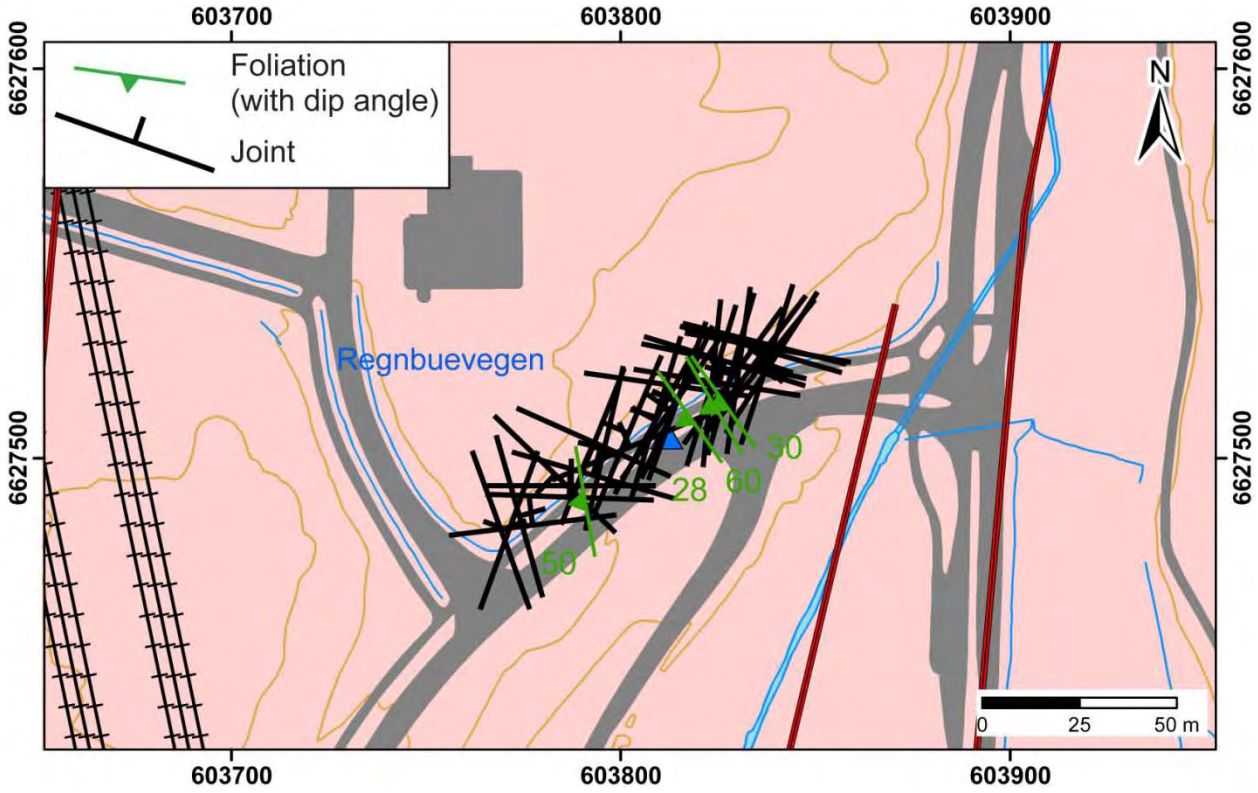

Figure 88. Structural field measurements at locality “Regnbuevegen” (caption of background map as Figure 34).

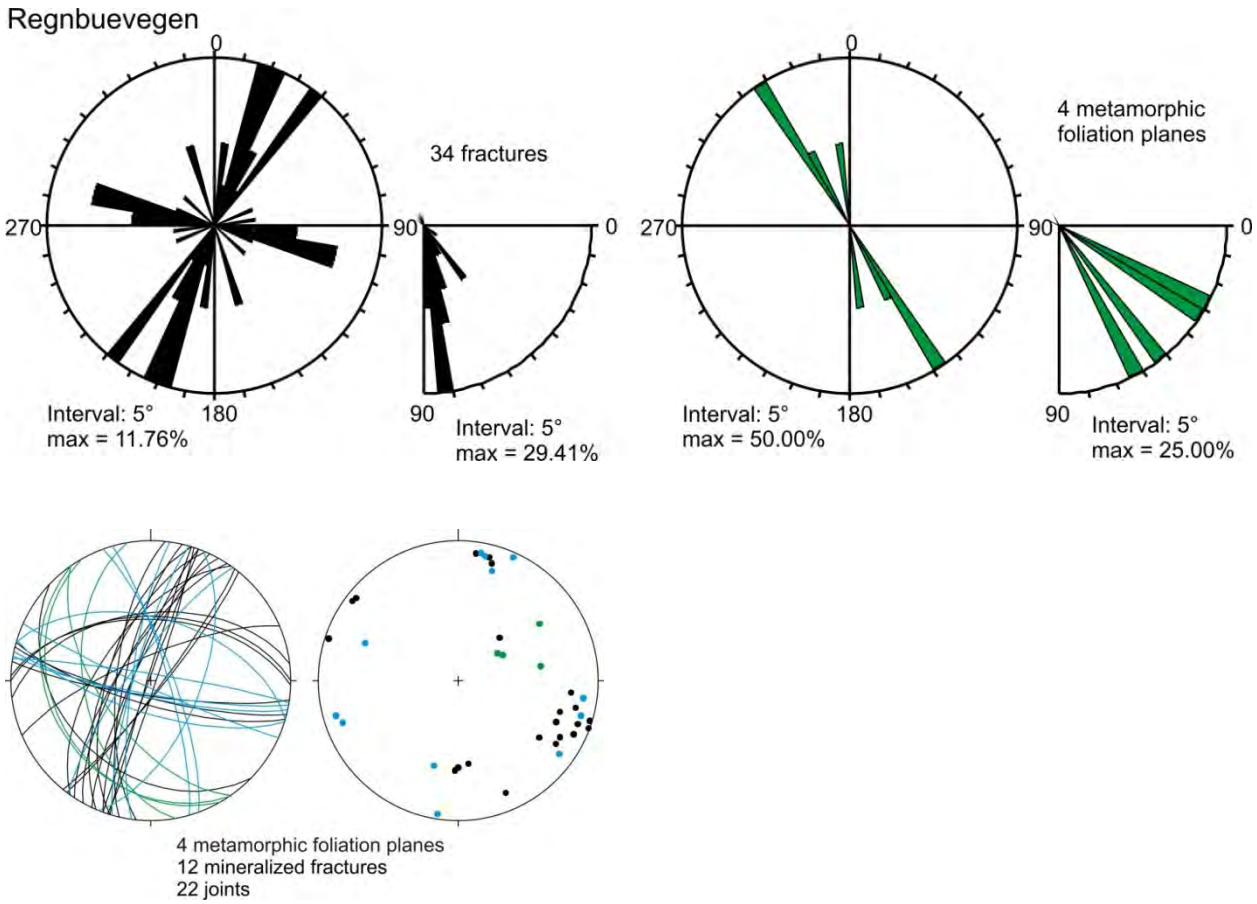

Figure 89. Structural field measurements displayed by rose diagrams and on stereonets at locality "Regnbuevegen" close to resistivity profiles 13, 14 and 15 (keys to stereonets on Figure 32).

5.6.2 Field locality "NE-Vevelstadveien"

"NE-Vevelstadveien" is a field locality between resistivity profiles 13 and 15. The c. 100 m long outcrop is aligned with a NNE-SSW mapped lineament (Figure 90).

The rocks alternate between felsic gneisses and amphibolites. The metamorphic foliation is gently dipping toward the west and WSW (Figure 90 and Figure 91). At field point "NE-Vevelstadveien_4" the contact between an overlying amphibolite and a felsic gneiss unit is faulted (Figure 92). The fault displays an undulated surface from a NE-SW vertical geometry to c. 50º WNW-dipping geometry corresponding to the two measurements of fault slips shown on Figure 90 and Figure 91. The two fault slips are sinistral as indicated by well-developed calcite steps (Figure 92). The fault measurements also correspond to the NNE-SSW mapped lineament (Figure 90). South-dipping 2 m and 5 cm wide pegmatitic veins are observed, respectively north and south of field point "NE-Vevelstadveien_4" (Figure 90, Figure 91 and Figure 92). Otherwise, the geometry of fractures is widespread and mineral coating is common on all direction (Figure 90 and Figure 91). NNW-SSE fractures, which are steeply dipping toward the WSW, form the most abundant set and commonly display zeolite- and calcite-coating (Figure 90 and Figure 91)

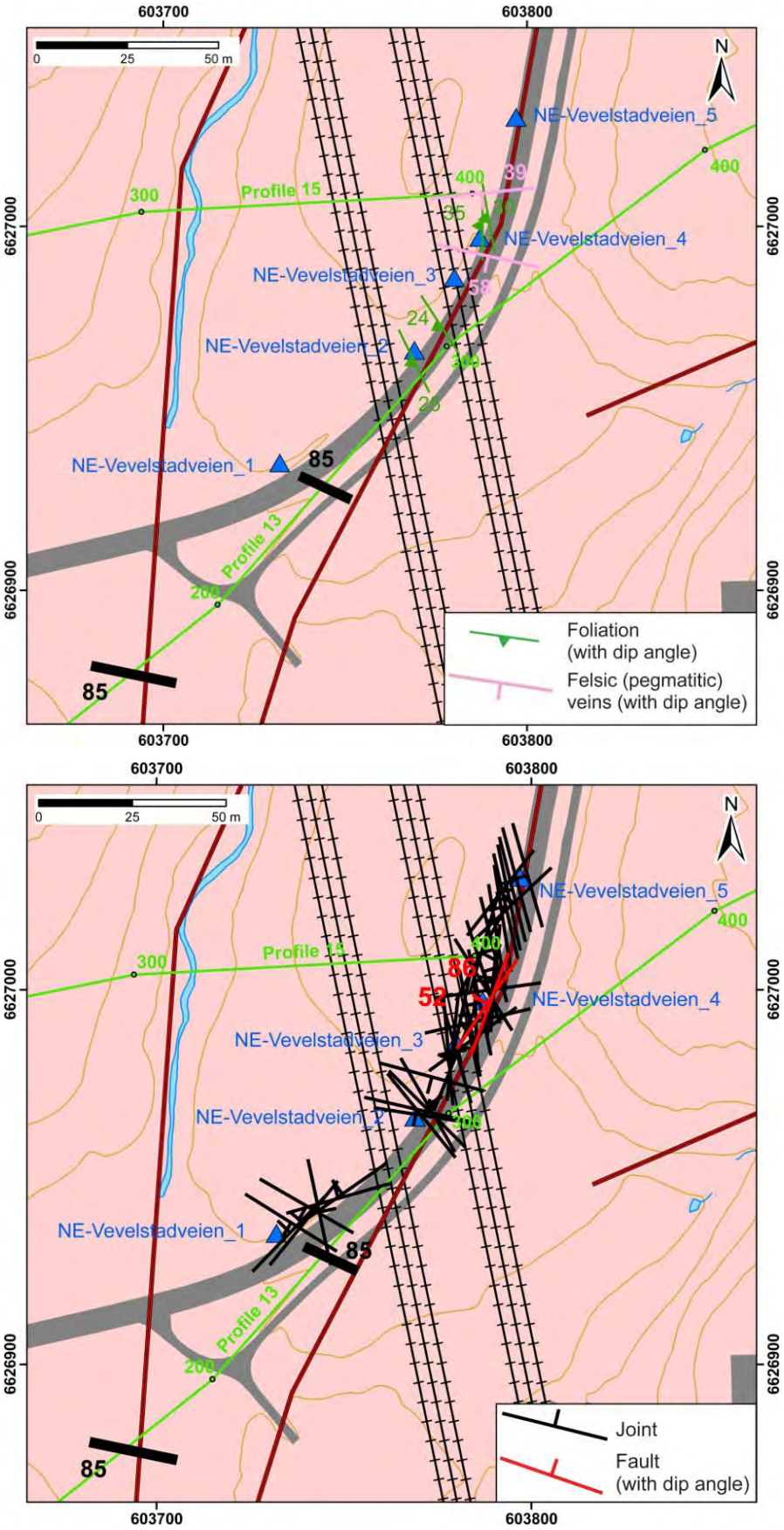

Figure 90. Structural field measurements at locality "NE-Vevelstadveien" close to resistivity profiles 13 and 15 (caption of background map as Figure 34 and of interpreted resistivity anomalies as Figure 5.

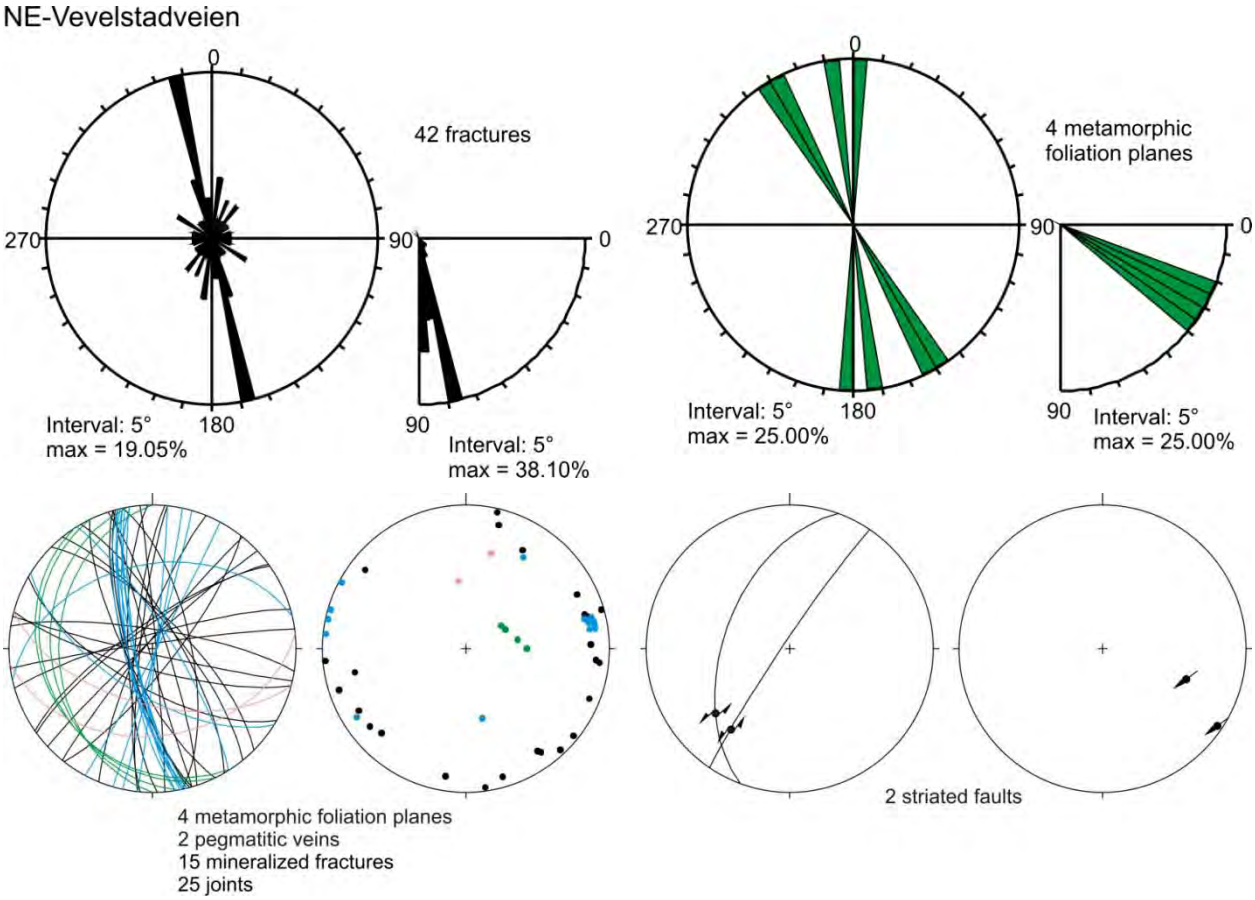

Figure 91. Structural field measurements displayed by rose diagrams and on stereonets at locality "NE-Vevelstadveien" close to resistivity profiles 13 and 15 (keys to stereonets on Figure 32 and Figure 33).

Figure 92. Faulted contact between a amphibolite and a felsic gneiss at field point "NE-Vevelstadveien_4" (located on Figure 90) and encapsulated photograph of the related calcite-stepped sinistral fault.

5.6.3 Field localities ”SW-Vevelstadveien” and ”East of Haugjordet Ungdomsskole”

The structures at the two field localities ”SW-Vevelstadveien” and ”East of Haugjordet Ungdomsskole” are analysed in the aim of identifying the 3 anomalies detected in resistivity profiles 13 and 15 and the nature of the N-S to NNE-SSW striking mapped lineaments (Figure 93).

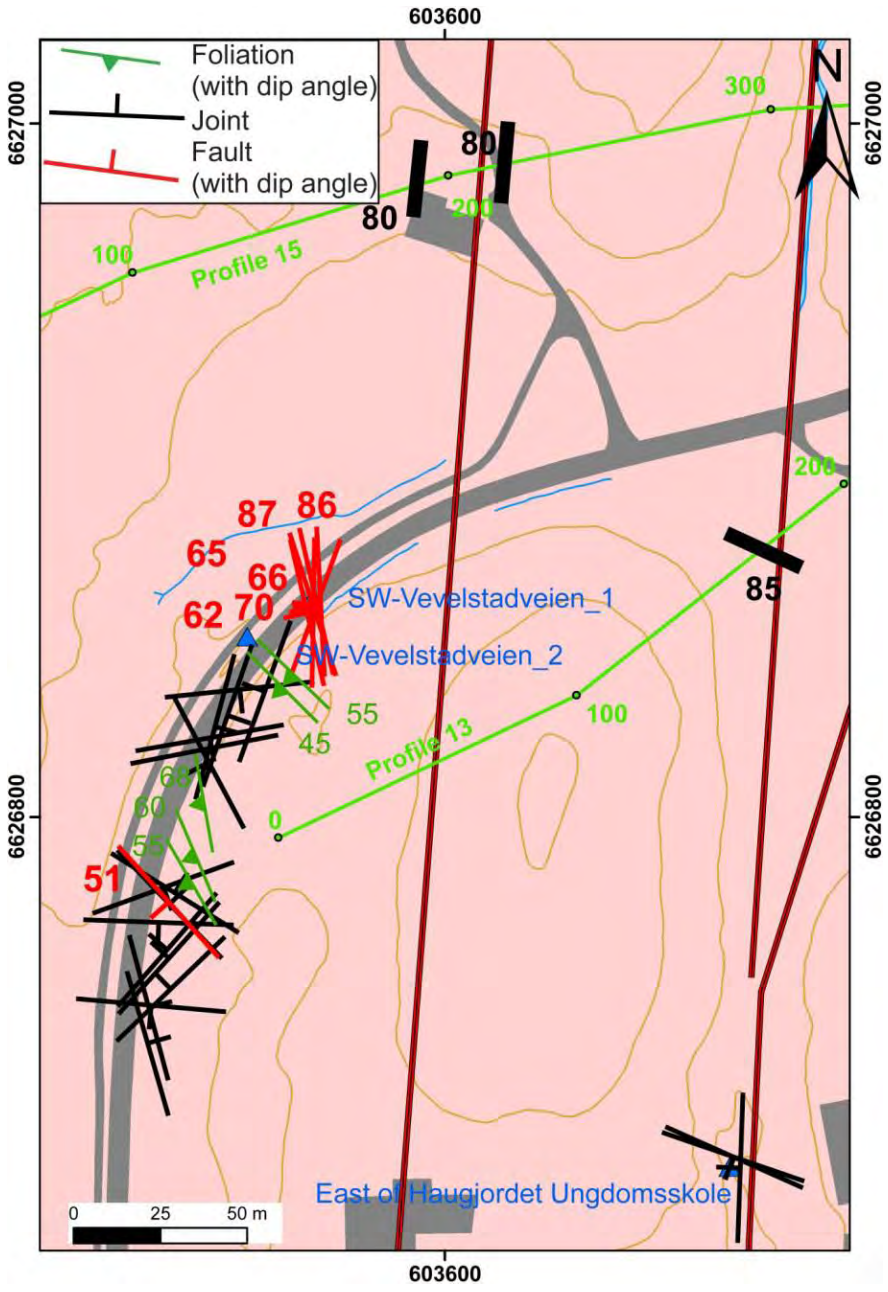

Figure 93. Structural field measurements at localities close to resistivity profile 13 (caption of background map as Figure 34 and of interpreted resistivity anomalies as Figure 5).

Field locality “SW-Vevelstadveien”

The field locality “SW-Vevelstadveien” is c. 50 m west of a N-S lineament that seems to correspond to the two anomalies along profile 15 (Figure 93). It is also a relevant place to investigate the anomaly indicated in profile 13 some 150 m to the east (Figure 93).

The outcrop of gneiss studied at this field locality is approximately 150 m long. The metamorphic foliation is rather constant in geometry with a moderate dip toward the SW and

WSW (Figure 93 and Figure 94). The dispersion of fractures is important both in terms of direction and dip angle (Figure 93 and Figure 94). A large set of steeply WSW dipping fractures has the same orientation as the striated faults measured at field point "SW-Vevelstadveien_1" (Figure 93 and Figure 94). These minor faults are found in the damage zones of a large N-S trending fault, which exhibits a 30 cm wide, chlorite-rich, fine-grained, brecciated fault core. The total width of the damage zone and the fault core is of approximately 2 m. South of the outcrop, in the wood, is a topographic step that aligns with the mapped fault (Figure 95).

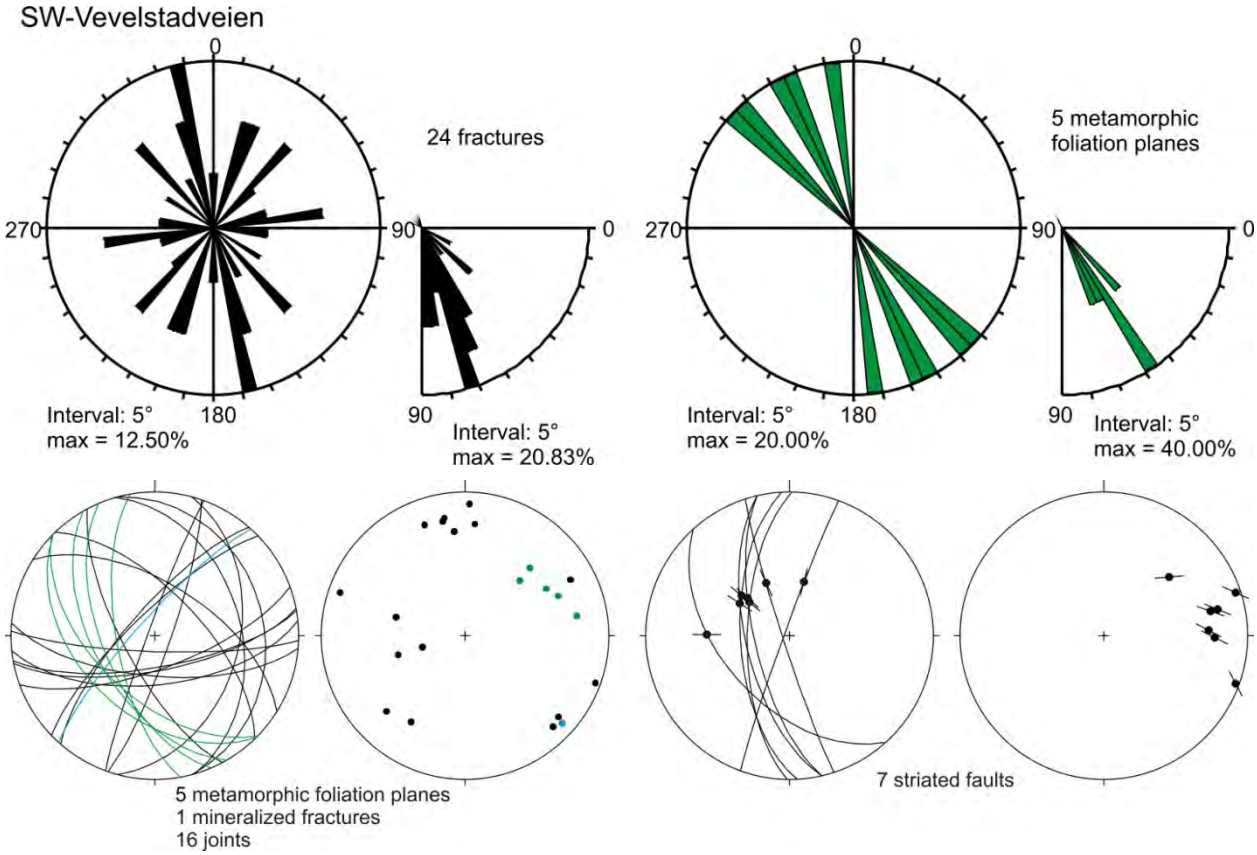

Figure 94. Structural field measurements displayed by rose diagrams and on stereonets at locality "SW-Vevelstadveien" close to resistivity profiles 13 and 15 (keys to stereonets on Figure 32 and Figure 33).

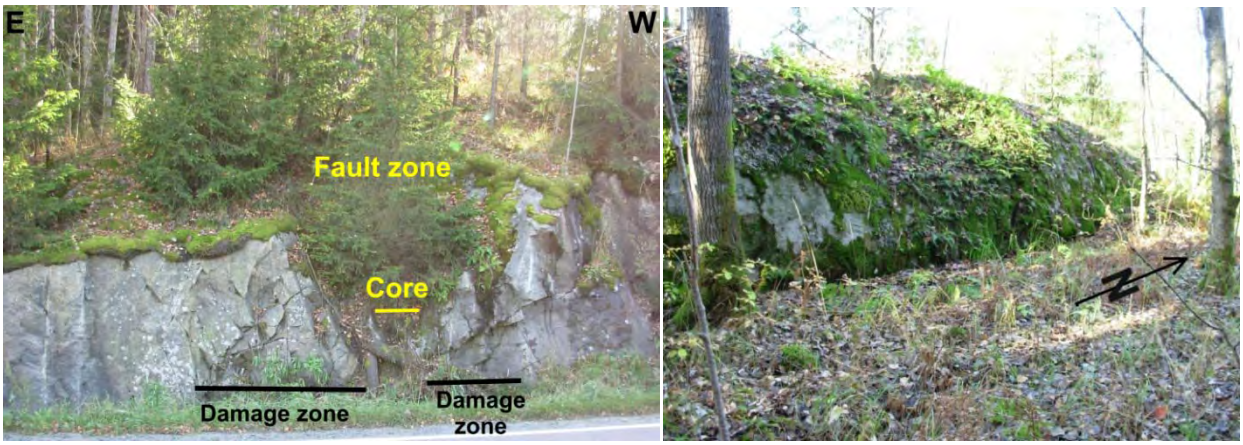

Figure 95. Left: large N-S trending and nearly vertical fault zone at field point "SW-Vevelstadveien_1" (located on Figure 93), with a 30 cm wide, chlorite-rich, fine-grained, brecciated fault core and adjacent damage zones, in which a dense population of minor striated fault planes is mapped; right: in the wood, south of the outcrop, is a topographic step that aligns with the fault.

Field locality "East of Haugjordet Ungdomsskole"

The field locality "East of Haugjordet Ungdomsskole" corresponds to a narrow, deeply incised, N-S striking gully from which issued the extraction of a N-S lineament (Figure 93). Although this location is accurate to determine the structural nature of this lineament, the outcrop is really difficult to study because of a widespread moss and lichen cover. Two main sets of steep joints are identified; one strikes N-S and the other, WNW-ESE (Figure 93 and Figure 96). Only three joints were measured but it was qualitatively observed that they were representative for the two sets at the outcrop.

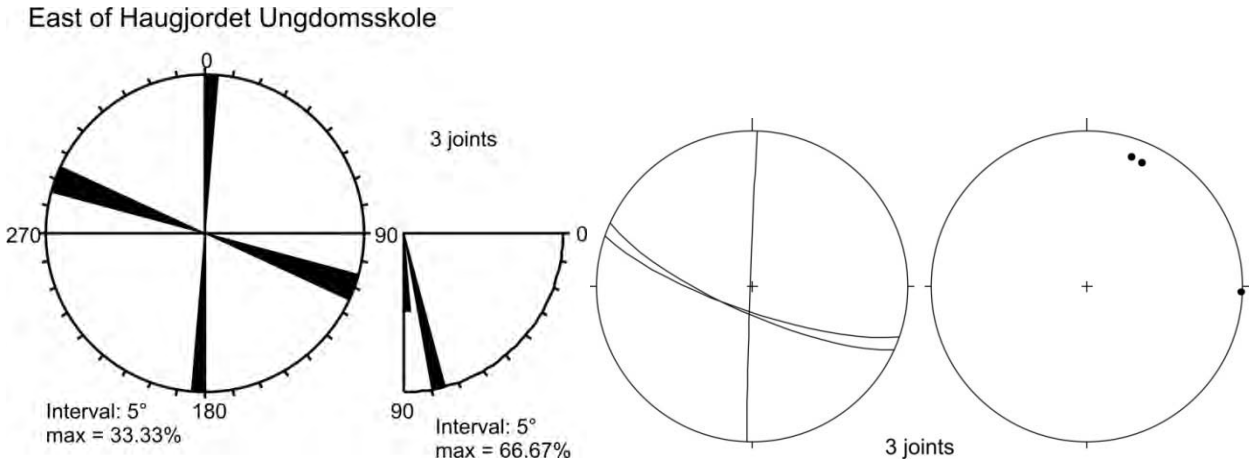

Figure 96. Structural field measurements displayed by rose diagrams and on stereonets at locality "East of Haugjordet Ungdomsskole" close to resistivity profiles 13 and 15 (keys to stereonets on Figure 32).

5.6.4 Field localities "South of Haugjordet Ungdomsskole" and "Vevelstad"

The two field localities "South of Haugjordet Ungdomsskole" and "Vevelstad" are respectively 50 m west of and on a NNW-SSE lineament (Figure 97) but 500 to 100 m south of the resistivity profiles 13, 14 and 15 (Figure 87).

Field locality "South of Haugjordet Ungdomsskole"

The outcrop at the field locality "South of Haugjordet Ungdomsskole" is several tens of meters long and c. 1 m high. The metamorphic foliation is WNW-ESE directed and vertical; it differs from the WSW-dipping trend found in the studied northern region and from the NW-dipping trend that characterises the eastern and western regions (see Figure 87). Nevertheless, the main structures observed at this field locality are steep NNW-SSE fractures, which commonly displayed mineral coating and moderately west-dipping normal faults with a 10 to 20 cm spacing between the fault planes (Figure 97, Figure 98 and Figure 99).

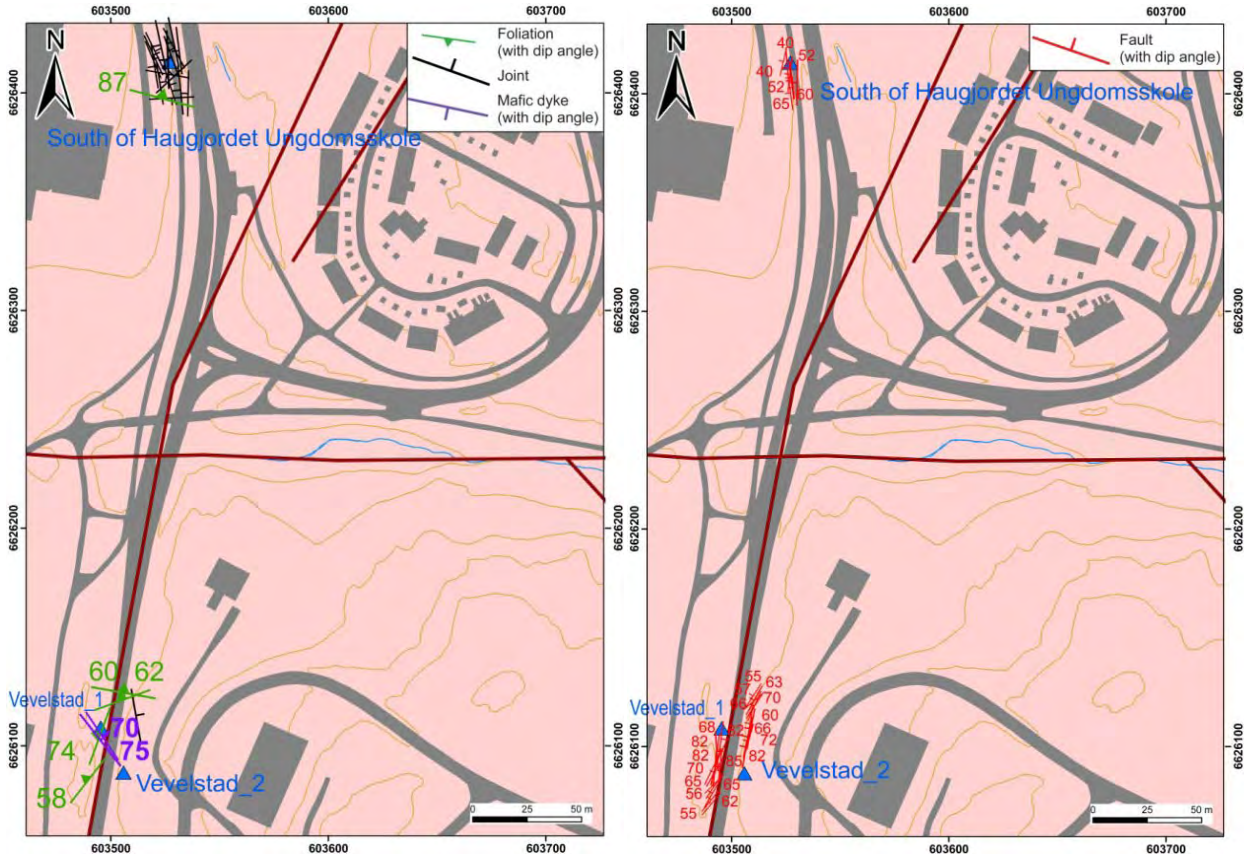

Figure 97. Structural field measurements at localities South of Haugjordet Ungdomsskole" and "Vevelstad" close to resistivity profiles 13, 14 and 15 (caption of background map as Figure 34).

Field locality "Vevelstad"

The outcrops of "Vevelstad" field locality comprise several tens of meters long and meters high road cuts,which are exactly along a N-S lineament (Figure 97). The metamorphic foliation shows a strong dispersion. A mean value corresponds to a NE-SW direction moderately dipping to the NW (Figure 97 and Figure 100), which strongly deviated from the NNW-SSE/NW-SE directed regional pattern found in the northern areas. The main important structural features at this field locality correspond to a very dense pattern of striated faults trending from NNE-SSW to N-S (Figure 97, Figure 100, Figure 101 and Figure 102). The NNE- SSW set dips 70º in average toward the WNW and the N-S set is nearly vertical. This observation strongly suggests that the N-S lineament mapped at this field locality (see Figure 97) correspond to a large fault zone. Another remarkable structure observed at field point "Vevelstad_1" is a 70-75º NE-dipping, 30 cm wide, gabbroic dyke (Figure 97, Figure 100 and Figure 101).

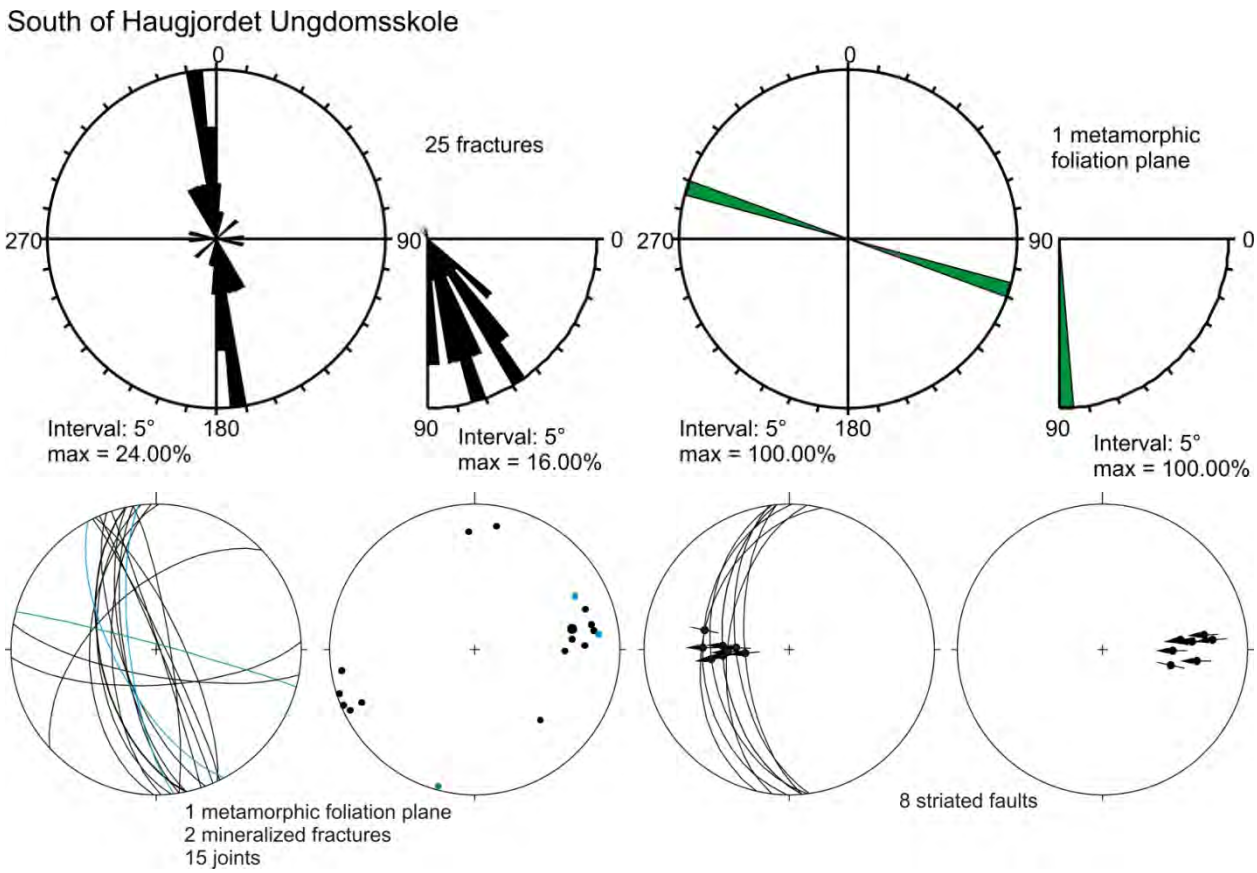

Figure 98. Structural field measurements displayed by rose diagrams and on stereonets at locality "South of Haugjordet Ungdomsskole" close to resistivity profiles 13 and 14 (keys to stereonets on Figure 32 and Figure 33).

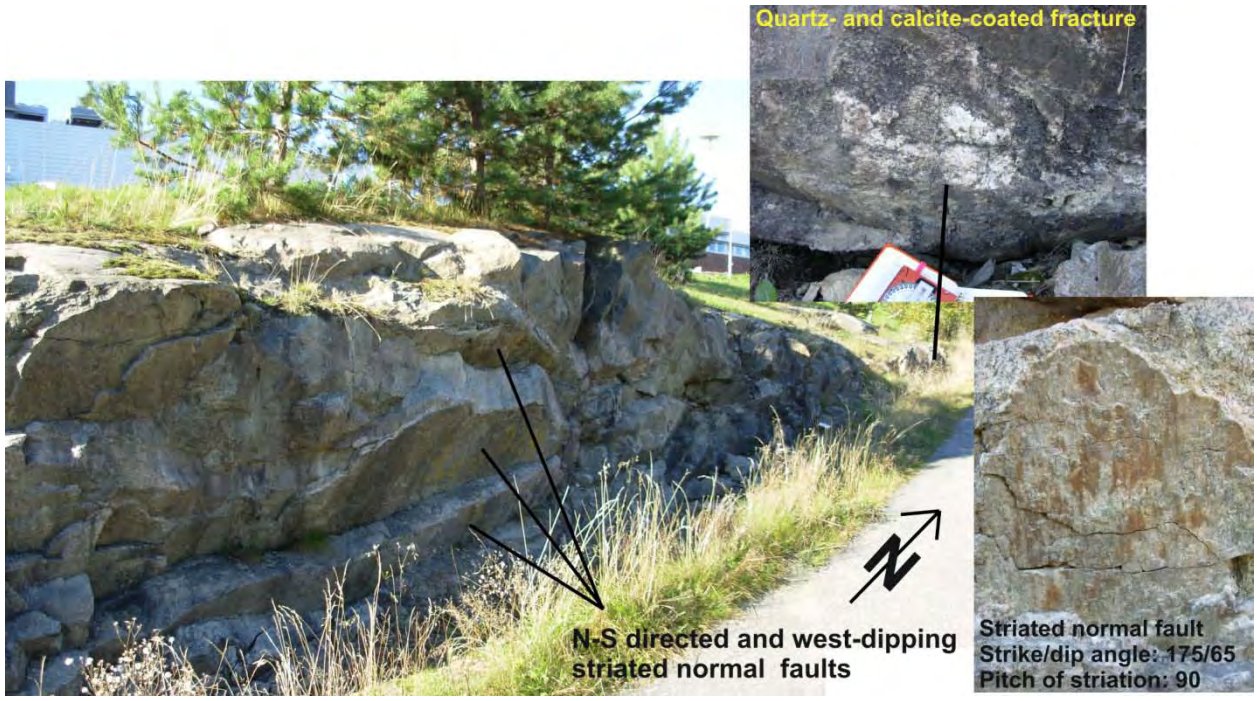

Figure 99. Photographs of the high density of faults at field locality "South of Haugjordet Ungdomsskole" (left), of a quartz- and calcite-coated NNW-SSE fracture (top right) and of normal striations on one of the fault plane (bottom right).

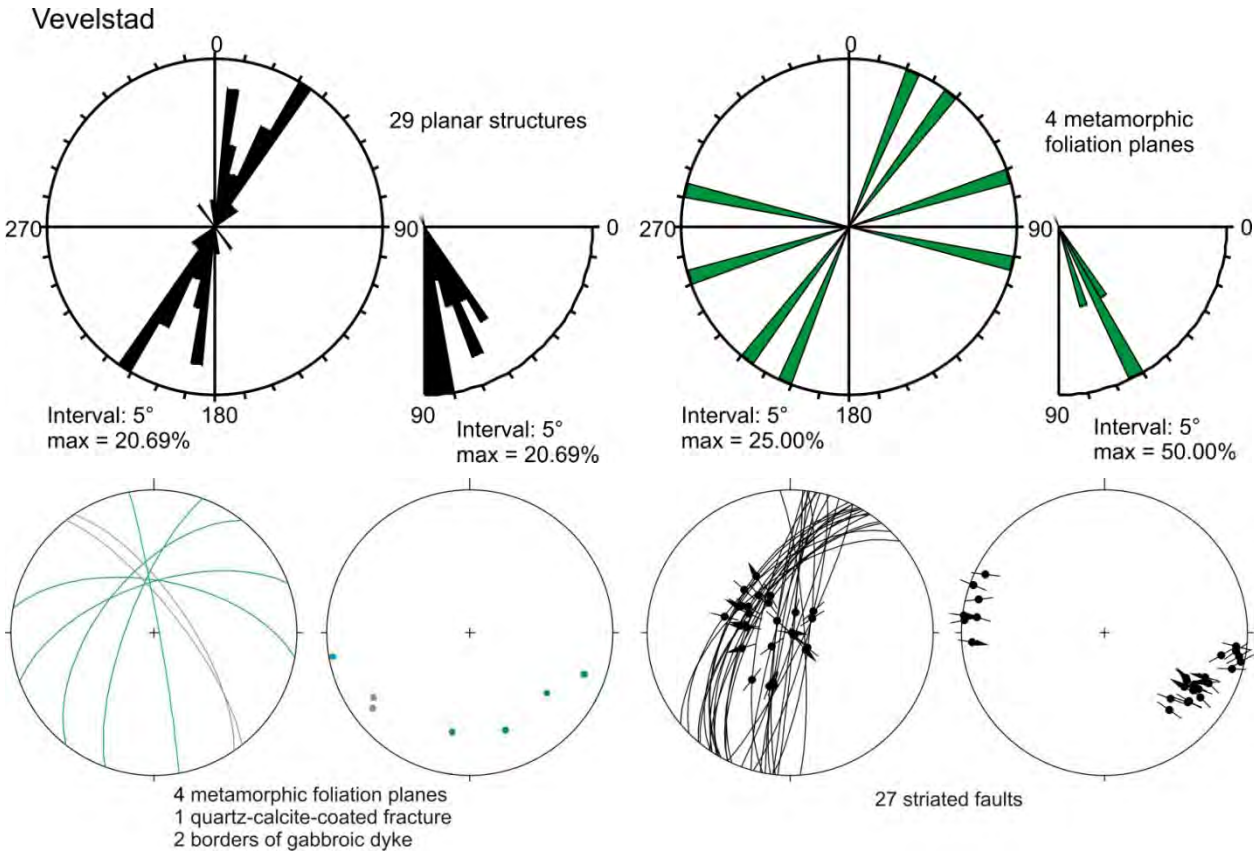

Figure 100. Structural field measurements displayed by rose diagrams and on stereonets at locality "Vevelstad" close to resistivity profiles 13 and 14 (keys to stereonets on Figure 32 and Figure 33).

Figure 101. Left: photograph showing the high density of dip-slip faults on the western side of the road "Vevelstadveien" at field point "Vevelstad_1" (located on Figure 97); right: 70-75º NE-dipping, 30 cm wide, gabbroic dyke at the same field point.

Figure 102. Top left: photograph of a large striated N-S nearly vertical fault observed on the eastern side of the road "Vevelstadveien" at field point "Vevelstad_2" (located on Figure 97), the other photographs show striated fault surfaces also observed at the same field point.

5.6.5 Field localities "Lyngåsen", "Bøleråsenskole" and "Skoglia"

The three field localities "Lyngåsen", "Bøleråsenskole" and "Skoglia" are close to the southern tip of resistivity profile 14 (Figure 103). This area is characterised by two perpendicular trends of lineaments that are NE-SW and NW-SE (Figure 103).

Field locality "Lyngåsen"

The outcrop of the field locality "Lyngåsen" is of limited extent and mainly comprises amphibolitic rocks. The main set of fractures corresponds to joints and is vertical and E-W striking (Figure 103 and Figure 104). Two other vertical sets are identified trending respectively NNE-SSW and NNW-SSE (Figure 103 and Figure 104). Both of them comprise quartz-, chlorite- or hematite- coated fractures. The set trending NNW-SSE also contains a sinistral striated fault (Figure 103, Figure 104 and Figure 105).

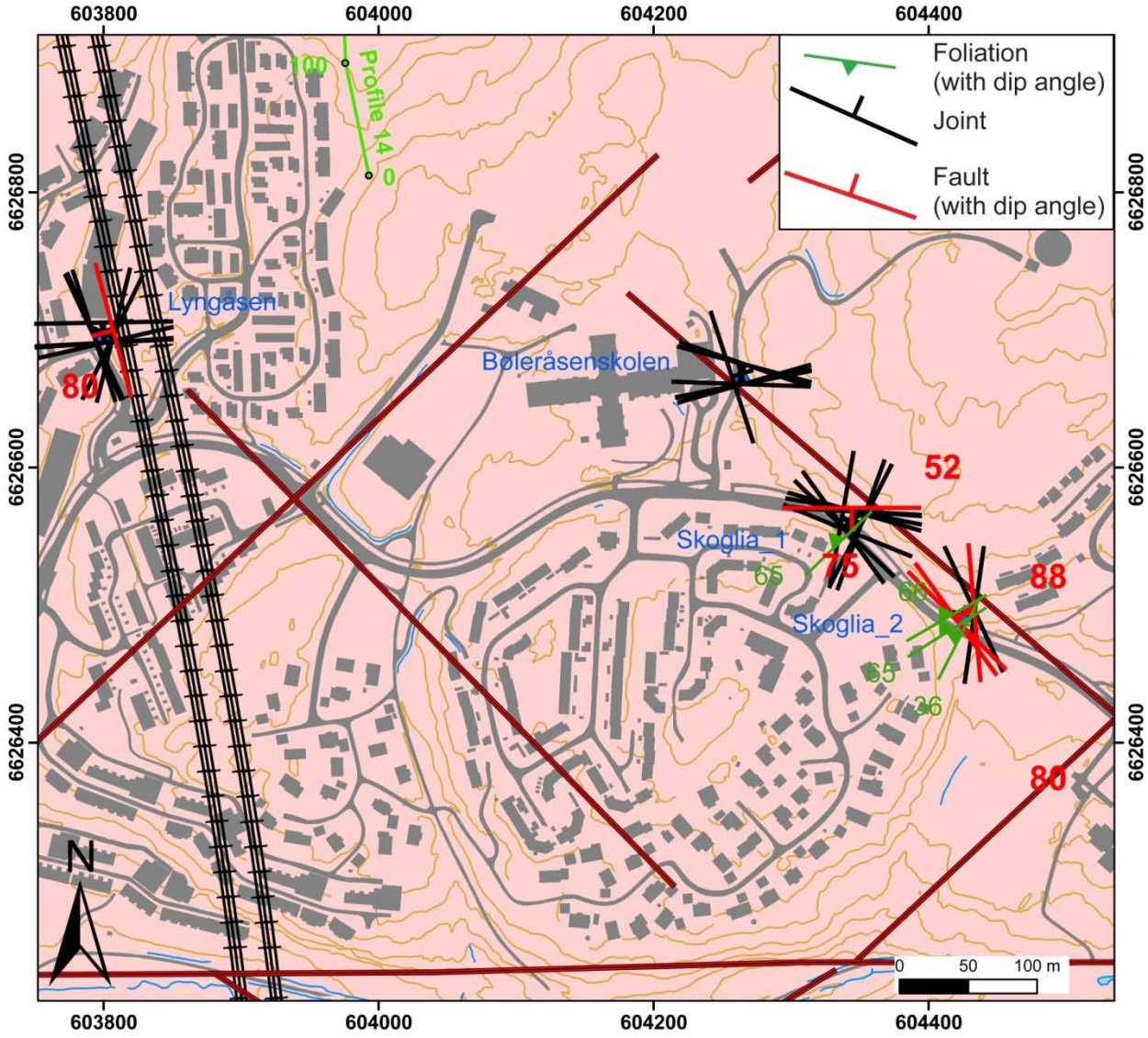

Figure 103. Structural field measurements at localities close to resistivity profile 14 (caption of background map as Figure 34).

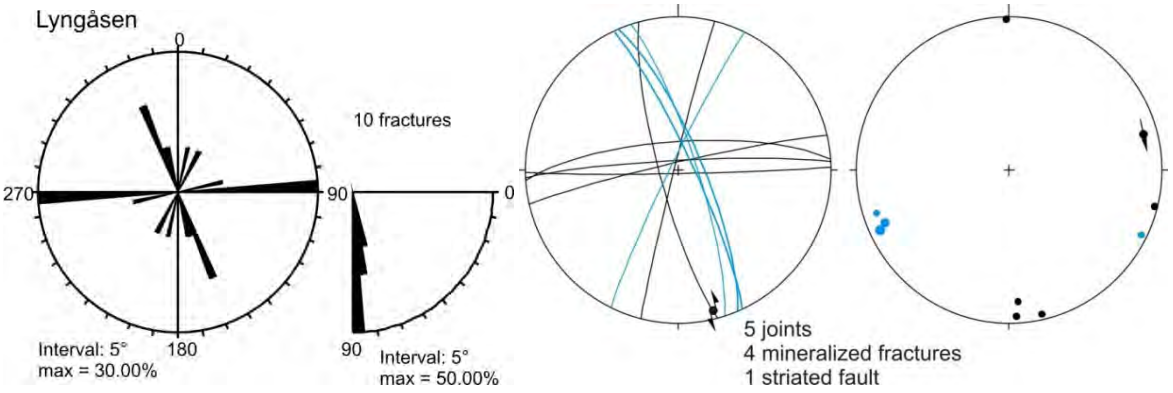

Figure 104. Structural field measurements displayed by rose diagrams and on stereonets at locality "Lyngåsen" close to resistivity profile 14 (keys to stereonets on Figure 32 and Figure 33).

Figure 105. Very steep, NNW-SSE trending, hematite-striated, sinistral fault at field locality "Lyngåsen".

Field locality "Bøleråsenskole"

The field locality "Bøleråsenskole" is an outcrop of limited extent. The fracture pattern of this locality (Figure 106) resembles the previously described steep E-W and NNW-SSE trending joint sets of field locality "Lyngåsen" (Figure 103).

Field locality "Skoglia"

The outcrop of the field locality "Skoglia" correspond to a woody road cut of c. 100 m long in a gneissic unit. The metamorphic foliation is the one identified in the area, that is steeply NW-dipping (Figure 103 and Figure 107), and therefore different of the regional metamorphic foliation in the northern region (see also Figure 87). The fractures are dispersed in their geometry (Figure 107). Striated faults are observed. The main set of fractures corresponds to vertical to moderately south-dipping planes and includes a dip-slip striated fault (Figure 103, Figure 107 and Figure 108). Another nearly vertical and NW-SE trending set of fractures is well represented that also contains two striated faults (Figure 103 and Figure 107). This set is parallel to the lineament mapped at this field locality (Figure 103). The N-S vertical dip-slip fault (Figure 103 and Figure 107) is the border of a 10 cm wide crushed zone.

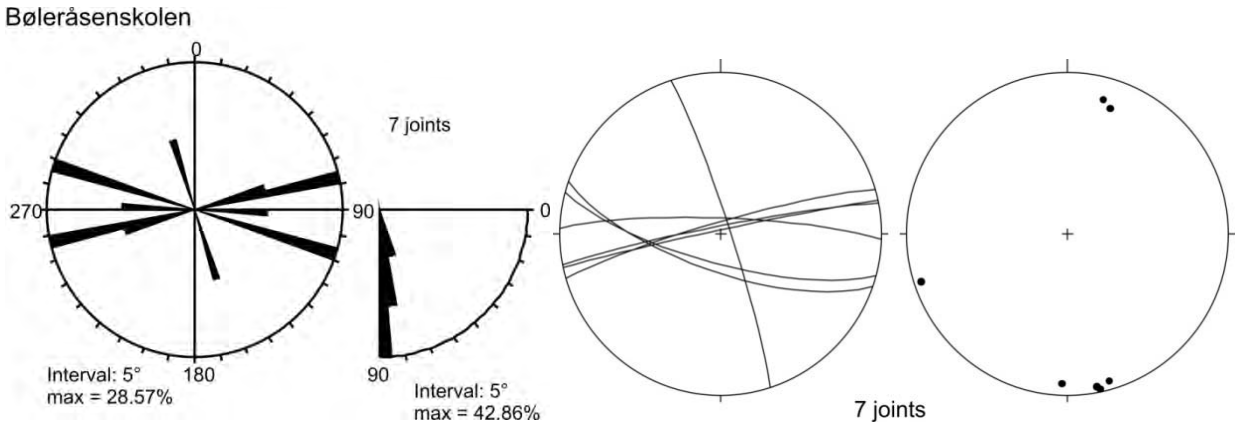

Figure 106. Structural field measurements displayed by rose diagrams and on stereonets at locality "Bøleråsenskole" close to resistivity profile 14 (keys to stereonets on Figure 32).

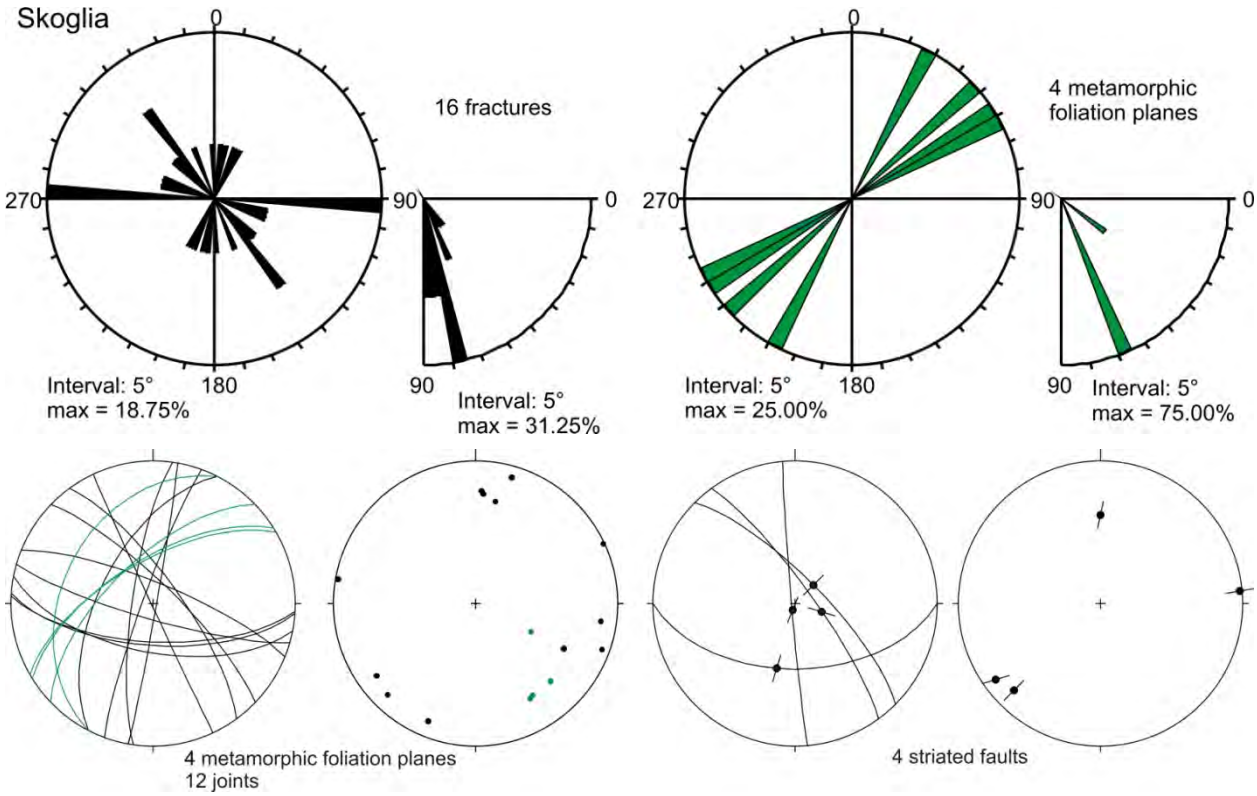

Figure 107. Structural field measurements displayed by rose diagrams and on stereonets at locality "Skoglia" close to resistivity profile 14 (keys to stereonets on Figure 32 and Figure 33).

Figure 108. Photograph (view to N) of a striated fault measured at field point "Skoglia_1" (located on Figure 103) with strike/dip angle: N090/52 and pitch of striation: 80W.

5.6.6 Structural analysis around resistivity profiles 13-15: summary

The cause of the anomalies along the resistivity profiles 13 and 14 are not accurately identified. The anomalies along profile 13 are expected to trend NW-SE parallel to the foliation. However they are also expected to steeply dip toward the SW while the foliation is shallow dipping to the SW (Figure 90 and Figure 93). However, NW-SE lineaments are quite commonly observed in the area (Figure 87) and we cannot exclude that they mark steep weak and fractured zones.

A WSW-ENE lineament is aligned with two of the anomalies of profiles 13 and 14 (Figure 87). This implies that the trend of the resistivity anomaly at 215 m along profile 13 would be WSW-ENE and not NW-SE as presented herein. None of the field localities have provided the observation of prominent WSW-ENE structures that may have explained the anomalies and unravelled the nature of the lineament. The only WNW-ESE trends observed at Sites 2, 3 and 4 (Figure 87; Lutro et al. 2007), "Vevelstad", "Skoglia" and "Bøleråsenskole" correspond either to the metamorphic foliation or to a set of steep joints (Figure 97, Figure 103).

The two anomalies along profile 13 are along a N-S to NNE-SSW striking lineament (Figure 87). Parallel faults are observed at several field localities and at "SW-Vevelstadveien" for the closest one (Figure 93). This would favour a N-S orientation of the resistivity anomalies rather than the NW-SE orientation presented herein and specifically for the resistivity anomaly at 165 m along profile 13 (Figure 87).

In turn, the two close anomalies along resistivity profile 15 (Figure 87) most likely correspond to a west-dipping fault zone as evidenced by the large number of striated faults with such attitude observed at field localities "NE-Vevelstadveien" (Figure 90), "SW-Vevelstadveien" (Figure 93), "South of Haugjordet Ungdomsskole" and "Vevelstad" (Figure 97), "Lyngåsen" and "Skoglia" (Figure 103) and at Sites 3, 5 and 7 (Figure 87; Lutro et al. 2007). At field point "SW-Vevelstadveien_1" (Figure 93), which aligns with the anomalies, the fault comprise a 30 cm wide brecciated fault core surrounded by its damage zones (Figure 95).

6. THE CAUSES OF THE ELECTRIC RESISTIVITY ANOMALIES

The structures or geological features in general that may explain the geophysical anomalies detected along the 18 profiles are listed in Table 4.

Profile no. and zone no. (Table 3**)**	**X** WGS 84, UTM 32	**Y** WGS 84, UTM 32	**Dip angle (°) dip direction**	Quality of interpreta-tion	**Proposed geological interpretation (with eventual correction on direction) and from the most to the less probable**
P 0 - 1	599303	6640223	70SW	Uncertain	Steep ENE-WSW fault or steep WSW-dipping fractured amphibolitic lens / fractured zone along steep SW-dipping foliation
P 0 - 2	599306	6640263	70SW	Uncertain	Steep ENE-WSW fault or steep WSW-dipping fractured amphibolitic lens / fractured zone along steep SW-dipping foliation
P 0 - 3	599338	6640391	80NE	Uncertain	Steep WSW-dipping fractured amphibolitic lens/ fractured zone along steep SW-dipping foliation
P 0 - 4	599481	6640527	90	.	Steep SW-dipping fractured amphibolitic lens/ fractured zone along steep SW-dipping foliation
P 0 - 5	599530	6640571	90	.	Steep SW-dipping fractured amphibolitic lens/ fractured zone along steep SW-dipping foliation
P 0 - 6	599634	6640648	90	.	Steep SW-dipping fractured amphibolitic lens/ fractured zone along steep SW-dipping foliation
P 0 - 7	599757	6640761	75NE	Uncertain	Steep SW-dipping fractured amphibolitic lens/ fractured zone along steep SW-dipping foliation
P 0 - 8	599925	6640992	80SW	Uncertain	NW-SE steep 20 m wide rhomb porphyry dyke
P 1 - 1	599479	6640090	35NW		Shallow north-dipping fault
P 1 - 2	599543	6640035	65SE	Uncertain	Steep E-W fault
P 2 - 1	599910	6640011	90	Uncertain	Steep E-W fault
P 3 - 1	600551	6638670	85W		Fractured zone along steep SW-dipping foliation/ steep SW-dipping fractured amphibolitic lens
P 3 - 2	600582	6638680	75W		Fractured zone along steep SW-dipping foliation/ steep SW-dipping fractured amphibolitic lens
P 3 - 3	600643	6638684	80W	Uncertain	Fractured zone along steep SW-dipping foliation/ steep SW-dipping fractured amphibolitic lens
P 4 - 1	600521	6638630	N80		Fractured zone along steep SW-dipping foliation/ steep SW-dipping fractured amphibolitic lens
P 4 - 2	600539	6638671	70S		Fractured zone along steep SW-dipping foliation/ steep SW-dipping fractured amphibolitic lens
P 5A - 1	600775	6637789	70E		Steep SW-dipping fractured amphibolitic lens / fractured zone along steep SW-dipping foliation

P 5B - 1	601119	6637816	60E	Uncertain	Steep WSW-dipping fractured amphibolitic lens / fractured zone along steep WSW-dipping foliation
P 5B - 2	601191	6637842	70W	Uncertain	Steep WSW-dipping fractured amphibolitic lens / fractured zone along steep WSW-dipping foliation
P 5B - 3	601241	6637862	75W	Uncertain	Fractured zone along steep WSW-dipping foliation /steep WSW-dipping fractured amphibolitic lens
P 6 - 1	601131	6637119	75E	Uncertain	Steep SW-dipping fractured amphibolitic lens / fractured zone along steep SW-dipping foliation
P 6 - 2	601230	6637151	85W		NW-SE steep 20 m wide rhomb porphyry dyke
P 7 - 1	601175	6637242	75S		Steep E-W fault
P 7 - 2	601166	6637305	70N	Uncertain	Steep E-W fault
P 8 - 1	600902	6636385	80W	Uncertain	Steep SW-dipping fault/ steep WSW-dipping fractured amphibolitic lens
P 8 - 2	601002	6636424	75W		Steep WSW-dipping fault /fractured zone along steep WSW-dipping foliation
P 8 - 3	601106	6636410	75W	Uncertain	Fractured zone along steep WSW-dipping foliation
P 8 - 4	601185	6636410	80W	Uncertain	Steep WSW-dipping fault/ steep WSW-dipping fractured amphibolitic lens
P 8 - 5	601240	6636414	85W		Steep WSW-dipping fault
P 8 - 6	601404	6636443	70E	Uncertain	NNW-SSE steep 20 m wide rhomb porphyry dyke
P 8 - 7	601482	6636465	85W	Uncertain	Steep WSW-dipping fractured amphibolitic lens
P 9 - 1	601486	6636128	80N		Steep E-W fault
P 9 - 2	601481	6636161	70N		Steep E-W fault
P 10 - 1	602184	6633987	80E		Fractured zone along steep WSW-dipping foliation*
P 10A - 1	602642	6633729	85E		NNW-SSE steep fault / fractured zone along steep WSW-dipping foliation*
P 10A - 2	602668	6633736	80E		NNW-SSE steep fault / fractured zone along steep WSW-dipping foliation*
P 10A - 3	602697	6633743	80W	Uncertain	NNW-SSE steep fault / fractured zone along steep WSW-dipping foliation*
P 11 - 1	602708	6632357	90		NNW-SSE steep fault / fractured zone along steep WSW-dipping foliation*
P 11 - 2	602867	6632325	85W		NNW-SSE steep fault / fractured zone along steep WSW-dipping foliation*
P 12 - 1	602655	6631582	70W		NNE-SSW steep fault *
P 12 - 2	602775	6631593	80E		NNE-SSW steep fault *
P 13 - 1	603688	6626875	85SW		Steep N-S fault zone / steep NW-SE weak and fractured zone
P 13 - 2	603724	6626907	85NE		Steep N-S fault zone / steep WSW-ESE fault zone / steep NW-SE weak and fractured zone

P 14 - 1	603975	6627014	75S		Steep WSW-ESE fault zone
P 15 - 1	603591	6626982	80W		Steep west-dipping fault zone
P 15 - 2	603620	6626989	80W		Steep west-dipping fault zone
P 16 - 1	603714	6624480	75NE		NW-SE fault*
P 16 - 2	603727	6624488	75NE		NW-SE fault *
P 16 - 3	603811	6624539	70SW		NW-SE fault *
P 17 - 1	603776	6624417	90		NW-SE fault *
P 17 - 2	603815	6624407	80E		NW-SE fault *
P 18 - 1	603693	6624247	80N		Fractured zone along the steep NW-dipping foliation*

Table 4. An attempt to define the geological structures that may create the resistivity anomalies along the 18 profiles (* means that no structural analysis was carried out in the surrounding of the anomalies).

7. CONCLUSIVE REMARKS

In 2010, NGU carried out a 2D electric resistivity survey with the acquisition of 18 profiles along the planned Oslo-Ski railroad tunnel. In some zones, the geophysical investigation was coupled with a detailed field study of structural geology. It is noticeable that the large urbanization in the northern part of the study area (profiles 0 to 8) has prohibited to fully take advantage of the 2D resistivity method due to extensive noises from underground installations. The structural field analysis in the same area was also not optimal due to the lack of outcrops and was consequently meaningless than in the southern half part of the studied area. Nevertheless, the 2D resistivity method has allowed, in most of the cases, the identification of soil covering the gneissic bedrock and of steep weakness zones. The latter mostly correspond to fractured zones in the gneissic host rock. The structural geology analysis carried out in the vicinity of some of the profiles has permitted to characterize that the fractures zones developed either along weak and severely fractured amphibolitic lenses or along faults within the gneiss, which are commonly both parallel to the gneissic foliation.

8. REFERENCES

ABEM 1999: ABEM Terrameter SAS 4000/SAS 1000. Instruction Manual. ABEM Printed Matter 93101. ABEM, Sverige.

Brøgger, W.C. 1933: Om rombeporfyrgangene og de dem ledsagende forkastninger i Oslofeltet. NGU 139, 51 pp.

Dahlin, T. 1993: On the Automation of 2D Resistivity Surveying for Engineering and Environmental Applications. Dr. Thesis, Department of Engineering Geology, Lund Institute of Technology, Lund University. ISBN 91-628-1032-4.

Dalsegg, E., Saintot, A. & Ganerød, G.V., 2010: Geofysiske og geologiske undersøkelser i forbindelse med Eikrem tunneltrase, Rv 70 Øydegard-Brunneset, Tingvoll, Møre og Romsdal. NGU Rapport 2010.006

Graversen, O. 1984: Geology and structural evolution of the Precambrian rocks of the Oslofjord - Øyeren area, Southeast Norway. NGU Bulletin 398, 50 pp.

Graversen, O. Naterstad, J., Nilsen, O., Nordgulen, Ø. and Lutro, O. 2009. Berggrunnskart Oslo 1914 IV, 1: 50 000, foreløpig utgave, NGU.

Loke. M.H. 2007: RES2INV ver. 3.56. Geoelectrical Imaging 2D & 3D. Instruction manual. www.geoelectrical.com.

Lutro, O., Saintot, A., Dehls, J., Olesen, O. & Nordgulen, Ø., 2007: Geologiske forhold langs planlagt jernbanetrasé Oslo-Ski. NGU report 2007.048, 79 pp.

Reiser, F., Dalsegg, E., Dahlin, T., Ganerød, G. & Rønning, J.S. 2009: "Resistivity Modelling of Fracture Zones and Horizontal Layers in Bedrock". NGU Report 2009.070, pp. 1-120, 2009 http://www.ngu.no/no/hm/Publikasjoner/Rapporter/2009/

Rønning, J.S., 2003: Miljø- og samfunnstjenlige tunneler. Sluttrapport delprosjekt A, Forundersøkelser. Statens vegvesen, Publikasjon nr. 102.

Rønning, J.S., Dalsegg, E., Elvebakk, H. & Storrø, G. 2003: Characterization of fracture zones in bedrock using 2D resistivity. 9th EEGS European Meeting, Prague, August 31 – September 4 2003. Extended Abstract: Proceedings P005.

Rønning, J.S., Dalsegg, E., Elvebakk, H., Ganerød, G.V. & Heincke, B.H. 2009: Characterization of fracture zones in bedrock using 2D resistivity. Proceedings from 5th Seminar on Strait Crossings, Trondheim, June 21 – 24 2009, p. 439 - 444 (SINTEF/NTNU)

9. APPENDIX 1

Locations of 2D resistivity profiles on 1/10 000 topographic map.

Overview map P 0, P 1 and P 2

Scale 1:10 000

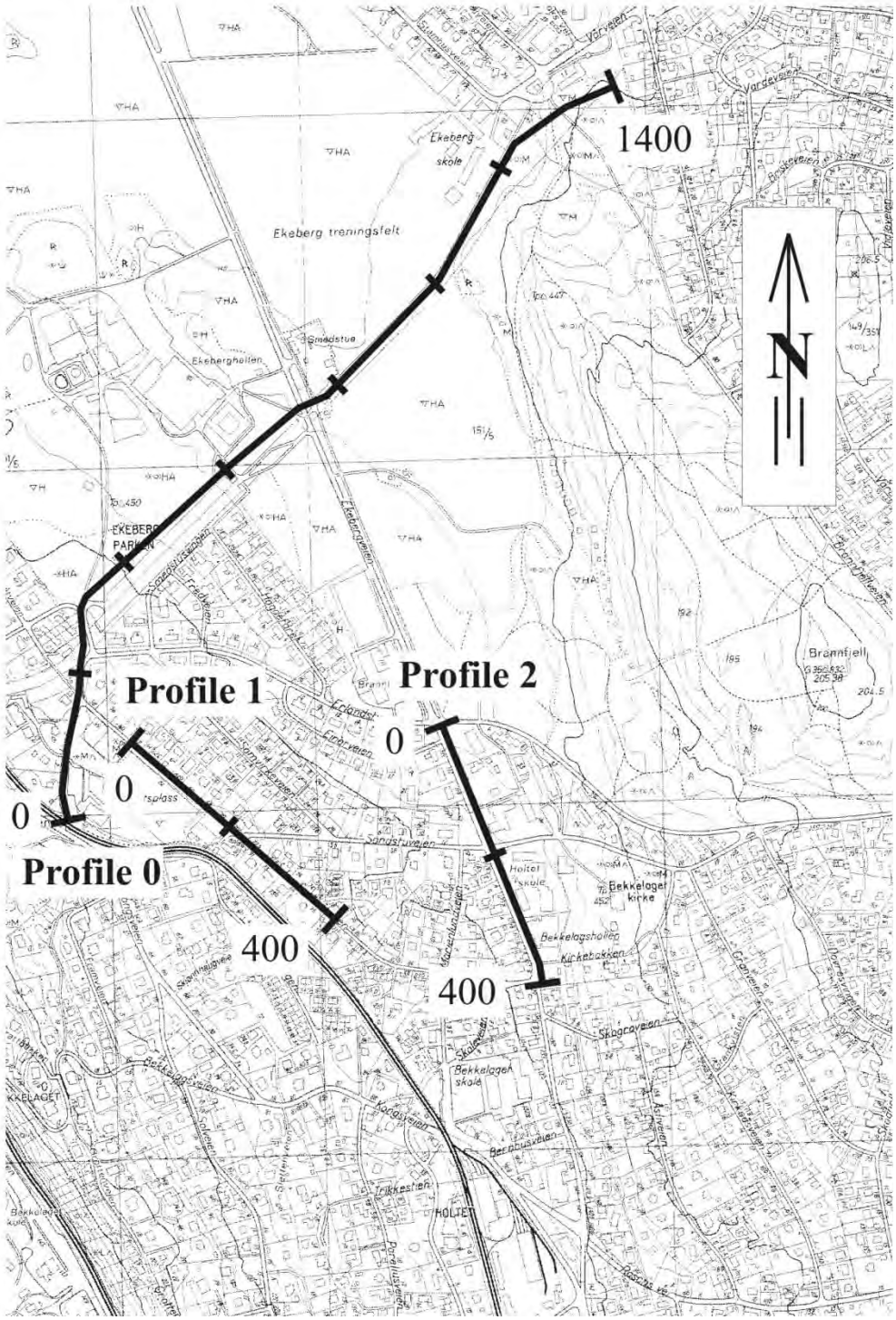

Overview map P 3, P 4, P 5A and P 5B

Scale 1:10 000

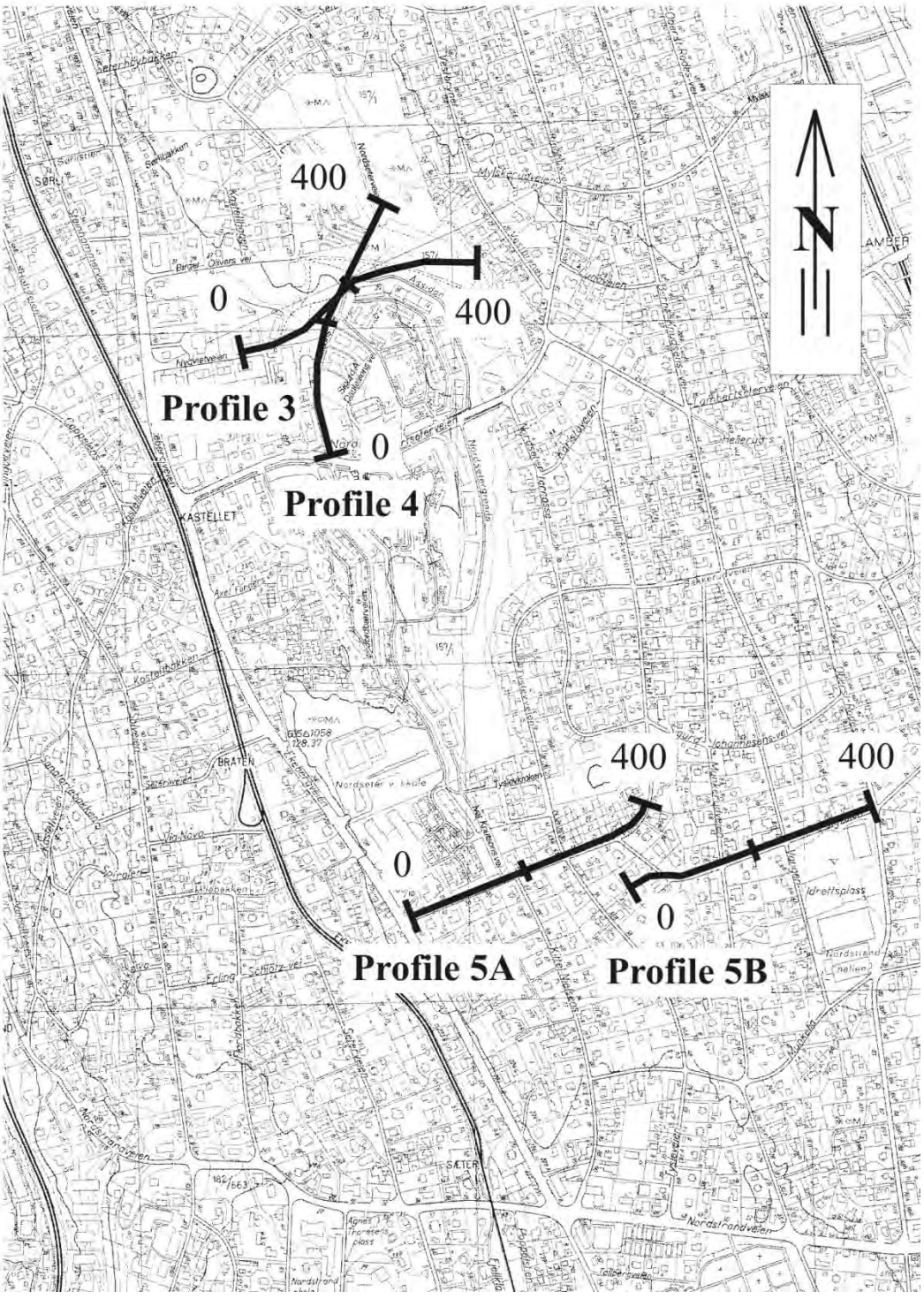

Overview map P 6, P 7, P 8 and P 9

Scale 1:10 000

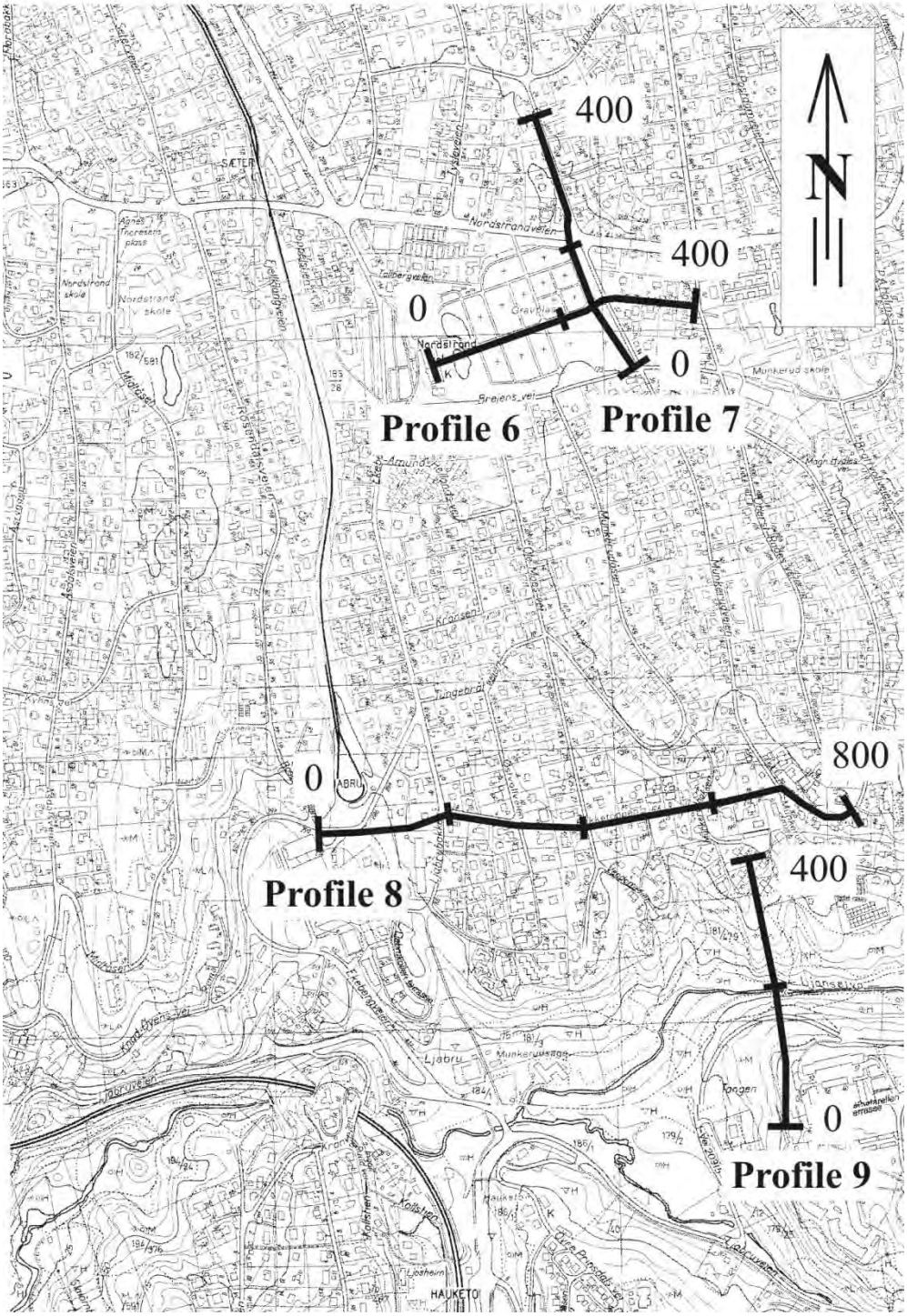

Overview map P 10 and P 10A

Scale 1:10 000

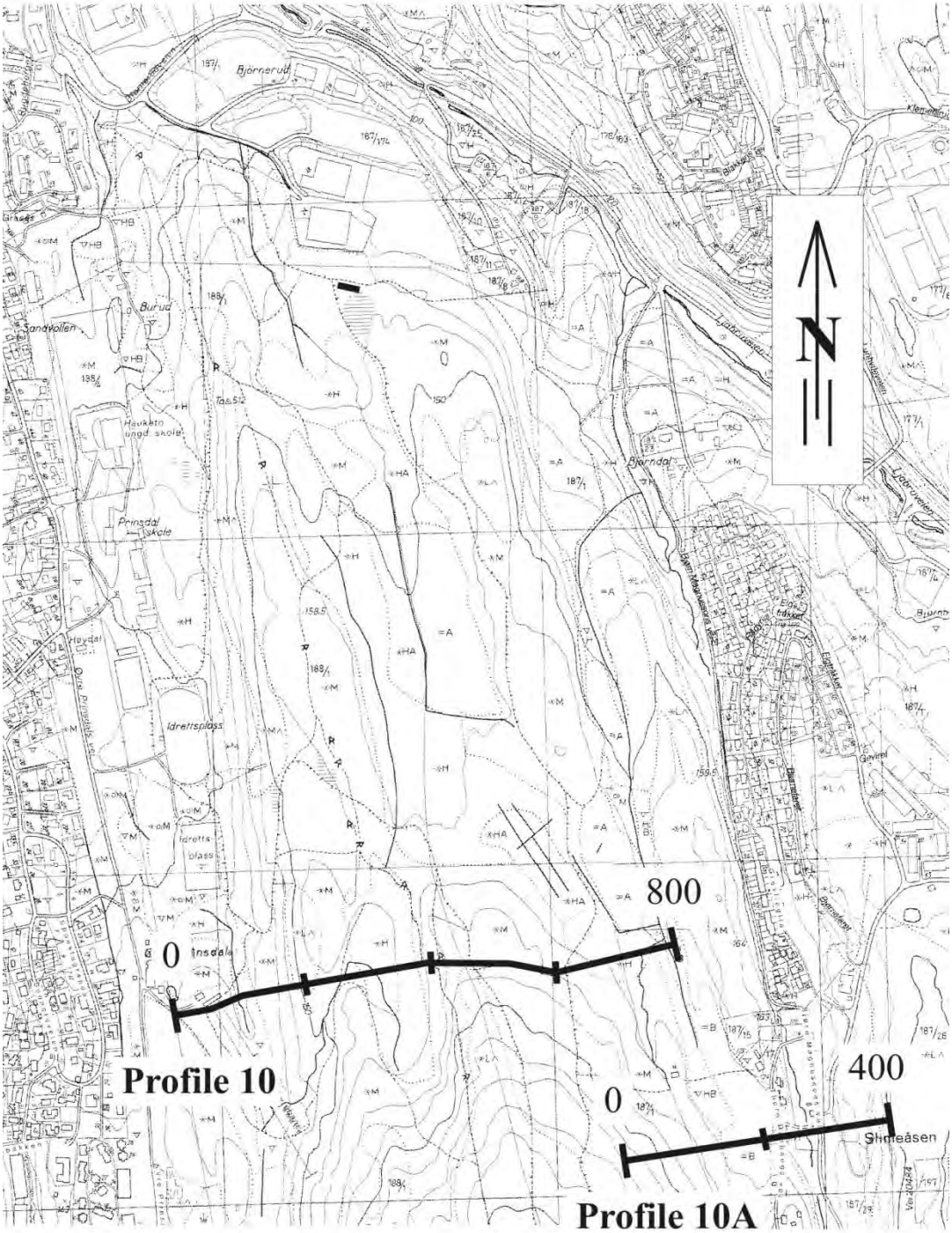

Overview map P 11 and P 12

Scale 1:10 000

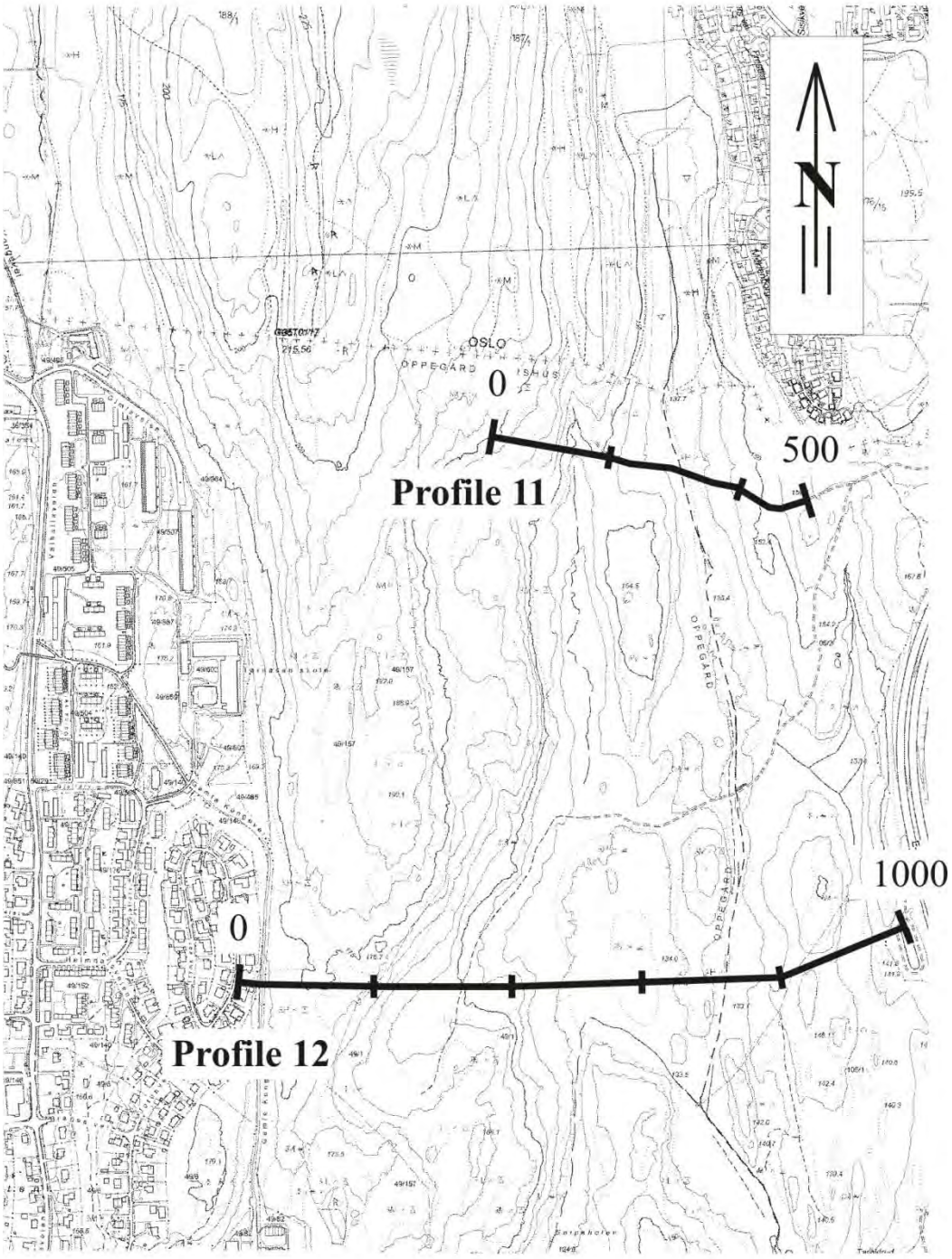

Overview map P 13, P 14 and P 15

Scale 1:10 000

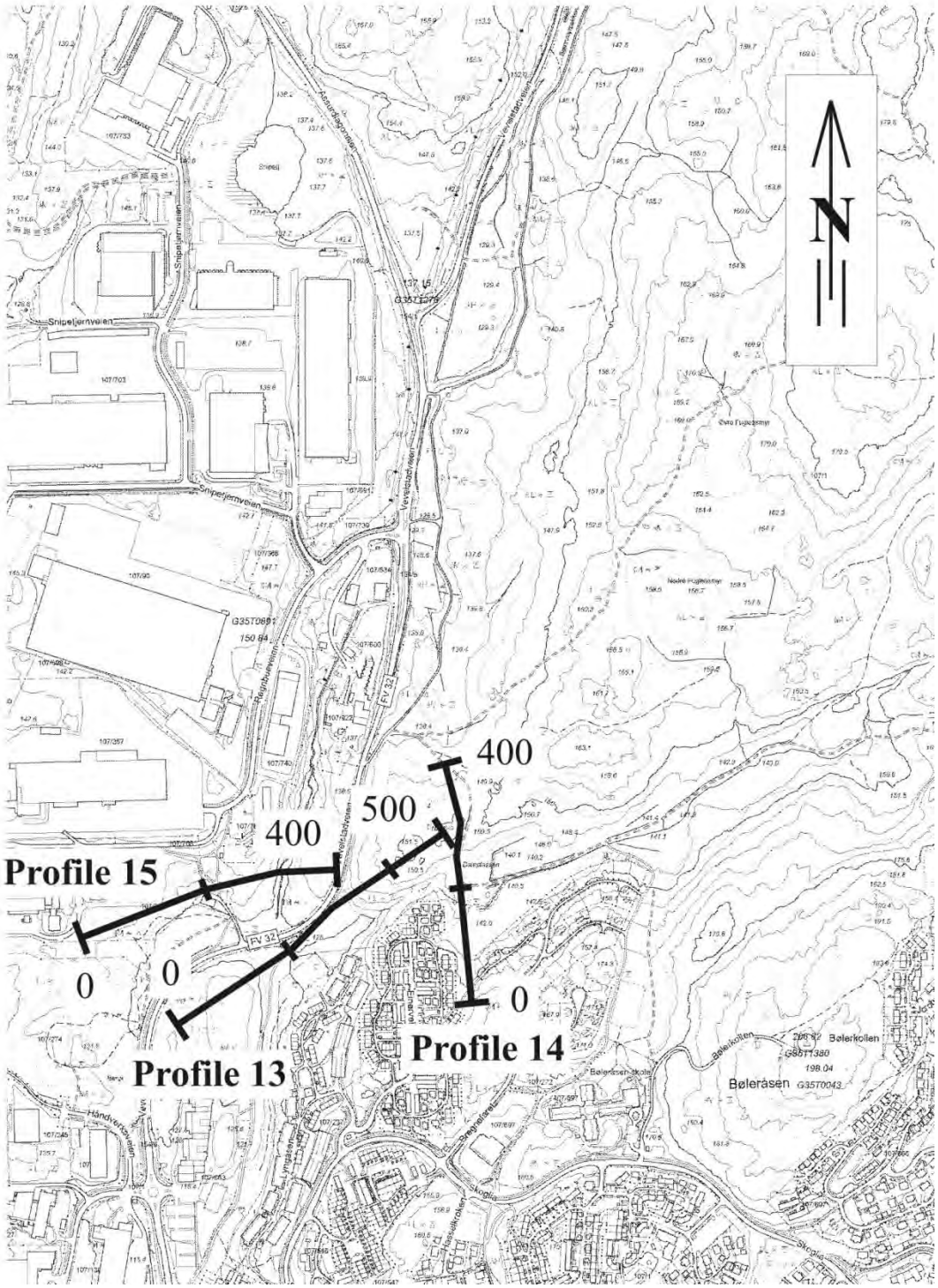

Overview map P 16, P 17 and P 18

Scale 1:10 000

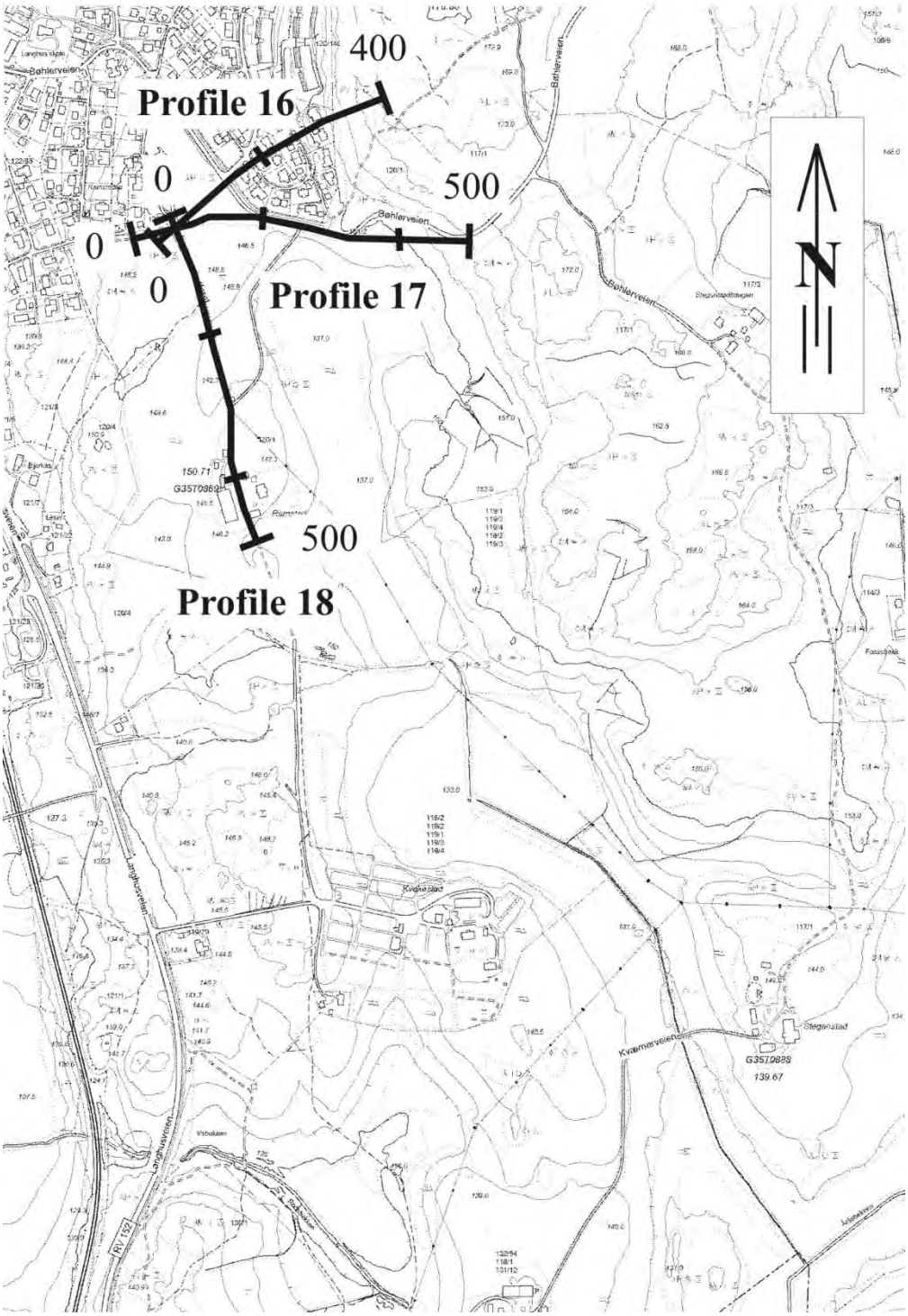

10. APPENDIX 2

Table of field measurements by field localities (in the order of appearance within the text). Strike and dip angle of planar structures according to the right hand rule. Abbreviations: MF, metamorphic foliation; J, joint; F, fault; CN, certainly normal fault; CS, certainly sinistral fault; PS, probably sinistral fault; Ca, calcite; Chl, chlorite; He, hematite; Qz, quartz.

Locality	Datum №	East	North	Structure	Strike	Dip angle	Pitch of striation	Comment	Date
AROUND RESISTIVITY PROFILES 0, 1 AND 2									
Ekeberghallen, poor outcrop, datum №1									13.10.2010
	1	599441	6640847	Amphibolite with WSW-ENE 40 cm wide and E-W 10 cm wide pegmatitic veins					
Ekeberg Rideskole, from datum №2 to datum №32									13.10.2010
Ekeberg Rideskole_1	2	599315	6640594	MF	158	67			
	3			J	264	62			
	4			J	255	68			
	5			J	66	62			
	6			J	259	71			
	7			J	130	45			
	8			J	286	79			
	9			J	182	80			
	10			MF	140	64			
	11			MF	165	69			
	12			J	276	49			
	13			J	254	65			
	14			J	282	55			
	15			J	134	55			
	16			J	33	37			
	17			J	35	88			
Ekeberg Rideskole_2	18	599231	6640717	J	303	60		Amphibolites in large pegmatitic body	
	19			J	303	73			
	20			J	300	58			
	21			J	182	50			
	22			J	83	88			
	23			J	27	55			

Locality	Datum №	East	North	Structure	Strike	Dip angle	Pitch of striation	Comment	Date
	24			J	110	81			
	25			J	68	81			
	26			J	20	88			
	27			MF	150	67			
	28			MF	149	68			
	29			MF	149	50			
	30			J	84	80			
	31			J	206	82			
	32			J	214	84			
Smedstusveien, from datum №33 to datum №46									13.10.2010
	33	599452	6640442	MF	140	58			
	34			MF	161	68			
	35			MF	142	64			
	36			J	273	59			
	37			J	92	85			
	38			J	17	86			
	39			J	279	47			
	40			J	12	89			
	41			J	12	85			
	42			J	26	81			
	43			J	282	40			
	44			J	285	66			
	45			J	26	42			
	46			J	274	80			
Jomfrubråtveien, 48, from datum №47 to datum №57									13.10.2010
	47	599199	6640392	Basaltic dyke	97	85		30 cm wide	
	48			Basaltic dyke	102	85		30 cm wide	
	49			J	247	81			
	50			J	11	85			
	51			J	276	84			
	52			J	278	84			

Locality	Datum №	East	North	Structure	Strike	Dip angle	Pitch of striation	Comment	Date
	53			J	101	87			
	54			MF	158	50			
	55			MF	144	70			
	56			J	246	82			
	57			J	247	85		Chl	
Frierveien, from datum №58 to datum №68									13.10.2010
	58	599205	6640329	MF	160	47			
	59			MF	158	65			
	60			J	346	81			
	61			J	197	85			
	62			J	240	79			
	63			J	71	88			
	64			J	356	62			
	65			J	260	81			
	66			J	353	70			
	67			J	77	86			
	68			J	71	88			
Sportsplassen, Jomfrubråtveien, from datum №69 to datum №100									13.10.2010
	69	599338	6640198	MF	142	60			
	70			MF	148	64			
	71			J	250	82			
	72			J	247	84			
	73			J	296	80			
	74			J	305	55			
	75			J	64	87			
	76			J	62	88			
	77			J	304	56			
	78			J	297	72			
	79			J	61	86			
	80			J	64	86			
	81			J	298	65			

Locality	Datum №	East	North	Structure	Strike	Dip angle	Pitch of striation	Comment	Date
	82			J	71	89			
	83			J	64	86			
	84			MF	156	48			
	85			MF	158	50			
	86			J	63	89			
	87			J	75	88			
	88			MF	147	58			
	89			J	267	81			
	90			J	291	68			
	91			J	84	84			
	92			J	82	83			
	93			J	304	61			
	94			J	264	88		Ca	
	95			CS	289	49	16W	Ca steps	
	96			CS	285	46	20W	Ca steps	
	97			J	270	62		Chl	
	98			MF	145	80			
	99			J	106	71		Chl + Ca	
	100			J	273	58		Chl + Ca	
Kongsveien, going from SE to NW, from datum №101 to datum №143									14.10.2010
Kongsveien_1	101	599177	6640106	MF	153	55			
	102			MF	152	57			
	103			J	33	45			
	104			J	298	65			
	105			J	24	65			
	106			J	85	87			
	107			J	81	89			
	108			J	200	66			
	109			J	60	86			
	110			J	48	89			
	111			J	63	78			

Locality	Datum №	East	North	Structure	Strike	Dip angle	Pitch of striation	Comment	Date
	112			J	317	65			
	113			J	318	63			
	114			J	105	76			
	115			J	145	53		Chl	
	116			J	82	73		Chl	
	117			J	76	87		Chl	
	118			F	155	55	89S	He, weathered plane	
	119			J	295	75			
	120			J	67	72			
	121			J	62	79			
	122			J	265	67			
	123			J	142	58		Weathered plane, MF-parallel	
	124			MF	142	58			
	125			J	103	70			
	126			J	181	60		Chl	
	127			J	66	89			
	128			J	87	80			
	129			J	285	67			
	130			J	300	76			
	131			J	147	56		Weathered plane, MF-parallel, spacing: 1 m	
	132			MF	147	56			
Kongsveien_2	133	599110	6640248	MF	150	25			
	134			MF	120	20			
	135			MF	160	10			
	136			J	264	70			
	137			J	264	62		Qz	
	138			J	270	72			
	139			J	355	65			
	140			J	50	86			
	141			J	276	65		White mineral coating	
	142			J	281	70			

Locality	Datum №	East	North	Structure	Strike	Dip angle	Pitch of striation	Comment	Date
	143			J	280	85		Amethyst coating	
Tramway station Sportsplassen, Jomfrustien, poor outcrop, data №144 and 145									13.10.2010
	144	599298	6640064	MF	168	69			
	145			J	84	83		Set of E-W joints	
Ekeberg, Brannfjell Skole, from datum №146 to datum №179									13.10.2010
Ekeberg, Brannfjell Skole_1	146	599799	6640197	MF	154	65			
	147			MF	156	64			
	148			J	30	70			
	149			J	263	59			
	150			J	233	81			
	151			J	264	58			
	152			MF	158	65			
Ekeberg, Brannfjell Skole_2	153	599715	6640218	J	250	82		Chl	
	154			MF	162	52			
	155			J	300	74			
	156			J	119	69			
	157			J	306	64			
	158			J	112	65		Basaltic patches	
	159			J	306	65			
	160			J	253	74		Chl	
	161			J	305	71			
	162			J	120	61			
	163			J	126	62		Ca	
	164			MF	174	54			
	165			MF	165	62			
	166			J	122	70			
	167			J	74	81			
	168			J	115	69			
	169			J	70	86			
	170			J	115	67		Ca	

Locality	Datum №	East	North	Structure	Strike	Dip angle	Pitch of striation	Comment	Date
	171			J	114	74		Ca	
	172			CN	267	66	72E	Ca steps	
	173			J	114	68		Ca	
	174			J	11	79		Ca	
	175			J	262	88			
	176			J	114	72			
	177			J	256	80			
	178			J	295	78			
	179			CN	111	74	44W	Chl + Ca	
Jomfrubråtveien, 78, from datum №180 to datum №201									13.10.2010
	180	599701	6639900	J	263	59			
	181			J	272	55			
	182			MF	147	37			
	183			MF	170	50			
	184			J	305	69			
	185			J	278	65			
	186			J	301	72			
	187			Pegmatitic vein, 20 cm wide	40	52			
	188			J	106	62		Chl + Ca	
	189			F	106	66	22W	Chl + Ca	
	190			J	155	74		Qz and late Ca	
	191			J	193	78			
	192			J	101	88			
	193			J	274	60			
	194			J	240	65			
	195			Pegmatitic vein, 4 cm wide	40	60			
	196			J	281	79			
	197			J	285	45			
	198			J	92	89			
	199			J	268	63			

Locality	Datum №	East	North	Structure	Strike	Dip angle	Pitch of striation	Comment	Date
	200			J	272	76			
	201			J	268	65			
Marienlundveien, small outcrop, from datum №202 to datum №204									14.10.2010
	202	599830	6639805	J	180	75			
	203			J	120	89			
	204			F	190	79	25S	He striae	
Erlandstuveien, Brannfjell, to the SE, from datum №205 to datum №252									14.10.2010
Erlandstuveien_1	205	600006	6640144	J	273	62		Massive garnet-bearing amphibolite	
	206			J	271	76			
	207			MF	140	60			
	208			MF	170	65			
	209			J	13	73			
	210			J	290	66			
	211			J	302	70			
	212			MF	154	62			
	213			MF	158	56			
	214			J	264	84			
	215			J	46	60			
	216			J	21	65			
	217			MF	154	59			
	218			J	285	48			
Erlandstuveien_2	219	600082	6640085	MF	176	66			
	220			MF	165	51			
	221			J	271	66			
	222			J	269	70			
	223			J	269	71			
	224			J	30	83			
	225			MF	145	53			
Erlandstuveien_3	226	600085	6640077	Basaltic dyke	225	69		4-5 m wide, western border	
	227			J in the dyke №226	45	75		Highly jointed, specially towards the borders, the eastern border is brecciated	
	228			J in the dyke №226	41	83			

Locality	Datum №	East	North	Structure	Strike	Dip angle	Pitch of striation	Comment	Date
	229			J in the dyke №226	37	83			
	230			J in the dyke №226	70	80			
	231			J in the dyke №226	6	89			
	232			J in the dyke №226	78	57			
	233			J in the dyke №226	42	66			
	234			J in the dyke №226	200	88		Joint spacing 3-5 cm	
	235			MF	200	80			
	236			MF	200	81			
	237			F	268	66	70W		
	238			J	276	70			
	239			J	294	75			
	240			J	130	71			
	241			J	256	76			
	242			J	250	80		Large, He + Chl	
	243			MF	171	64			
	244			J	274	60			
Erlandstuveien_4	245	600099	6640070	Basaltic dyke	15	65		40 cm wide, western border	
	246			Basaltic dyke	17	60		40 cm wide, eastern border	
	247			MF	168	67			
	248			J	298	66			
	249			J	142	70		Large, He + Chl	
	250			J	305	85		Large, He + Chl	
	251			MF	190	78			
Erlandstuveien_5	252	600109	6640064	Amphibolitic body	226	60		Western contact with gneiss	
AROUND RESISTIVITY PROFILES 3 AND 4									
Kastellet, from datum №253 to datum №353									13.10.2010
Kastellet_1	253	600428	6638662	MF	180	64			
	254			MF	160	50			
	255			MF	163	56			
	256			J	64	89			
	257			J	51	69			

Locality	Datum №	East	North	Structure	Strike	Dip angle	Pitch of striation	Comment	Date
	258			J	115	68			
	259			J	285	82			
	260			J	100	78			
	261			J	110	63			
	262			J	304	62			
	263			J	293	59			
	264			J	10	53			
	265			MF	180	55			
	266			MF	180	60			
	267			J	80	89			
	268			J	225	54			
	269			J	113	54			
	270			J	129	72		Garnet-bearing gneiss	
	271			J	271	62			
	272			J	305	60			
	273			J	240	70			
	274			J	110	50			
Kastellet_2	275	600508	6638638	MF	170	60			
	276			J	220	70			
	277			J	250	80			
	278			J	270	75			
Kastellet_3	279	600576	6638711	MF	175	60			
Kastellet_4	280	600625	6638783	MF	170	70		Amphibolite	
	281			MF	190	70			
	282			MF	190	66			
	283			J	295	71			
	284			J	124	88			
	285			J	304	81			
	286			J	309	72			
	287			J	300	80			
	288			J	280	85			

Locality	Datum №	East	North	Structure	Strike	Dip angle	Pitch of striation	Comment	Date
	289			J	270	63			
	290			J	310	73			
	291			MF	174	70			
	292			MF	160	60			
	293			J	38	52			
	294			J	49	71			
	295			J	16	60			
	296			J	25	54			
	297			J	261	49			
	298			MF	172	62		Garnet-bearing gneiss	
	299			J	306	88			
	300			J	280	40			
	301			J	34	58			
	302			MF	166	71			
	303			J	110	72			
	304			J	270	84			
	305			J	272	82			
Kastellet_5	306	600597	6638844	MF	155	60			
	307			J	34	55			
	308			J	264	80			
	309			J	266	65			
	310			J	37	51			
	311			J	250	87			
	312			MF	160	50			
	313			J	93	69			
	314			J	50	72			
	315			J	33	58			
	316			J	102	72			
	317			J	37	56			
	318			J	32	47			
	319			MF	157	58			

Locality	Datum №	East	North	Structure	Strike	Dip angle	Pitch of striation	Comment	Date
	320			J	37	45			
	321			J	298	81			
Kastellet_6	322	600715	6638586	MF	160	63		Garnet-bearing gneiss	
	323			J	120	75			
	324			J	87	75			
	325			J	30	70			
	326			J	102	87			
	327			J	254	87			
	328			J	253	78			
	329			J	250	86			
	330			J	30	62			
	331			J	27	60			
	332			J	114	75			
	333			J	120	82			
	334			J	270	88			
	335			J	34	73			
	336			J	41	60			
	337			MF	145	65			
	338			MF	155	58			
	339			J	40	58			
	340			J	88	87			
	341			J	285	77			
	342			J	265	88			
	343			J	101	86			
	344			J	291	72			
	345			J	246	68			
	346			J	67	78			
	347			MF	150	55			
	348			MF	161	64			
	349			J	25	55			
	350			J	308	60			

Locality	Datum №	East	North	Structure	Strike	Dip angle	Pitch of striation	Comment	Date
	351			J	218	44			
	352			J	69	88			
	353			MF	155	49			
Mylskerudveien, garnet-rich massive amphibolite, quite highly fractured, from datum №354 to datum №375									12.10.2010
Mylskerudveien_1	354	600854	6638798	J	27	75			
	355			J	190	80			
	356			J	240	85			
	357			J	290	42			
	358			J	70	85			
	359			J	305	50			
	360			J	220	89			
	361			J	60	75			
	362			J	340	59			
Mylskerudveien_2	363	600880	6638807	J	75	85		Main joint set	
	364			F	255	58	30W		
	365			F	256	53	32W		
	366			J	260	80			
	367			J	270	65			
	368			J	10	42			
	369			J	310	57			
	370			J	74	80			
	371			J	86	78			
	372			J	196	76			
	373			J	62	86			
	374			J	70	80			
	375			J	342	47			
Holtveien, small outcrop, from datum №376 to datum №390									14.10.2010
	376	600018	6638744	MF	149	58			
	377			MF	176	75			
	378			J	222	84			
	379			J	74	89			

Locality	Datum №	East	North	Structure	Strike	Dip angle	Pitch of striation	Comment	Date
	380			J	221	85			
	381			J	250	81			
	382			J	216	58			
	383			J	238	76			
	384			J	248	86			
	385			J	263	88			
	386			J	245	80			
	387			J	85	88			
	388			J	250	87			
	389			J	249	86			
	390			J	77	86		Spacing: 50 cm	
Torsborgveien, small outcrop, from datum №391 to datum №407									14.10.2010
	391	599821	6639047	MF	150	50			
	392			MF	152	56			
	393			MF	160	68			
	394			J	248	78			
	395			J	78	87			
	396			J	70	86			
	397			J	59	49			
	398			J	80	68			
	399			J	60	88			
	400			J	223	76			
	401			J	224	76			
	402			J	45	80			
	403			MF	165	66			
	404			J	238	79			
	405			MF	160	68			
	406			Basaltic dyke 3 cm thick	280	51			
	407			MF	157	67			
AROUND RESISTIVITY PROFILES 5A, 5B, 6 AND 7									

Locality	Datum №	East	North	Structure	Strike	Dip angle	Pitch of striation	Comment	Date
Nordstrand Hallen, from datum №408 to datum №416, glacial polished surface									12.10.2010
	408	601303	6637772	MF	165	55			
	409			J	70	88			
	410			J	275	68			
	411			J	32	60			
	412			J	45	50			
	413			J	55	85			
	414			J	280	63			
	415			J	262	65			
	416			J	255	60			
Munkelia, going eastward from datum №417 to datum №435									12.10.2010
Munkelia_1	417	601080	6637490	J	120	72		Ca	
	418			MF	163	58			
	419			J	275	72		Ca	
Munkelia_2	420	601174	6637498	MF	160	73			
	421			J	257	73			
	422			J	257	72			
	423			J	90	86			
	424			J	342	54			
	425			MF	160	72			
	426			J	269	88			
Munkelia_3	427	601213	6637553	MF	143	60			
	428			MF	150	50			
Munkelia_4	429	601274	6637610	MF	156	59			
	430			MF	167	64			
	431			MF	168	67			
	432			J	254	80			
	433			J	230	88			
	434			J	258	79			
	435			J	255	81			
Nordstrand Kirke, from datum №436 to datum №457									14.10.2010

Locality	Datum №	East	North	Structure	Strike	Dip angle	Pitch of striation	Comment	Date
Nordstrand Kirke_1	436	601011	6637107	J	257	63		Amphibolite	
	437			J	146	82			
	438			J	230	80			
	439			J	120	72			
	440			J	253	60			
	441			MF	326	87			
Nordstrand Kirke_2	442	600932	6637142	J	286	46		Amphibolite	
	443			J	165	82			
	444			J	164	68			
	445			F	288	83	55W	Chl	
	446			J	130	77			
	447			J	104	79			
	448			J	280	46			
	449			J	112	70			
	450			J	162	60			
	451			J	106	80			
	452			J	286	75			
	453			J	282	74			
	454			J	278	80			
	455			J	276	85			
	456			J	147	59			
	457			J	306	62			
Breiens veien, from datum №458 to datum №465									14.10.2010
	458	601002	6637005	MF	155	77		Strongly foliated gneiss	
	459			MF	154	70			
	460			J	247	87			
	461			J	236	86			
	462			J	70	85			
	463			MF	161	66			
	464			J	80	85			
	465			J	71	85			

Locality	Datum №	East	North	Structure	Strike	Dip angle	Pitch of striation	Comment	Date
AROUND RESISTIVITY PROFILES 8 AND 9									
Munkerudåsen, from datum №466 to datum №483									12.10.2010
Munkerudåsen_1	466	601263	6636690	MF	176	56		Amphibolites and pegmatites	
Munkerudåsen_2	467	601281	6636666	J	60	64			
	468			J	77	82			
	469			J	275	84		White mineral coating	
	470			MF	166	65			
	471			Pegmatite	67	59	60 cm wide		
	472			F	262	71	70W	Thin striae	
	473			J	294	55		Qz	
	474			MF	170	62			
	475			J	270	86		White mineral coating	
Munkerudåsen_3	476	601344	6636556	MF	161	69			
	477			J	67	88			
	478			J	76	84			
Munkerudåsen_4	479	601261	6636557	CN	272	73	60W	Ca-Chl striae	
	480			MF	154	58			
	481			J	78	87			
	482			J	90	84			
Munkerudåsen_5	483	601228	6636591	Pegmatite	120	80		2 m wide	
Bakketoppen, from datum №484 to datum №487									12.10.2010
Bakketoppen_1	484	601410	6636442	MF	165	75			
	485			Rhomb porphyry dyke				20 m wide	
Bakketoppen_2	486	601292	6636418	MF	155	70			
	487			F	276	76	60W	Thin striae	
Vendomveien, from datum №488 to datum №493									12.10.2010
	488	601304	6636272	J	260	88			
	489			J	268	65			
	490			J	9	42			
	491			MF	163	70			
	492			MF	171	58			

Locality	Datum №	East	North	Structure	Strike	Dip angle	Pitch of striation	Comment	Date
	493			MF	161	60			
Munkerudvollen, from datum №494 to datum №516									12.10.2010
Munkerudvollen_1	494	601579	6636424	J	250	75		Large, white mineral coating	
	495			J	261	80			
	496			J	265	85			
	497			J	262	89			
	498			MF	165	42			
	499			MF	161	50			
Munkerudvollen_2	500	601566	6636412	J	316	63			
	501			MF	174	54			
	502			J	95	85			
	503			J	84	84			
	504			J	100	88			
	505			J	270	84		Ca	
Munkerudvollen_3	506	601513	6636426	J	274	55		Qz	
	507			J	115	85			
	508			J	105	76			
	509			J	258	88			
	510			MF	170	53			
	511			MF	165	79		MF steepens westward	
	512			MF	165	70			
	513			J	261	82		Qz	
	514			J	266	84			
	515			MF	166	76			
	516			J	290	86			
Ljabru, going north from datum №517 to datum №570 (from Ljabru_1 to Ljabru_2) and poor outcrop from datum №571 to datum №573 (Ljabru_3)									14.10.2010
Ljabru_1	517	600972	6636159	PS	113	89	17W		
	518			CS	298	76	5W		
	519			CS	113	82	22W		
	520			MF	170	65		Garnet-bearing gneiss	
	521			J	120	73			
	522			J	121	79			

Locality	Datum №	East	North	Structure	Strike	Dip angle	Pitch of striation	Comment	Date
	523			J	268	65			
	524			MF	163	76			
	525			J	120	70			
	526			J	122	71			
	527			J	76	86			
	528			J	116	72			
	529			J	278	66			
	530			J	122	72			
	531			F	270	61	35W	Chl	
	532			J	61	85			
	533			J	91	81			
	534			J	121	73			
	535			MF	172	64			
	536			MF	164	55			
	537			J	105	87			
	538			J	107	75			
	539			J	257	65			
	540			J	280	54			
	541			J	74	81			
	542			MF	176	62			
	543			J	176	62		Large	
	544			CN	181	50	89S		
	545			J	124	72			
	546			CN	168	60	70N	2 m west from fault №544, with proto-breccia	
	547			J	123	71			
	548			MF	165	72			
	549			J	276	56			
	550			J	263	61			
	551			J	260	55			
	552			MF	142	77			
	553			J	254	60			
	554			J	67	81			

Locality	Datum №	East	North	Structure	Strike	Dip angle	Pitch of striation	Comment	Date
	555			MF	154	76			
	556			J	66	81			
	557			J	257	58			
	558			MF	152	65			
	559			MF	144	62			
	560			MF	154	75			
	561			J	200	88			
	562			J	252	52			
	563			J	34	60			
	564			J	74	83			
	565			J	244	66			
	566			J	238	89			
	567			J	235	85			
	568			J	259	57			
	569			J	9	75			
Ljabru_2	570	600940	6636277	MF	158	63			
Ljabru_3	571	600993	6636201	F?	147	88	25N		
	572			MF	147	68			
	573			J	268	54			
Knud Øyes vei, from datum №574 to datum №645									14.10.2010
Knud Øyes vei_1	574	600698	6636293	MF	138	64			
	575			MF	155	45			
	576			MF	158	52			
	577			J	55	88			
	578			J	58	83			
	579			J	70	83		Mafic gneiss with pegmatites	
	580			J	267	82		He + Chl	
	581			MF	160	50			
	582			J	67	81			
Knud Øyes vei_2	583	600712	6636227	J	276	69		Mafic gneiss with pegmatites	
	584			MF	150	58			
	585			MF	152	56			

Locality	Datum №	East	North	Structure	Strike	Dip angle	Pitch of striation	Comment	Date
	586			J	266	70		Ca	
	587			J	13	67			
	588			J	304	32			
	589			J	54	84			
	590			J	28	71			
	591			J	320	70			
	592			J	167	71			
	593			MF	200	30			
	594			MF	198	34			
	595			MF	180	35			
	596			J	320	54			
	597			J	50	64			
	598			J	53	70			
	599			MF	169	40			
	600			MF	180	44			
	601			J	50	43			
	602			MF	204	35			
	603			J	245	80			
	604			J	244	85			
	605			J	330	85			
	606			MF	186	25			
	607			MF	160	44			
	608			J	75	69			
	609			MF	170	51			
	610			CN	162	51	53W		
	611			J	268	78			
	612			MF	164	68			
	613			J	164	68			
	614			J	246	58			
	615			J	50	68			
	616			MF	155	65			
	617			J	245	89			

Locality	Datum №	East	North	Structure	Strike	Dip angle	Pitch of striation	Comment	Date
	618			J	121	68			
	619			J	242	85			
Knud Øyes vei_3	620	600656	6636149	J	22	76			
	621			J	72	88			
	622			MF	185	20			
	623			J	270	73		Large, Chl	
	624			J	6	82			
	625			MF	235	9			
	626			J	327	73			
	627			J	326	72			
	628			J	270	81			
	629			MF	178	12			
	630			J	14	75			
	631			J	82	87			
	632			J	117	68			
	633			CN	170	55			
	634			J	178	70		Fracture associated to normal fault	
	635			J	174	75		Fracture associated to normal fault	
	636			J	173	65		Fracture associated to normal fault	
	637			J	166	55		Fracture associated to normal fault	
	638			MF	208	17			
	639			J	14	83		Chl	
	640			J	134	88			
	641			J	82	85			
	642			J	114	65			
	643			F	173	85	40S	He + Chl striae	
	644			J	35	74			
	645			J	79	88			
East Kantarellen, going eastward from datum №646 to datum №678									12.10.2010
East Kantarellen_1	646	601621	6636067	MF	137	75			
	647			J	265	62		Large	
	648			J	218	75			

Locality	Datum №	East	North	Structure	Strike	Dip angle	Pitch of striation	Comment	Date
	649			J	254	82			
	650			Pegmatite	80	75			
	651			MF	150	60			
	652			J	262	78			
	653			MF	148	38		Going eastward the foliation flattens	
	654			J	260	74			
	655			J	95	68			
	656			J	240	62			
East Kantarellen_2	657	601646	6636084	Basaltic dyke 1.5 m wide	17	84			
	658			Basaltic dyke 1.5 m wide	15	82			
	659			MF	157	46			
	660			J	270	55		Large	
	661			MF	142	59			
	662			J	251	89			
	663			MF	160	74			
	664			MF	158	55			
	665			J	69	72			
	666			J	276	80			
	667			MF	165	50			
	668			J	264	69			
	669			MF	170	58			
	670			J	268	53			
	671			J	340	60			
	672			J	96	87			
	673			J	266	66			
	674			MF	163	67			
	675			J	269	69			
	676			J	273	69			
	677			MF	156	48			

Locality	Datum №	East	North	Structure	Strike	Dip angle	Pitch of striation	Comment	Date
East Kantarellen_3	678	601686	6636084	J	50	76			
West Kantarellen, going westward from datum №679 to datum №712									12.10.2010
West Kantarellen_4	679	601586	6636087	MF	161	60			
	680			Basaltic dyke 10 cm wide	161	60			
	681			CS	84	79	34E		
	682			CS	82	82	36E		
	683			J	266	75			
	684			MF	164	72			
	685			J	76	79			
	686			F	266	64	75W	Badly preserved He striae	
	687			MF	158	60			
	688			J	276	82			
	689			J	270	58			
	690			MF	168	58			
	691			J	90	89			
West Kantarellen_5	692	601496	6636119	CS	125	70	56E	Calcite steps	
	693			MF	160	68			
West Kantarellen_6	694	601488	6636121	CS	114	78	13E		
	695			F	110	79	26E		
West Kantarellen_7	696	601480	6636118	Rhomb porphyry dyke	180	89		20 m wide Eastern border	
West Kantarellen_8	697	601460	6636114	Rhomb porphyry dyke				20 m wide Western border	
	698			MF	169	78			
	699			J	224	75			
	700			J	114	89			
	701			J	200	70			
	702			J	261	68			
West Kantarellen_9	703	601435	6636102	MF	163	58			
	704			MF	162	67			

Locality	Datum №	East	North	Structure	Strike	Dip angle	Pitch of striation	Comment	Date
	705			J	92	82			
	706			J	274	74		Ca	
	707			J	271	72			
West Kantarellen_10	708	601423	6636091	F	100	56	20E		
	709			MF	153	67			
	710			F	125	65			
	711			MF	153	65			
West Kantarellen_11	712	601403	6636076	MF	163	56			
AROUND RESISTIVITY PROFILES 13, 14 AND 15									
Regnbuevegen, going from W to E, from datum №713 to datum №750									15.10.2010
	713	603845	6627516	J	200	80		Fine-grained amphibolite	
	714			J	340	77		Chl	
	715			J	344	80		Chl	
	716			J	263	50			
	717			J	134	35			
	718			J	272	54			
	719			J	270	52			
	720			MF	170	50		Felsic gneiss	
	721			J	286	53		He, fine-grained amphibolite	
	722			J	114	86		Orange mineral coating	
	723			J	193	75			
	724			J	22	61		Orange mineral coating	
	725			J	247	76			
	726			J	203	65			
	727			J	209	72			
	728			J	197	65		Coarse massive gneiss	
	729			J	215	60			
	730			J	98	81			
	731			J	205	80			
	732			J	200	89			
	733			MF	145	60			
	734			MF	150	30			

Locality	Datum №	East	North	Structure	Strike	Dip angle	Pitch of striation	Comment	Date
	735			MF	145	28			
	736			J	186	70			
	737			J	197	88			
	738			J	188	79		Chl	
	739			J	279	86		Chl	
	740			J	196	80		Chl	
	741			J	102	80		Chl	
	742			J	107	71		Qz	
	743			J	216	78		Chl	
	744			J	104	80			
	745			J	213	72			
	746			J	106	76			
	747			J	37	84			
	748			J	39	83			
	749			J	100	82		Chl	
	750			J	18	87			
NE-Vevelstadveien, going from S to N along the western side of the road, from datum №751 to datum №798									15.10.2010
NE-Vevelstadveien_1	751	603732	6626935	J	224	75		Gneiss	
	752			J	122	64		Chl	
	753			J	219	86			
	754			J	120	68			
	755			J	348	68			
	756			J	254	82			
	757			J	235	76			
	758			MF	154	25			
NE-Vevelstadveien_2	759	603769	6626966	J	103	87			
	760			J	279	79			
	761			J	321	75			
	762			J	315	72			
	763			J	330	75			
	764			MF	147	24			
	765			J	105	78			

Locality	Datum №	East	North	Structure	Strike	Dip angle	Pitch of striation	Comment	Date
	766			J	202	82			
	767			J	164	88			
NE-Vevelstadveien_3	768	603780	6626986	J	355	88		Amphibolite, more fractured	
	769			J	6	88		White mineral coating	
	770			J	234	78			
	771			J	169	80		White mineral coating	
	772			J	178	76			
	773			J	12	88		Zeolite	
	774			J	257	41		White mineral coating	
	775			Qz pegmatite	105	58		2 m thick	
	776			J	168	80		Ca, amphibolite	
NE-Vevelstadveien_4	777	603787	6626997	CS	200	52	42S	Faulted gneiss-amphibolite contact	
	778			CS	214	86	31S		
	779			J	185	80		Gneiss	
	780			J	262	87			
	781			J	186	83			
	782			MF	180	35			
	783			MF	170	30			
	784			J	328	79		Mineral coating	
	785			J	342	82			
	786			Pegmatitic vein	84	39		5 cm wide	
	787			J	166	79		Ca + Zeolite	
	788			J	28	88		Ca + Zeolite	
	789			J	171	80		Ca + Zeolite	
	790			J	16	88		Ca + Zeolite	
	791			J	171	76		Ca + Zeolite	
	792			J	167	76		Ca + Zeolite	
	793			J	168	76		Ca + Zeolite	
	794			J	166	74		Ca + Zeolite	
	795			J	227	86			
	796			J	38	78			
	797			J	165	76			

Locality	Datum №	East	North	Structure	Strike	Dip angle	Pitch of striation	Comment	Date
NE-Vevelstadveien_5	798	603797	6627030	J	164	75			
SW-Vevelstadveien, along the eastern side of the road from N to S, from datum №799 to datum №827									15.10.2010
SW-Vevelstadveien_1	799	603561	6626862	Fault zone	177	62	66N	with 30 cm core and 1 m wide damage zones on each side, chlorite-rich fine-grained fault rock in the core	
	800			Fault zone	167	65	66N		
	801			Fault zone	200	87	58N		
	802			Fault zone	162	86	57N	A topographic line N160-165 highlights the fault (data №799-804) to the south	
	803			Fault zone	181	66	72N		
	804			Fault zone	167	70	64N		
SW-Vevelstadveien_2	805	603543	6626852	MF	134	55		Gneiss	
	806			MF	135	45			
	807			J	200	86			
	808			J	84	62			
	809			J	19	81			
	810			J	15	41			
	811			J	80	72			
	812			J	79	70			
	813			J	152	72			
	814			MF	170	68			
	815			MF	157	60			
	816			MF	150	55			
	817			J	302	60			
	818			J	316	65			
	819			J	70	71			
	820			F	138	51	60W	Badly preserved striae	
	821			J	92	81			
	822			J	221	75			
	823			J	222	80		Ca	
	824			J	226	77			
	825			J	345	25			
	826			J	95	67			
	827			J	344	40		Many pegmatites	

Locality	Datum №	East	North	Structure	Strike	Dip angle	Pitch of striation	Comment	Date
East of Haugjordet Ungdomsskole, weathered outcrop in a deep woody gully, from datum №828 to datum №830									15.10.2010
	828	603682	6626699	J	114	76		Gneiss	
	829			J	182	89			
	830			J	109	77			
South of Haugjordet Ungdomsskole, high density of faults with quartz, sporadically calcite and proto-breccias, from datum №831 to datum №856									15.10.2010
	831	603527	6626415	J	334	85			
	832			J	335	75			
	833			J	337	88			
	834			J	168	58		Large	
	835			J	152	67		Qz	
	836			F	193	40	90		
	837			J	171	72		Data №837-840: spacing 10-20 cm	
	838			J	168	71			
	839			J	178	65			
	840			J	160	70			
	841			J	173	75		Qz + Ca	
	842			CN	175	52	90		
	843			CN	187	55	85S		
	844			J	100	75			
	845			J	351	82			
	846			J	227	56			
	847			J	342	88			
	848			CN	173	45	90		
	849			CN	175	65	90		
	850			CN	181	40	90		
	851			CN	175	52	85N		
	852			CN	172	60	85N		
	853			J	174	57			
	854			J	181	52			
	855			J	87	70			
	856			MF	285	87			
Vevelstad, high density of faults, from datum №857 to datum №890									15.10.2010

Locality	Datum №	East	North	Structure	Strike	Dip angle	Pitch of striation	Comment	Date
Vevelstad_1	857	603490	6626076	MF	200	74		From datum №857 to datum №875: from N to S on the western side of the road and high density of faults with a spacing down to 10 cm	
	858			F	7	79	83S		
	859			Gabbro dyke, 30 cm wide	322	75			
	860			Gabbro dyke, 30 cm wide	326	70			
	861			CN	206	68	70S	Chl	
	862			CN	7	89	89S		
	863			CN	356	82	80S		
	864			F	20	87	89S		
	865			F	186	82	84N		
	866			F	5	88	78N		
	867			F	15	80	75N		
	868			CN	210	56	73N		
	869			F	26	82	77N		
	870			MF	218	58			
	871			F	225	55	71S		
	872			F	214	70	83N		
	873			F	210	62	89N		
	874			F	220	65	75S		
	875			F	219	65	84S		
Vevelstad_2	876	603492	6626096	F	190	85	60S	From datum №876 to datum №890: from S to N on the eastern side of the road and high fault density with a spacing of 1 m	
	877			F	196	82	80S		
	878			F	192	87	58S		
	879			F	191	72	60S		
	880			F	188	82	58S		
	881			CN	211	66	81S		
	882			CN	204	66	83S		
	883			CN	214	57	86S		
	884			J	350	87		Qz + Ca	
	885			F	230	60	79S	Chl	

Locality	Datum №	East	North	Structure	Strike	Dip angle	Pitch of striation	Comment	Date
	886			F	206	70	76N		
	887			F	209	55	82N		
	888			F	213	63	82N		
	889			MF	250	62			
	890			MF	280	60			
Lyngåsen, mostly amphibolite, from datum №891 to datum №900									15.10.2010
	891	603800	6626698	J	342	80		White mineral coating	
	892			J	89	88			
	893			J	206	86		Chl	
	894			J	257	86			
	895			J	194	88			
	896			J	266	75			
	897			J	267	85			
	898			J	337	77		Large, qz	
	899			J	335	82		Large, qz	
	900			CS	165	80	6S	Chl + He	
Bøleråsenskolen, from datum №892 to datum №898									15.10.2010
	892	604264	6626668	J	109	71		Large pegmatitic bodies	
	893			J	254	84			
	894			J	105	75			
	895			J	342	85			
	896			J	258	88			
	897			J	259	86			
	898			J	272	82			
Skoglia, from datum №899 to datum №918									15.10.2010
Skoglia_1	899	604426	6626494	F	175	88	86S	Crushed infill	
	900			J	188	78			
	901			J	155	89			
	902			MF	207	36			
	903			F	315	75	89N		
	904			MF	238	65			
	905			F	324	80	77S		

Locality	Datum №	East	North	Structure	Strike	Dip angle	Pitch of striation	Comment	Date
	906			MF	240	66			
Skoglia_2	907	604344	6626561	MF	226	65			
	908			J	370	88			
	909			J	314	78			
	910			J	106	81			
	911			J	324	75			
	912			J	93	68			
	913			J	200	84			
	914			J	101	62			
	915			J	94	66			
	916			J	207	59			
	917			J	292	78			
	918			F	90	52	80W	He	